Maintenance Optimization of Tidal Energy Arrays

Design of a Probabilistic Decision Support Tool for Optimizing the Maintenance Policy

R.C. de Nie

Master Thesis
MSc Offshore & Dredging Engineering
Delft University of Technology

In collaboration with:
Damen Shipyards

TU Delft

Maintenance Optimization of Tidal Energy Arrays

Design of a Probabilistic Decision Support Tool for Optimizing the Maintenance Policy

by

R.C. de Nie

to obtain the degree of Master of Science

at the Delft University of Technology,

to be defended publicly on Friday December 16, 2016 at 10:00 AM.

Student number: 4023358

Chairman:	Prof. dr. ir. A.R.M. Wolfert,	TU Delft
Thesis committee:	ir. A. Jarquin Laguna,	TU Delft
	ir. G. Leontaris,	TU Delft
	BEng C.F.D. Hoogendoorn,	Damen Shipyards

This thesis is confidential and cannot be made public until December 16, 2026.

TU Delft

Abstract

The increasing demand for electricity offers many opportunities for renewable energy production, of which one alternative is tidal stream energy. Several feasibility studies have shown that the global tidal stream energy potential can contribute significantly to producing renewable energy. This tidal energy can mostly be produced at the 'tidal hotspots', where the kinetic energy density is very high due to fast flowing tidal currents. However, the tidal technology is not yet cost competitive in comparison with other renewables, such as photovoltaic and wind energy, which is why further cost reductions and efficiency improvements are to be achieved. Interviews with existing tidal system developers provided insight in the cost breakdown and showed that maintenance accounts for a significant share of the total project costs. This is due to the harsh environmental conditions that impose a large uncertainty, which increase the complexity of selecting an optimal maintenance policy. Damen Shipyards has shown interest in entering the tidal industry and is exploring the cost reduction possibilities by developing their own tidal system.

This thesis contributes to Damen Shipyards' research by performing a time series analysis of a tidal hotspot to identify and model the multivariate dependence of the governing environmental phenomena. A probabilistic decision support tool is developed for selecting the optimal maintenance policy. The decision support tool primarily determines when and to what extent corrective maintenance should be performed. The corresponding overall maintenance costs are also calculated and secondary information regarding the activity duration is given. By means of the probabilistic approach, which captures the weather window uncertainty due to the environmental randomness, the results can be interpreted by the user based on the desired confidence level.

In this research the weather window uncertainty is implemented by simulating a large number of random, but statistically identical environmental time series, which are based on available measurement data of the tidal field at EMEC, located at the Orkney Islands in the United Kingdom. The multivariate dependence between the significant wave height, wave peak period, wind velocity and current velocity is identified in the measurement set and fully represented in the generated time series by means of a pair-copula construction simulation. The necessity for having time independence cannot be met in the original dataset, which is why a new simulation approach is developed. This method consists of a sequential simulation of pair-copula constructions to include both the time dependence and multivariate dependence in the synthetic time series. Simulation of the set of synthetic time series showed to be more effective for describing uncertainty with respect to exclusively using the original dataset, due to the possibility of including more environmental realizations.

The tidal array is represented as a semi-Markov decision process, which captures all costs and transition processes related to the deterioration and maintenance decisions. A policy optimization algorithm can then be used to find the optimal set of decisions and the corresponding maintenance cost rate which includes both the direct and indirect maintenance costs.

The novel tidal system design of Damen Shipyards is then plugged into the decision support tool in order to determine the optimal maintenance policy and maintenance costs. The effect of different levels of detail for representing the tidal system have been compared and the benefits in terms of cost reductions of using this decision support tool with respect to less advanced approaches have been highlighted. Furthermore, multiple scenarios have been elaborated to identify the sensitivities in the cases of accounting for unreliability in the failure rates, varying the number of platforms in the array and including the economic fluctuations of the maintenance vessel day rates.

Preface

Before you lies the thesis "Maintenance Optimization of Tidal Arrays: Design of a Probabilistic Decision Support Tool for Optimizing the Maintenance Policy", which contributes to the research on cost reductions for tidal energy systems. It has been written to fulfill the graduation requirements of the Offshore Engineering and Dredging master program at Delft University of Technology and has been performed under the supervision of Damen Shipyards.

The process of conducting the research for this thesis proved to be a challenge, which I would not have been able to tackle without support and guidance from numerous people. I would therefore like to dedicate a few words of acknowledgement to those who kept me going strong during the last twelve months.

I am very grateful to the chairman of my thesis committee, Prof. Rogier Wolfert, for showing trust in me and my research. I believe that by being challenged constantly throughout the course of my graduation, the quality of my research exceeded my initial expectations of what would be possible. The discussions were always interesting and led to new insights on exciting subjects which would normally not be touched upon in the master program.

I would also like to express my sincere gratitude to George Leontaris for his excellent guidance as my daily supervisor. The numerous meetings we had were great to exchange ideas and discuss the latest developments. George always motivated me to push my limits and further improve the research.

I would also like to thank Antonio Jarquin Laguna for his contribution to my graduation committee as the representative from my master track. I was very delighted with the liberty I enjoyed to further expand my knowledge beyond that of the regular Offshore and Dredging master program. Antonio has also further sparked my interest in ocean energy systems, which will most certainly play a significant role to meet the growing energy demand.

Furthermore, I would like to compliment and give credit to Don Hoogendoorn for being my mentor at Damen Shipyards. Not only was he a source of motivation and understanding, but he also actively involved me in the Damen culture, which truly was a great experience.

Lastly, I would like to give a big word of thanks to my friends, girlfriend, roommates and family who I have not given as much attention as I would like to have done during my graduation. I highly appreciate the countless of times that I could blow off steam with all of you and take a step back to see the wider perspective. It has been quite the ride and I hereby promise that copulas and maintenance model optimization will not be brought up as a topic of conversation, at least not for a while...

For those having made it up to this point, I congratulate you with having read at least one page of my thesis and I hope you will enjoy reading the rest as much as I did when writing it.

R.C. de Nie
Delft, December 2016

Acronyms

ACF Auto Correlation Factor.

ADCP Acoustic Doppler Current Profiler.

AIC Akaike Information Criteria.

AWAC Acoustic Wave and Current.

BIC Bayesian Information Criteria.

CAPEX capital expenditures.

DP Dynamic Positioning.

DR Decision Regime.

EMEC European Marine Energy Centre.

FiT Feed-in Tariff.

FMEA Failure Modes and Effect Analysis.

FORCE Fundy Ocean Research Center for Energy.

GoF Goodness-of-Fit.

LCOE Levelized Cost Of Electricity.

MAD median absolute deviation.

MC Monte Carlo.

MET meteorological.

MLE Maximum Likelihood Estimation.

MTBF mean time between failure.

MTTR mean time to repair.

NAC nested Archimedean copula.

O&M Operations & Maintenance.

OPEX operational expenditures.

PCC pair-copula construction.

PM prime mover.

PSV Platform Supply Vessel.

PV photovoltaic.

SMDP Semi-Markov Decision Process.

TEC Tidal Energy Converter.

TRL Technology Readiness Level.

TSR tip-speed ratio.

VAT Vertical Axis Turbine.

List of Figures

1.1 Global energy trends up to 2035 . . . 1
1.2 Quantified global tidal energy resources . . . 2
1.3 Simulated maximum depth-averaged velocities within a sub-section of the northwest European shelf seas . . . 3
1.4 Cost breakdown for current stage of development (left) and commercial target (right) . . . 4
1.5 Cost breakdown for large scale offshore wind farms . . . 4
1.6 Maintenance optimization . . . 7
1.7 Flowchart of this thesis' topics and the chapter relations . . . 10

2.1 Fréchet-Hoeffing bounds . . . 15
2.2 Original, survival and rotated copula variants . . . 16
2.3 Contour plots of copulas with standard normal marginals ($\tau = 0.60$) . . . 18
2.4 Model structures for construction of multivariate dependence . . . 20
2.5 Four parameter D- and Canonical vines . . . 21
2.6 Visualisation of D-vine simulation for one sample set . . . 23

3.1 Example of Markov chain and transition probabilities . . . 27
3.2 Policy iteration flow chart . . . 28

4.1 The 'bathtub curve' . . . 32
4.2 Reliability function and failure probability distribution function for a constant failure rate . . . 33
4.3 Serial system of n components . . . 33
4.4 Parallel system failure . . . 34
4.5 MTBF of parallel systems . . . 35

5.1 Artist impression of the Damen Tidal Energy Converter (TEC) design . . . 40
5.2 TEC power curve . . . 42
5.3 Fault tree of the tidals array . . . 44
5.4 Exponential failure distribution of individual assemblies and TEC . . . 46
5.5 Fraction of assembly failure rate w.r.t. TEC failure rate . . . 47

6.1 Process flow chart for generating the order of maintenance tasks . . . 49
6.2 Spot day rate of Platform Supply Vessels (PSVs) in the North Sea area . . . 53

7.1 Model framework . . . 57

8.1 Geographical location of European Marine Energy Centre (EMEC) [35] . . . 62
8.2 Rose plots of the absolute and relative wave and current velocity directionality . . . 63
8.3 Current and wave direction time series . . . 63
8.4 Histograms for current velocity and significant wave height for two relative propulsion directions (same vs. opposite) . . . 64
8.5 Prevailing wind direction and effect on significant wave height . . . 64
8.6 Frequency spectrum plots of directional and absolute current velocity data . . . 65
8.7 Frequency spectrum plots of the significant wave height and peak wave period . . . 66
8.8 Factorisation of variables at D-vine base level . . . 68
8.9 Scatter plots of pseudo-observations . . . 69
8.10 Copying a fraction of the original Ucurr time series . . . 71
8.11 Correlograms of EMEC timeseries (1 lag = 10 minutes) . . . 73
8.12 Univariate time series simulation algorithm . . . 74
8.13 Simulated time series of U_{wind} for different lags ($\triangle t = 10$ min) . . . 75

8.14 Error between simulation methods when increasing the time steps of the Uwind data 76
8.15 Simulated time series of U_{wind} for different copula families 77
8.16 Visual comparison of original and two synthetic U_{wind} time series 78
8.17 Histograms of mean and standard deviation of synthetic U_{wind} time series 79
8.18 Transition matrix of original U_{wind} time series 80
8.19 Statistical properties of error distribution for different time lags 80
8.20 Comparison of original time series and one synthetic time series realization 82
8.21 Comparison of the cumulative distribution functions of the persistence in the original and synthetic time series 83
8.22 Comparison of activity duration with original and synthetic time series (fixed starting point) . . 84
8.23 Comparison of activity duration with original and synthetic time series (variable starting point) 85
8.24 Comparison of activity duration of synthetic time series with and without multivariate dependence (replace 9 TECs) 85

9.1 Example of deterioration and maintenance states 88
9.2 Decision sets for system states in SMDP representation 90
9.3 Tidal array example: deterioration & maintenance states 90
9.4 Tidal array example: deterioration transitions (decision: D_1) 91
9.5 Process for calculating the TEC's long term mean power production 94
9.6 Tidal array example: Maintenance transitions from S_{M5} 95
9.7 Fitting limits on time series and identifying non-operability 97
9.8 Overall non-operability for task 'TEC replacement' for the observed time series 97
9.9 Weather window starting points for task 'TEC replacement' (green = pass, red = no pass) 98
9.10 Cumulative task durations for the replacement of 1 TEC: $D_{2.1}$ (1000 simulations) 99
9.11 Cumulative task durations for the replacement of 1 to 6 TECs: $D_{2.1} \rightarrow D_{2.6}$ (1000 simulations) . . 99
9.12 Tidal array example: $N_{TEC,fail}$ during the maintenance activity 102
9.13 Example tidal array: Maintenance cost rates and optimal policies for $N_{sim} = 1000$ 104
9.14 Example tidal array: Maintenance cost rates for $N_{sim} = 1000$ 104
9.15 Optimal policy results of case 1a 105
9.16 Optimal policy results of case 1b 105
9.17 Results of case 2 105
9.18 Optimal policy results of case 3a 106
9.19 Optimal policy results of case 3b 106

10.1 Mean power production distribution for different cut-out velocities 108
10.3 Maintenance cost rates and optimal policies of the base case 109
10.4 Percentage of non-maximum TEC replacements if maintenance is initiated 110
10.5 TEC replacements in states with high non-maximum replacements 110
10.6 Decisions per state for the three analyzed policies within DR 2 of policy G 112
10.7 Comparison of the maintenance cost rate per analyzed policy 113
10.8 reference case: Optimal maintenance cost rate 115
10.9 Selection of simulation points from identified optimal policies 116
10.10 Maintenance cost rates and optimal decisions for different λ_{TEC} 117
10.11 Cumulative distribution of maintenance cost rates for different λ_{TEC} 117
10.12 Cumulative distribution of maintenance cost rates for different $N_{platform}$ 118
10.13 Cumulative distribution of maintenance cost rates for different vessel day rates 119

A.1 Pearson Linear Correlation cases 125
A.2 Differences between Pearson and Spearman correlation 126
A.3 D-vine node labels 129

B.1 Darrieus types 131
B.2 tip-speed ratio (TSR)-C_p relation for different prime movers (PMs) 132

C.1 Tidal array example: Maintenance transitions from S_{M5} 136

D.1 Acoustic wave and current ADCP 137

D.2 Window used for the median absolute deviation . . . 138
D.3 Timeseries of H_s . . . 139
D.4 Timeseries of T_p . . . 139
D.5 Timeseries of U_{wind} . . . 140
D.6 Timeseries of U_{curr} . . . 140
D.7 Boxplot of significant wave height per current velocity bin: same and opposite direction . . . 141
D.8 Properties of the used D-vine . . . 142
D.9 Time independence analysis . . . 143
D.10 Required time interval for full time dependence of all 4 variables . . . 143
D.11 Auto- and Cross-correlations of EMEC data . . . 144
D.12 Simulated time series of U_{wind} for different lags ($\triangle t$ = 10 min) . . . 144
D.13 Simulated time series of U_{wind} for different lags ($\triangle t$ = 20 min) . . . 145
D.14 Simulated time series of U_{wind} for different lags ($\triangle t$ = 30 min) . . . 145
D.15 Simulated time series of U_{wind} for different lags ($\triangle t$ = 1 hour) . . . 145
D.16 Comparison of activity duration with original and synthetic time series (fixed starting point) . . . 146
D.17 Comparison of activity duration with original and synthetic time series (variable starting point) 147

E.1 Input - Simulation data . . . 149
E.2 Input - Operational data . . . 149
E.4 Maintenance activity duration and costs of maintenance for Decision D2.1: 'Replace 1 TEC' . . . 150
E.5 Maintenance activity duration and costs of maintenance for Decision D2.2: 'Replace 2 TECs' . . . 151
E.6 Maintenance activity duration and costs of maintenance for Decision D2.3: 'Replace 3 TECs' . . . 151
E.7 Maintenance activity duration and costs of maintenance for Decision D2.4: 'Replace 4 TECs' . . . 151
E.8 Maintenance activity duration and costs of maintenance for Decision D2.5: 'Replace 5 TECs' . . . 152
E.9 Maintenance activity duration and costs of maintenance for Decision D2.6: 'Replace 6 TECs' . . . 152
E.10 Maintenance activity duration and costs of maintenance for Decision D2.7: 'Replace 7 TECs' . . . 152
E.11 Maintenance activity duration and costs of maintenance for Decision D2.8: 'Replace 8 TECs' . . . 153
E.12 Maintenance activity duration and costs of maintenance for Decision D2.9: 'Replace 9 TECs' . . . 153
E.13 Flowchart of D-states and transitions of policy G . . . 155
E.14 Maintenance activity duration and costs of maintenance loop 1 . . . 156
E.15 Maintenance activity duration and costs of maintenance loop 2 . . . 156
E.16 Maintenance activity duration and costs of maintenance loop 3 . . . 157
E.17 Maintenance activity duration and costs of maintenance loop 4 . . . 157
E.18 Maintenance activity duration and costs of maintenance loop 5 . . . 158
E.19 Maintenance activity duration and costs of maintenance loop 6 . . . 158
E.20 Maintenance activity duration and costs of maintenance loop 7 . . . 159

List of Tables

1.1 Levelized cost of electricity for different power sources . . . 3

2.1 Copula tail dependence properties [64] . . . 18
2.2 Relations between θ and τ . . . 19

5.1 Numerical values of the TEC power generating properties . . . 43
5.2 Wind turbine assemblies' reliability field data . . . 45
5.3 Product costs of assembly and TEC . . . 47

6.1 Required weather window of the maintenance operation . . . 51
6.2 Damen Utility vessel fuel consumption . . . 53
6.3 Vessel operation cost rates . . . 54

8.1 Peak data analysis of current velocity frequency spectrum (directional data) . . . 65
8.2 Peak data analysis of current velocity frequency spectrum (absolute data) . . . 66
8.3 Kendall's Tau rank correlations of environmental bivariate data . . . 67
8.4 Copula fitting statistics for bivariate data U_{wind}-H_s . . . 69
8.5 Copula fitting statistics for bivariate data H_s-T_p . . . 70
8.6 Copula fitting statistics for bivariate data T_p-U_{curr} . . . 70
8.7 D-vine copula parameters . . . 70
8.8 Kendall rank correlation of the conditional distributions at each vine tree and copula parameter 75
8.9 Kendall rank correlation of time lags and copula parameter . . . 76
8.10 Comparison of statistical properties of original and synthetic time series of U_{wind} . . . 79
8.11 States of the U_{wind} time series . . . 80
8.12 Kendall's Tau rank correlations of ne synthetic time series realization . . . 81

9.1 Example of deterioration state duplicates (2 platforms with 2 TECs, 1 failure) . . . 89
9.2 Example of deterioration state generation . . . 89
9.3 Examples values of transition probabilities . . . 92
9.4 Example values of deterioration transition rates . . . 93
9.5 Examples values of maintenance transition probabilities . . . 96
9.6 Example array: Optimal policy (1 simulation) . . . 102

10.1 Power production properties for different cut-out velocities . . . 108
10.2 Comparison of failure times and maintenance activity durations . . . 109
10.3 Boundaries of the decision regimes for analyzed policies . . . 112
10.4 Maintenance cost rates of the identified optimal policies for different confidence levels . . . 113
10.5 Unique maintenance loops of policy G . . . 114
10.6 Comparison of P90 values for minimum cost rates . . . 115
10.7 Relative difference in maintenance cost rate at P90 due to changing λ_{TEC} . . . 117
10.8 Maintenance cost rates of simulations with varying λ_{TEC} values for different confidence levels . 118
10.9 Normalized maintenance cost rates for different $N_{platform}$ . . . 118

A.1 Satisfaction or not of properties for various constructions . . . 126

C.1 Tidal array example: Maintenance task generation . . . 136

D.1 Extreme value limits for EMEC dataset . . . 138
D.2 Kendall's Tau rank correlations of reference study on sea states . . . 141
D.3 All possible factorisations and their combined Tau values . . . 142

Contents

Abstract iii

Acronyms vi

List of Figures ix

List of Tables xiii

1 Introduction 1
- 1.1 Emerging markets for tidal energy converters . . . 1
  - 1.1.1 Global energy trends . . . 1
  - 1.1.2 Tidal energy potential . . . 1
  - 1.1.3 Cost competitiveness . . . 2
- 1.2 Cost breakdown and reduction potential of tidal systems . . . 4
  - 1.2.1 Total cost breakdown of tidal systems . . . 4
  - 1.2.2 OPEX cost breakdown of offshore wind farms . . . 4
- 1.3 Maintenance management . . . 5
  - 1.3.1 Strategy definition . . . 5
  - 1.3.2 Policy optimization . . . 5
- 1.4 Uncertainties in maintenance of tidal arrays . . . 5
  - 1.4.1 Weather windows uncertainty . . . 5
  - 1.4.2 Limited data and experience . . . 6
- 1.5 Necessity for a probabilistic maintenance model . . . 6
- 1.6 The Damen solution . . . 6
  - 1.6.1 Novel tidal system design . . . 6
  - 1.6.2 Maintenance management implementation . . . 7
- 1.7 Purpose statement . . . 8
- 1.8 Research objectives . . . 8
- 1.9 Research questions . . . 9
- 1.10 Research methodology . . . 9
- 1.11 Outline . . . 9

I Theoretical background 11

2 Multivariate dependence modeling using copulas 13
- 2.1 Introduction to dependence . . . 14
  - 2.1.1 Common methods for describing dependence . . . 14
  - 2.1.2 Tail dependence . . . 14
- 2.2 Copulas . . . 14
  - 2.2.1 Bivariate copula properties . . . 15
  - 2.2.2 Popular bivariate copula families . . . 16
  - 2.2.3 Tail dependence properties . . . 17
- 2.3 Fitting a copula to bivariate data . . . 18
  - 2.3.1 Build the empirical copula . . . 18
  - 2.3.2 Determine the optimal copula parameter . . . 19
  - 2.3.3 Selecting the best fitting copula . . . 19
- 2.4 Copula constructions for describing multivariate dependence . . . 20
  - 2.4.1 Pair Copula Constructions . . . 20
  - 2.4.2 Vine copula representation . . . 21
  - 2.4.3 The h-function . . . 22
- 2.5 Building a vine copula . . . 22

2.6 Vine copula simulation . . . 22
2.7 Simulation of data with time dependence . . . 23
2.7.1 Necessity of i.i.d. input data . . . 23
2.7.2 Research gap . . . 24

3 Maintenance Decision Models 25
3.1 Group maintenance strategy . . . 25
3.2 Limitations of analytical models . . . 25
3.3 Semi-Markov Decision Processes . . . 26
3.3.1 General Markov process . . . 26
3.3.2 Extension into a Semi-Markov Decision Process . . . 26
3.3.3 SMDP system representation . . . 27
3.4 Policy optimization methods . . . 28
3.4.1 Policy iteration . . . 28

4 Equipment failure 31
4.1 Modeling failures . . . 31
4.2 Random failures . . . 31
4.3 Multi-component failure . . . 33
4.3.1 Serial failure . . . 33
4.3.2 Parallel failure of identical equipment . . . 34

II Damen solution - System overview 37

5 Damen Tidal Energy Converter 39
5.1 Tidal array location . . . 39
5.1.1 Feed-in tariff . . . 39
5.2 TEC system overview . . . 40
5.2.1 System description . . . 40
5.2.2 Subsystem & assembly identification . . . 41
5.3 TEC power generation . . . 41
5.3.1 Power curve . . . 41
5.3.2 Optimal control strategy . . . 42
5.3.3 Power generation related assumptions . . . 43
5.4 TEC failure . . . 43
5.4.1 Included failure modes . . . 43
5.4.2 Usage of wind turbine reference data . . . 44
5.4.3 Adjustment factors . . . 45
5.4.4 Bundling of assembly failure rates and product costs . . . 45
5.4.5 Failure related assumptions . . . 47

6 Maintenance strategy 49
6.1 Maintenance tasks . . . 49
6.1.1 Maintenance process flow . . . 49
6.1.2 Weather windows . . . 51
6.2 Maintenance vessel . . . 51
6.2.1 Sailing speed . . . 52
6.2.2 Deck space . . . 52
6.2.3 Day rate . . . 52

III Model development & results 55

7 Maintenance model framework 57
7.1 Model overview . . . 57
7.2 Input . . . 57
7.3 Process flow . . . 58
7.3.1 Environmental generation . . . 58
7.3.2 System and decision representation . . . 58
7.3.3 Maintenance policy optimization . . . 59

7.4 Output . . . 59
7.4.1 Deterministic output of a single simulation . . . 59
7.4.2 Analysis of probabilistic results . . . 59
7.5 Model assumptions . . . 59
7.5.1 Failure related assumptions . . . 60
7.5.2 Maintenance related assumptions . . . 60
7.5.3 Electricity production related assumptions . . . 60

8 Generation of environmental time series including dependence 61
8.1 Analysis of EMEC environmental measurement data . . . 61
8.1.1 Data availability . . . 61
8.1.2 Influence of directionality on the wave-current interaction . . . 62
8.1.3 Influence of directionality on the wind-wave interaction . . . 64
8.1.4 High frequency wave-current interaction . . . 65
8.2 Vine construction . . . 67
8.2.1 Bivariate dependence . . . 67
8.2.2 Vine type selection . . . 68
8.2.3 Base level factorisation . . . 68
8.2.4 Copula selection . . . 68
8.2.5 Vine property overview . . . 70
8.3 Existence of time dependence in time series . . . 71
8.3.1 Univariate time dependence . . . 72
8.3.2 Disadvantages of increasing the sampling time interval . . . 72
8.4 New approach for simulating time and multivariate dependence . . . 73
8.4.1 Developed simulation algorithm . . . 73
8.4.2 Analysis of univariate case . . . 74
8.4.3 Goodness of Fit tests . . . 78
8.4.4 Expansion to multivariate case . . . 81
8.4.5 Synthetic time series validation . . . 82
8.5 Added value of using copulas for time series simulation . . . 83
8.5.1 Original TS $\longleftrightarrow$ Synthetic TS . . . 83
8.5.2 Synthetic TS with/without multivariate dependence . . . 85

9 Maintenance policy optimization using Semi-Markov Decision Processes 87
9.1 State generation . . . 87
9.1.1 Unique states . . . 88
9.1.2 Maximum allowable array failures . . . 89
9.2 Decisions . . . 89
9.2.1 Primary decision set: 'Should maintenance be performed?' . . . 90
9.2.2 Secondary decision set: 'If so, how many TECs should be replaced at once?' . . . 90
9.3 Illustrative example . . . 90
9.3.1 Clarification on observed maintenance transitions . . . 91
9.4 Deterioration module . . . 91
9.4.1 Failure transition probabilities . . . 91
9.4.2 Failure transition rates . . . 92
9.4.3 Production downtime costs ('*Reward*') . . . 92
9.5 Maintenance module . . . 94
9.5.1 Transition probabilities . . . 94
9.5.2 Maintenance task generation algorithm . . . 96
9.5.3 Maintenance activity duration algorithm ('*Transition rates*') . . . 97
9.5.4 Maintenance costs ('*Rewards*') . . . 100
9.6 Policy optimization module . . . 102
9.6.1 Primary output interpretation . . . 102
9.6.2 Probabilistic output due to environmental randomness . . . 103
9.6.3 Decision making . . . 103
9.7 Model verification . . . 104
9.7.1 Case 1a: High set-up vessel, low variable costs costs . . . 104

9.7.2 Case 1b: Low set-up vessel, High variable costs costs . . . 105
9.7.3 Case 2: No weather window requirements . . . 105
9.7.4 Case 3a: High TEC failure rate . . . 106
9.7.5 Case 3b: Low TEC failure rate . . . 106

10 Model results **107**
10.1 Damen base case . . . 107
10.1.1 Complete description of uncertainty . . . 107
10.1.2 General findings . . . 107
10.1.3 Identifying optimal policies . . . 109
10.1.4 Comparison of optimal policies . . . 111
10.1.5 Analysis of recommended maintenance policy . . . 113
10.2 Reference case: Optimal policy without unique failure combinations . . . 114
10.2.1 Approach . . . 114
10.2.2 Comparison of results . . . 114
10.3 Sensitivity analysis . . . 115
10.3.1 Selecting representative simulations . . . 115
10.3.2 Scenario 1: TEC failure rate . . . 115
10.3.3 Scenario 2: Array size . . . 118
10.3.4 Scenario 3: Maintenance vessel . . . 119

11 Conclusions & recommendations **121**
11.1 Conclusions . . . 121
11.2 Recommendations . . . 123
11.2.1 Environmental analysis and modeling . . . 123
11.2.2 Decision support tool . . . 123

A Copulas and Vines **125**
A.1 Common methods for describing dependence . . . 125
A.1.1 Pearson product-moment correlation coefficient . . . 125
A.1.2 Spearman's rank correlation coefficient . . . 125
A.1.3 Kendall rank correlation coefficient . . . 126
A.2 Properties of the copula construction methods . . . 126
A.3 A pair-copula decomposition of a general multivariate distribution . . . 127
A.4 Vine density distributions . . . 127
A.4.1 D-vine . . . 128
A.4.2 C-vine . . . 128
A.5 D-vine copula simulation algorithm . . . 128
A.5.1 D-vine . . . 128
A.5.2 Node labels . . . 129

B Darrieus turbine power generation **131**
B.1 Types of Darrieus turbines . . . 131
B.2 Power curve . . . 131
B.2.1 Power coefficient . . . 132
B.2.2 Darrieus swept area . . . 132
B.2.3 Power coefficient . . . 132

C Model properties **135**
C.1 Deterioration Module . . . 135
C.1.1 Calculate $N_{TEC,fail,pos}$ . . . 135
C.2 Maintenance Module . . . 136
C.2.1 Numerical example of maintenance task generation . . . 136

D Environmental analysis **137**
D.1 Acoustic Wave and Current ADCP . . . 137
D.2 Filtering & smoothing . . . 137
D.2.1 Extreme value removal . . . 138
D.2.2 Outlier filtering . . . 138

D.3 EMEC measurement data . . . 139
D.4 Influence of directionality on wave-current interaction . . . 141
D.5 Reference study on dependence of sea state variables. . . . 141
D.6 All possible factorisations and their combined Tau values . . . 142
D.7 D-vine contours. . . . 142
D.8 Time independence analysis . . . 142
D.9 Auto- and Cross-correlations of EMEC data . . . 144
D.10 Simulated time series of U_{wind} for different lags and time steps . . . 144
D.11 Copula comparison study . . . 145
D.11.1 Original TS ⟷ Synthetic TS . . . 145

E Model results **149**
E.1 Base case input parameters . . . 149
E.1.1 Determining $N_{fail,max}$ . . . 150
E.2 General results . . . 150
E.2.1 Maintenance activity . . . 150
E.3 Properties of policy G . . . 155
E.3.1 Flowchart of D-states and transitions . . . 155
E.3.2 Maintenance loop activity properties . . . 156

Bibliography **161**

1 Introduction

1.1. Emerging markets for tidal energy converters

1.1.1. Global energy trends

Today's world is developing at a pace with a rapid growth of the global electricity demand. Data from the U.S. Energy Information Administration [24] describe an increase of the electricity net generation of the world between 1990 and 2012 by more than 90%. This trend will also continue the next decades when analyzing British Petroleum's global energy outlook [75], which predicts a continuation of this growth due to the growing population and the overall development of higher living standards. Between 2013 and 2035 the primary energy production is projected to increase by 37%, with growth averaging 1.4% per year, as is depicted in figure 1.1a. In addition to this trend, an increase of the fraction of generated electricity with respect to the total energy produced is expected from 42% today to 47% in 2035, as can be seen in figure 1.1b.

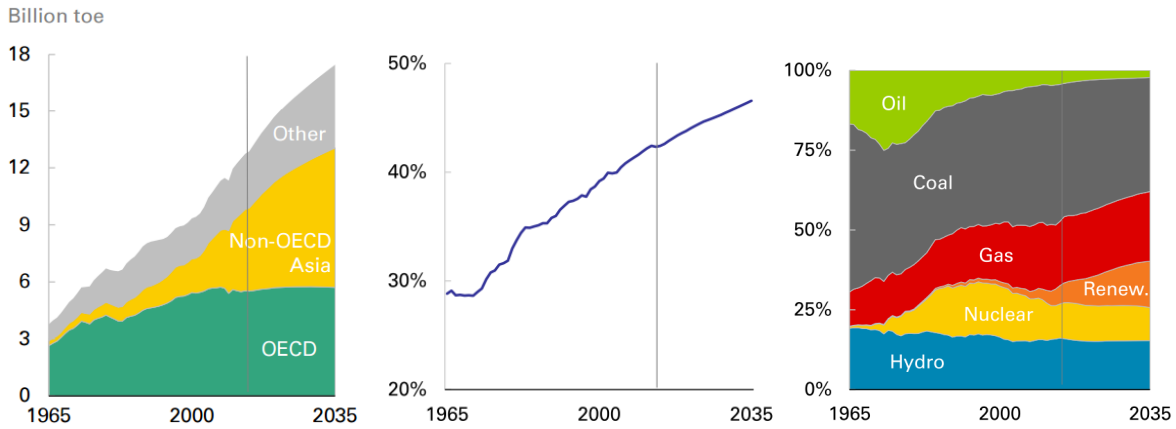

(a) Primary energy production per region

(b) Inputs to power as a share of total primary energy

(c) Primary inputs to power

Figure 1.1: Global energy trends up to 2035 by British Petroleum [75]

The increase in the electricity demand offers many opportunities for governments to develop different deployment strategies to meet the demand. Given the growing awareness for sustainability and CO_2 reduction, this has resulted in a vast increase in market share of renewable energy sources, shown in figure 1.1c.

1.1.2. Tidal energy potential

Whilst the vast majority of the renewable energy developments focuses on solar photovoltaic (PV) and wind energy, several studies [30, 34, 42, 84] have shown that the global tidal stream energy potential can still con-

tribute significantly at the so-called 'tidal hotspots', where the kinetic energy density is very high due to fast flowing tidal currents. An overview of the most significant resources is shown in figure 1.2. The estimates of global potential of tidal energy generation vary, but it is widely agreed that tidal stream energy capacity could exceed 120 GW globally, which accounts for 4.36% of the global electricity production in 2015 [76].

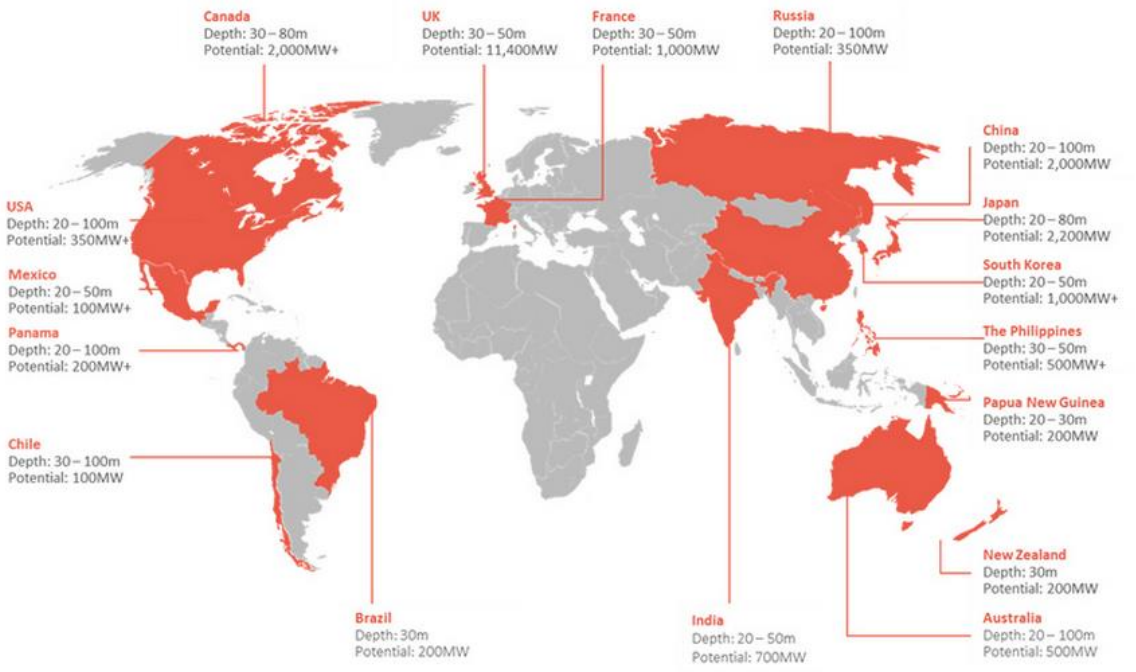

Figure 1.2: Quantified global tidal energy resources by Atlantis Resources Limited [8]

In addition to the availability of tidal stream energy, the technology may bring a number of advantages over comparable renewable energy sources, such as (offshore) wind and solar PV systems:

1. The predictive behavior of the tides enables a very predictable electricity production profile, which reduces the necessity of expensive electricity buffer stations.
2. Depending of the rating of the turbine, tidal current power can achieve capacity factors in excess of 40% (peaking at 66% so far [60]) on commercial scale sites. Whilst the capacity factors of most offshore wind farms in the United Kingdom and Denmark balance around 40% [26, 27], the annual capacity factors of wind turbines and solar PV were in 2015 well below that with factors of 32.5% and 28.6% [104], respectively.
3. Smaller tidal systems are needed than offshore wind systems for an equivalent power production due to the higher density of the water relative to air. This may enable a reduction in material costs, but also savings on installation and Operations & Maintenance (O&M) activities since smaller vessels may be used.
4. The floating or submerged positioning of tidal systems results in a minimal visual disturbance and may even be placed in shipping lanes in some cases if the tidal systems are fully submerged [98].

Figure 1.3 shows the tidal flow velocities near the United Kingdom, generated by a numerical model [81]. The dark red areas group all potential TEC sites – totaling 9500 km2 where water depths exceed 25m and mean spring peak velocities exceed 2m/s.

1.1.3. Cost competitiveness

The most common index for determining the effectiveness and comparing energy sources is the Levelized Cost Of Electricity (LCOE). Lower values of the LCOE lead to cheaper electricity generation costs and are highly preferred. It is defined as follows:

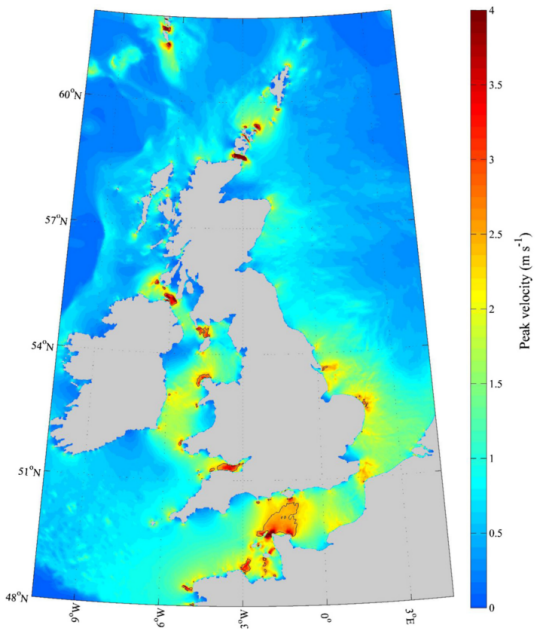

Figure 1.3: Simulated maximum depth-averaged velocities within a sub-section of the northwest European shelf seas

$$LCOE = \frac{\text{sum of discounted costs over lifetime}}{\text{sum of discounted electrical energy produced over lifetime}} = \frac{\sum_{t=1}^{n} \frac{CAPEX_t + OPEX_t}{(1+r)^t}}{\sum_{t=1}^{n} \frac{E_t}{(1+r)^t}} \tag{1.1}$$

The tidal industry is relatively new and so far no optimal design has been found. The current cost of electricity generated by the tidal industry is still significantly higher than other renewable energy sources, as is listed in table 1.1.

Table 1.1: Levelized cost of electricity for different power sources

Source of energy	LCOE [ct/kWh]
Onshore wind	2.9 - 11.4 [78]
Offshore wind	6.7 - 16.9 [78]
Solar PV	3.5 - 18.0 [78]
Tidal stream	23.3 - 34.5 [29]

In order to make the tidal energy systems a viable alternative for existing forms of renewable energy, and thus more cost competitive, it is required to drastically reduce the LCOE. As is stated in equation 1.1, this can be achieved through one or more of the following actions:

- Reduction of capital expenditures (CAPEX), related to design, production and installation activities
- Reduction of the operational expenditures (OPEX), related to O&M and removal activities
- Increase of the produced electricity (E_t)
- Extension of the system's lifetime (n). However, this is usually fixed at 20 years as current site lease contracts only last for that duration.
- Reduction of discount rate (r). This risk driven factor significantly influences the LCOE, but can be accounted for by postponing expenses and bringing income forward in time. Once the Technology Readiness Level (TRL) increases to a commercial level, the discount rate will decrease due to a risk reduction for the investments.

1.2. Cost breakdown and reduction potential of tidal systems

1.2.1. Total cost breakdown of tidal systems

Several studies have been conducted on developing strategies for the reduction of the LCOE. One of such studies [71] has interviewed existing tidal system developers to identify key contributing factors, so appropriate developments can be initiated. Based on these interviews, the breakdown of costs was determined for the existing tidal devices, which can be seen in figure 1.4.

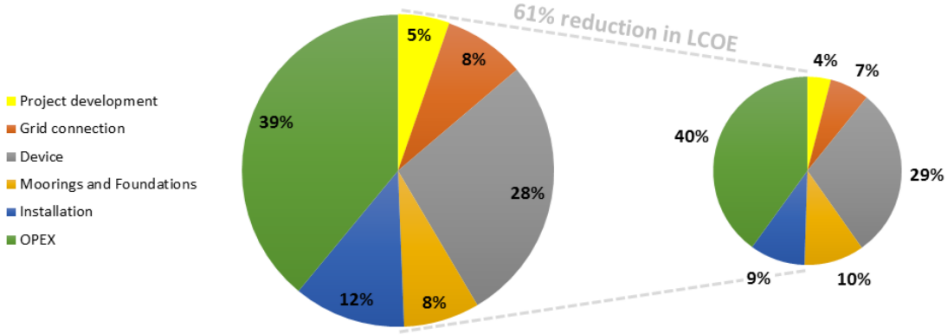

Figure 1.4: Cost breakdown for current stage of development (left) and commercial target (right)

It can be noted that the OPEX covers 39% of the costs for the current stage of development. The commercial target shows that this part remains nearly unchanged, which implies that significant cost savings are required to obtain this result. Based on the interviews it was assumed the overall costs are to be reduced by 61% in order to reach the commercial target. The OPEX is therefore required to reduce with the same factor.

1.2.2. OPEX cost breakdown of offshore wind farms

A reference study on the lifetime costs for large scale offshore wind farms[88] has identified the OPEX cost breakdown, which include the processes listed in figure 1.5a. The operational aspects cannot be easily reduced by technological and policy related measures and are thus more or less dependent on external developments.

On the other hand, the maintenance related aspects are fully based on the selected maintenance strategy and corresponding policy, which is the responsibility of the tidal developer. Assuming that the offshore wind farm OPEX breakdown is similar to that of tidal arrays, it can be observed that the maintenance accounts for 43% of the total OPEX costs.

Cost element	Cost		% Contribution
	Total ($\times 10^3$ £)	Per MW installed (£/MW)	OPEX
O&M			
C_{rent}	1,947.5	3,895	2.5%
$C_{O\&M\text{-}ins}$	7,280	14,560	9.2%
$C_{transmission}$	35,895	71,790	45.3%
$C_{M\text{-}indirect}$	5,033.7	10,067	6.3%
C_{ProM}	15,690.6	31,381	19.8%
C_{CM}	13,394.7	26,789	16.9%
$C_{O\&M}$	79,241.5	158,483	100%

(a) OPEX cost breakdown of offshore wind reference study

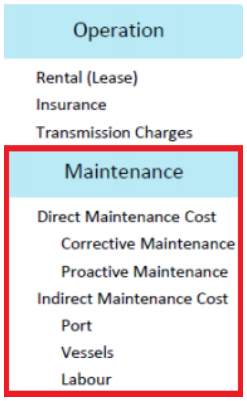

(b) Included processes in the OPEX

Figure 1.5: Cost breakdown for large scale offshore wind farms

The executing of maintenance of tidal arrays thus accounts for almost 17% of the total cost breakdown. Whilst

these costs can never be reduced to zero, it is relatively easy to perform a maintenance optimization by means of a maintenance decision model. Application of the identified optimal maintenance policy can then result in direct cost savings, which show to be significant in the total cost breakdown. It is therefore decided to focus on reducing the maintenance costs by means of a maintenance optimization.

1.3. Maintenance management

Maintenance [19] is formally defined as the combination of all technical, administrative and managerial actions during the life cycle of an item intended to retain it in, or restore it to, a state in which it can perform the required function (function or a combination of functions of an item which are considered necessary to provide a given service).

Besides the operational aspects, much attention is paid to the management of maintenance. Maintenance management embodies all processes answering the question of what activities should be done when, by whom and with what intention. The management of maintenance can be split into two main processes [22], the definition of the strategy and the implementation of the strategy, often referred to as the maintenance policy.

1.3.1. Strategy definition

Maintenance management starts with the definition of the maintenance strategy. The strategy can be composed by first identifying the overall maintenance objectives and applying the right maintenance strategy on the system (comparable to validation). The effectiveness of the maintenance strategy is valued based on the correctness of the process and to what extend the system objectives are met during its lifetime [22]. This enables to find an optimal strategy in this phase which allows to minimize the maintenance indirect costs [105], such as loss of production.

1.3.2. Policy optimization

After having defined the maintenance strategy, the implementation of the strategy is what is most important (comparable to verification). In this stage the key objective is to ensure optimization of the policy, referring to the formal set of rules that describe the performance of the maintenance activities within the predefined boundaries of the strategy. It describes how well the task is being performed, not whether the task itself is correct. Efficiency is then understood as providing the same or better maintenance for the same cost [22].

1.4. Uncertainties in maintenance of tidal arrays

Uncertainty can be considered in two categories, aleatory and epistemic [62]. Aleatory uncertainty can be considered as uncertainty arising from inherently probabilistic systems, such as the environmental conditions at the tidal site. The epistemic uncertainty compromise elements that are unknown but have the ability to be, such as the effect of a new vessel operator, who may deviate from the predefined policy. In this research only the aleatory uncertainty is included, as this is most significant and does not require actual insights in the discrepancies of the maintenance execution.

For determining the optimal maintenance of a tidal array the aleatory uncertainties need to be included which affect the system's performance. For tidal systems two main uncertainties can be identified, namely the environmental influences which affect the weather windows and the limited operational data.

1.4.1. Weather windows uncertainty

Tidal array locations are characterized by fast flowing currents, together with wind and waves. These three environmental phenomena pose a direct limitation to the operability of the maintenance vessel, since waiting for a weather window may take longer than initially expected.

The wind and wave influence on weather window uncertainty is a well-known problem and has been extensively studied for the installation and maintenance activities of offshore wind farms [51, 62, 92]. Probabilistic

models have been developed which include the weather window uncertainty and its effect on the total maintenance costs and optimal policy.

For tidal array locations the fast flowing currents add more complexity to the model, as this is a severe limitation for performing maintenance activities. Dynamic positioning capabilities of the maintenance vessel are generally not sufficient to effectively perform station-keeping during an activity. The recurring character of the tidal current further reduces the possibility of extended weather windows, so the combination of the tidal current limitations and those of the wind and waves is one to be analyzed extensively.

Since tidal energy is relatively new with respect to offshore wind technology, and has a considerable lower number of deployed systems, less research has been conducted on the unique environmental conditions at tidal locations. In order to effectively include the uncertainty due to the waves, wind and currents, it is thus first required to gain insights in the physical interactions. This thesis will contribute to this cause by analyzing the multivariate dependence between the currents, waves and wind, so it can be included in the developed model.

1.4.2. Limited data and experience

A recurring theme from the previously mentioned interviews with tidal developers is that the operating costs are uncertain because of the early stage of technology development [93]. Some device developers can now point to data of prototype operation for significant periods but for others lack of experience of long term operation means that there is uncertainty about the frequency and cost of maintenance interventions.

Only very limited measurement data is available, which further complicates the process of gaining insight in the weather window uncertainty. Additionally, no failure related data of the tidal components is available, which requires current maintenance models to be run with data from reference studies, such as available data from the offshore wind industry. This research attempts to give realistic values for both the equipment failures and product costs, which may be a first step in quantifying these properties for tidal energy systems.

1.5. Necessity for a probabilistic maintenance model

The mentioned uncertainties form the foundation of this research, together with the implementation of a maintenance model which allows the tidal array to be described in such detail. Existing analytical maintenance models [6, 73, 77] require numerous assumptions and simplifications to be made when describing the equipment failures and maintenance activities. In addition to the already required assumptions due to the data limitations, it is therefore desired not to apply further simplifications on the system which further decrease the degree of realism.

It is therefore decided that an alternative maintenance decision model is to be developed, which is able to realistically represent the tidal array, the failures and the maintenance activities. A probabilistic approach is applied to include the weather window uncertainty to support the decision making for selecting an optimal maintenance policy. Chapter 3 describes the selected maintenance decision model and its characteristics in more detail.

1.6. The Damen solution

1.6.1. Novel tidal system design

Damen Shipyards is developing a novel tidal system design which aims to bring the LCOE down to a level which is more in line with the existing renewable systems. Contrary to the majority of existing tidal systems, the product of Damen will focus on accomplishing significant cost reductions of the total system by an integral design approach, instead of marginally improving the efficiency of the system's individual assemblies. The current top level tidal system design of Damen will be explained more in detail in chapter 5.

1.6.2. Maintenance management implementation

In terms of maintenance strategies, it is desirable to avoid corrective maintenance as much as possible by planning preventive maintenance activities [22]. However, for TEC arrays the optimal approach for maintenance activities may deviate from this widely accepted view due to the previously mentioned uncertainties. These uncertainties may influence the preventive strategies more due to their complexity and increased dependence on the correctness of the inputs of decision making processes.

Also, in this early stage of development, it is more desirable for Damen to obtain extensive insight in the characteristics of a more conservative strategy, which is less sensitive to the uncertainties, and consider the corresponding optimal policy as a realistic upper bound. Alternative strategies may still be analyzed at a later stage if the initial results are promising.

Therefore, the maintenance strategy which is implemented by Damen is a corrective group maintenance strategy. The application and optimization of this strategy will be the center piece of this research.

Definition of the corrective group maintenance strategy

The developed maintenance strategy is strictly corrective and thus only initiates maintenance upon a failure in the tidal array. The failure modes which are part of this research are described in subsection 5.4.1 and only include the main assemblies that are related to the electricity producing functions.

The extension to a group based corrective strategy implies that an economical dependence between the failures and maintenance activity is present. This dependence can be exploited to reduce the maintenance costs, as can be read in section 3.1. Due to set-up costs, which are independent of the number of failed TECs, the costs of performing maintenance on multiple TECs differs from maintaining the same quantity individually.

Policy optimization

For the effective implementation of the group based maintenance strategy it is essential to find the optimal moment of maintenance and define how many TECs should be replaced when maintenance is initiated. The break-even point should be found to economically optimize the maintenance, as is depicted in figure 1.6. The tidal array may be left to deteriorate, since performing maintenance as that moment is not economically optimal. If so, the failed TEC(s) will be unable to produce electricity, introducing downtime costs. At some moment, when more TECs have failed, the decision may be to perform maintenance and replace one or multiple TECs. The tasks and phases of the maintenance operation will be extensively explained in chapter 6. The developed model will assist with the decision making by producing the optimal decision for every single identified failure combination within the array.

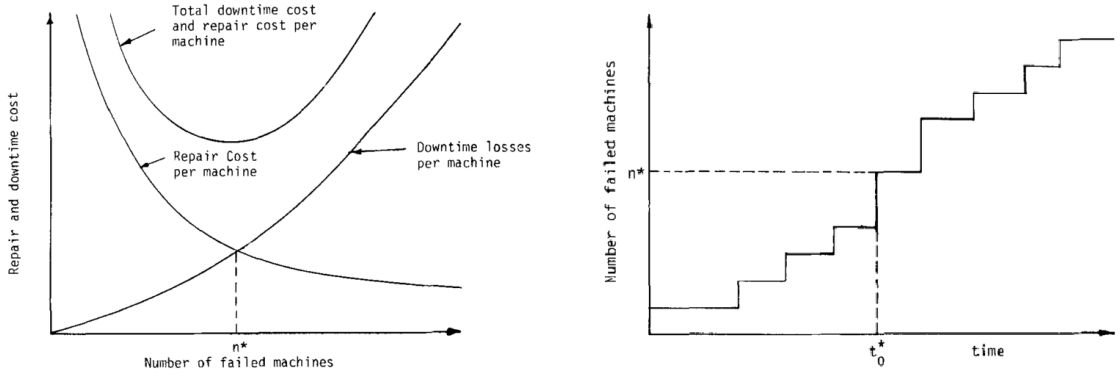

(a) Maintenance cost curve

(b) Moment of optimal maintenance

Figure 1.6: Maintenance optimization

1.7. Purpose statement

Studies and early array projects have shown that the recent developments of tidal energy converters can significantly contribute in generating energy at fast flowing locations. This transition to renewable energy production may well have a noticeable impact on the environment by replacing the current conventional energy sources. However, in order to achieve this, the LCOE of the tidal systems is required to reduce to a comparable level of the alternative (renewable) energy sources for cost competitiveness. So far no single aspect of the system has been identified which can solely account for the desired cost reduction, so it can only be achieved by an integral approach of both technological innovations and operational optimization [7].

Recent interviews with TEC developers gave insight in the current LCOE breakdown, which stated that O&M related activities are the most dominant contributors and account for 39% [71] of the total LCOE. This is a noticeably higher share than that of comparable energy sources, such as the offshore wind, and can be explained by a number of internal and external factors. Firstly, the (semi-)submerged positioning of the TECs renders the devices difficult to access and often requires the use of specialized vessels. Additionally, the operability of maintenance vessels may be severely limited by the combination of wind and waves, but especially fast tidal flows, which characterize the high potential tidal locations. Furthermore, since the tidal industry is still in its development phase only limited long-term operational experience and data on component failure rates is available. The current lack of insight in failure properties makes it hard to develop an efficient maintenance policy to minimize the overall costs.

The early stage of development of the tidal industry also brings the challenge that no convergence to an optimal design has been identified yet. Tidal developers each have their own focus points of development, which results in a large variation of TEC designs. Whilst the continuation of the search for optimal designs is desirable, the learning rate of the individual developers is mostly limited to the findings of their own specific system performances. The design methodologies for TECs [68] is therefor still mostly orientated at (technical) feasibility, after which an appropriate, but most probably sub-optimal, maintenance policy is fitted, resulting in higher overall costs.

For an effective reduction of the LCOE it is therefore required to improve the existing design methodology by integrating the maintenance strategy definition and the optimization of its policy at an early stage in the TEC development. The implementation of this methodology into a computer model is highly desirable to formalize the economic optimization of the maintenance policy and identify the influence of the uncertainties on the maintenance costs.

The purpose of this study is twofold. First, this study will assess how the governing environmental conditions can be effectively characterized and implemented in a model to describe its effect on the uncertainty of maintenance. Secondly, the failure and maintenance characteristics of the tidal array will be formalized into a decision support tool. This decision support tool is both used to identify an optimal maintenance policy, but also to provide insight in the effect of the various uncertainties on both the proposed policy and its corresponding maintenance cost.

The decision support tool described in this study is developed in collaboration with Damen Shipyards and a case study will be performed to economically optimize the maintenance policy of the existing top level TEC design and provide insight. An extensive analysis will be performed which determines the added value of this decision support tool by evaluating the recommended maintenance policy and comparing this to that of other maintenance models.

1.8. Research objectives

The research objective of this study is to increase the understanding of the maintenance uncertainty of tidal arrays due to the environmental influences and include this uncertainty in the optimization of the maintenance policy. This will be achieved by developing a decision support tool which captures all significant internal and external system characteristics.

1.9. Research questions

The research questions of this thesis are:

RQ 1 How can the environmental effects at tidal hotspots be realistically modeled?
- (a) Can dependence between the variables be identified and explained?
- (b) What model is best used to generate time series which includes multivariate dependence?

RQ 2 How can the uncertainty in the maintenance activities of the TEC array be included in the model?

RQ 3 How can the resulting optimal maintenance strategy influence the decision making?
- (a) How does this model relate to other generic analytic group based maintenance models?
- (b) What are the main sensitivities that affect the total maintenance cost?

1.10. Research methodology

The research methodology which is applied consists out of the following consecutive steps:

Step 1 Perform a literature study
- **1.1** Simulation of realistic environmental time series
- **1.2** Description of component failures
- **1.3** Developing a decision model framework

Step 2 Identify the main contributions of the maintenance process
- **2.1** Tidal system properties
- **2.2** Maintenance vessel properties
- **2.3** Analysis of environmental measurement data

Step 3 Develop the decision support tool which can optimize maintenance policies

Step 4 Perform a case study with Damen's tidal system design to obtain insight in the system characteristics and sensitivities

1.11. Outline

To facilitate the reading of this research, three parts are introduced which each consist out of multiple chapters to structure the different topics. The outline of this thesis is depicted below in figure 1.7. The main chapter interactions have also been included to give more insight in the overall realization of this research.

Chapter two, three and four provide the theoretical background which will be applied to answer the research questions and develop the decision support tool.

Chapter five and six describe the tidal system and the selected maintenance strategy, which will serve as the model's base case. By means of reference studies and assumptions, the relevant system parameters will be presented that are implemented in the model.

Chapter seven presents the model framework and gives an overview of the related main processes and model assumptions of the developed model.

Chapter eight answers *research question 1*. First environmental measurement data is analyzed to answer *subquestion 1a*. Secondly, the development of a new method for generating time series which includes dependence is extensively described. This method provides an answer to *subquestion 1b*.

Chapter nine describes the development of the policy optimization model by combining the results from various chapters. An extensive description of the model characteristics are presented to answer *research question 2*.

Chapter ten contains the results of the base case simulation. The optimal policy and corresponding costs will be identified and insight will be provided in the results and the model sensitivities to answer *research question 3*.

Chapter eleven gathers all the conclusions from the individual chapters and presents the main findings of this research. Also, recommendations are given for further research.

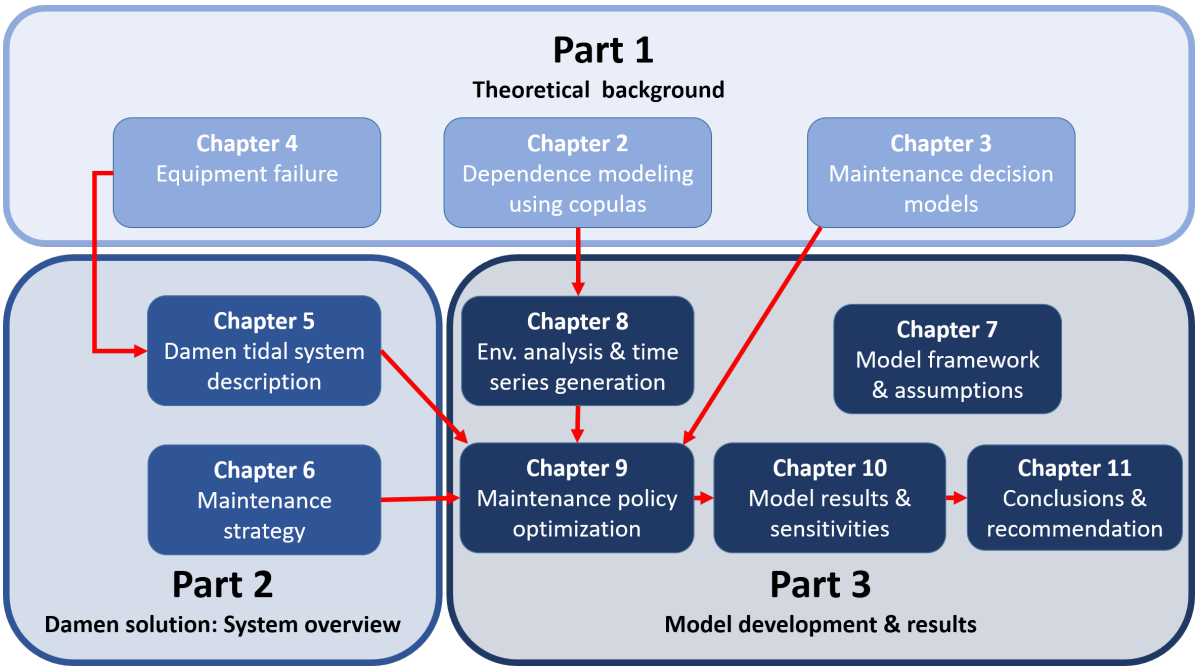

Figure 1.7: Flowchart of this thesis' topics and the chapter relations

Part I

Theoretical background

2

Multivariate dependence modeling using copulas

During the operational period of the tidal array, it is subjected to a number of environmental phenomena, of which the most governing are waves, wind and tidal currents. The combination of these phenomena describe sea states which pose the limiting factor for a vessel's workability when performing maintenance activities. Also, the electricity produced by the TECs is directly related to the tidal velocity profile. In order to develop the model for finding an optimal maintenance policy, it is thus required to obtain insight in the environmental variables and their dependencies to generate reliable and realistic samples.

The environmental variables which are included in this research are:

- Wave height *[m]*
- Wave period *[s]*
- Wind speed *[m/s]*
- (Horizontal) current speed *[m/s]*

Multiple approaches may be used to represent the environmental conditions, such as creating a numerical model for the location of interest, as has been performed at the EMEC tidal testing site [55]. Developing such numerical model requires accurate information for determining the boundary conditions and is computationally heavy to run simulations, so reducing the complexity of the problem is preferred. This can be achieved by evaluating measurement data and applying a probabilistic analysis for a statistical representation. This method exclusively relies on the availability of measurement data and is relatively easy, though versatile, to implement.

Because of this it is decided to describe and simulate the occurring environmental conditions of the tidal location by means of a stochastic approach. It includes the use of copulas for describing the dependence between variables and generating weather time series with identical statistical characteristics for running the maintenance model simulations. Previous studies on the application of copulas for describing sea states have described the dependence between the wind and waves [57, 65], but the inclusion of the tidal velocity has not yet been performed.

This chapter commences with an introduction to variable dependence, describing what copulas are and giving arguments why copulas are the preferred method for describing dependence. Also, the methods are introduced to identify and model the multivariate dependence. Lastly, the approach and data requirements for simulating samples which contain this multivariate dependence are explained.

One of these data requirements for simulating samples cannot be met with the current environmental dataset, which is why an extension of the current simulation methods has been developed to still enable the simulation of synthetic time series. This extension will be extensively described in section 8.3, but the corresponding requirement and research gap is already introduced in this chapter, in section 2.7.

2.1. Introduction to dependence

2.1.1. Common methods for describing dependence

Various methods and models are available for describing the dependence between distributions and variables. Three of the most commonly used types for describing the correlation between two variables are the Pearson Correlation Coefficient, Kendall's Tau and Spearmans's rho [108]. The Pearson correlation coefficient describes linear correlation whereas the latter two resemble rank correlation methods. The characteristics and notations of all three types are listed in appendix A.1.

Whilst each of above mentioned types can provide valuable information regarding the relations between variables, none of them is able to model full dependence, i.e. dependence structure and tail behavior, due to only describing monotone dependence. It is exactly these properties which are interesting when interpreting and sampling the interaction between sea state related physical phenomena.

2.1.2. Tail dependence

Definition

The tail dependence of a bivariate distribution is a measure of the dependence in the upper-right- and lower-left-quadrant of the distribution. The definition is divided into two parts, one for upper and one for lower [25].

Tail dependence in a bivariate distribution can be represented by the probability that the first variable exceeds its q-quantile, given that the other exceeds its own q-quantile. The limiting probability, as q goes to infinity, is called the upper-tail dependence coefficient [89], and a copula is said to be upper-tail dependent if this limit is not zero.

Tail dependence between environmental variables

Tail dependence properties are particularly important in many applications that rely on non-normal multivariate families [45], which is often the case when observing the interaction between sea state related physical phenomena [5, 50, 57, 65]. The upper tail dependence during extreme weather cases, such as fast winds which induce high waves, are especially of interest for determining the potential working window of the maintenance vessel and is perfectly captured in the tail dependence property.

Since the tidal array location will also be subjected to fast flowing currents, the possible tail dependence between the current velocity and wave properties could also contribute significantly. Studies have been performed on the interaction between current-wave interactions [109], but little is known for the unique circumstances of the tidal arrays. The sheltered location with extremely high currents may well give different interactions. Therefore, there is a necessity for a more advanced and comprehensive method for describing the tail dependence between distributions.

Describing tail dependence using copulas

As will be described in section 2.2, the use of copulas accounts for all this and is the preferred method for describing dependence. It should be noted that throughout this report the Kendall's Tau will be used regularly, since this correlation coefficient is closely related to the copula theory. This will be further elaborated on later in the report. The equation for determining the Kendall's Tau value is listed in appendix A.1.3.

2.2. Copulas

Copulas are functions that couple multivariate distribution functions to their one-dimensional marginal distributions. These marginal distributions are uniformly distributed in the range of [0,1] [69]. The use of copulas enables studying the dependence structure of multivariate distributions by means of decoupling the marginal properties of the random variables and the dependence structures. The first publication on copulas was by Sklar [90] in 1959, who developed a theorem which still remains essential for defining copulas. The

name 'copula' was chosen to emphasize the manner in which a copula 'couples' a joint distribution function to its univariate margins.

2.2.1. Bivariate copula properties

Sklar's theorem

Theorem (**Sklar's theorem**). *Let H be a joint distribution function with margins F and G. Then there exists a copula C such that for all x,y in* $\bar{R}$,

$$H(x,y) = C(F(x),G(y)) \tag{2.1}$$

If F and G are continuous, then C is unique; otherwise, C is uniquely determined on RanF & RanG. Conversely, if C is a copula and F and G are distribution functions, then the function H defined by 2.1 is a joint distribution function with margins F and G.

Fréchet-Hoeffding bounds

In this section the existence of a maximal and a minimal bivariate copula is shown, usually referred to as the Fréchet-Hoeffding bounds. All other copulas take values in between these bounds on each point of their domain, the unit square. The Frechet upper bound corresponds to perfect positive dependence and the lower bound to perfect negative dependence. For bivariate copulas, the Fréchet-Hoeffding states that the cumulative distribution function of the copula is bounded by the equation below.

$$max(u+v-1,0) \leq C(u,v) \leq min(u,v) \tag{2.2}$$

The upper and lower bounds have been visualized in figure 2.1.

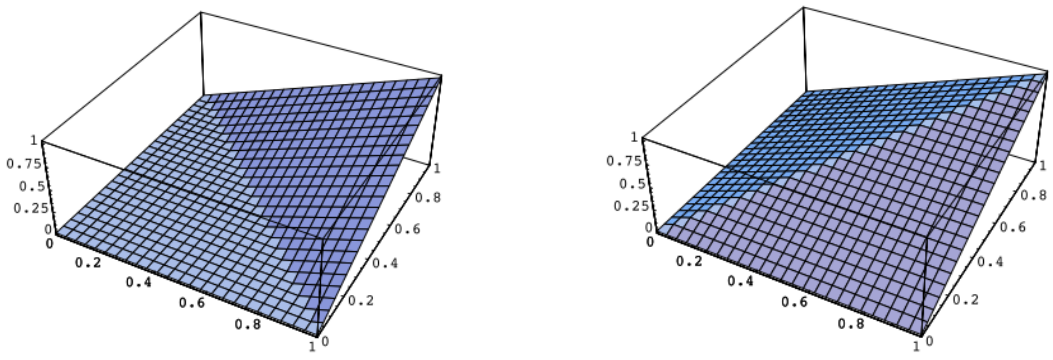

(a) Fréchet-Hoeffing lower bound (b) Fréchet-Hoeffing upper bound

Figure 2.1: Fréchet-Hoeffing bounds

Survival and rotated copulas

Every bivariate copula has a survival copula associated with it that gives the probability of two random variables both to exceed a certain value.

The survival copula $\bar{C}(u,v)$ associated with the copula $C(u,v)$ is

$$\bar{C}(u,v) = u+v-1+C(1-u,1-v) \tag{2.3}$$

The purpose of a survival copula may not seem evident at first, but when looking at the graphical representation it can be observed that the survival copula is in fact the 180 degrees rotated copula. By including survival copulas dependence may be defined more efficiently without implementing more copula families.

Similarly, rotation by 90 and 270 degrees is also possible for most bivariate copulas and further extend the possibilities of also describing negative dependence with the initial set of copulas. An example of the Clayton copula, described in paragraph 2.2.2, is shown below in figure 2.2 together with the rotated and survival variant.

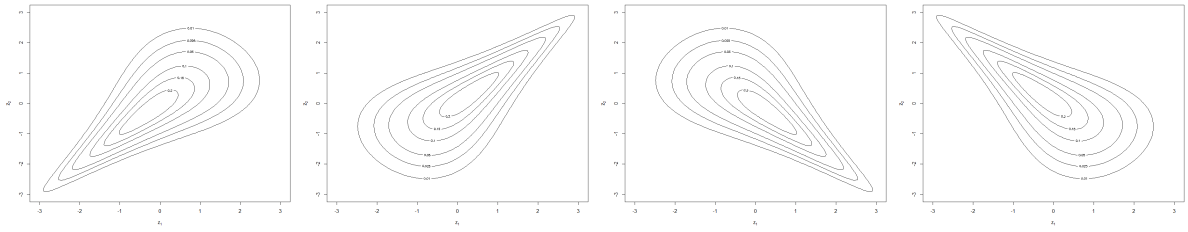

(a) Clayton copula (original) (b) Survival Clayton copula (180 deg) (c) Rotated Clayton copula (90 deg) (d) Rotated Clayton copula (270 deg)

Figure 2.2: Original, survival and rotated copula variants

2.2.2. Popular bivariate copula families

Many copula families have been developed, each with their own distinct characteristics to effective describe dependence, either bivariate or in some cases multivariate. Some main properties can be identified which clearly distinct themselves from one another. The copulas can either describe have one or two parameters, and may or may not have a degree of tail dependence and skewness.

Whilst it is possible to use a single copula for describing multivariate dependence, the application of (sets of) bivariate copulas is often preferred due to its ease of implementation. For this reason, only the properties of bivariate copulas are explained in the upcoming paragraphs. Additional arguments for this choice are mentioned in 2.4.

Archimedean copula family

Archimedean copulas are very popular because they can be described in a closed form and only have one parameter to determine the strength of dependence. Three of the most well known Archimedean copulas are the Clayton, Frank and Gumbel copulas. Due to their different properties regarding tail dependence, as will be explained in subsection 2.2.3, these three Archimedean copulas are included in the analysis of chapter 8.

The equations for cumulative distribution functions are given below.

Clayton copula

$$C_\theta(u,v) = [max\{u^{-\theta} + v^{-\theta} - 1; 0\}]^{-1/\theta} \tag{2.4}$$

$$\theta \in [-1,\infty) \setminus \{0\} \tag{2.5}$$

Gumbel copula

$$C_\theta(u,v) = exp\left[-((-log(u))^\theta + (-log(v))^\theta)^{1/\theta}\right] \tag{2.6}$$

$$\theta \in [-1,\infty) \setminus \{0\} \tag{2.7}$$

Frank copula

$$C_\theta(u,v) = -\frac{1}{\theta} log\left[1 + \frac{(exp(-\theta u) - 1)(exp(-\theta v) - 1)}{exp(-\theta - 1)}\right] \tag{2.8}$$

$$\theta \in \mathbb{R} \setminus \{0\} \tag{2.9}$$

Elliptical copula family

Elliptical distribution families are widely applied in statistics and econometrics, especially in finance [32]. They are so-called implicit copulas because they do not have a simple closed form.

Gaussian copula

There is no simple analytical formula for the Gaussian copula function, but it can be upper or lower bounded, and approximated using numerical integration [15, 16]. The bivariate Gaussian copula is defined as:

$$C_{Ga}(u,v) = \Phi_\rho\left(\Phi^{-1}(u), \Phi^{-1}(v)\right) \tag{2.10}$$

where

$$\Phi_\rho(x,y) = \int_{-\infty}^{x}\int_{-\infty}^{y} \frac{1}{2\pi\sqrt{1-\rho^2}} e^{\frac{2\rho st - s^2 - t^2}{2(1-\rho^2)}}\, ds\, dt \tag{2.11}$$

Gaussian copulas have no tail dependency unless $\rho = 1$.

Student-t copula

Let t_ν denote the central univariate Student-t distribution function, with ν degrees of freedom:

$$t_\nu(x) = \int_{\infty}^{x} \frac{\Gamma((\nu+1)/2)}{\sqrt{\pi\nu}\Gamma(\nu/2)} \left(1 + \frac{s^2}{\nu}\right)^{-\frac{\nu+1}{2}} ds \tag{2.12}$$

where Γ is Euler function and t_ν, $\rho \in [0,1]$, the bivariate distribution corresponding to t_ν:

$$t_\nu(x,y) = \int_{-\infty}^{x}\int_{-\infty}^{y} \frac{1}{2\pi\sqrt{1-\rho^2}} \left(1 + \frac{s^2 + t^2 - 2\rho st}{\nu(1-\rho^2)}\right)^{-\frac{\nu+2}{2}} ds\, dt \tag{2.13}$$

The bivariate Student-t copula $C_{\rho,\nu}$ is defined as

$$C_{\rho,\nu}(u,v) = t_{\rho,\nu}\left(t_\nu^{-1}(u), t_\nu^{-1}(v)\right) \tag{2.14}$$

2.2.3. Tail dependence properties

All of the described bivariate copulas, except for the Frank and Gaussian copulas, have different strength of dependence in the tails of the bivariate distribution. See [46] for an overview of other copulas. The Clayton copula is lower-tail dependent, but not upper. The Gumbel copula is upper-tail dependent, but not lower. The Student copula is both lower- and upper-tail dependent, while the Gaussian and Frank are neither lower- nor upper-tail dependent.

To illustrate the different behaviors of the tails of several copula densities, the contours of the probability density functions corresponding to the copulas cited above are presented in figure 2.3. The parameters are chosen in such way that the associated Kendall's Tau is identical in all figures ($\tau = 0.60$).

Table 2.1: Copula tail dependence properties [64]

Copula	Upper tail dependence	Lower tail dependence
Gumbel	$2-2^{1/\theta}$	0
Clayton	0	$\begin{cases} 2^{1/\theta}, & \text{for } \theta > 0 \\ 0, & \text{for } \theta \leqslant 0 \end{cases}$
Frank	0	0
Gaussian	0	0
Student	$2t_{\nu+1}\left(-\sqrt{\frac{(\nu+1)(1-\rho)}{(1+\rho)}}\right)$	$2t_{\nu+1}\left(-\sqrt{\frac{(\nu+1)(1-\rho)}{(1+\rho)}}\right)$

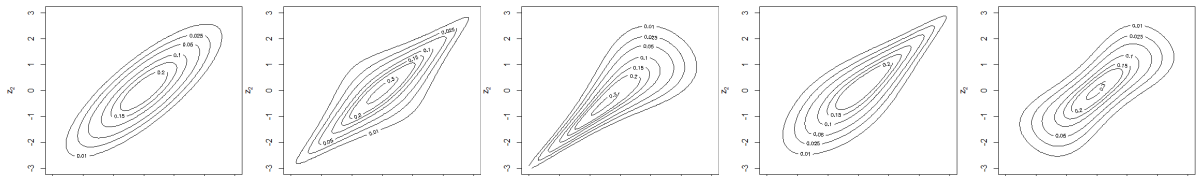

(a) Gaussian copula (b) Student-t copula (c) Clayton copula (d) Gumbel copula (e) Frank copula

Figure 2.3: Contour plots of copulas with standard normal marginals ($\tau = 0.60$)

2.3. Fitting a copula to bivariate data

Having identified which bivariate copulas are included in this research, the next step is to describe the method for fitting a copula to bivariate data. The bivariate data in this research may be any combination between the four identified environmental variables and each have their own best fitting copula (and corresponding copula parameter). Having found a good fit, the copula can then be used to represent the bivariate dependence for further analysis and simulation purposes.

To fit a copula to data three steps are to be performed:

Step 1 Build the empirical copula
Step 2 Determine the optimal copula parameter for the included copula families
Step 3 Compare the copulas and select the best fit

2.3.1. Build the empirical copula

Conversion to pseudo-observations

Converting the original data to pseudo-observations enables to find an estimate of the margins, as these will change to an uniform distribution. This is achieved by using the ranks of the samples, which is defined as follows

$$\hat{U}_{ij} = \frac{R_{ij}}{n+1} \tag{2.15}$$

where n is the number of observations and the R_{ij} can be determined by using the expression for Kendall's Tau, shown in appendix A.1.3.

The asymptotically negligible scaling factor of $(n+1)$ instead of n is used to force the variates to fall inside the open unit hypercube, $[0,1]^d$, to avoid problems with density evaluation at the boundaries [67].

Calculating the empirical copula

Once the pseudo-observations are known of the marginal distributions, the empirical copula can be calculated as follows

$$\tilde{C}(u) = \frac{1}{n+1} \sum_{j=1}^{n} I\left(Z_{j1} \leq u_1, \ldots, Z_{jd} \leq u_d\right) \tag{2.16}$$

2.3.2. Determine the optimal copula parameter

Method-of-Moments using rank correlation

A straight forward method for estimating the copula parameter, θ, without knowing the marginal distribution is by using Kendall's tau [46, 67]. This method takes advantage of the property that many copulas have a one-to-one correspondence between their parameter and Tau. Table 2.2 shows the relation between the two.

Table 2.2: Relations between θ and τ

Copula	Kendall's tau	Parameter range
Gaussian	$sin(\tau \frac{/pi}{2})$	$-1 < \theta < 1$
Student-t	$sin(\tau \frac{/pi}{2})$	$-1 < \theta < 1$
Clayton	$2\frac{\tau}{1-\tau}$	$0 < \theta$
Gumbel	$\frac{1}{1-\tau}$	$1 \leq \theta$
Frank	$1 - 4\theta^{-1}(1 - D_1(\theta))$	$\theta \in \mathbb{R}$

$D_1(\theta) = \theta^{-1} \int_0^\theta \frac{t}{e^t - 1} \mathrm{dt}$

It must be stated that the Kendall's Tau is only directly related to the first copula parameter. In this research this only poses a problem for the Student-t copula, which also has a second parameter. Also, the expression for the Frank copula parameter does not have a closed form, which makes the one-to-one correspondence ineffective to use. To still be able to fit the Frank and Student-t copula on bivariate data, a second approach is introduced which uses the Maximum Likelihood Estimation (MLE) and is can be applied to all copulas.

Maximum Likelihood Estimation

An alternative for fitting the best copula parameter is calculating the MLE between the empirical copula, created from the bivariate dataset, and the theoretical copula. An essential step in calculating the MLE is converting the data to pseudo-observations [64]. This approach uses a numerical maximization, such as gradients or finite differences to find the best fit. Several software packages [85, 96] are readily available to perform these calculations and make this a very effective method for finding the optimal fit.

In this research the model uses the MLE approach, but afterwards the results were verified by comparing them to the found values of the one-to-one relation between Kendall's Tau and the copula parameter.

2.3.3. Selecting the best fitting copula

After the parameter of each of the copulas has been identified, the best fitting copula must be identified. The best fitting copula can be selected according to the Akaike Information Criteria (AIC) [3] and Bayesian Information Criteria (BIC) [87]. The criteria are computed for all available copula families (e.g., if u and v are negatively dependent, Clayton and Gumbel and their survival copulas are not considered) and the family with the minimum value is chosen. For observations u_i, i = 1, ..., N, the AIC of a bivariate copula family c with parameter(s) θ is defined as

$$AIC = -2 \sum_{i=1}^{N} ln\left(c(u_i, v_i|\theta) + 2k\right. \tag{2.17}$$

where k = 1 for one parameter copulas and k = 2 for the two parameter Student-t copula. Similarly, the BIC is given by

$$BIC = -2\sum_{i=1}^{N} ln\left(c(u_i, v_i|\theta) + ln(N)k\right) \tag{2.18}$$

Evidently, if the BIC is chosen, the penalty for two parameter families is stronger than when using the AIC.

2.4. Copula constructions for describing multivariate dependence

There are multiple copula construction methods to describe multivariate dependence, each having different properties and limitations with respect to the ease of implementation and desired complexity of modeling the dependence. Indepth studies on copula dependence modeling [1, 47] have compared the set of available copula construction methods and listed some desirable properties and limitations, which are listed in appendix A.2. The six identified methods can be placed into two distinct groups, constructions which are described by multivariate copulas and those which can also fully describe the overall dependence by using bivariate copulas.

2.4.1. Pair Copula Constructions

This latter group, consisting of the nested Archimedean copulas (NACs) and pair-copula constructions (PCCs), is highly preferred and can model multivariate data sets by using a cascade of lower-dimensional bivariate copulas. Visual representations of both types of constructions are depicted in figure 2.4 to give better understanding in what the copula constructions look like and the differences between the two constructions.

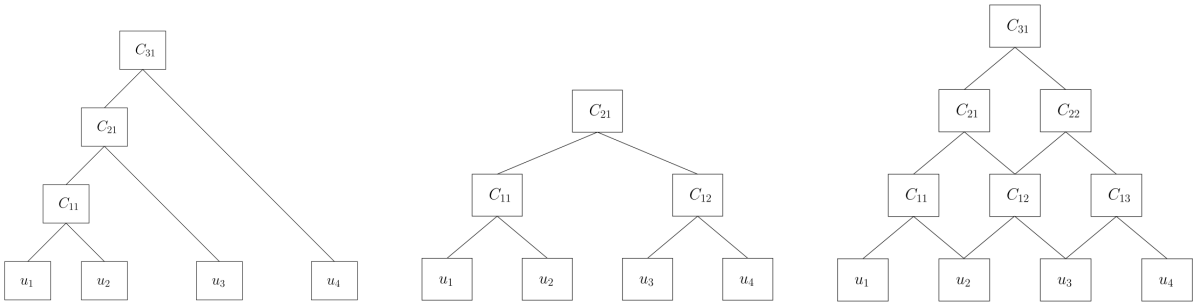

(a) Fully nested Archimedean construction (d=4)

(b) Partially nested Archimedean construction (d=4)

(c) Pair copula construction (d=4)

Figure 2.4: Model structures for construction of multivariate dependence

For the objectives of this research, namely the interpretation and sampling of the four environmental variables, the preferred option is to describe the multivariate dependence by means of a PCC. This is due to three main advantages of PCCs with respect to NACs [1].

- Since only bivariate copulas are involved in a PCC, the partial derivatives of may be obtained relatively easily for most parametric copula families.
- The copulas involved in a PCC do not have to belong to the same family. In contrast to the NAC they do not even have to belong to the same class.
- The simulation procedure for the PCC is in general much simpler and faster than for the NAC.

Initially Joe [45] gave a probabilistic construction of multivariate distributions functions based on simple building blocks called pair-copulas. Bedford and Cooke [10, 11] organized these constructions in a graphical way called regular vines.

2.4.2. Vine copula representation

The concept of vines are used to model a multivariate data set through pair-copula construction in a satisfactory fashion. Vines serve as an aid to take advantage of information known in advance (about the dependency structure), before dividing a multivariate distribution function into bivariate copulas and univariate distribution functions.

Within this research the two main vine types are included, namely the Canonical vine and the D-vine. Both vines have their own distinct construction, as is shown in figure 2.5. The details and arguments for selecting either of the vines is explained in the upcoming paragraphs, but first the notation and interpretation of the vine structure is explained.

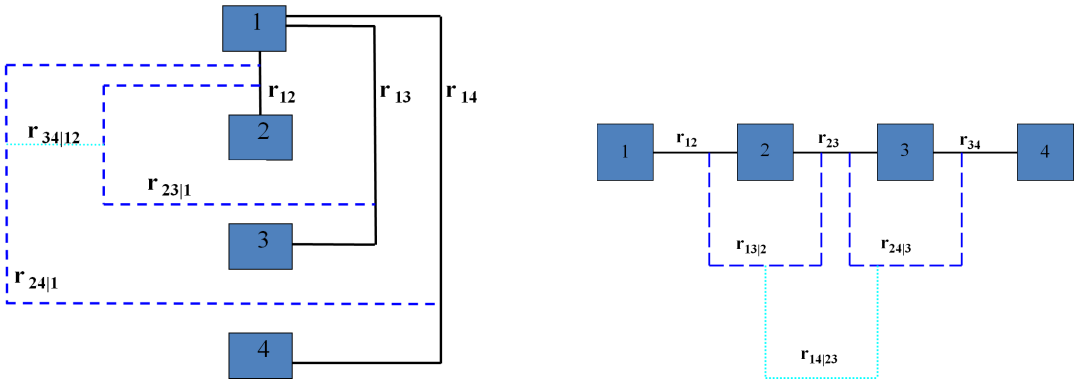

(a) Canonical vine (b) D Vine

Figure 2.5: Four parameter D- and Canonical vines

Interpretation of the vine components

Within any vine, the following components can be identified[2]:

Trees The trees denote the level in the vine. The vine is built from its base level up to its top node, after which the multivariate dependence is full described by the vine.

Nodes The nodes represent the univariate data in the vine. At the base level these represent the actual input data, but higher level nodes describe the derived data by applying the 'h-function'. This will be explained in subsection 2.4.3.

Edges Each edge corresponds to a pair-copula density and the edge label corresponds to the subscript of the pair-copula density.

The four-dimensional ($n = 4$) vines in figure 2.5 consist of three trees T_j , $j = 1,2,3$. Tree T_j has $6-j$ nodes and $5-j$ edges. The whole decomposition is defined by the $n(n-1)/2$ edges and the marginal densities of each variable.

The nodes in tree T_j are only necessary for determining the labels of the edges in tree T_{j+1}. As can be seen, two edges in T_j , which become nodes in T_{j+1}, are joined by an edge in T_{j+1} only if these edges in T_j share a common node.

Vine selection

As stated before, each vine type has its own advantages. Fitting a Canonical vine might be advantageous when a particular variable is known to be a key variable that governs interactions in the data set. In such a situation one may decide to locate this variable at the root of the canonical vine, as is done with variate 1 in figure 2.5. The D-vine is mostly preferred if no key variable can be identified in the data and the bivariate combinations have a more or less equal level of dependence.

In chapter 8 the analysis is performed to select the best fitting vine. The analysis shows that the multivariate dependence of the environmental data is best represented by the D-vine, due to the absence of a key variable. More on this analysis can be read in subsection 8.2.2.

Bedford and Cooke [10] give the density of an n-dimensional distribution for a D-vine (and the C-vine), which has been described in appendix A.4.

2.4.3. The h-function

An expression for $cu, v_j|v_{-j}$'s arguments, $F_{u|v-j}$ and $_{Fv_j|v_{-j}}$ is found in [67] . In [45] the following relation is derived (under certain regularity conditions) and given that v is univariate,

$$F_{u|v} = \frac{\partial C_{u,v}}{\partial F_v} \tag{2.19}$$

and when u and v are uniform, this is defined as the h-function [2].

$$h(u,v,\theta) = F_{u|v} = \frac{\partial C_{u,v}(ux,v,\theta)}{\partial v} \tag{2.20}$$

In equation 2.20, θ is the set of parameters for the current copula, and the second parameter of h() is the conditioning variable. The inverse of the h-function is defined as $h{-}1(u,v,\theta) = F^{-1}_{u|v}$, which is as the inverse of $h(u,v,\theta)$ with respect to u. The inverse h-function is required when simulating from a vine construction.

2.5. Building a vine copula

First one has to choose which variables to join at the first level of the vine. Then the variables that have the highest rank correlation, expressed in the Kendall Tau, are joined together. Having chosen the order of the variables at the first level, one has also determined which factorisation to use. Given data and the chosen factorisation, one must then specify the parametric shape of each pair-copula involved. The parametric shapes may for instance be determined using the following procedure [2]:

Step 1 Determine which copula families to use at level 1 by plotting the observations, and/or applying a Goodness-of-Fit (GoF) test (AIC or BIC).
Step 2 Estimate the parameters of the selected copulas.
Step 3 Determine the observations required for level 2 as the partial derivatives of the copulas from level 1.
Step 4 Determine which copula families to use at level 2 in the same way as at level 1.
Step .. Repeat step 1-3 for all levels of the construction.

2.6. Vine copula simulation

Once the vine has been constructed and all copula families and their respective parameters has been selected, using the procedure from section 2.5, it is possible to simulate new samples. This simulation method is applied to generate synthetic time series which are based on the original environmental measurement data.

The algorithm for the D-vine is available in appendix A.5.1. In addition figure 2.6 visualizes a single simulation loop of a D-vine with 4 variables (d=4), producing four variates, including the multivariate dependence which was described by the PCCs. In the description of the simulation procedure the nodes are labeled as $v(i,j)$. Only the relevant nodes are depicted in figure 2.6, but appendix A.5.2 can be consulted for a full overview of the node labels, which are also required in the formal algorithms.

The steps which are taken per simulation loop are as follows:

1. Generate four random numbers from an uniform distribution, $w_1, \ldots, w_4$
2. Calculate U_1
   a Start from the bottom-left and let $U_1 = w_1$
3. Calculate U_2
   a Again, start from the bottom-left and use plug in U_1 and w_2 into the inverse h-function of $C(1,1)$ to calculate U_2

4. Calculate U_3
   a Plug in U_1 and U_2 into the h-function to calculate the conditional distribution $v(2,2)$ at the second tree
   b Plug in $v(2,2)$ and w_3 into the inverse h-function of $C(2,1)$ to calculate the intermediate value, $U_3^\star$
   c Plug in U_2 and the intermediate value $U_3^\star$ into the inverse h-function of $C(2,1)$ to calculate U_3
5. Calculate U_4
   a Use the same methodology to calculate $v(3,2)$, $v(3,3)$ and $v(3,4)$ using the h-function and corresponding input
   b Plug in $v(3,4)$ and w_4 into the inverse h-function of $C(3,1)$ to calculate the intermediate value, $U_4^\star$
   c Plug in $v(2,1)$ and the intermediate value $U_4^\star$ into the inverse h-function of $C(2,2)$ to calculate the second intermediate value, $U_4^{\star\star}$
   d Plug in $v(3,1)$ and the intermediate value $U_4^{\star\star}$ into the inverse h-function of $C(1,3)$ to calculate U_4

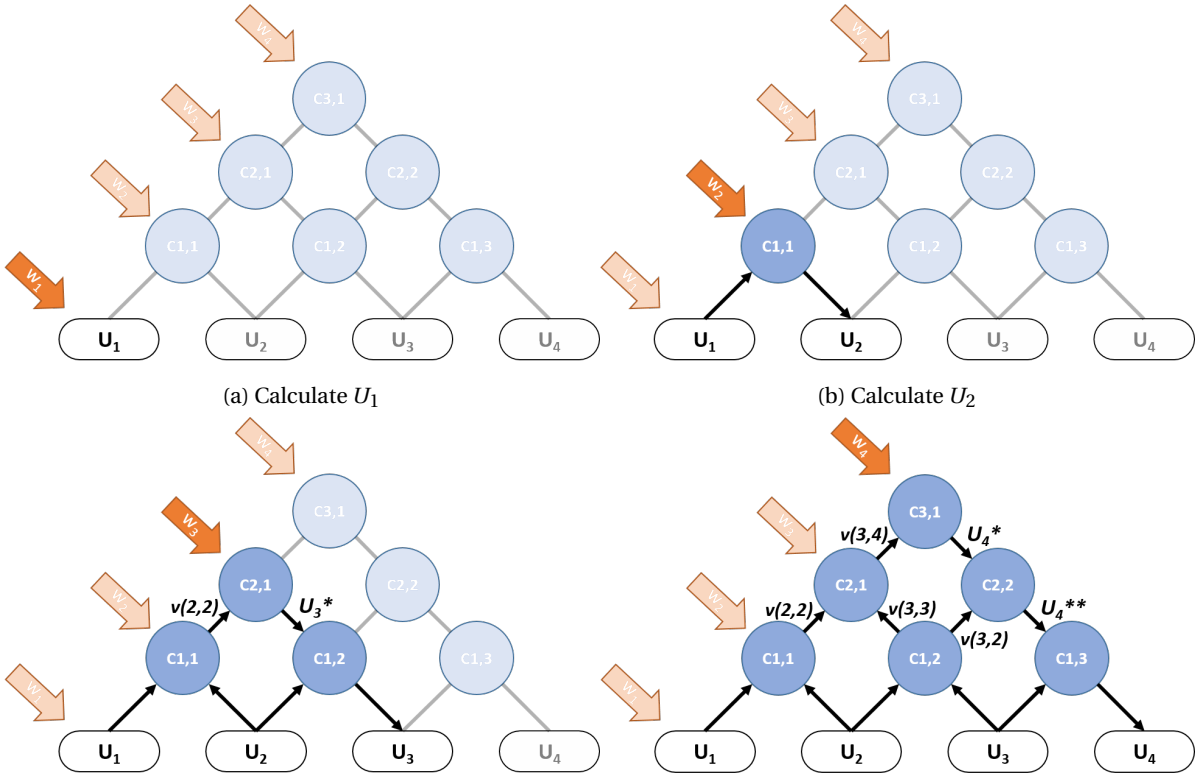

(a) Calculate U_1 (b) Calculate U_2

(c) Calculate U_3 (d) Calculate U_4

Figure 2.6: Visualisation of D-vine simulation for one sample set

2.7. Simulation of data with time dependence

2.7.1. Necessity of i.i.d. input data

One important property of the analyzed data set should be carefully checked, since each set of samples is generated independently from previous simulations. This requires the original dataset to be independent and identically distributed too for a good representation with the synthetic one. To enable vines to effectively simulate synthetic time series this necessity implies that the input datasets should be time independent, as is stated in many publications on copula simulation [2, 65, 67].

Obtaining this state of time independence in the dataset can be either achieved by applying filtering, such as a GARCH(1,1) [14] model, or by increasing the time step to reduce the dependence between lags, as can be inspected by plotting the Auto Correlation Factor (ACF) of the input time series.

2.7.2. Research gap

There may be cases in which either of proposed solutions is undesirable to implement. This happens to be the case with the measurement data for this research, since only a very limited time series is available. The number of samples is therefore too small to perform filtering or increasing the time step.

For now it is more important to mention that the described copula and vine theory cannot be directly applied to generate synthetic time series which contain (near) identical multivariate and time dependence properties, such as the persistence, as the original time series.

Having performed an extensive literature study, it is to the author's best beliefs that the copula theories have in fact not, or very limited, been applied for describing both types of dependence by means of a formal algorithm. This research gap will be studied more extensively in chapter 8 and new methodologies will be proposed to overcome this limitation.

3

Maintenance Decision Models

For production equipment, ensuring the system function is often the prime objective. Here, maintenance has to provide the right (but not the maximum) reliability, availability, efficiency and capability (i.e. producing at the right quality) of production systems in accordance with the need for these characteristics. In principle it is possible to give an economic value to the maintenance results, and a cost-balance can be done.

In this chapter the application of a semi-Markov decision process is explained to represent the group maintenance strategy. The limitations of analytical maintenance models are also touched upon, which prove that these models are inadequate.

3.1. Group maintenance strategy

The most important characteristic is that the process of replacing components is economically dependent, as was already mentioned in paragraph 1.6.2. In this thesis a positive economical dependence is identified, which implies that replacing multiple components at once results in lower costs with respect to replacing them one after each other in independent activities. Important to state is that in the mentioned studies and this research as well, all components are assumed to be identical and fail independent.

A fixed cost C_0 occurs when initiating a maintenance activity. The cost of repairing an individual component consists of two components, one fixed and the other time related. Specifically, C_f is the fixed cost of repairing a component and includes such costs as the price of replacement parts, while C_r denotes the cost per unit time of replacing one component. Each component that fails accumulates down time costs at a rate of C_d per unit time. By using a objective function the optimal moment of maintenance can be found which minimizes the sum of all these costs, as is depicted in figure 1.6.

3.2. Limitations of analytical models

Multiple studies have been performed to describe a system in which a group maintenance strategy is applied, each with their own assumptions. Some studies [6, 73, 77] assume that the replacement is instantaneously and the costs per unit of time can be neglected. Jacob [44] extends these analytical models by including random repair times and thus represents the maintenance process more realistically. Assaf [6] has combined group maintenance optimization theories with the possibility of adding maintenance interval restrictions. Still, all studies aim to minimize the maintenance costs based on a set of analytical equations.

Whilst these models are able to give an acceptable representation of the tidal array, there are a number of limitations which render the existing analytical methods useless for accurately describing the system. The corresponding optimized maintenance policy can thus not be representative.

First of all, the tidal array includes clustering of components since they are spread over a finite number of tidal platforms. This results in the necessity of differentiating between possible failure combinations, in case more

than one component has failed. As will be explained in chapter 5 this affects both the fixed (C_f) and variable (C_r) cost aspect of the maintenance process and thus these values cannot be taken as constants.

A second important limitation is that of the inclusion of uncertainty. It was mentioned in the introduction that the maintenance duration, and thus costs, depend on the availability of weather windows. In this research an accurate representation of the environmental conditions is desired, which is why a numerical approach is preferred which can fully describe the randomness of the weather. This numerical approach for including the uncertainty cannot be effectively combined with the less complex analytical models, which is why these will not be used. Chapter 7 presents the maintenance model which has been developed to determine the optimal policy.

3.3. Semi-Markov Decision Processes

Semi-Markov Decision Process (SMDP) have been extensively used to describe maintenance planning problems and have shown to be an effective approach for minimizing the long-term maintenance costs [9, 36, 102]. Semi-Markov decision processes allow engineers to model complex systems more accurately and enable the best decision policy to be obtained by means of optimization algorithms. This process type is an extension of the general Markov processes. The general Markov property and the model extensions into a semi-Markov decision process will be explained in the next subsections.

3.3.1. General Markov process

A Markov model is a special type of dynamic model with which the probabilistic evolution of a system can be modeled in time.

The Markov property [61] means that evolution of a stochastic process in the future depends only on the present state and does not depend on past history. The corresponding Markov process can thus be described as being 'memory-less', which corresponds to the property of the exponential distribution.

Any arbitrary system or process can be described using Markov chains by means of defining a finite number of states which each describe an unique situation in time and/or space. The probability of changing from one state to another are defined by a set of transition probabilities representing the probability to go from the state i to the state j in one step, or specific time interval [22].

$$S = \{1, 2, .., n\} \tag{3.1}$$

$$p_{ij} \quad \text{,with} \quad i, j = 1, 2, .., n \tag{3.2}$$

For a system with n states, these probabilities can be grouped in a matrix called stochastic matrix of transition probabilities, in the following form:

$$P = \begin{bmatrix} p_{11} & p_{12} & \cdots & p_{1n} \\ p_{21} & p_{22} & \cdots & p_{2n} \\ \vdots & \vdots & \ddots & \vdots \\ p_{n1} & p_{n2} & \cdots & p_{nn} \end{bmatrix} \tag{3.3}$$

Each element in matrix P is a probability and therefore its value is within the interval [0,1]. Also, and given that each row contains the probability of a finite number of events, the sum of all elements of each row should be equal to unity. In other words, P is a stochastic matrix for which each row contains a probability vector.

3.3.2. Extension into a Semi-Markov Decision Process

The general Markov process is extended with two additional properties in order to obtain a Semi-Markov Decision Process, namely the addition of the following properties:

- Adjustable sojourn times

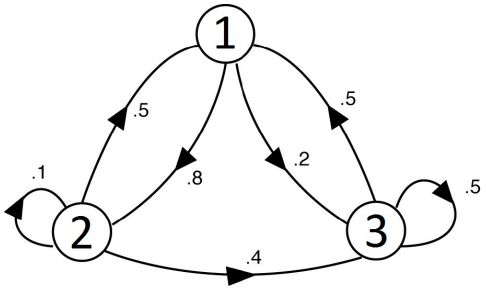

$$P = \begin{bmatrix} 0.0 & 0.8 & 0.2 \\ 0.5 & 0.1 & 0.4 \\ 0.5 & 0.0 & 0.5 \end{bmatrix}$$

Figure 3.1: Example of Markov chain and transition probabilities

- Decisions

The steps of this transition are explained below to give insight in the properties of a semi-Markov decision process.

State holding times: Semi-Markov processes

Semi-Markov processes allow the amount of time spent in each state to be any positive value and not just an exponential distribution. This ensures that various transition rates $\lambda_{i,j}$ can be used between any of the states. This is a very important property, as it allows physical processes, such as the failure rates and the maintenance rate, to be effectively implemented in the model to be more comparable to the actual situation [80].

Furthermore, the length of a visit in a state is called the sojourn time (t_i). The sojourn times of each state can by calculated by the transition rates. Each sojourn time $\lambda_{i,j}$ is the inverse of the sum of the departe rates for state S_i. [83]

$$t_i = \frac{1}{\sum \lambda_{i,dep}} \tag{3.4}$$

The accuracy of estimating the sojourn times directly results in the accuracy of the overall model. Thus, a sojourn time that is not well represented leads to poor model results. It is therefore important to acquire realistic values for describing the transition rates between the states to ensure that the corresponding sojourn times represent reality as much as possible.

Decision making & rewards: Semi-Markov Decision Processes

The second extension adds decision making properties to the semi-Markov process, which converts it into a semi-Markov decision process. This is achieved by enabling the user to define a set of decisions (sometimes called actions in liturature) for each of the states [99]. Whilst the states itself remain unchanged, each of the decisions has their own set of transition rates and rewards, based on what it represents.

3.3.3. SMDP system representation

The semi-Markov decision process is defined by a four-tuple:

- States
- Decisions
- Transition probabilities
- Costs

Let $p_{ij}(a)$ be the probability of going from state i to state j when action a is chosen and $c_i(a)$ is the cost from a transition to state j from state i when action a is chosen. Then the total reward of choosing action a while in state i is [40]

$$c_i(a) = \sum_{j=1}^{N} c_{i,j} \cdot p_{ij}(a) \tag{3.5}$$

The time spent in each state must also be considered. So it is then necessary to find the reward per unit time called the earning rate while choosing action a finally giving the best initial policy. This is found by [100]

$$q_j(a) = \frac{c_i(a)}{t_i} \tag{3.6}$$

3.4. Policy optimization methods

Two methods are used to solve SMDPs, namely a value iteration method and a policy iteration method [101]. The selection of the method is based on whether a finite or an infinite horizon problem is observed. A finite horizon problem is when the system considered is only being solved for a finite time interval, ensuring the transient effects when approaching the end of lifetime to be also included.

Using a finite horizon in combination with the value iteration method, it is possible to simply count the reward for each decision and sum the total reward for the entire policy at the end of the time interval. However, when the time interval is infinite, the rewards obtained will grow without bound over time and disable the possibility of finding an optimal policy.

In this thesis, a policy iteration method in combination with an infinite is applied as the optimization method. This can be safely assumed since the operational lifetime of such tidal systems is generally 20 years and the transient effects on the optimal decisions are negligible, as the sojourn times are significantly shorter than 20 years.

The reward will be measured by the gain that one decision has over another alternative. It is desirable to maximize this gain for each state in which a choice is present. Then the final policy will be independent of time. A policy iteration method is advantageous because it is a much more efficient search method for larger systems.

3.4.1. Policy iteration

The long-run average cost per time unit is taken as the criterion which is to be optimized. For this criterion the semi-Markov decision process is determined by the following characteristics:

- $p_{ij}(a)$ = the probability that at the next decision epoch the system will be in state j if action a is chosen in the present state i,
- $t_i(a)$ = the expected time until the next decision epoch if action a is chosen in the present state i,
- $c_i(a)$ = the expected costs incurred until the next decision epoch if action a is chosen in the present state i.

The policy iteration algorithm can be found in several formats, but the results remains identical. In this research the approach of Tomasevicz [101] for using an educated guess as the initial policy (step 1), whereas the remainder of the algorithm is described by Tijms [99].

Figure 3.2: Policy iteration flow chart

Step 1: Initial policy

To determine the best policy using the policy iteration method it is first necessary to select an initial policy. This policy can be selected at random, but this may result in a number of unneeded iterations to reach to the final optimal policy. Therefore, the first step is to choose an initial policy that is not random, but an educated guess. The initial policy d_1 is the policy in which the highest earning rate, thus the lowest value of $c_i(a)$, is selected for each state.

Step 2: Policy Evaluation

Next, the iteration process begins by the Policy Evaluation step. It is necessary to obtain a scalar that represents the gain of the selected alternative along with N relative values, v_i, for the system. The gain of the policy is the average reward per unit of time. This provides method of comparison between policies. Note that there are N relative values and one scalar g in which to solve, giving $N+1$ unknowns with only N equations. Therefore one of the relative values, usually v_N, is arbitrarily set to zero [40]:

$$v_i = c_i(d_i) - g \cdot t_i(d_i) + \sum_{j \in I} p_{ij}(d_i) \cdot v_j \tag{3.7}$$

$$v_N = 0 \tag{3.8}$$

Step 3: Policy Improvement

For each state $i \in I$, determine an action a_i yielding the minimum in

$$\min_{a \in A(i)} \left\{ c_i(a) - g(d) \cdot t_i(a) + \sum_{j \in I} p_{ij}(a) \cdot v_j(d) \right\} \tag{3.9}$$

The new stationary policy $\bar{d}$ is obtained by choosing $\bar{d}_i = a_i$ for all $i \in I$ with the convention that $\bar{d}_i$ is chosen equal to the old action d_i when this action minimizes the policy-improvement quantity.

Step 4: Convergence test

If the new policy $\bar{d} = d$, then the algorithm is stopped with policy d. The constant $g*$ is uniquely determined as the minimal average cost per time unit.

Otherwise, go to step 2 with d replaced by $\bar{d}$.

4

Equipment failure

Failures are essential events when developing a corrective maintenance model. A failure is defined as the termination of the ability of equipment to perform a required function [19]. The cause of a failure may not always be known, but can be related to errors in the design, manufacturing, installation, operation and/or maintenance.

In this thesis the focus will be on how often the equipment fails and the probability of occurrence, and less on why and how the equipment has failed. This chapter explains the essential theoretical background and equations are provided for describing failures in a system.

4.1. Modeling failures

Four basic functions are used to describe equipment failures: [22]

- $f(t)$ - Failure probability density function (pdf)
- $F(t)$ - Failure probability distribution function (cdf)
- $R(t)$ - Reliability function
- $\lambda(t)$ - Failure rate

The failure probability density function, $f(t)$, describes the probability of failure at time 't' and integrating this function gives $F(t)$, the probability of failure until time 't'. The reliability function, $R(t)$ gives the probability to survive until time 't'. Failure rate (λ) is the frequency with which equipment fails, expressed in failures per unit of time.

Each of these four functions are directly related to each other and once one is known, the others can be derived. The complete derivation of each function can be found in [22], but for this research the following equations are most important.

$$\int_0^t f(t)dt = F(t) = 1 - R(t) \tag{4.1}$$

$$R(t) = exp\left\{-\int_0^t \lambda(t)dt\right\} \tag{4.2}$$

4.2. Random failures

The hazard function describes the failure rate in time and is often referred to as the 'bathtub curve', which is depicted in figure 4.1. Whilst there is no general consensus on the applicability of this curve [52], a significant part of literature represents the bathtub curve as the superposition of three independent hazard rates: [41, 54]

- Decreasing hazard function - Infant mortality failure
- Constant hazard function - Random failures
- Increasing hazard function - Wear out failures

In this thesis all failure rates are assumed constant. In section 5.4 the arguments are given to substantiate this assumption of which one important reason is the lack of detailed failure data. Reference failure data is used, but only fixed failure rates are available for the observed equipment, not the distribution in time. Therefore the exponential distribution is applicable, as it only requires one parameter to fully describe its distribution.

If the failure rate is constant ($\frac{d\lambda}{dt} = 0$), it implies that only random failures occur. Depending origin of the failure data, two approaches are possible. Either the failure data describes all equipment failures during its lifetime or the constant failure rate has been identified during its operational lifetime. If equipment failure data of the entire lifetime is fitted with an exponential failure distribution, the constant hazard function attempts to fit the realistic, 'observed failure rate' hazard function. This gives an underestimation during the early and ending life time, but an overestimation during the operational lifetime. If the failure data only describes the lifetime with constant failures, it represents that specific region very well, but cannot be used to describe the other two regions, or it will severely underestimate the observed failure rates.

In this research the exponential failure rates the second approach is used, so only the constant failure rate region is included the development of the maintenance model. This approach is most commonly used and the failure rate data which is presented in chapter 5 is also exclusively applicable for the constant failure rate region [4]. In figure 4.1 the approximation of the observed failure rate by using a constant failure rate is depicted by the solid red line.

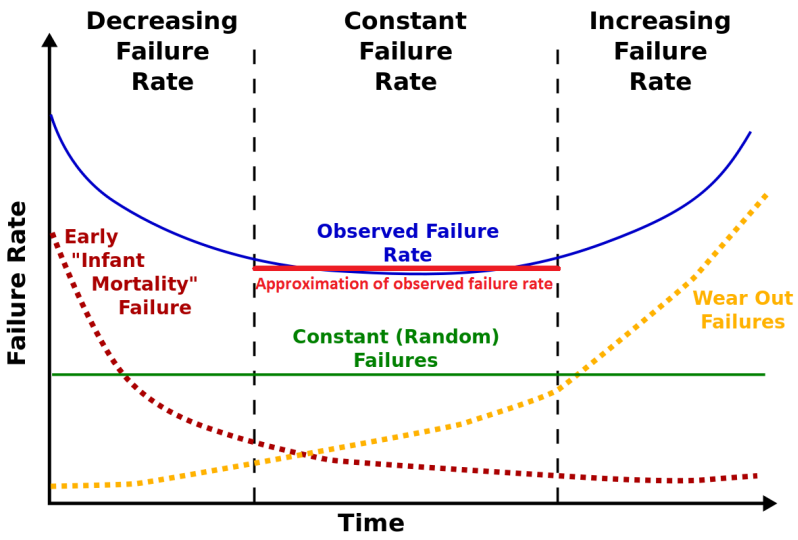

Figure 4.1: The 'bathtub curve'

Since a constant failure rate is used, the equation of the reliability function can then be rewritten to an exponential function. Equation 4.4 is called the exponential failure distribution and can thus be applied for equipment under the assumption that the failure rate is constant in time.

$$R(t) = e^{-\lambda \cdot t} \tag{4.3}$$

$$F(t) = 1 - e^{-\lambda \cdot t} \tag{4.4}$$

$$f(t) = \lambda \cdot e^{-\lambda \cdot t} \tag{4.5}$$

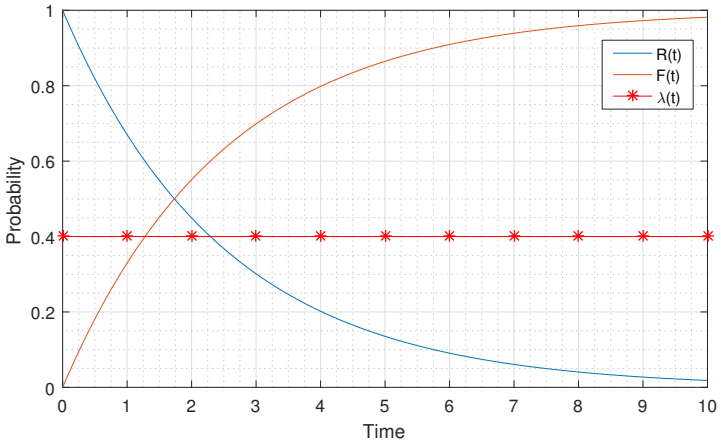

Figure 4.2: Reliability function and failure probability distribution function for a constant failure rate

In practice, the mean time between failures (mean time between failure (MTBF), $1/\lambda$) is often reported instead of the failure rate.

$$MTBF = \frac{1}{\lambda} \tag{4.6}$$

4.3. Multi-component failure

The tidal system consists of multiple assemblies, so a description of multi-component failures is required as well. To do so, it is assumed that all assemblies of the tidal system are described by an exponential failure distribution, as has been explained in section 4.2. In this section both series and parallel systems reliability will be explained, including their application in the tidal system failure representation.

4.3.1. Serial failure

A series system is a configuration such that, if any one of the system components fails, the entire system fails. Conceptually, a series system is one that is as weak as its weakest link. [82]. Figure 4.3 gives a schematic representation of a series system with 'n' components.

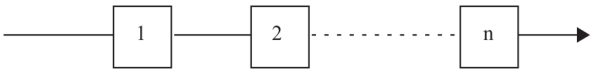

Figure 4.3: Serial system of n components

It is possible to convert the failure distributions of all individual components into one overall failure distribution. For serial failures the following holds [82]:

$$\textit{"System success"} \equiv \textit{"Success of every individual component"}$$

This can be written in terms of reliability as follows:

$$R_{sys} = R_1 \cdot R_2 \cdot \ldots \cdot R_n \qquad \text{(if component reliabilities differ)} \tag{4.7}$$

$$R_{sys} = [R_i]^n \qquad \text{(if i=1,...,n components are identical)} \tag{4.8}$$

When plugging the exponential distribution into the equations for serial reliability the following is found:

$$R(t) = e^{-\lambda \cdot t} \tag{4.9}$$

$$\lambda_{sys} = \sum_{i=1}^{n} \lambda_i \tag{4.10}$$

$$R_{sys}(t) = e^{-\sum_{i=1}^{n} \lambda_i \cdot t} \tag{4.11}$$

$$F_{sys}(t) = 1 - R_{sys}(t) = 1 - e^{-\sum_{i=1}^{n} \lambda_i \cdot t} \tag{4.12}$$

The failure rates of individual components add up to the system's failure rate. This results in failure probability distribution function that has an increased steepness and thus the system fails faster on average.

This property is especially important when representing the serial system that is responsible for the electricity generation. Different assemblies are connected serially and failure of one will result in an overall subsystem failure, since no electricity can be produced anymore. This does not mean that all individual assemblies are broken and are to be replaced, but the function of the overall subsystem cannot be executed anymore. Section 5.4 gives a detailed description of how the tidal system is represented by means of combining individual assembly failure distributions.

4.3.2. Parallel failure of identical equipment

A second type of multi-component failures is the parallel system, in which redundancy is included. The overall system only fails if all of the individual components have failed. Figure 4.4a shows a parallel system of 'n' components. Parallel systems are usually implemented to increase the MTBF of the overall system, as the inclusion of more parallel linked components require a longer time before all components have failed. The example

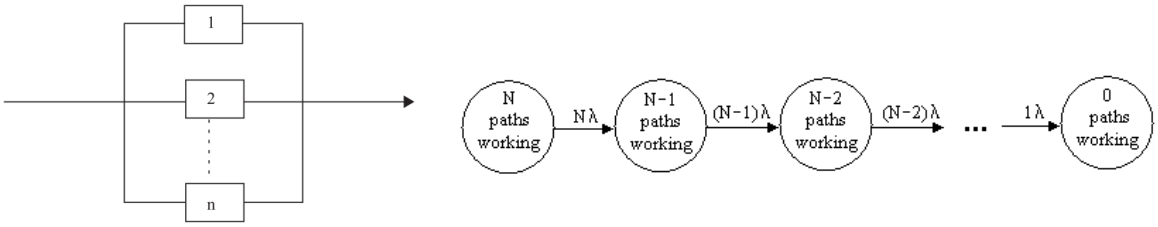

(a) Parallel system of n components

(b) Parallel failure in states

Figure 4.4: Parallel system failure

Since all failure rates are constant in this thesis, the mean time from the 'n paths working' state to the '0 paths working' state is the sum of the mean times from each state to the next [63]. The transition from one state to another can be described by means of a serial system failure. Only one of the working paths is required to fail in order to transit to the next state, in which the same occurs but with one less path working, as is depicted in figure 4.4b. This immediately gives the well known result that the MTBF of a system with 'n' parallel redundant paths (without repairs) is proportional to the partial sum of the harmonic series

$$MTBF(N) = \frac{1}{\lambda} \cdot \left(1 + \frac{1}{2} + \frac{1}{3} + \frac{1}{4} + \ldots + \frac{1}{N}\right) \tag{4.13}$$

Figure 4.5 gives an example of a parallel system with 10 identical components and $\lambda = 0.4$. For the different number of working paths the overall failure rate, using the serial failure equations, is determined. The corresponding MTBF is depicted, together with the sum from the initial state up to the observed state. As the number of parallel components increase, the benefit of the increased redundancy decreases, as the serial failure rate between the states increases as well.

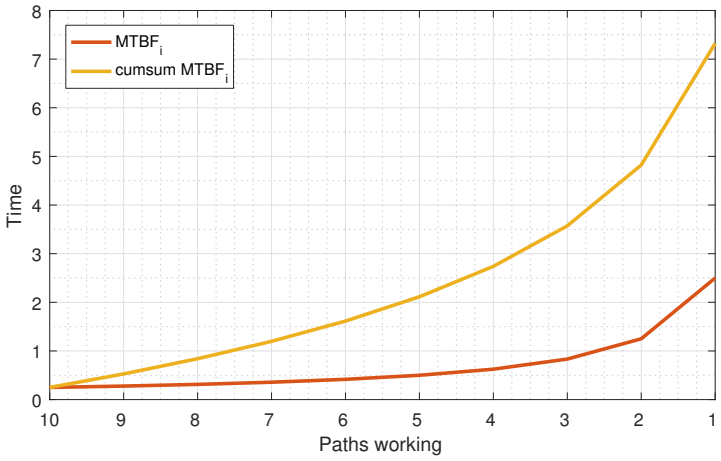

Figure 4.5: MTBF of parallel systems

In this research the tidal system will be represented by a number of parallely connected electricity generating subsystems, which operate independently. The system failure can be described as a full array failure when no electricity is produced.

Part II

Damen solution - System overview

5

Damen Tidal Energy Converter

In this chapter the current top level design of Damen is described and insight is provided on the design philosophy of the tidal platform and how this affects the design and maintenance tasks. Furthermore, the power production capacities are explained of the TECs. Lastly, the failure modes, rates and costs are presented in this chapter.

The system which is described in this chapter, together with the maintenance strategy in chapter 6, will serve as the base case during the execution of the maintenance model and the interpretation of results, which are extensively described in part III.

5.1. Tidal array location

The majority of the current tidal systems are developed for implementation at high resource tidal locations (V_{msp} > 3.5 m/s) [28], which prove to be most suitable for the initial deployment round [81]. Tidal feasibility studies state that the initial pre-commercial development phase should focus on a small-scale array infrastructures, producing in the range of 3MW to 20MW. [56].

As mentioned in the introduction, the tidal location in this study is chosen to be the Orkney Islands, United Kingdom. Feasibility studies have shown that this region contains multiple tidal hotspots [8, 55], as can be seen in figure 1.3. EMEC is the operator of the tidal location at the Orkney Islands and environmental time series will be used from their in-house measurements to represent the wave, wind and current characteristics at that specific location.

For this location the tidal array which is to be developed will consist out of five systems, which are positioned in a grid with enough spacing to provide good vessel accessibility, no overlap in the mooring footprint and negligible inter-TEC influence due to the wake disturbance of the current flow.

5.1.1. Feed-in tariff

A Feed-in Tariff (FiT) is a policy mechanism designed to accelerate investment in renewable energy technologies. This is being achieved by offering long-term contracts to renewable energy producers, typically based on the cost of generation of each technology.

Each government has its own FiTs and may differ per renewable energy generation technology. The base case which is used in this thesis uses the EMEC location for the tidal array, for which the United Kingdom FiT is applied. Several FiTs may apply, depending on the production capacity and TRL of the system [72].

For the base case it is assumed that the FiT for the developed tidal systems at EMEC is 11 cents/kWh and remains constant for the projected lifetime of 20 years. This may change in time however and is considered a political uncertainty. The effect of changing the FiT will therefore be investigated in the sensitivity analysis.

5.2. TEC system overview

5.2.1. System description

Damen's latest developments regarding a novel TEC design for reducing the LCOE have lead to a top level design which deviates from current TEC designs. An artist impression of the current Damen design which will be used in this study is shown in figure 5.1. Whilst the dimensions and selection of included system components are still in a preliminary phase and should not be observed as part of the final design, the artist impression clearly shows what design philosophy is applied by Damen.

The tidal platform design describes a floating system which includes 16 vertically orientated Darrieus turbines that produce electricity by rotation of the respective shafts, which in turn power the generators. Contrary to most of the industry, this design focuses on using readily available components to reduce the cost of the system. Also, feasibility studies of Damen [39] have shown that by implementing multiple smaller turbines and connecting these to individual generators is more cost effective than merely one or two larger turbines to generate the same amount of electricity, due to the complexity and non-availability of these large custom components .

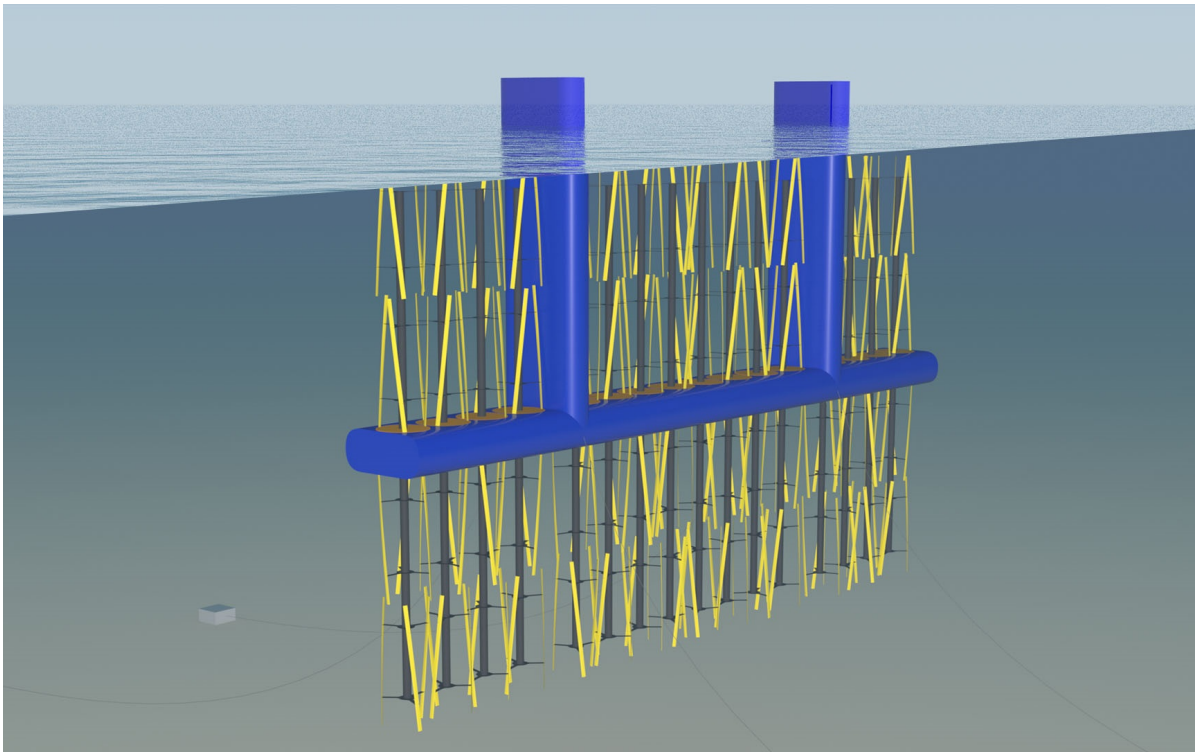

Figure 5.1: Artist impression of the Damen TEC design

Plug&Play connection

An important characteristic of the tidal system is its ease for performing maintenance. As stated, the design has a strong focus on using multiple smaller components instead of one equivalent counterpart with identical power production. The shift from a CAPEX to an OPEX orientated system requires a different approach during the development of the top level system design.

One result which is derived from this design approach is the Plug&Play connection of the TEC onto the floater. The TEC, including all its components, can easily be connected and disconnected onto the floater by means of inclined outer surfaces, which cling into the similarly shaped slot of the floater. Upon placement, the TEC will remain in position due to its gravitational force and surface friction. Whilst no final connection has been designed by Damen yet, all of the alternatives can be traced back to a variant of the 'slide and lock' mechanism. The operation for the placement follows the reversed procedure.

It must be noted that the actual maintenance activity involves more steps, such as having the platform enter maintenance mode. These tasks will be explained more into detail in the next paragraph and chapter 6, including the required weather windows.

Maintenance mode

In order to perform the TEC replacement the tidal platform first needs to emerge to the water surface, which is achieved by creating positive buoyancy as a result of filling the buoyancy tanks with air. After surfacing, the TEC replacement takes place. After having replaced the correct number of TECs, the platform submerges again and leaves maintenance mode once it is position.

During the maintenance mode, from the emerging to being fully submerged again, none of the TECs is operational and thus the entire system is affected by downtime. This effect will also be included in the model and introduces additional set-up costs for the maintenance activity, which are both fixed (platform emerging/-submerging) and variable (number of TECs to be replaced).

It is important to state that maintenance mode is only initiated if a weather window for the entire set of tasks is available. Depending on the weather conditions this will require the vessel to wait until the weather window occurs.

5.2.2. Subsystem & assembly identification

Multiple subsystems can be identified in the design of an individual tidal platform, each directly related to the main functions of the system. However, as will be explained more in detail in subsection 5.4.1, only the TECs and its main assemblies will be included in this research since these account for the majority of the random failures. The functions and failures of remaining subsystems, such as the floater, mooring lines and export cable, are excluded from this research.

Each tidal platform houses 16 identical TECs which are responsible for generating electricity from the tidal flow. The assemblies of a TEC which can be identified within this research are:

- Darrieus turbine blades (also called the Prime Mover)
- Generator
- Invertor
- Brake
- Gearbox
- Shaft and bearings

5.3. TEC power generation

As stated, each of the 16 TECs consists out of a PM, which is responsible for converting the kinetic energy of the current flow into mechanical energy within the system, and a number of components which transfer the energy (gearbox) before the mechanical energy is converted into electricity (generator). Whilst the PM's main function is to maximize the production output, the other assemblies designed to minimize the losses during energy transport. The power production properties of the tidal system are discussed in this section, describing parameters which will be used throughout this research.

5.3.1. Power curve

The most common way of representing the production capacity of a PM, and connected assemblies, is by means of a power curve. The power curve describes the relation between the flow velocity, in this case that of the tidal current, and the power. The relation between these two parameters is derived from hydrodynamics and can be written as

$$P = \frac{\eta_{DT} \cdot C_p(TSR) \cdot \rho_{water} \cdot A \cdot U_{curr}^3}{2} \tag{5.1}$$

where:

P	Generated power	$[W]$
$C_p(TSR)$	Power coefficient	[-]
ρ_{water}	Density of water	$[kg/m^3]$
A	Swept area of the PM	$[m^2]$
U_{curr}	Current velocity	$[m/s]$
η_{DT}	Drive train efficiency	$[-]$

Power curves generally have a similar profile to that in figure 5.2, which shows the power curve of the TEC, including its drive train losses. A number of characteristic points can be identified which, if the data is available, can be implemented easily to construct the power curve:

U_{cut-in} The minimum flow velocity required to start operating. This is either determined by the inertia of the PM or controlled by the brake

U_{rated} The design flow velocity at which P_{rated} is first reached.

P_{rated} The power for which the system is designed. By active braking (mechanical or via the generator) the power is upper bounded at this value

$U_{cut-out}$ The maximum flow velocity for which the power production is upper bounded. If this value is exceeded the PM enters its survival mode by bringing the system to a stand-still. This is to prevent the system from failing in extreme weather conditions.

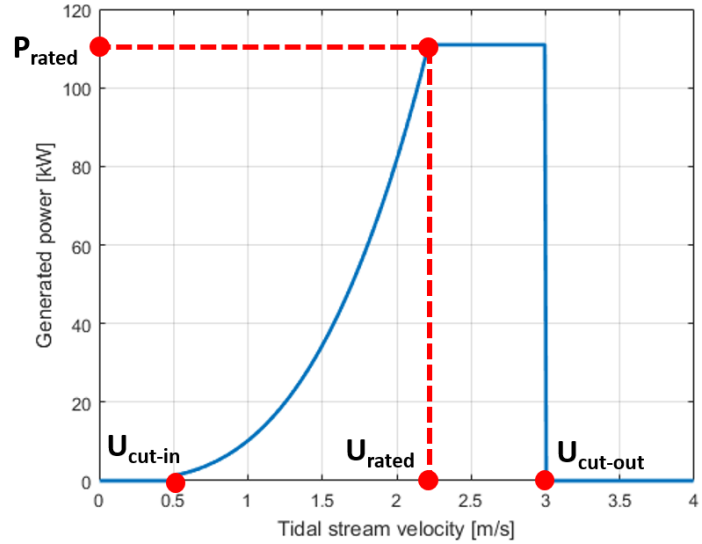

Figure 5.2: TEC power curve

The power curve can be analytically described by the following equation:

$$P(U_{curr}) = \begin{cases} 0, & \text{for } U_{curr} < U_{cut-in} \\ \frac{\eta_{DT} \cdot C_p(TSR) \cdot \rho_{water} \cdot A \cdot U_{curr}^3}{2}, & \text{for } U_{cut-in} \leq U_{curr} < U_{rated} \\ P_{rated} & \text{for } U_{rated} \leq U_{curr} < U_{cut-out} \\ 0, & \text{for } U_{curr} \geq U_{cut-out} \end{cases} \tag{5.2}$$

The power generating properties of Darrieus turbine and related components, which will be applied in the base case, are listed in table 5.1.

5.3.2. Optimal control strategy

Using a control strategy enables the Darrieus turbine to operate at its optimal TSR, either by changing its pitch angle or by adjusting the rotational speed of the blades. Optimizing TSR for each current flow velocity maximizes C_p and thus results in an increase of the power production.

The slowly changing character of the current velocity enables the use of a quasi-static approach for determining the optimal control strategy. It is therefore assumed that the fluctuations in U_{curr} are slow enough for the control system to always use the best TSR for the optimal power coefficient.

This assumption results in a slight overestimation of the electricity production, as in reality dynamic fluctuations will always result in efficiency losses. However, it is not in the scope of this research to describe the power production capabilities of the TEC in more detail, as it is an arbitrarily input in the maintenance model.

Table 5.1: Numerical values of the TEC power generating properties

Parameter	Value
P_{rated}	110 kW
U_{cut-in}	0.5 m/s
U_{rated}	2.2 m/s
$U_{cut-out}$	3.0 m/s
C_p	0.38
η_{DT}	90 %
A	58.24 m^2
L x D	11.2 x 2.6 m

5.3.3. Power generation related assumptions

In this research a number of assumptions are made to simplify the developed maintenance model. More detailed information about the Darrieus turbine and the assumptions made to obtain the production related values can be read in appendix B.

- The power generation properties of all TECs are identical to each other.
- The TECs in the array are not subject to wake effects due to nearby water-structure interaction.
- No efficiency losses occur due to wear-out of the assemblies.
- Marine fouling (and its negative effects) is considered negligible, due to the design of the blades and use of fouling control coatings [110].
- The control system is assumed to be optimal, which is why a fixed value for C_p can be used.

5.4. TEC failure

The failure of the different components within the system play a central role within this research. The optimal maintenance policy is highly dependent on the failure rates and the direct and indirect costs in the event of maintenance in case of failure. Hence, insight in the failure related data is given in this section to clearly demarcate the scope of this research and the model.

5.4.1. Included failure modes

The main elements of the Damen tidal system can be subdivided into two groups:

- Electricity production related elements
- Miscellaneous elements

An important assumption of this research is that during the operational lifetime of the tidal array, only maintenance is required on the electricity producing elements, as these consist out of moving parts. The dynamic character of these components results in a non-negligible chance of failure due to wear, which is why this is posed as the main failure mechanics of the system.

This implies that the latter group, which includes the mooring system, the floater and the export cable, are excluded from the maintenance model and are considered to experience no failure. The structural integrity of the tidal platform is thus for the system lifetime sufficient to withstand all (extreme) loads.

Additionally, it is assumed in this research that only random failure occurs, described by the exponential distribution. When a certain assembly has failed, the remainder of the assemblies is still considered to be 'as new' and thus has the same constant failure rate throughout its lifetime. No infant mortality and wear-out effects are included in this research.

Fault tree

The failure modes that can be identified in the tidal array are thus only described by the failure of TECs, due to a local assembly failure. This is represented in figure 5.3 in the fault tree of one tidal platform. The other platforms depicted have identical fault trees to describe the platform failure, but are not included in the figure.

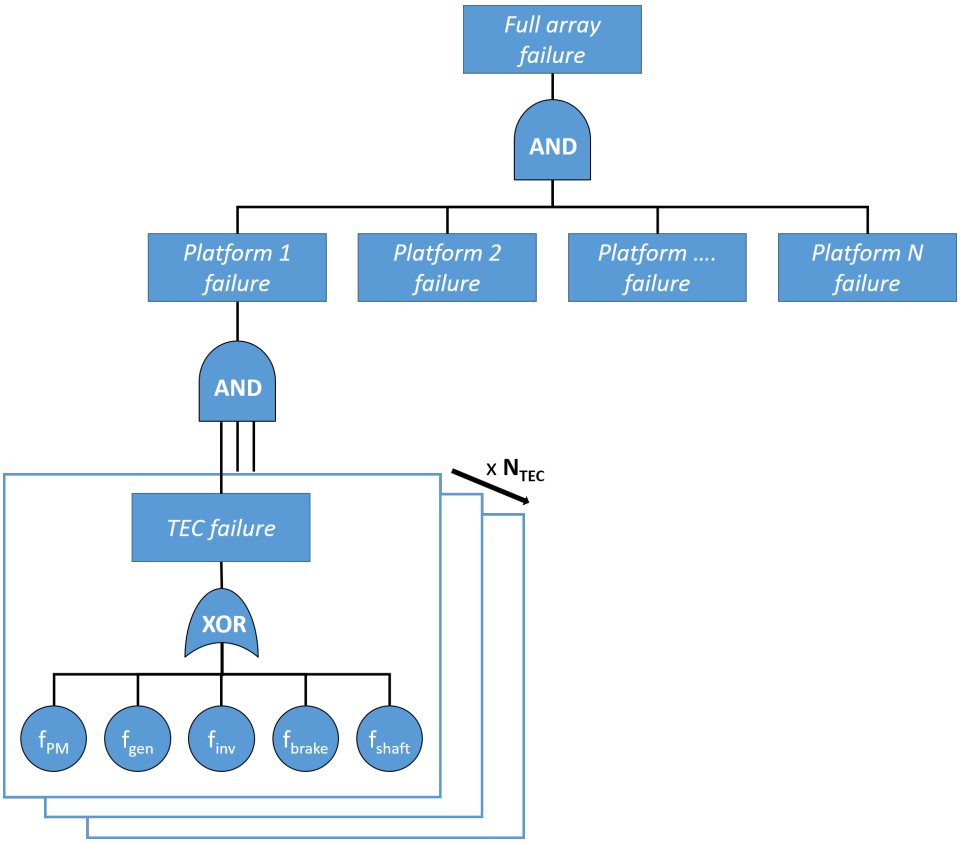

Figure 5.3: Fault tree of the tidals array

The TECs are considered to operate independently of each other and are thus are represented parallel. In the failure tree this relation is displayed by an 'AND-gate' until the event of full platform failure occurs.

On the other hand, the individual assemblies with a TEC are connected serially and are considered to fail mutually exclusive to each other. If one assembly fails, the entire TEC stops operating immediately, rendering it impossible for other assemblies to fail at the same time. This relation between the assemblies within a TEC is represented by a 'XOR-gate' in the fault tree.

5.4.2. Usage of wind turbine reference data

At first, the failure rates for different components of the Damen tidal system are taken into account. At this point, it needs to be mentioned that the full-scale application of tidal energy devices is not at a mature stage in order to recuperate actual failure rates for the different modules of the device. A valid alternative to this is the use of actual failure rates from other related fields of research and application in the renewables sector (e.g. wind turbines, other renewable energy devices).

Reliability data from wind turbine assemblies has become available in recent years from surveys [79, 111] and has been combined in a recent study [4] to perform a Failure Modes and Effect Analysis (FMEA) on wind turbines. Table 5.2 shows a typical comparison between reliability field data of a small wind turbine, 300 kW, and a 1 MW wind turbine main assembly failure rates based on [79]. The exponential model and constant failure rate region are considered for failure rate field data [111]. As mentioned, the exponential failure model describes merely random failures during the operational lifetime of the system.

Table 5.2: Wind turbine assemblies' reliability field data

Assembly	Failure rate of LWK WTs	
	300 kW WT	1 MW WT
Blades	0.078	0.308
Generator	0.059	0.126
Brake	0.029	0.056
Gearbox	0.079	0.255
Shaft/bearings	0.002	0.046
Converter	0.045 - 0.2 [79]	

As only two data sets are available, 300 and 1000 kW, extrapolating the data to match the Darrieus turbine power (110 kW) cannot be effectively performed as the relation between the power and failure rates remain unknown. By applying for instance a linear extrapolation, the failure rate of the shaft and bearings will even exceed zero, resulting in non-existent negative values. Thus, in order to maintain the level of data reliability within this thesis as much as possible, it is chosen to use the failure rate data of the 300 kW wind turbine to represent the tidal system's failure rates.

5.4.3. Adjustment factors

A similar study [53] which calculates the O&M costs for a specific tidal device uses the same approach of using wind failure rates as reference data, but on top of that also employs certain adjustment factors. These factors are:

- f1 (= 6.3) to account for the naval underwater environment
- f2 (= 1.1) for the data uncertainty origination (data compiled from various sources such as research papers and other project reports)

Application of these adjustment factors would lead to the following calculation of the failure rate for a component:

$$\lambda_{adj} = \lambda_{ori} * f_1 * f_2 \tag{5.3}$$

Whilst the use of such adjustment factors may in specific cases increase the accuracy when describing tidal device failure rates, the magnitude of the mentioned factors could not be justified and thus these will not be included in this research. Instead, the 300 kW WT reference values will be used as the base case and in section 10.3 the model sensitivity will be observed when varying the failure rate inputs. This approach is more meaningful and provides extensive insight in the effect of uncertainty in component failure rates.

In case of the converter data, which is obtained from a different study, the lower boundary (0.045) is selected to represent the tidal system's converter failure rate. This assumption is done to be in correspondence with the decision of also selecting the lower boundary for the other assemblies.

5.4.4. Bundling of assembly failure rates and product costs

In the model which has been developed in this research, the individual failure rates and product costs are combined into one overall value, which represents the properties of an entire TEC. This assumption reduces both the complexity of the model and significantly cuts the simulation time, as the number of unique failure states reduces exponentially. The bundling of failure rates and product costs can be done due to number of reasons which are system specific and may not be blindly applied in any situation.

First of all, the described failure rates are all constant and only random failures are included in the model. The failure distribution of the assemblies are described by the exponential model, as described in subsection 5.4.2. This enables the summation of rates into one overall failure rate, which describes the exponential failure distribution of a TEC.

Secondly, when looking at the physical interaction of the assemblies within a TEC and the corresponding failure tree, as is depicted in figure 5.3, it is apparent that failure of one assembly leads to the failure of the entire TEC. Still, only the failed assembly is broken and needs to be replaced, but the developed corrective maintenance strategy states that the entire TEC will be replaced and repaired onshore.

Characteristic TEC failure rate

Due to the above two arguments, the ratio of assembly failure rates (r_i) with respect to the characteristic TEC failure rate can be calculated as follows:

$$\lambda_{TEC} = \sum_{i=1}^{n} \lambda_{ass,i} \tag{5.4}$$

$$r_i = \frac{\lambda_i}{\lambda_{TEC}} \tag{5.5}$$

with λ_{TEC} being the failure rate of one TEC. It is easily notices that the inclusion of more assemblies, which each may bring the entire TEC to a failure, increases the characteristic TEC failure rate. The cumulative distribution function of the exponential failure model in figure 5.4 also shows the same effect of adding the failure rates.

$$F(t) = 1 - exp^{-\lambda \cdot t} \tag{5.6}$$

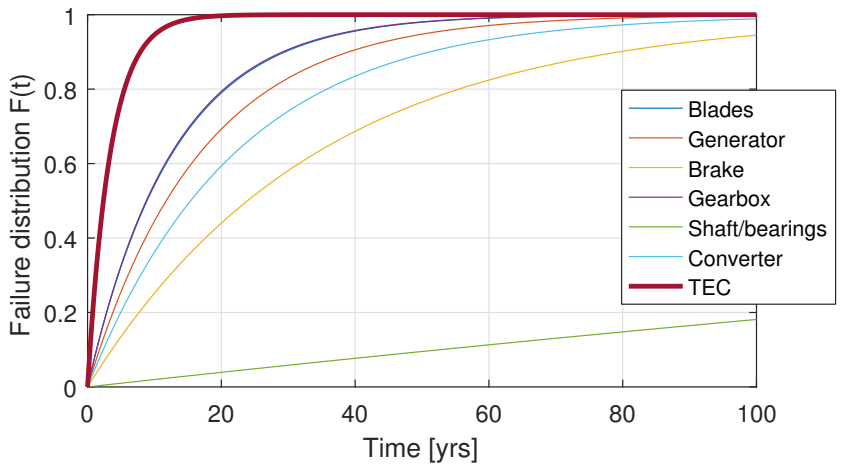

Figure 5.4: Exponential failure distribution of individual assemblies and TEC

Given the assembly failure rates in table 5.2, the ratios of the assembly failure rates with respect to the TEC failure rate are shown in figure 5.5.

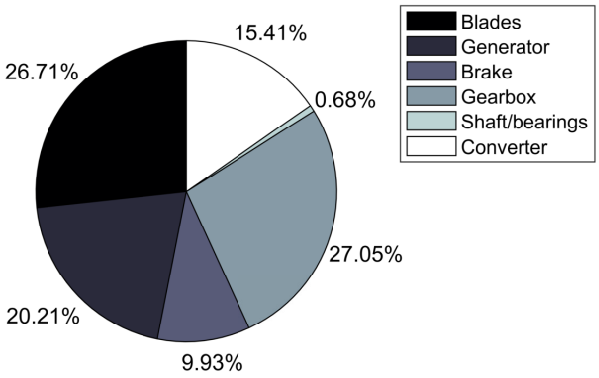

Figure 5.5: Fraction of assembly failure rate w.r.t. TEC failure rate

It is found that each of the TECs has a failure rate of $\lambda_{TEC} = 0.2920$ failures per year. To make this number easier to grasp, it can be converted into the MTBF, as follows:

$$MTBF_{TEC} = \frac{1}{\lambda_{TEC}} \tag{5.7}$$

Using this equation the MTBF of an individual TEC is 3.4 years.

Characteristic TEC product costs

If a TEC failure occurs due to a local failure of an assembly, the entire TEC gets replaced with a new one and the failed TEC will be repaired. It is assumed that this is done by replacing the broken assembly with an 'as new' product, whilst not performing cost-related maintenance on the other assemblies. Thus, the characteristic TEC product cost for a replacement is the sum of all partial assembly costs, based on its failure ratio.

$$C_{TEC} = \sum_{i=1}^{n} r_i \cdot C_i \tag{5.8}$$

The TEC product costs upon failure are determined using the ratios listed in 5.5. Damen has performed a product cost estimation [39] for the individual assemblies. Since the CAPEX is excluded from this model and it is assumed that only the TEC related components can fail, the cost estimation is limited to these assemblies. The product costs are listed in table 5.3.

Table 5.3: Product costs of assembly and TEC

Assembly	Product cost (C_i)	Failure ratio (r)	Cost contribution ($r_i \cdot C_i$)
Blades	€1260	0.2671	€983
Generator	€10200	0.2021	€6018
Brake	€10200*	0.0993	€2958
Gearbox	€13950	0.2705	€11021
Shaft/bearings	€11100	0.0068	€222
Converter	€20400	0.1541	€9180
TEC	**C_{TEC} = €10405**		

* Braking is performed by using the generator, so identical costs are shared if one of the two failures occur

5.4.5. Failure related assumptions

A few important assumptions regarding the failure must be mentioned to substantiate the calculations and processes in the maintenance policy optimization model:

- Individual assembly failures are represented by an exponential model, and are thus random failures during the operational lifetime of the system.
- If one assembly fails, the remaining non-failed assemblies are considered to still be 'as new'. This follows implicitly from the first assumption, since only random failures are included.
- Failures are fully independent of each other, both for identical assemblies and between different assemblies.
- For each TEC, the assembly failure is calculated as being mutually exclusive. This implies that if one assembly fails, the entire TEC fails due to this and no situation will occur in which multiple assemblies will fail simultaneously.
- It is assumed that in case of maintenance of a TEC no additional repair costs are charged for product related processes such as onshore logistics and labor. These are all assumed to be included in the product costs of table 5.3.

6

Maintenance strategy

This chapter provides information regarding the implemented maintenance strategy, the vessel which is used and the activity breakdown into individual tasks. Each of these tasks have their own required duration, costs and the execution may be bounded by operational limits.

6.1. Maintenance tasks

In order to determine the optimal maintenance policy for the group based corrective maintenance strategy, it is required to look at the individual tasks and in what order these are executed. As has been mentioned before, all possibilities of replacing different number of TECs are considered, and each require an unique combination of tasks. The identified tasks and their ordering within the replacement operation are be discussed in subsection 6.1.1.

6.1.1. Maintenance process flow

A process flow of the individual vessel related tasks has been developed for describing the maintenance activity. The process flow, as seen in figure 6.1, applies to all maintenance activities in this research, regardless of how many TECs are decided to be replaced at once. Each of the tasks will be explained more in detail in the remainder of this chapter.

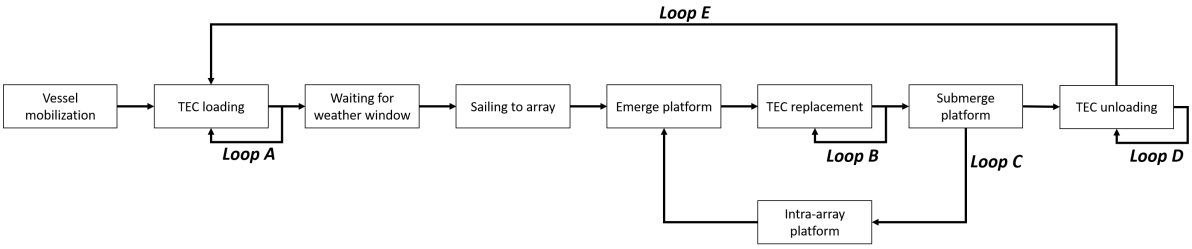

Figure 6.1: Process flow chart for generating the order of maintenance tasks

In figure 6.1 several loops are be observed. Based on the conditions of the maintenance activity and the tidal array, these loops are initiated. The loops describe the following:

Loop A More than one TEC is loaded, since multiple failed TECs will be replaced at once
Loop B Multiple failed TECs at the same tidal platform will be replaced sequentially
Loop C Failed TEC(s) at another platform will be replaced if the vessel still has 'as new' TECs left
Loop D More than one failed TEC has been replaced and is sequentially unloaded at the port
Loop E The maintenance activity requires more TECs to be replaced than the vessel's deck capacity

Vessel mobilization

When the decision is made to perform maintenance, the vessel will first need to sail to the port which has the TECs stored. No dedicated vessel is used, but instead a rented one which is available at that time, as will be explained in subsection 6.2.3. This task thus describes the sailing of the rented vessel towards to port for loading the TECs and personnel.

TEC (un)loading

If the maintenance vessel arrives in the port, it will load the selected number of TECs onto its deck to prepare for operation. Likewise, after switching out the failed TEC(s) with functioning one(s), it will unload the failed TEC(s) at the port, so reparations can commence onshore.

Also, if more TECs are to be replaced than can be loaded at once, the vessel will return to port during operation to resupply and thus unloading and loading activities are initiated.

Waiting for weather window

Given the weather forecast, it may or may not be possible to perform the TEC replacement operation immediately. The vessel will therefore wait in the port until the forecast shows a weather window in which the required number of TECs can be replaced at once for at least one tidal platform.

Sailing to/from array

For the EMEC tidal location the distance between the port and the tidal array is approximately 45 kilometers. For the implementation in this research the influence of external effects, such as the current velocity, are not considered for the sailing speed. This is a valid assumption, since the mean of the current velocity is zero due to its sinusoidal velocity profile.

Emerge/submerge platform

These two tasks are directly related to the tidal platform entering its 'maintenance mode'. This is performed by filling or emptying the floater ballast tanks. The tidal platform enters its 'maintenance mode' when it starts emerging and leaves it again when submerged after one or multiple TECs have been replaced. During the emerging and submerging process all TECs are non-functioning and thus produce no electricity. This process has also been described in paragraph 5.2.1.

TEC replacement

Once the platform is submerged, the failed TEC can be removed by using the vessel's crane and is positioned on deck. Afterwards, a functioning TEC is picked up from the deck and installed in the empty slot of the floater, as is described in paragraph 5.2.1. During the TEC replacement process all TECs are non-functioning and thus produce no electricity. This process has also been described in paragraph 5.2.1.

Intra-array transport

When the number of TECs which are to replaced at once are spread out over multiple tidal platforms, it is required to first commence maintenance at one platform and then, after submerging it, move on to the next platform. The sailing process between the different tidal platforms costs time and is thus a unique task.

More importantly, whilst the vessel waits in the port until it can perform its initial replacement activity, this is not the case for consecutive tidal platforms if more than one requires a TEC to be replaced. If there is no weather window for completing the replacement of the TECs at the next platform, the vessel will wait near the array until it becomes possible.

6.1.2. Weather windows

For a safe and successful execution of a number of tasks a weather window is required since operational limits apply, which are dependent on the harshness of the weather conditions.

The included operational limits are determined by three criteria, namely:

Limit 1 Vessel sea-keeping performance
Limit 2 Vessel station-keeping (using Dynamic Positioning (DP)) when interacting with the tidal platform
Limit 3 Motions of the vessel and tidal platform during the TEC lifting operation

The task durations and operational limits are determined by using the properties described in subsection 6.1.1 and expert judgment from within Damen [39].

Table 6.1: Required weather window of the maintenance operation

Task	Duration [hours]	Limit	Environmental limits			
			Hs [m]	Tp [s]	Uwind [m/s]	Ucurr [m/s]
Vessel preparation	48	-				
TEC loading	1	-				
TEC unloading	1	-				
Waiting for weather window	0*	-				
Port-array transport	2	1	2.5		9	
Array-port transport	2	1	2.5		9	
Intra-array transport	0.5*	1	2.5		9	
Platform emerging	2	2	2		7	2.5
Platform submerging	2	2	2		7	2.5
TEC replacement	1	3	1.5		6	2

* The mentioned duration is applied when no weather window related delays occur. This duration will therefore increase if waiting for a weather window of successive maintenance tasks is required.

Lack of T_p limits

It must be mentioned that, although in this analysis no limits are set with regard to T_p, it will still be included in the maintenance model. This is due to the fact that Damen uses in-house tools, which also take the combination of weather conditions into account, for calculating the DP vessel limits in which T_p is also included as a limit. Whilst the implementation of the respective tools is not included in the scope of this research, it was desired by Damen to build a model framework which can easily incorporate this in the future.

Additionally, T_p is used to describe the multivariate dependence between environmental variables more realistically. This multivariate dependence will be explained further in chapter 8 and further substantiates the decision to include T_p from a modeling point of view.

6.2. Maintenance vessel

Damen Shipyards is interested in using vessels from their current portfolio to perform the maintenance activities. It is therefore decided that the vessel of choice is the Damen Utility Vessel 6516 [23], which is commonly used for light duty supporting and maintenance tasks at offshore locations. It is very similar to the regular PSV design, but its equipment is carefully selected for performing maintenance activities, such as the A-frame crane located at the aft of the vessel for lifting operations.

The vessel is represented in this thesis' model by means of three parameters, namely the sailing speed, the deck space and the day rate. Each of these parameters is explained more in the next paragraphs.

6.2.1. Sailing speed

The sailing speed is essential for calculating the time it requires to sail from the port to the tidal array. For the Damen Utility Vessel the sailing speed is 12.0 knots, which is equal to 22.2 km/h. In this research the sailing speed is assumed to be constant, even though this may differ in reality (both in positive and negative sense) due to the influence of environmental influences.

6.2.2. Deck space

The available deck space determines how many TECs can be transported at once. This influences the overall maintenance time in the case that more than the maximum transportable TECs are desired to be replaced. In this case the vessel will need to sail back to the port to resupply after the initial replacement until the total number of replacements has been completed.

The selected Damen Utility Vessel has 450 m^2 of deck space, being roughly 15 meters wide and 30 meters long. Whilst no exact sea keeping regulations for these new loads are known at this moment, it's been assumed that the TECs will most probably be placed in transverse direction on the deck. This enables the operator to position four TEC carriage constructions on the vessel of which three can carry a new TEC for replacement. The last one is required to place the initial failed TEC at, since this one is first removed from the tidal platform before one of the new TECs is lifted from the vessel.

In the maintenance optimization model the option of increasing the maximum TECs is also considered, which may be realized by rearranging the TEC placement if less restrictions turn out to apply.

6.2.3. Day rate

The day rate of the Utility Vessel varies greatly and is subject to numerous factors which are related to the job availability, market status and the duration the vessel is rented for. The industry commonly distinguishes rates based on the type of contract:

- Spot contract: contracting a vessel when it is needed
- Term contract: contracting a vessel for a predefined term

Term contracts, and especially long term contracts, most often lead to a discount in the day rate and are thus favorable if the required vessel activities are certain for an extended amount of time. In this case, since the deployment of commercial tidal devices has only recently started, it is assumed that for the base case only spot contracts are used. This also gives a conservative approach for determining the maintenance costs, as the most expensive day rate type is used.

Spot contract day rates

The day rates of offshore vessel are closely monitored by a number of market analysts. For determining the vessel rates of the Damen Utility Vessel the analyses performed by Clarksons Platou [20] are used, which is a renowned maritime data analyst company. The selected Utility Vessel agrees best with the spot day rates of medium sized PSVs in the North Sea area with a deck space of 500-899m^2. The Utility Vessel 6515 has 450m^2, so this assumption is reasonably substantiated.

A large fluctuation in the day rates throughout the years can be observed in figure 6.2. In the last 10 years the day rates ranged from about 5,000 GBP to 24,000 GBP per day. This variation in rates will most probably continue throughout the life time of the tidal array, so several cases can be defined. For the base case the day rate is selected to be constant at 12,000 GBP per day ($\approx$ €13,500). However, in section 10.3 a sensitivity study will be performed which analyzes the effect of applying different day rates.

Additional operation costs

Besides the vessel day rates, some other cost centers cannot be neglected and should also be included when calculating the overall operation cost rate. Within this research the following two cost centers are also included:

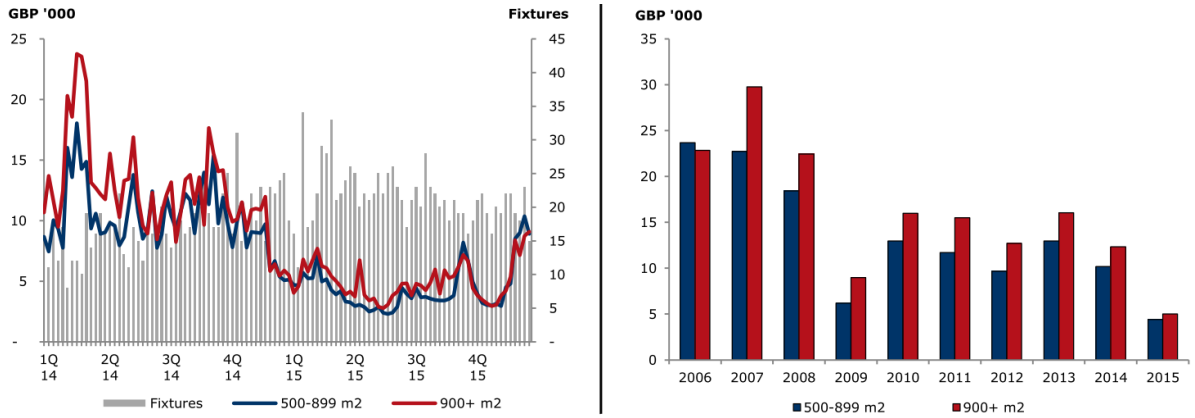

Figure 6.2: Spot day rate of PSVs in the North Sea area

- Specialized personnel/technicians for supervising the offshore maintenance operation
- Fuel costs of the vessel

Personnel

The following is assumed with regard to specialized personnel:

- A team of two specialized technicians should always be present on the vessel when maintenance is being performed for supervising and troubleshooting.
- The personnel enters the vessel just before departure from the port and remains on board until the vessel has returned to port after a successful operation. They are thus not present during the loading and unloading of TECs.
- The technicians are paid $ 125/h (≈ €110) per person [70].
- Limitations to personnel maximum working hours are excluded from the model, so the possible necessity of multiple shifts with additional personnel is disregarded. In practice this could be represented by two 2-man teams which each have a 12-hour shift.

Fuel costs

The fuel costs of the vessel are also included in the cost rate calculation, by means of a number of simplifications. Fuel consumption data of a reference vessel [107] is used to define three rates of fuel consumption, which are shown in table 6.2. The price of the required MGO fuel type is assumed to be 400$/$MT$ (≈ €360), based on current market prices [18].

Table 6.2: Damen Utility vessel fuel consumption

Idle in port	Sailing	Maintenance operation (DP)
1 MT day	13 MT/day	6 MT/day
360 €/day	4680 €/day	2160 €/day

Task cost rate overview

The three identified operation related cost contributions can be added together in order to determine the overall vessel operation cost rates per defined task. Table 6.3 gives an overview of the costs per hour, rounded off to the nearest €5, and will be used as the base case input for the model.

Table 6.3: Vessel operation cost rates

Task	Vessel costs [€/h]	Personnel costs [€/h]	Fuel costs [€/h]	**Net costs [€/h]**
Vessel preparation	565	-	195	**760**
TEC loading	565	-	15	**580**
TEC unloading	565	-	15	**580**
Waiting for weather window	565	-	15	**580**
Port-array transport	565	220	195	**980**
Array-port transport	565	220	195	**980**
Intra-array transport	565	220	195	**980**
Platform emerging	565	220	90	**875**
Platform submerging	565	220	90	**875**
TEC replacement	565	220	90	**875**

Part III

Model development & results

7

Maintenance model framework

This chapter provides information regarding the maintenance model framework. Section 7.1 visually represents the framework and introduces the three main processes of the decision support tool. The remainder of this chapter will give a brief explanation of each process of the model. This will assist to put the outcomes of chapter 8 and 9 into the correct perspective.

7.1. Model overview

As was already briefly touched upon when describing the thesis outline in section 1.11, the model which has been developed consists out of three main processes, namely the generation of environmental time series with multivariate dependence, the failure and maintenance representation of the observed tidal system and lastly the optimization of the maintenance policy. In figure 7.1 the model's main framework is visualized.

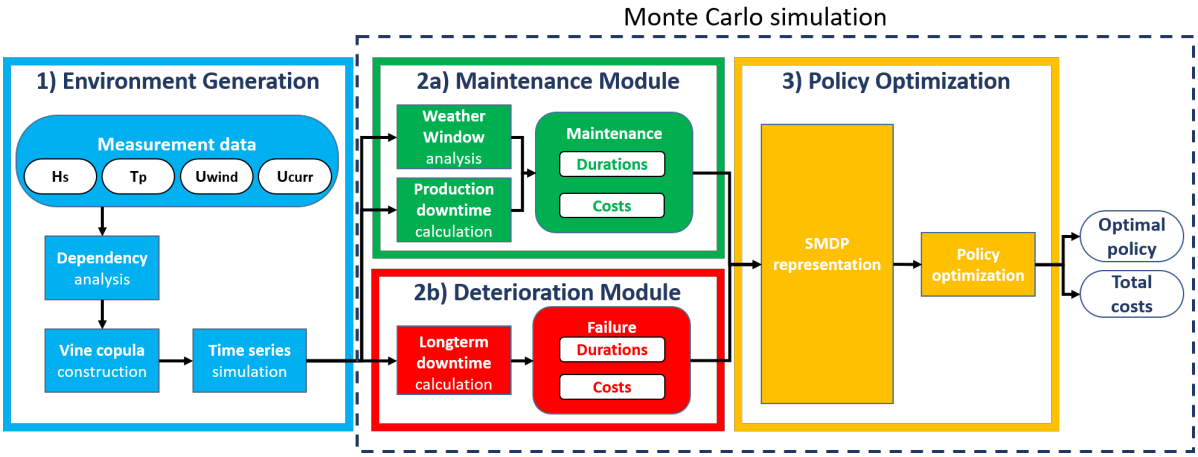

Figure 7.1: Model framework

7.2. Input

Multiple input types are identified within this model, which are either defined by the user (e.g. system topology) or based on the availability of external data (e.g. environmental measurements). The main input categories are listed below. An overview of the model inputs can be observed in appendix E.1 and gives a good understanding on what parameter sensitivities can be analyzed by using this model.

- Environmental measurements

- Tidal system parameters
- Power generation parameters
- Vessel parameters
- Maintenance activity parameters
- Financial parameters

7.3. Process flow

7.3.1. Environmental generation

As can be noted in figure 7.1 this module consists of three steps:

1. Analyze the multivariate measurement data
2. Build a vine copula which describes the identified dependence
3. Simulate synthetic time series from the vine

Probabilistic modeling using Monte Carlo simulations

The first two steps are executed only once per measurement set to build the vine copula and determine its parameters. Then, numerous synthetic time series are simulated randomly, but do have identical statistical properties. Due to this, the randomness of the environment can be described by implementing this set of time series (e.g. N_{sim}=1000) in the remainder of the model, similar to a Monte Carlo (MC) approach.

This results in a large number of independent time series which are independently run through the remainder of the model. Each simulation will have its own respective properties being calculated by the other processes and also result in an unique optimal policy, which by itself is a deterministic result.

Having run all the simulations, the individual policy and cost outputs can be combined to generate a probabilistic distribution. This ensures that the maintenance uncertainty due to the environmental influence is also included in the model results.

7.3.2. System and decision representation

This process consists of two modules, which are directly related to the available decisions when attempting to optimize the maintenance policy. The decision can either be to perform maintenance by replacing one or more TECs, or to let the system deteriorate due to TEC failures. Each module calculates the required data in order to provide the decision making process with the required input to optimize the policy, based on all available decisions.

Maintenance module

Each of the simulated synthetic time series is forwarded to this module, in which the following occurs:

1. Determine all possible maintenance activities based on TEC component quantities and topology
2. Determine the weather window using the operational limits for all combinations of maintenance activities and synthetic time series
3. Calculate the total duration and the direct costs (due to vessel day rates) of all maintenance activities for each synthetic time series

In section 7.3.1 it was already described that a large number of synthetic time series are generated, which are run through the model. This implies that, as is stated above, each of these time series is used to calculate the total duration for all possible maintenance activities.

Doing so will result in a distribution of the total maintenance duration, based on the predefined task durations and corresponding operational limitations. An algorithm has been developed to perform all these tasks and will be further explained in chapter 9.

By multiplying the duration of the maintenance activity by the day rate of the vessel, the direct costs of maintenance are determined.

Failure module

Two processes occur in this module:

1. Calculate the indirect maintenance costs due to the lack of electricity production during the TEC down-time
2. Calculate the overall failure rate and product cost of each TEC based on the individual component failure rates and costs

The indirect costs consist out of the lack of electricity production for a given duration, multiplied with the cost of electricity, due to down-time after a failure. To calculate the production losses during downtime, the U_{curr} time series is used as an input for the current velocity and combined with the power curve of a TEC.

The second process in this module, calculating the overall failure rate and product costs, run independently from the above-mentioned process. All individual component failure rates are combined and represented as one characteristic failure rate for the TEC. Likewise, the ratio between the components is used to determine the overall product cost of new TEC.

7.3.3. Maintenance policy optimization

The maintenance policy optimization process is extensively described in chapter 9 and is responsible for two tasks:

1. Correctly formatting the calculated data into the SMDP format
2. Optimizing the SMDP problem to determine the optimal group based maintenance policy

As is shown in figure 7.1, all data which describe the transition probabilities, rewards, transition rates and decisions have been calculated in the previous modules. Several algorithms then combine this to represent it in the correct format for the SMDP by linking it to the set of possible system states.

This data is then fed to the policy optimization algorithm, which iterates until the optimal maintenance policy is obtained which minimizes the costs per time unit, and thus has the highest gain.

7.4. Output

7.4.1. Deterministic output of a single simulation

The formal output of a single simulation in the model is a deterministic optimized maintenance policy for the described system. The output of the model answers the following question:

If a TEC fails, should maintenance be performed and if so, how many TECs should be replaced at once?

7.4.2. Analysis of probabilistic results

In the model numerous of MC simulations take place, which may not result in the same optimal policy, given the randomly generated environmental inputs. The combined output which is generated by all simulations thus should be interpreted as the probabilistic results due the the maintenance uncertainty which is imposed by the environment.

The obtained distributions for all of the optimal policies and total maintenance costs must then be analyzed in order to select one, or multiple, policies which are defined as optimal. The selection of an optimal policy is fully dependent on the required certainty that the decision maker desires and this research will only make recommendations.

7.5. Model assumptions

Numerous assumptions are made in each of the modules, and will all be explained in the corresponding chapter. In order to give a first insight in the possibilities and restrictions of the developed model, some main

assumptions are already listed below. The argumentation for the inclusion of each of these assumptions are described in the respective chapters.

7.5.1. Failure related assumptions

1. A constant component failure rate is assumed, this implies that only random assembly failures are modeled. Wear-out failures are not considered.
2. Multiple TECs will never fail at exactly the same time, so deterioration occurs in singular steps of one failure at the time.
3. TECs can fail during maintenance operations, but this is limited to a maximum of one.
4. Failure can only occur when the TECs are operational.
5. Assemblies within the same TEC will never fail at exactly the same time. This means only one assembly can be broken simultaneously within each TEC, as the TEC stops operating immediately after failure.

7.5.2. Maintenance related assumptions

1. Minimum reliability constraints, such as a minimum required number of operating TECs, are not considered.
2. A maintenance vessel is always available when deciding to perform maintenance, albeit at a distance which requires sailing time. The mean sailing time has been defined as the duration of the 'vessel preparation' task.
3. The delays in the overall operation duration are exclusively due to waiting for weather windows.
4. The TEC repairs will be performed onshore for the calculated representative assembly costs.
5. The components are 'as new' after reparation.
6. Functioning TECs are always directly available at the port.
7. The number of function TECs on stock is always sufficient for any maintenance operation. This can be achieved by having as many TECs on stock as will be maximally replaced at once and assuming a negligible replacement time of the failed assembly.
8. Once the maintenance activity is initiated, it cannot be canceled anymore.
9. The TEC with most failures will always be maintained first.

7.5.3. Electricity production related assumptions

1. The TECs in the array are not subject to wake effects due to nearby water-structure interaction.
2. All TECs have identical power curves
3. The power generation properties of all TECs are identical to each other.
4. No efficiency losses occur due to wear-out of the assemblies.
5. Marine fouling (and its negative effects) is considered negligible, due to the design of the blades and use of fouling control coatings [110].
6. The control system is assumed to be optimal, which is why a fixed value for C_p can be used.

8

Generation of environmental time series including dependence

This chapter will provide answers to the first research question posed in this research by performing an extensive analysis on the generation of multivariate environmental time series which contain multivariate dependence. For realistically describing the maintenance uncertainty in the decision support tool, it is of great importance to include the multivariate dependence in the synthetic time series, as this resembles reality better.

RQ 1 How can the environmental effects at tidal hotspots be realistically modeled?
- (a) Can dependence between the variables be identified and explained?
- (b) What model is best used to generate time series which includes multivariate dependence?

Section 8.1 describes the measurement dataset which is used in this research. Multiple tests are included which have been performed to determine what environmental effects and interactions are significant enough to be included when simulating time series. Together with the bivariate dependence analysis in section 8.2, which also compares the results to a reference study, research question 1a is attempted to be answered.

It was already mentioned in subsection 2.7.2 that existing theories on copulas and vines do not have a readily available solution if the analyzed data contains strong time dependence. This is highly undesirable, as incorrect dependence will be attempted to be modeled in the vine algorithm. Section 8.3 identifies the time dependence in the data set used in this research.

Section 8.4 proposes two new methods for effectively simulating univariate time dependence and multivariate dependence from the data set. The best method will be used to answer research question 1b. The generated synthetic time series can then be used to describe the maintenance uncertainty due to the environmental influence. This introduces a probabilistic property to the model and will be achieved by running MC simulations for the remainder of the maintenance model.

Lastly, section 8.5 is dedicated to identifying and explaining the added value of using the newly developed method to describe the environmental influence in the maintenance model. This is achieved by performing three comparison studies between properties of the simulated synthetic time series and alternatives, such as using the original time series or removing the multivariate dependence.

8.1. Analysis of EMEC environmental measurement data

8.1.1. Data availability

EMEC's tidal testing location has two sensors which have been logging environmental data. A bottom-founded Acoustic Wave and Current (AWAC) is used to log the wave and current data and a meteorological (MET) station measures the wind speed and direction. More information regarding the measure technology can be

read in appendix D.1. Below the variables are presented will be used in this analysis. These were obtained from EMEC's data logs.

AWAC data:
- Significant wave height *[m]*
- Peak wave period *[s]*
- Peak wave direction *[deg]*
- Horizontal current velocity *[m/s]*
- Horizontal current direction *[deg]*

MET data:
- Wind velocity *[m/s]*
- Wind direction *[deg]*

The measurement dataset consists of 7922 samples with an interval of 10 minutes, which describe the period from July to September. No additional data was available for this research, so the seasonality of the environmental conditions could not be observed.

It is therefore important to state that the conclusions in this research cannot be extrapolated for long-term statistics without further research. However, for the purpose of this thesis, the available data will be assumed to represent long term environmental conditions in order to be able to feed the maintenance model with input data.

Data quality

The environmental dataset contains raw measurement data and has not been quality checked by EMEC. The data contains both negative and extreme values for H_s and T_p, including a small period of no measurements. In order to determine the multivariate dependence using copulas, the measurement data of all four variates needs to be usable for each sample.

By filtering the dataset for each of the four variables, the time samples for negative (if applicable) and extreme values are identified, so these can be removed from the analysis. Furthermore, the data is smoothed to reduce local fluctuations and measurement errors. The exact process of filtering and sampling can be read in appendix D.2.

Location of sensors

A bottom-founded AWAC is located at the position of the red dot in figure 8.1, which is part of EMEC's tidal location. What is important to notice is that this tidal array, like many others, resides in a sheltered area. The nearby islands and shallow water are the reason why the tidal current flows significantly faster than in nearby open water locations.

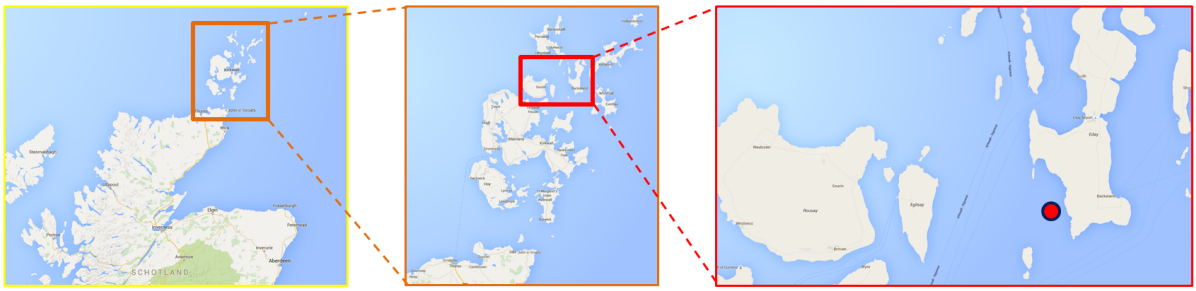

Figure 8.1: Geographical location of EMEC [35]

8.1.2. Influence of directionality on the wave-current interaction

Extensive research has been done on the interaction between the waves and currents [48, 109] which have identified a number of effects which may be important to include in the time series modeling. It was found that waves are strongly modulated by the tide. Significant wave height and period are mainly controlled by time-varying water depth, but wave periods are also affected by a Doppler shift produced by the current [13]. Also, a numerical model at EMEC showed local occurrences of tidal lumps, which is the amplification of the wave height when waves and current are in opposing direction [55].

The dependence between the variables can be effectively described by using copulas. Still, it must be considered whether the directional data of the waves and currents is to be included in the dependence analysis or whether this can be excluded since it does not affect the vessel's working windows. Therefore, an analysis is performed on the influence of directionality on the wave propagation direction and the presence of tidal lumps.

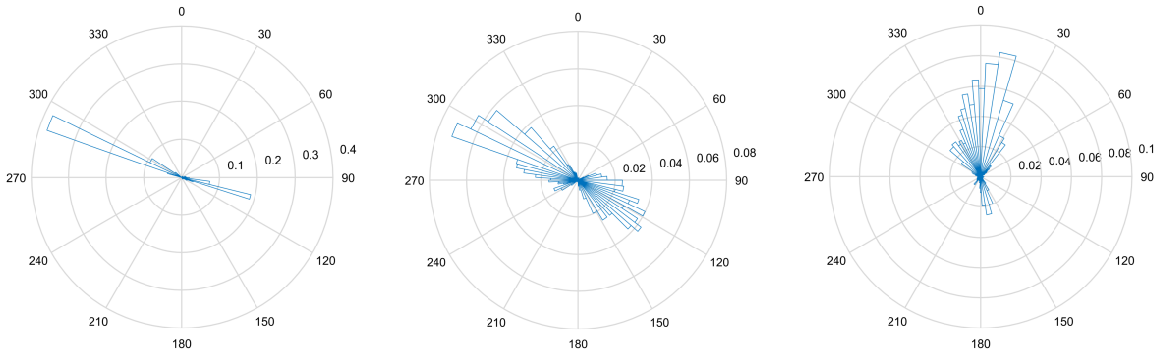

(a) Current velocity direction [deg] (b) Wave propagation direction [deg] (c) Angle between current velocity and waves propagation [deg]

Figure 8.2: Rose plots of the absolute and relative wave and current velocity directionality

The wave and current directions have been plotted in figure 8.2. The number of occurrences when the current and waves have opposing directions is not significant when inspecting figure 8.2c and it seems that at the EMEC measurement location the recurring character of the tidal current direction is dominant for the peak wave direction. This can also be observed in figure 8.3, which show the directions of waves and current in time.

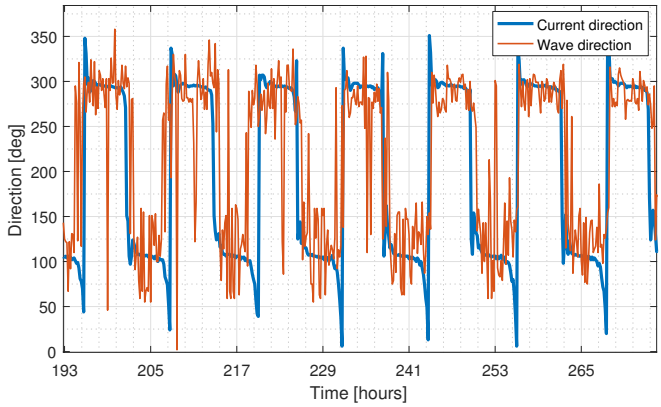

Figure 8.3: Current and wave direction time series

The effects which occur at opposing directions are analyzed more extensively. It can be observed in figure 8.4b that no amplification of the wave height occurs in the event of opposing directions of the current and waves. Figure 8.4a shows that this situation mostly occurs when the current velocity is relatively low, showing a peak at 0.5 m/s. This may be an indication that the wave propagation direction generally follows the current direction with a slight lag. This could explain why the peak in occurrence for opposing direction is found at low current velocities. This is further analyzed by plotting the time series of both the current and wave propagation direction. The resulting time series is shown in figure 8.3 and shows that mean wave propagation follows the current accurately, but does show relatively small fluctuations (<30 deg) around its mean.

From figure 8.4 the absence of tidal lumps cannot be fully explained, significant wave height and current velocity are uncoupled as the time of occurrence is not included. In order to further substantiate the evidence for the lack of tidal lumps, both variables are coupled in a boxplot to observe what environmental combinations occur in case of having the same and opposite direction. The boxplot is depicted in appendix D.4 and shows that no significant change in the significant wave heights can be seen between the samples de-

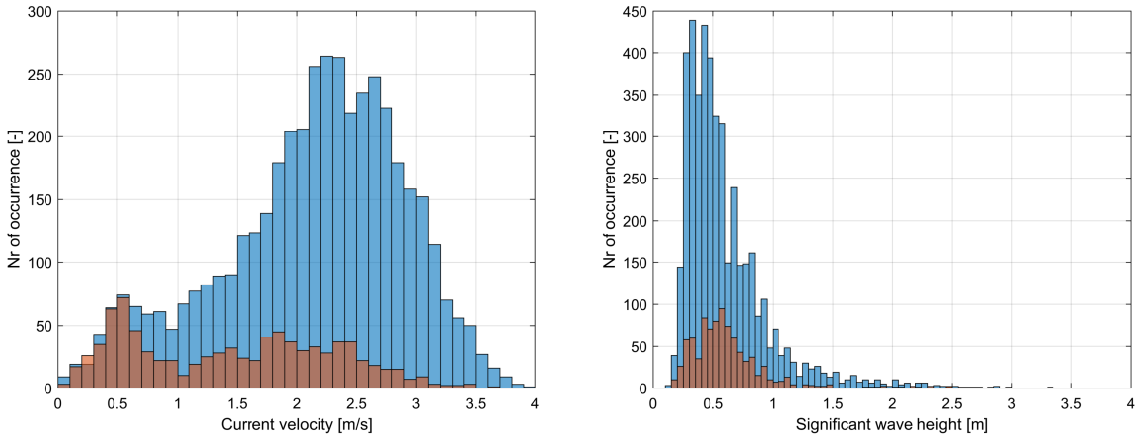

(a) Current velocity: Same (blue) & opposing direction (red) (b) Wave Height: Same (blue) & opposing direction (red)

Figure 8.4: Histograms for current velocity and significant wave height for two relative propulsion directions (same vs. opposite)

scribing the same and opposing direction. Given the available measurement data from EMEC, it can thus be concluded that no amplification of the wave heights can be observed due to its directionality. It is therefore decided to exclude the directionality data of the wave and current variables in this research, as it does not noticeably influence the resulting output.

8.1.3. Influence of directionality on the wind-wave interaction

In the previous subsection it was shown that the current and waves directions can be excluded from the dependence analysis. It still is of interest to check whether the wind direction may have a significant influence on the vessel operability, as the wind may blow unfavorably from the transverse direction. Figure 8.5a shows the rose plot for the wind direction and it can be observed that North-North-West (note that the figure shows the 'To' direction) was the prevailing wind direction during the months July and August, with only little fluctuations from other directions.

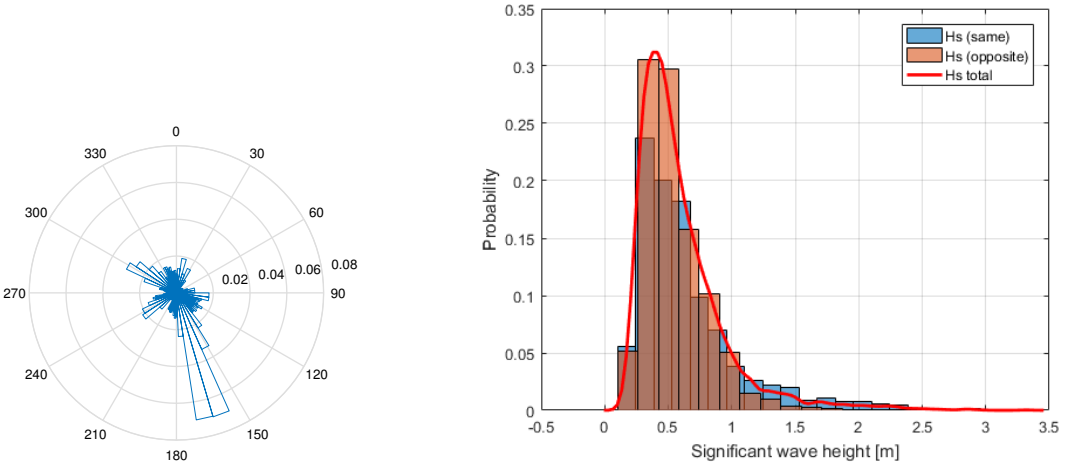

(a) Rose plot of wind directions [deg] (b) Histograms for significant wave height with the same and opposite direction as the wind

Figure 8.5: Prevailing wind direction and effect on significant wave height

The prevailing direction only deviates 30 degrees from the mean wave and current direction (120/300 deg), so the wind, waves and current are reasonably co-linear. Figure 8.5b shows a difference in the significant wave height can be observed when the wind and waves direction is either the same or opposite. Still, the two distributions do not vary significantly, with the exception of a slightly longer tail for waves propelling

Table 8.1: Peak data analysis of current velocity frequency spectrum (directional data)

Npeak	f [10^{-4} Hz]	T [h]	Phenomenon
1	0.1161	23.92	*2x Semi-diurnal period*
2	0.2246	12.37	Semi-diurnal period
3	0.4453	6.24	*1/2x Semi-diurnal period*
4	0.6699	4.15	*1/3x Semi-diurnal period*
5	0.9020	3.08	*1/4x Semi-diurnal period*

in the South-East direction. Additionally, the wind is a driving force and is not influenced by the waves and currents.

Excluding the wind direction would remove this variation of significant wave height occurrences, based on the wave propagation direction. Instead, the total significant wave height distribution would then be applied for both wave propagation directions, giving a corresponding probability distribution of the wave height which is depicted in figure 8.5b as the solid red line. It can be seen that the discrepancy between each of the directional histograms and the total distribution is relatively small. In this research it is therefore decided to also remove the wind direction, as its effect on the wave height is negligible and the wind direction itself is mostly fixed.

8.1.4. High frequency wave-current interaction

The tidal current velocity profile is a recurring semi-diurnal process, due to the position moon and sun being the major driving forces. The low frequency phenomenon is easily detected in the actual tidal velocity, but this does not necessarily result in the optimal way of defining dependence between the current velocity and the wind and wave variates. High frequency interaction may occur, which are related to the wind and wave phenomena and can possibly describes the dependence better. It is thus desirable to analyze whether this hypothesis can be accepted and dependence should be modeled by implementing exclusively the high current velocity frequencies, rather than the absolute current velocities which also include the semi-diurnal process.

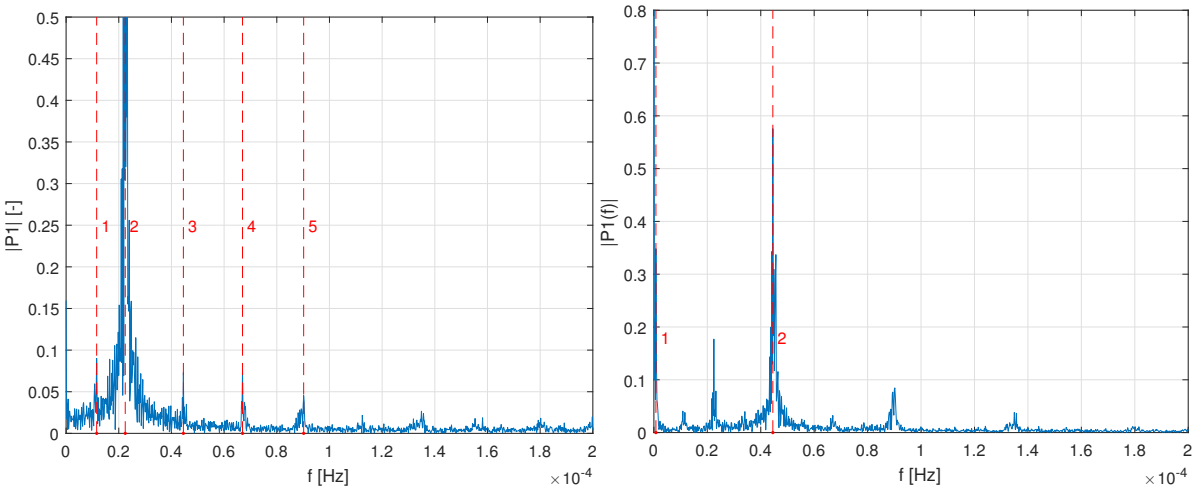

(a) Single-sided amplitude spectrum of current velocity frequencies (directional data)

(b) Single-sided amplitude spectrum of current velocity frequencies (absolute data)

Figure 8.6: Frequency spectrum plots of directional and absolute current velocity data

Table 8.1 shows the frequency and period information of the identified peaks of the current velocity frequency spectrum in figure 8.6a, which is composed using the measurement data at EMEC. The identified amplitude peaks in the frequency spectrum exclusively describe tidal related phenomenon, as peak 2 resembles the semi-diurnal tide period (T_{tsd} = 12.25 hours). The small discrepancy between measurement and actual period is explained by an uncertainty bandwidth of the measurement data when determining the actual peak

frequencies. The remainder of the identified peaks are directly related to the semi-diurnal tide period, as they are ratios of this phenomenon, which can be explained by the fact that the recurring peaks are not identically shaped. This results in this numerical effect, which attempts to describe this slight discrepancy by adding more frequencies. Also, the peak describing the semi-diurnal tide (peak 2) is significantly higher with respect to its linked peaks, which expresses itself in a dominant presence within the measurement data.

The Fourier analysis has also been performed on the absolute current velocity measurements, as an attempt to identify initially hidden characteristics. The resulting plot is depicted in figure 8.6b in which only the largest two peaks are highlighted. Peak 1 occurs at a frequency which was insignificant at the Fourier analysis with directional data. Its frequency fully corresponds to the spring tide period, as this occurs almost twice a month, around new moon and full moon. The sun, moon, and earth form a line (a condition known as syzygy [94]), which amplifies the tidal range and velocities to its maximum. The second peak can also be fully explained, as it describes the semi-diurnal period of the tide, albeit twice as small due to using the absolute value.

Table 8.2: Peak data analysis of current velocity frequency spectrum (absolute data)

Npeak	f [10^{-4} Hz]	T [h]	Phenomenon
1	0.0076	364.96 (=15.21 days)	Spring tide
2	0.4453	6.24	Semi-diurnal period (absolute, thus x2)

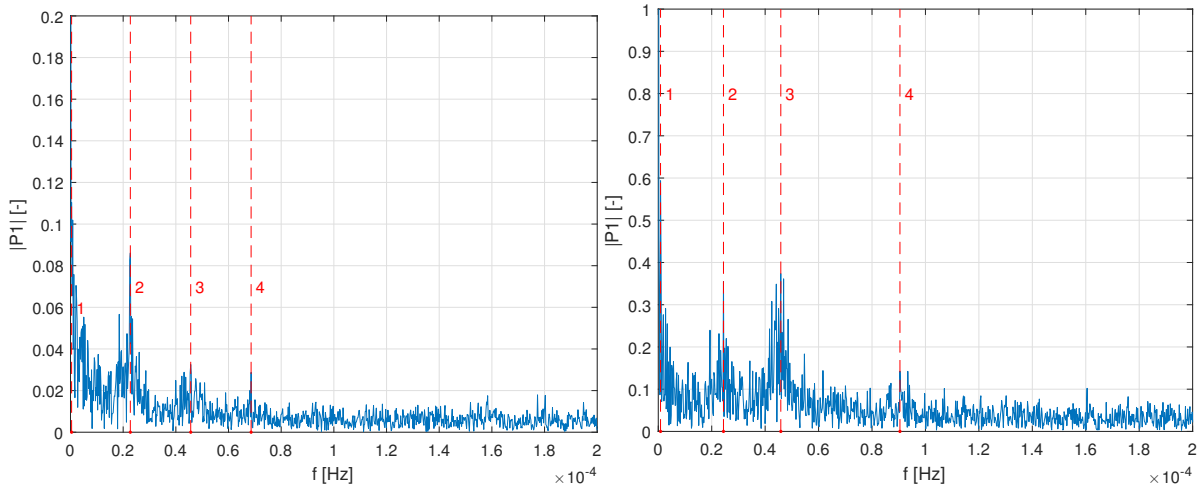

(a) Single-sided amplitude spectrum of significant wave height frequencies

(b) Single-sided amplitude spectrum of peak wave period frequencies

Figure 8.7: Frequency spectrum plots of the significant wave height and peak wave period

Having identified the five largest peaks in the directional frequency spectrum and two in the absolute frequency spectrum, the remainder of the frequencies consist mostly of white noise and produce no significant amplitude. The occurring frequencies of wave height and wave period are significantly higher, as can be seen in figure 8.7a and 8.7b. These frequencies cannot be identified in the current velocity frequency spectrum. This absence of non-tidal related amplitude peaks in the frequency spectrum implicitly proves that the current velocity at the EMEC site is not subjected to noticeable high frequency interaction with the occurring waves.

The observations in this analysis prove that no high frequency current-wave interaction can be identified in the measurement data. This results in two conclusions which relate to the copula analysis and sample generation later in this chapter. First of all, the representation of the tidal velocity variate should be performed in its absolute form, instead of attempting to filter out the semi-diurnal frequency components and perform the multivariate dependence analysis with high frequency components. Secondly, as no significant peaks occur at the wave frequencies, it can be assumed that the current velocity variable is dominant and one of the driving forces in the system. This characteristic will be applied in section 8.4 for the sampling of multivariate time series.

8.2. Vine construction

Having shown that for this instance the directionality of the wind, wave and current can be excluded from this dataset for effectively describing the governing sea states at the EMEC tidal location, the next step is developing the vine pair-copula construction to describe the multivariate environmental dependence.

8.2.1. Bivariate dependence

The first step in constructing the vine is determining the factorisation of the variables at the base level. This is done by calculating the Kendall's Tau rank correlation and connecting the strongest bivariate pairs to function as the vine's base.

Using Kendall's Tau, as described in subsection A.1.3, the following Kendall rank correlations can be observed from the bivariate data. The value 0 implies full independence and +1/-1 imply full positive and negative rank correlation, respectively.

Table 8.3: Kendall's Tau rank correlations of environmental bivariate data

	Uwind	Hs	Tp	Ucurr
Uwind	1.000	0.121	-0.089	-0.003
Hs	0.121	1.000	0.077	-0.069
Tp	-0.089	0.077	1.000	0.394
Ucurr	-0.003	-0.069	0.394	1.000

it shows that the highest dependence can be found between:

- Ucurr-Tp (0.394)
- Uwind-Hs (0.121)
- Uwind-Tp (-0.089, *negative*)

Comparison to results of related studies

Having shown this, it should be noted that the the identified bivariate dependence is significantly lower than existing research results [65], as shown in appendix D.5 on the dependence between H_s,T_p and U_{wind} at sea. This fundamental difference in results can be explained due to a number of reasons, which should be carefully considered to uphold the validity of both researches and interpret the data in this research correctly.

Firstly, the EMEC location is geographically different than the location at which dependence were found. The values from the reference study correspond to the open sea, with a water depth of 650 meters where the wind is prevalent as the driving force. Hence, wind driven waves are expected to be observed at that location, which is clearly seen in the dependence between the wind and wave variables. As is seen in figure 8.1, the north east direction of the EMEC tidal location is blocked by the island. This creates blockage of the wind, so the fetch is very limited and it can thus be assumed that wind-driven waves are less occurring at the shallow water tidal location.

Secondly, the inclusion of the high current velocities as an additional environmental driving force, besides the wind, creates a different situation in which the waves are not exclusively wind-driven at the tidal location. Figure 8.2c shows that the wave direction is near identical to the tidal current direction in most samples, which indicates that the current influence is much more dominant than the wind. Whilst these current forces will never occur at open water locations, it does give a possible explanation why the bivariate dependence does not correspond well.

Lastly, the comparison study uses multi-year datasets in which the extremes are observed. The time interval is 30 hours, which ensures that the the logged data is time independent, as is also shown by the calculation in this thesis in subsection 8.3.2. The EMEC data only describes short-term measurement data of 2 months, with a 10 minute interval. This has resulted in data which does not contain extreme weather events, in which a possible strong (upper tail) dependence can be observed.

8.2.2. Vine type selection

Before walking through steps 1 to 5 in the vine building procedure, as described in section 2.5, the vine type should be determined to determine which bivariate copula pairs are to be developed at each level. Within this research only the well described C- and D-vines are included for the vine type selection. Fitting a C-vine is usually considered when a particular variable is known to be a key variable that governs interactions in the data set. In such a situation one may decide to locate this variable at the root of the canonical vine to ensure the system dependence can be best described by copulas.

However, when observing table 8.3, it becomes clear such key variable is not present in this situation and thus the C-vine does not bring advantage in terms of representing the multivariate dependence. Instead, due to a relative evenly spread of dependence pairs amongst the variables, a D-vine is preferred and will be used to describe the multivariate dependence throughout the remainder of this research.

8.2.3. Base level factorisation

Having selected the D-vine construction, the necessity of the base level factorisation arises. The four variables have to be factorized in such way that the highest Kendall Tau rank correlation pairs are observed at the base level. Whilst no widely accepted method is described in the literature, besides a full model comparison based on AIC and BIC, a simple approach is proposed in this research, which maximizes the sum of the absolute Tau values of the three bivariate pairs. Table D.3 display the result of this approach and demonstrate that the optimal factorisation is as shown in figure 8.8.

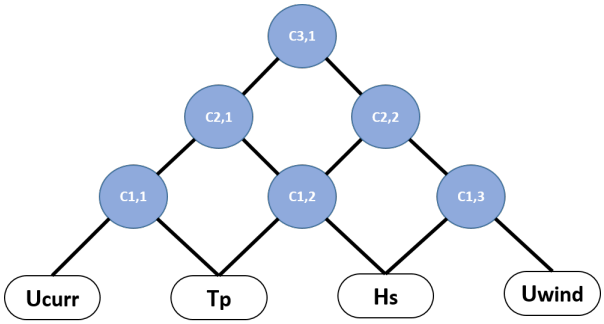

Figure 8.8: Factorisation of variables at D-vine base level

8.2.4. Copula selection

Once the factorisation is known it is possible to determine what copula families best describe the three pairs of bivariate dependence at the base level.

Pseudo-observations

Initially the processed measurement data need to be converted to its corresponding pseudo-observations in order to enable the representation using copulas. The method has been described in paragraph 2.3.1 and enables to describe the empirical dataset into uniform marginal distributions.

For the selected factorisation, as seen in figure 8.8, the following bivariate sets of pseudo-observations are obtained:

By visually inspecting the pseudo-observations of the three bivariate pairs, a difference in dependence can already be identified. Since the Kendall Tau correlation values are not especially large (i.e. $\tau > 0.5$), the best corresponding copula family for describing the bivariate dependence may not be selected by merely visual inspection. Still, given the distribution of the scatter plots, some preliminary conclusions can be drawn on the most likely copula families for each of the pairs.

Figure 8.9a shows a clustering of scatter points in the upper right corner, which implies that some magnitude of upper tail dependence is present between U_{wind} and H_s. Given the mentioned copula tail dependence properties, a Gumbel or Survival Clayton copula will most likely best fit this data.

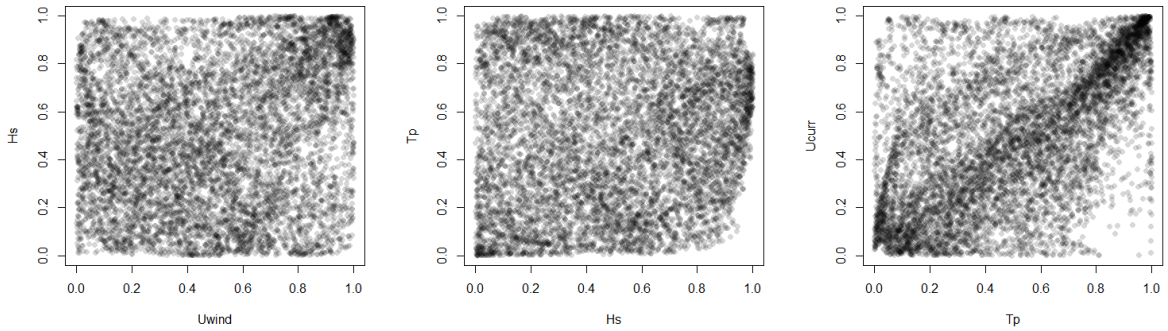

(a) Uwind - Hs (b) Hs - Tp (c) Tp - Ucurr

Figure 8.9: Scatter plots of pseudo-observations

Figure 8.9b depicts a near uniform spreading of the points, with a very small clustering in the lower left corner, which indicates a weak, but noticeable lower tail dependence between H_s and T_p. This can lead to the conclusion that either a Clayton or Survival Gumbel describes this dependence best.

The last subplot, figure 8.9c, has a distinct cluster of pseudo-observations in both bottom left and top right corner. This may indicate that this dependence is best represented by the Student-T, with both lower and upper tail dependence, but in the SouthEast-NorthWest diagonal some clustered pseudo-observations can be noticed, possibly indicating that the bivariate dependence can describe the entire range. For this dataset the Student-T, Gaussian and Frank copulas have the closest resemblance to the pseudo-observation plots.

Fitting copulas to the data

The visual inspection of the pseudo-observations already gave a hint about which copula families best describe the dependence of the three pairs. Still, to ensure the best fitting copula family is selected, the GoF test is conducted, as described in subsection 2.3.3. First the Kendall's Tau rank correlation is used to determine the copula parameter(s) and then these are compared using AIC and BIC. The results are plotted below for the bivariate sets.

Table 8.4: Copula fitting statistics for bivariate data U_{wind}-H_s

Copula family	logLik	AIC	BIC
Gaussian	122.79	-243.57	-236.60
Student-t	117.63	-231.26	-217.31
Clayton	4.09	-6.18	0.80
Gumbel	175.90	-349.80	-342.82
Frank	138.07	-274.13	-267.15
Survival Clayton	**232.20**	**-462.41**	**-455.43**
Survival Gumbel	27.19	-52.38	-45.40

Table 8.4 shows that the Survival Clayton performs best when fitted to the data, with the Gumbel as the second best. This was already predicted when visually inspecting the pseudo-observations and thus matches with our initial findings. The Survival Clayton copula will be applied for representing the dependence between U_{wind} and H_s, with the corresponding copula parameter, $\theta_{Clayton} = 0.29$.

Table 8.5 also has a good resemblance of what could be visually identified from the pseudo-observation plots. The Clayton copula performs best when fitted to the data, with the Survival Gumbel as the second best. The Clayton copula will be applied for representing the dependence between U_{wind} and H_s, with the corresponding copula parameter, $\theta_{Clayton} = 0.19$.

The copula fitting statistics of T_p and U_{curr} data already gave uncertainty when inspecting the pseudo-observations. Looking at table 8.6 it can be noted that the Student-t, Gumbel and Frank copulas fit the data

Table 8.5: Copula fitting statistics for bivariate data H_s-T_p

Copula family	logLik	AIC	BIC
Gaussian	72.44	-142.88	-135.90
Student-t	55.46	-106.92	-92.97
Clayton	**114.14**	**-226.28**	**-219.30**
Gumbel	6.61	-11.22	-4.25
Frank	48.36	-94.73	-87.75
Survival Clayton	7.19	-12.38	-5.40
Survival Gumbel	89.37	-176.74	-169.76

Table 8.6: Copula fitting statistics for bivariate data T_p-U_{curr}

Copula family	logLik	AIC	BIC
Gaussian	1276.97	-2551.94	-2544.97
Student-t	1402.30	-2800.61	-2786.65
Clayton	754.95	-1507.89	-1500.91
Gumbel	**1479.73**	**-2957.46**	**-2950.49**
Frank	1439.98	-2877.97	-2870.99
Survival Clayton	1307.06	-2612.12	-2605.14
Survival Gumbel	1048.87	-2095.75	-2088.77

best. Based on the fitting analysis, the Gumbel copula is the most optimal fit by a small margin. However, since the both a lower and upper tail was identified in figure 8.9c, selecting the Gumbel copula would result in a loss of the lower tail dependence characteristics when sampling synthetic time series, whereas a Student-t copula would be able to effectively describe it.

Still, the Gumbel copula is selected for describing the dependence betwen T_p and U_{curr} since we are mainly interested in the upper tail dependence, e.g. the variable dependence at rough seas, to use a conservative approach for determining the available weather windows during maintenance activities. The corresponding Gumbel copula parameter is, $\theta_{Gumbel} = 1.58$.

8.2.5. Vine property overview

The described method in section 2.5 was used to build the of the D-vine and describe the copulas at the different levels. Table 8.7 gives an overview of the best fitting copulas at each level, including the corresponding Kendall's Tau of the conditional distributions. The corresponding contour plots of the copulas with standard normal marginals can be seen in appendix D.7. It can be observed that the dependence decreases as the level of the vine increases, which corresponds with literature. However, this results in an even weaker dependence between the variables which are not linked at the base level.

Table 8.7: D-vine copula parameters

Copula	Copula family	Copula parameter	Kendall's Tau
Tree 1			
C(1,1)	Gumbel	1.58	0.37
C(1,2)	Clayton	0.19	0.09
C(1,3)	Survival Clayton	0.29	0.13
Tree 2			
C(2,1)	Rot. Clayton 270 degrees	-0.24	-0.11
C(2,2)	Rot. Gumbel 90 degrees	-1.12	-0.11
Tree 3			
C(3,1)	Gumbel	1.11	0.10

8.3. Existence of time dependence in time series

As is stated in section 2.6, to apply copulas vines to simulate a dataset, the time series should consist out independent of identically distributed random variates [2, 65, 67]. Several methods have been identified to obtain time independence in time series, such as using an ARIMA [38] and GARCH [14] models. These require a thorough analysis of the data and may not be easy to implement, hence they are excluded from the possible solution space. The most straight forward method is by increasing the time interval between samples, effectively reducing the number of data points which are included in the copula analysis. As will be shown in subsection 8.3.2, this approach results in the removal of valuable data, especially since the original EMEC dataset only describes a limited time span.

This section describes the identification of the univariate time dependence and a new approach for describing the univariate time dependence by using the existing vine copula theory. This approach is then further extended to combine the, in section 8.2 described, multivariate dependence of the four variables together with the respective time dependence.

Exclusion of tidal current variable during simulation

Whilst this method can be widely implemented to describe the time dependence, in this research a special case arises for the current velocity. The magnitude and occurrence in time of U_{curr} does not depend on quasi-random processes and can to a high accuracy already be predicted, based on the major driving forces behind it, namely the Earth's rotation and the influence of the Sun and Moon. Therefore, to preserve the consistency of the recurring tidal velocity profile, it is decided that the synthetic time series of this variable will not be simulated using the D-vine.

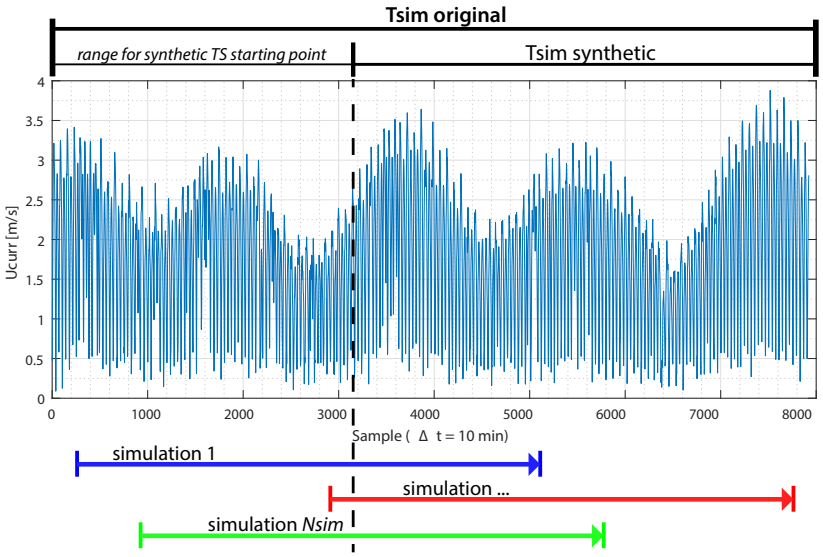

Figure 8.10: Copying a fraction of the original Ucurr time series

Instead the entire U_{curr} time series will be copied from the existing dataset and plugged into the D-vine for each time step, using a randomly selected starting point in the original time series. Figure 8.10 shows how the range is determined in which the starting point is randomly selected. This ensures that the sinusoidal character of the current velocity is maintained and the current velocity acts as the simulation input for the other environmental variables in the D-vine.

It must be noted that two disadvantages arise when applying this method to maintain the current velocity profile. Firstly, any local error or discrepancy in the U_{curr} dataset will be repeatedly included in the simulation of the synthetic time series. Secondly, using the existing U_{curr} data limits the maximum time series length to that of the original dataset. When the desired length of the synthetic time series approaches that of the

original set, the randomness of the starting point and thus the entire time series also reduces, which is an important side effect to take into account.

Still, within this research the synthetic time series are applied to calculate the weather windows of the vessel upon TEC failure and the indirect losses due to reduced production capacity. The original measurement set contains 7922 data points with 10 minute interval, describing a period of over 2 months. This is significantly longer than the maintenance activity will, if the maintenance policy requires a call to action.

8.3.1. Univariate time dependence

Univariate time dependence is best described by calculating the ACF of a time series and plotting its respective correlogram.

The autocorrelation coefficient at lag h is given by [17]

$$r_h = \frac{c_h}{c_0} \tag{8.1a}$$

$$c_h = \frac{1}{N}\sum_{t=1}^{N-h}(Y_t - \bar{Y})\cdot(Y_{t_h} - \bar{Y}) \tag{8.1b}$$

$$c_0 = \frac{1}{N}\sum_{t=1}^{N}(Y_t - \bar{Y})^2 \tag{8.1c}$$

The upper and lower confidence bounds (B) for correlation with a significance level (α) can also be plotted in the same correlogram. When the upper or lower bound are exceeded, the null hypothesis that there is no autocorrelation for the given lag is rejected. A test of randomness is conducted by observing the autocorrelation factor for adjacent timesteps (lag = 1) with a significance level of 0.95.

$$B = \pm z_{1-\alpha/2}\cdot SE(r_h) \tag{8.2a}$$

$$SE(r_1) = \frac{1}{\sqrt{N}} \tag{8.2b}$$

$$SE(r_h) = \sqrt{\frac{1+2\sum_{i=1}^{h-1} r_i^2}{N}} \text{ for } h > 1 \tag{8.2c}$$

8.3.2. Disadvantages of increasing the sampling time interval

Observing the correlograms in figure 8.11 it can be noted that the EMEC measurement data can not be considered to be time independent. The blue line in the figures represents the criterion to pass the test of randomness and at lag 1 this is not met. When increasing the time interval, it becomes evident in the plots in appendix D.8 that the increase in sample interval required (14.5 hours) to obtain time independence does not suffice. Too much data is lost in the process, bringing two disadvantages.

Firstly the characteristic current velocity profile is no longer described by the time independent data. The simulated time series from the D-vine will have the same time interval. Since these time series are applied for a weather window analysis, the minimum duration of each maintenance task will also inevitably increase together with the selected time interval. As we are interested in performing relatively short maintenance tasks in favorable weather conditions, such as during neap tide, the time interval should be in the same order of magnitude.

Secondly, the reduction in data also impacts the results of the multivariate analysis. When performing the bivariate dependence analysis with a time step of 870 minutes (=14.5 hours), ensuring full time independence of all three variables (U_{curr} is excluded), the number of samples reduces from 7922 to 92 points. This further decreases the reliability of the fitted copula with respect to the actual dependence, as less data is available for the fitting procedure. This loss in dependence is undesired and thus we continue with the original 10 minute

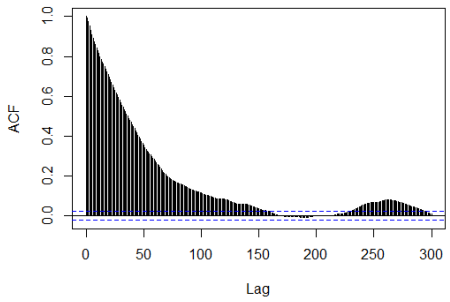

(a) Autocorrelation - Uwind

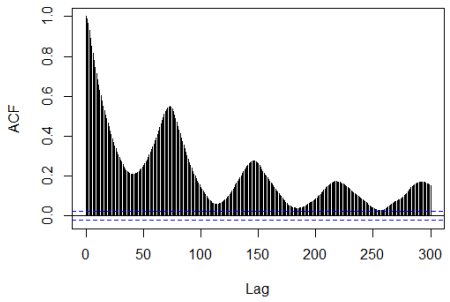

(b) Autocorrelation - Hs

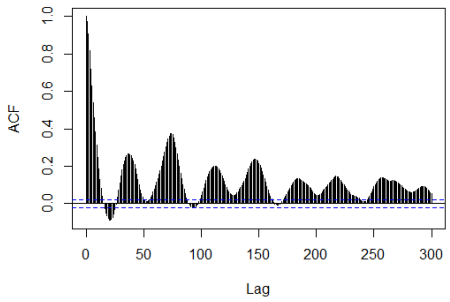

(c) Autocorrelation - Tp

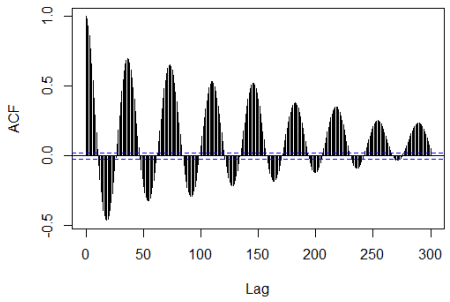

(d) Autocorrelation - Ucurr

Figure 8.11: Correlograms of EMEC timeseries (1 lag = 10 minutes)

time steps and develop a method to describe time dependence within the D-vine structure to preserve the limited measurement data.

8.4. New approach for simulating time and multivariate dependence

Several approaches are possible to combine the univariate time dependence with the multivariate dependence, each with their own distinct characteristics. Two methods have been considered in this research, which both apply a sequential simulation algorithm:

- Multivariate dependence → Univariate time dependence ($x3$)
- Univariate time dependence ($x3$) → Multivariate dependence

Both methods are considered sequential as they use a two-step algorithm to simulate synthetic time series with both types of dependence. Part of the proposed algorithm , the multivariate dependence modeling, has already been extensively explained in section 8.2. The sequential simulation method combines default multivariate D-vine with new D-vines. Each of these new D-vines, one for each variable in the multivariate D-vine, is filled with its own univariate time lagged variates. Simulation from this D-vine should result in synthetic time series which describe time dependence.

8.4.1. Developed simulation algorithm

The developed algorithm uses the existing D-vine simulation method as its foundation, but extends the simulation methodology to enable the simulation of univariate time series which include time dependence. Before explaining how the multivariate vines are coupled to the univariate vines, it is first required to elucidate the simulation process of univariate time series which include time dependence.

Univariate time series simulation

The univariate time series simulation process is as follows:

Step 1 Build the D-vine by using N lagged sets of the univariate time series ($N = 3$ in figure 8.12)
Step 2 Simulate the full D-vine once using the method described in section 2.6 (figure 8.12a)
Step 3 Shift all generated variates and D-vine parameters one time lag (figure 8.12b)
Step 4 Simulate a new sample using only one random input and the shifted vine parameters (figure 8.12c)
Step 5 Repeat step 3 and 4 T_{sim} times to generate the full synthetic time series

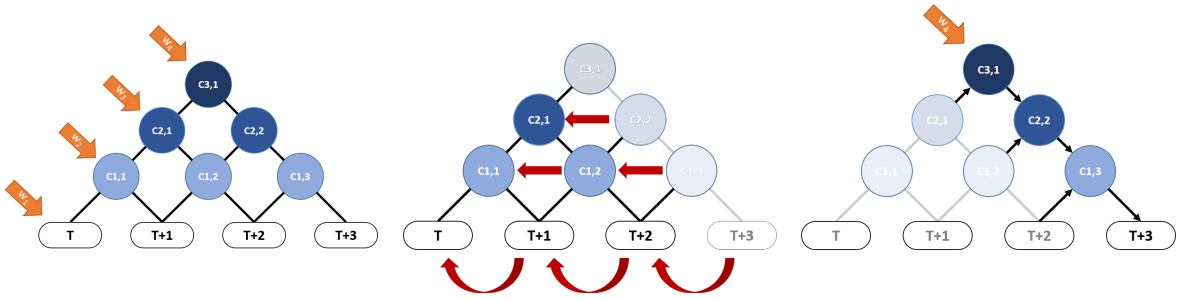

(a) Simulate full D-vine (b) Shift variates one lag (c) Simulate a new sample

Figure 8.12: Univariate time series simulation algorithm

By plugging lagged versions of the original univariate time series into the D-vine, the copulas in the vine are used to describe the time dependence between the lags. Simulation of a new sample, as seen in figure 8.12c includes the identified time dependence between the included lags and thus the persistence can be modeled.

Coupling of lagged univariate and multivariate vines

As mentioned, the results from the univariate time dependence vines are coupled to the existing multivariate D-vine, of which the characteristics are mentioned in subsection 8.2.5. The two approaches differ in the order of which the vine inputs and outputs are linked in order to analyze what the difference is on the overall result. Both approaches will be explained below to give more insight in the developed algorithm.

Approach '*Multivariate dependence → Univariate time dependence (x3)*' first simulates T_sim samples from the multivariate D-vine. The samples of the intermediate U_{wind}, H_s and T_p time series are then for each time step as the w_4 simulation input, as depicted in figure 8.12c. This will create three synthetic time series for the mentioned variables, which are added to the existing U_{curr} time series to obtain the final output.

Approach '*Univariate time dependence (x3) → Multivariate dependence*' does the exact opposite and first uses random numbers to simulate from each of the three univariate D-vines. This creates three independent time series (excluding U_{curr}). These are then plugged into the multivariate D-vine as w_2, w_3, w_4 input, sample per sample. The time series which are generated by the multivariate D-vine are the final output of this approach.

8.4.2. Analysis of univariate case

Before simulating any of the proposed methods, an analysis is performed on simulating time dependence in a time series for each of the three variables. Again, U_{curr} is implemented differently in the D-vine, so this variable is excluded from the analysis.

Two properties will be looked into, namely the number of time lags which is required as a minimum to sufficiently represent the original data and the influence of using different bivariate copulas. For both properties the quality of representation between the original and synthetic time series is investigated in terms of statistical properties and persistence.

As mentioned, the analyses will be performed for U_{wind}, H_s and T_p. However, only the results of U_{wind} will be visually presented in the next paragraphs, whereas the results of the other variables will only be mentioned if these vary from the U_{wind} case.

Influence of increasing time lags

To gain insight in the effect of increasing the time lags the time series of U_{wind} is represented by four PCCs, in which the time lags are included as follows in the base level of the D-vine structure:

1. $t_i - t_{i+1}$ $(d = 2)$
2. $t_i - t_{i+1} - t_{i+2}$ $(d = 3)$
3. $t_i - t_{i+1} - t_{i+2} - t_{i+3}$ $(d = 4)$
4. $t_i - t_{i+1} - t_{i+2} - t_{i+3} - t_{i+4}$ $(d = 5)$

For this specific analysis, the D-vine is restricted to only use the bivariate Gaussian copula for creating identical simulation conditions in which only the time lag varies. Also, the synthetic time series are simulated with a 10 minute interval, just as the original, and the seed for generating random numbers is kept fixed for all four simulation alternatives.

The D-vines are composed using the copula parameters that are listed in table 8.8. which in their turn are calculated from the Kendall Tau rank correlation of the bivariate, namely the original and lagged, dataset. The same rank correlation is found for all the lagged variants, e.g. $t_i - t_{i+1}$ and $t_{i+3} - t_{i+4}$, which both are described by a single lag. This is due to the fact that the bivariate samples have identical variate sets, except for a different starting and ending point in the dataset. Calculations showed that this is effect is negligible and thus all bivariate pairs within the same lag have identical properties.

Table 8.8: Kendall rank correlation of the conditional distributions at each vine tree and copula parameter

Tree	τ	θ_{Gaus}
1	0.92	0.99
2	-0.55	-0.76
3	0.42	0.61
4	-0.09	-0.14

Upon plotting one instance of each of the synthetic time series of U_{wind}, as is depicted in figure D.12, a number of phenomena can be observed when comparing the output. Bear in mind that a fixed seed is used for generating random numbers, so the comparison focuses on the characteristic differences between simulations and less on the actual representation of the original time series.

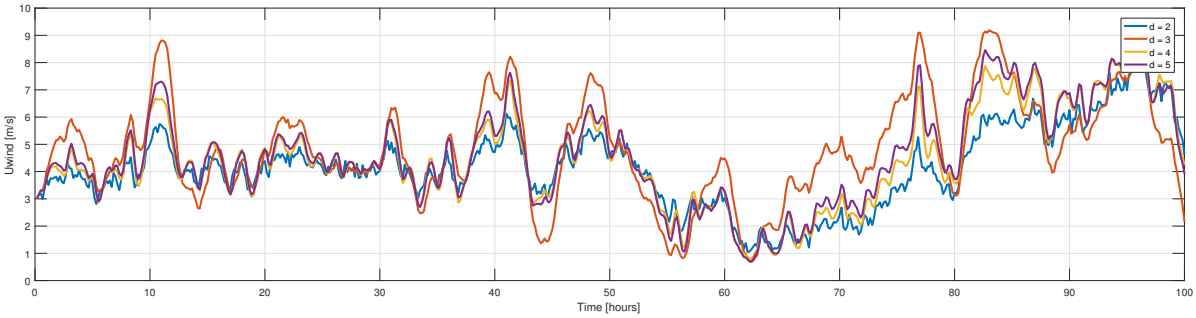

Figure 8.13: Simulated time series of U_{wind} for different lags ($\triangle t$ = 10 min)

It can be observed that all four simulation methods show a strong correspondence in the time series profile. Still, discrepancies can be seen, which are related to the number of used time lags in the D-vine base level. It seems that using one time lag (d=2) generates a relatively stable output signal, which is not sensitive to extremes. Using two time lags (d=3) does exactly the opposite and generally describes the maximum outlier when an extreme, both peaks and troughs, occurs. The other two methods (d=4 and d=5) give intermediate values and show a reasonably good correspondence with each other.

In this case, as described by table 8.8, the Kendall's Tau deteriorates as the time lag is increased. This phenomenon is very similar to that of what can be observed when plotting the correlogram of an univariate time series. Applying the same methodology, the number of included time lags should depend on the magnitude of the Kendall's Tau number, which may or may not exceed a threshold value, stating time independence of that time lag.

To further elucidate this new insight in the use of bivariate D-vine trees for describing time dependence, the simulated time series and the Kendall Tau values for the different D-vines are also displayed in figure D.13, D.14 and D.15 and table 8.9 for the situation in which only every second ($\triangle 20min$), third ($\triangle 30min$) and every sixth ($\triangle 1hour$) datapoint is used in the D-vine copula analysis.

Table 8.9: Kendall rank correlation of time lags and copula parameter

Lag	$\tau(\triangle 10min)$	$\tau(\triangle 20min)$	$\tau(\triangle 30min)$	$\tau(\triangle 1hour)$
1	0.92	0.85	0.79	0.67
2	-0.55	-0.27	-0.10	0.04
3	0.42	0.22	0.08	0.02
4	-0.09	-0.10	-0.01	-0.03

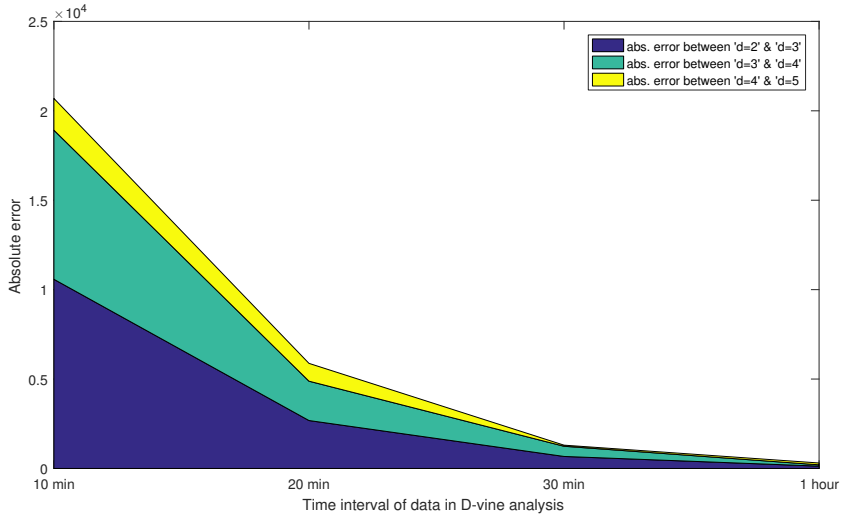

Figure 8.14: Error between simulation methods when increasing the time steps of the Uwind data

Bivariate independence test

As expected, the error between the $d = k$ and $d = k+1$ time series, plotted in figure 8.14, becomes smaller as the Kendall Tau number reduces to values near zero, indicating independence between the respective time lags and thus no significant improvement when increasing the number of time lags in the D-vine tree.

This observation can be formalized using a test of bivariate copula independence, similar to the threshold value when calculating the auto-correlation. The bivariate independence test [33] is based on Kendall's Tau and exploits the asymptotic normality of the test statistic:

$$statistic := T = \sqrt{\frac{9N(N-1)}{2(2N+5)}} \cdot |\tau| \tag{8.3}$$

where N is the number of observations and τ the empirical Kendall's Tau of the data vectors u1 and u2. The p-value of the null hypothesis of bivariate independence hence is asymptotically

$$p = 2(1-\Phi(T)) \tag{8.4}$$

where Φ is the standard normal distribution function.

In essence the extension of the D-vine for describing time dependence is not required to be any longer than the maximum non-independent time lag, using the above test. By varying the threshold of the p-value, which is usually set at 0.95, the allowable error between the different time lag methods of the synthetic time series can be further altered. This is especially useful when also considering the additional simulation time when extending the D-vine. A balance needs to be found between the level of accuracy of the synthetic time series and the simulation time of running the D-vine model.

Influence of changing copulas

In addition to varying the time lag, the influence on the synthetic time series is observed upon changing the bivariate copula family, which is implemented for describing the dependence between the lagged variates. In the previous paragraph it was proven that no significant difference was seen between using one lag and multiple when using one hour intervals and a noticeable discrepancy was observed with 10 minute intervals. In order to use this in our advantage, the comparison of different copula is done with 10 minute intervals and only one included time lag to amplify the effect of disturbance. Doing so will give insight in the stability of the copula families for the least accurate time interval.

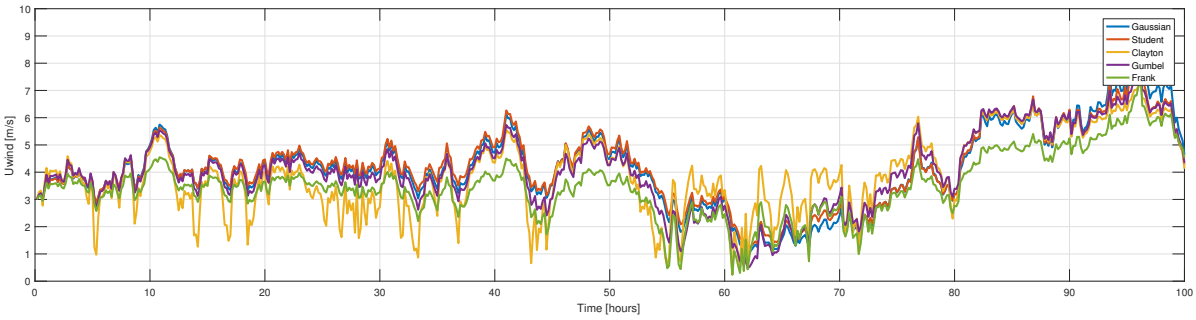

Figure 8.15: Simulated time series of U_{wind} for different copula families

Figure 8.15 depicts that varying the copulas results in significant differences in the U_{wind} profile. It can be noted that the time series which is related to the Clayton copula contains a large number of peaks, which return throughout the time series, both above and below the other time series. This peaked behavior is not realistic for describing wind velocities, since these rapid fluctuations of are rarely observed in measurements, whereas a more smoothed flow with only small local fluctuations, such as in the time series of the other four copulas, resembles wind profiles more accurately.

Additionally, the Frank copula time series seems to describe an underestimation of U_{wind}, when comparing it to the other simulated time series. When excluding the negative peaks of the Clayton time series it can be concluded that the Frank time series describes the lower limits of this time series. Whilst no theoretical explanation can be provided, this does state that the Frank copula is not a good copula for simulation, since it is conservative with respect to the others.

In this set of synthetic time series, no clear distinction can be made between the Gaussian, Student-t and Gumbel copula, so no concrete conclusion can be made on the choice of preference. What must be noted is that when running the copula fitting analysis, as described in paragraph 8.2.4, the preferred choice is the Student-t copula.

To further validate the findings and assumptions, this analysis has been rerun for the same dataset with three variations which are implemented both exclusively and simultaneously in different runs to check whether the Student-t copula family does indeed represent the lagged data best. These variations were changing the time step to one hour, including four lagged variates (d=5) and redoing the analysis up to now for the H_s and T_p variables. Results showed that the Student-T copula fitted the data best for all conditions, so it can be concluded that choosing the Student-t copula family is the preferred option for describing univariate time dependence, given the current dataset.

8.4.3. Goodness of Fit tests

In paragraph 8.4.2 and 8.4.2 the influence of changing the time lag and the copula families for simulating synthetic time series were analyzed qualitatively, as the results were only compared with respect to each other. This was possible due to the fact that, for a fixed seed, the time series looked relatively comparable and extraordinary behavior could be studied. However, now a selection has been made on the preferred simulation properties, namely simulating with either Gaussian, Student-t or Gumbel copula with a time interval of 10 minutes and 4 time lags (d=5), it is required to test the goodness of fit of the synthetic time series with respect to the original one.

Several tests have been developed to check the goodness of fit, which are each explained below. The purpose of these tests is not only to determine whether the choice of preferred simulation properties is valid. More importantly the goal is to gain additional insight in the fitting characteristics when simulation large numbers of synthetic time series and whether bivariate copulas can be applied in general to effectively model time dependence.

For the goodness of fit tests below, 1000 synthetic time series of U_{wind} were simulated, each with a different random seed and the following simulation properties:

- 4 time lags: $t_i - t_{i+1} - t_{i+2} - t_{i+3} - t_{i+4}$ $(d = 5)$
- Student-t copula
- 10 min time interval

Visual inspection

The first test to perform is a visual inspection in which the original time series of U_{wind} is compared to a number of synthetic time series. This test alone cannot give definitive conclusions, as the randomness of the synthetic time series will never give (near) identical fits. However, the trends of the time series can already indicate whether the synthetic time series do have a similar persistence to some extend.

In figure 8.16 the original time series of U_{wind} is plotted over two randomly selected synthetic time series for a duration of 100 hours.

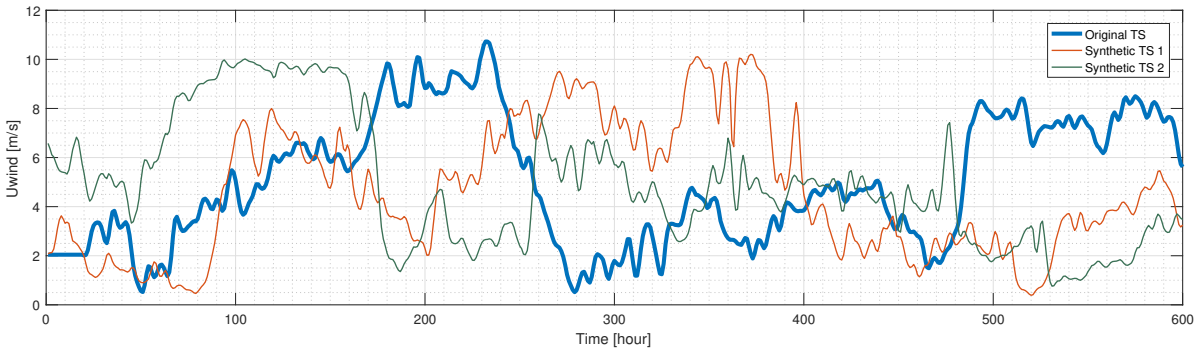

Figure 8.16: Visual comparison of original and two synthetic U_{wind} time series

Statistical properties

A second simple test is to calculate the mean and standard deviation for both the original and synthetic time series and compare the results. Since a large number of synthetic time series have been simulated, the individual values are not of particular interest. Instead, the distribution of the mean and standard deviation have been calculated, as can be seen in figure 8.17, which gives valuable information about the spreading of the synthetic time series. Table 8.10 contains all relevant data.

The results in table 8.10 show that the mean of the mean and mean standard deviation correspond very well with the original time series, which indicates a good fit. The spreading of statistical properties within the set of synthetic time series is more interesting however, since this says something about the accuracy of the simulation algorithm. Looking at figure 8.17, the spreading of the mean and standard deviation follows a

Table 8.10: Comparison of statistical properties of original and synthetic time series of U_{wind}

	$Original$	$Synth_{mean}$	$Synth_{std}$
$Mean$	4.9005	4.9035	0.2299
std	2.0522	2.0704	0.1047

normal distribution. This implies that the majority of the values is clustered around the mean value. By also inspecting the standard deviation of the two statistical properties, it becomes clear that the spreading is very limited and each of synthetic time series has a mean value between 4.4436 and 5.3633, and a standard deviation between 1.8610 and 2.2798, given a 95% confidence. Although no existing threshold is available in literature, this spreading stay well within the acceptable range from a simulation point of view. A larger spreading of the standard deviation would lead to more extremes in the time series, whereas an increase in the spreading of the mean would result in larger shifts of the entire dataset, which is also undesirable.

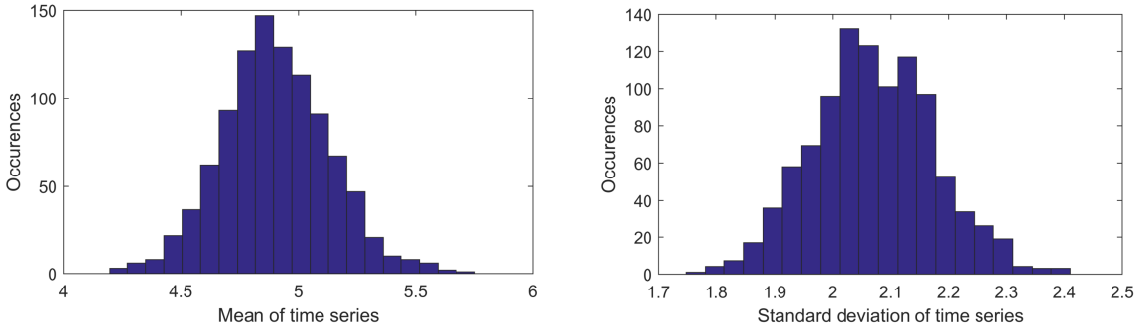

(a) Histogram of mean

(b) Histogram of standard deviation

Figure 8.17: Histograms of mean and standard deviation of synthetic U_{wind} time series

Markov Chain transition probabilities

The last test which is conducted to test the goodness of fit of the synthetic time series with respect tot the original time series is by means of Markov Chain transition probabilities. The Markov Chain has already been introduced in chapter 3 and this analysis applies the theory to define multiple states and the corresponding transition probabilities to get an indication on the persistence of the time series.

The analyses initiates by defining the states. In this analysis the states consist out of bins in which the value of U_{wind} resides in as time progresses. The states are chosen arbitrarily after some iterations on the bin bandwidths. It is important to state that the selection of bins has a significant influence on the result and should not be chosen too small. The approach for finding the correct number of states included the fulfilling of two conditions, whilst attempting to create as maximize the number of states to use as much data as possible:

- The transition matrix should not contain zero elements on the diagonal, implying too small bins in which states get skipped
- The only the first positive and negative non-diagonal entry should contain data

The selection of states which fulfill these conditions have been found and are listed in table 8.11.

Markov transition matrix

By calculating the transition of states for each time step, the transition matrix for the original U_{wind} time series is composed. The 3D bar plot of the transition matrix is depicted in figure 8.18a. The three non-zero diagonals are plotted in figure 8.18b, which describe the transition to a lower state (S_i to S_{i-1}), remaining in the same state (S_i to S_i) and transition to a higher state (S_i to S_{i+1}). The latter plot is basically a 2D projection of the 3D bar plot, as seen from the origin.

Table 8.11: States of the U_{wind} time series

State	bin [m/s]	State	bin [m/s]
1	[0,1)	7	[6,7)
2	[1,2)	8	[7,8)
3	[2,3)	9	[8,9)
4	[3,4)	10	[9,10)
5	[4,5)	11	[10,11)
6	[5,6)	12	[11,12)

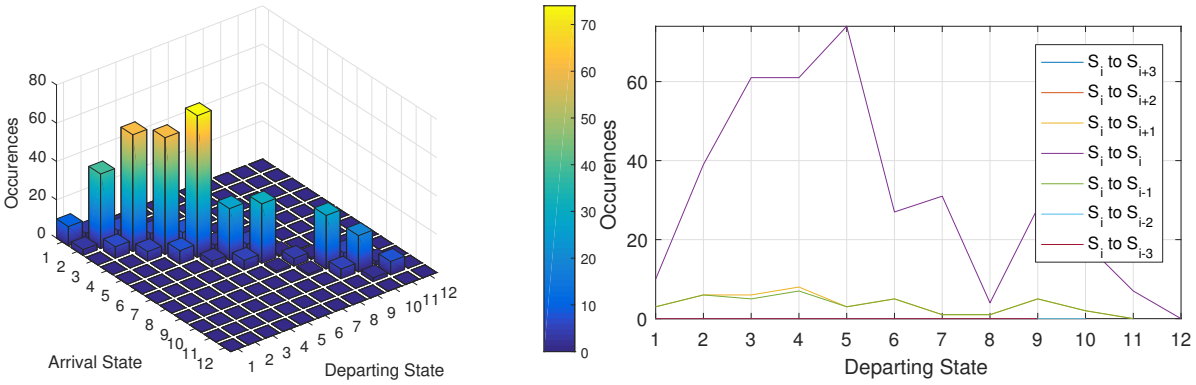

(a) 3D bar plot of transition matrix

(b) Plot of state transitions

Figure 8.18: Transition matrix of original U_{wind} time series

Index of dispersion

The index of dispersion [21] is a normalized measure of the dispersion of a probability distribution: it is a measure used to quantify whether a set of observed occurrences are clustered or dispersed compared to a standard statistical model.

$$D = \frac{\sigma^2}{\mu} \tag{8.5}$$

In figure 8.19 the mean, standard deviation and index of dispersion of the error distributions are depicted for different time lags. It can be observed that all three parameters decline as the time lag increases and approach a horizontal asymptotic value. Interesting about these plots is that the error margin and its spreading decrease as the time lag increase, which indicate that the representation of the persistence of synthetic time series with respect to the original time series improves as larger time periods are observed.

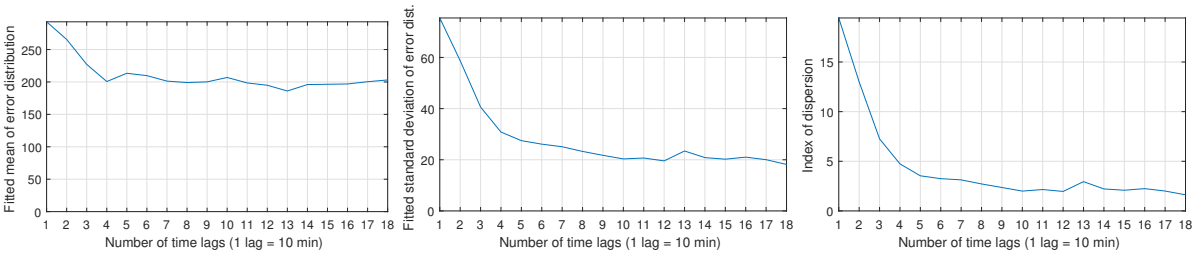

(a) Mean value

(b) Standard deviation

(c) Index of dispersion

Figure 8.19: Statistical properties of error distribution for different time lags

The mentioned findings rely on a qualitative approach, since the error values of the time lags are only compared to that of the original time interval ($\triangle t$ = 10 min). Still, combined with the previous two goodness of fit tests, it can be said that the use of bivariate copulas to describe univariate time dependence is indeed

possible and the persistence in the original time series has increasingly matching properties when analyzing longer time intervals.

8.4.4. Expansion to multivariate case

It's been proven in subsection 8.4.3 that the bivariate copulas can be applied for describing time dependence in univariate time series by simulating from a D-vine with lagged variates. The final step is to expand this method from the univariate case to the multivariate case. This will combine three sets of univariate time dependence (as stated, U_{curr} is copied from the existing dataset to preserve its profile) and the multivariate dependence. In the following paragraphs the newly proposed method is described and some results are discussed.

It is important to state that the cross-correlation, e.g. the dependence between Hs_t and Tp_{t+1}, is excluded from this analysis to prevent these unexplained effects from affecting the simulation results. However, with the same methodology as is stated in previous sections for the univariate time dependence D-vine modeling, it is also possible to construct the cross-correlation if desired.

Both simulation methods were executed and it was observed that the synthetic time series of '*multivariate dependence → univariate time dependence*' lost all of their multivariate dependence, but did include the univariate time dependence. Whilst this multivariate dependence was significantly lower than the univariate dependence between lagged variates, it is significant enough not to be neglected. Given this undesired result, this method was thus not optimal for simulating both time dependence and multivariate dependence.

The '*univariate time dependence → multivariate dependence*' method showed considerable better results when inspecting the synthetic time series. Since the multivariate D-vine algorithm is placed at the end of the simulation, this dependence is fully included, which is one of the key properties which the synthetic time series should have. The corresponding Kendall's tau rank correlation of one simulation is seen in table 8.12 and shows good correspondence with the rank correlation of the original time series, noted in table 8.3.

Table 8.12: Kendall's Tau rank correlations of ne synthetic time series realization

	Uwind	Hs	Tp	Ucurr
Uwind	1.000	0.087	-0.074	-0.004
Hs	0.087	1.000	0.061	-0.059
Tp	-0.074	0.061	1.000	0.327
Ucurr	-0.004	-0.059	0.327	1.000

Having identified that the algorithm which is placed at the end presumably is dominant when simulating synthetic time series, it was expected to see a lack of time dependence, and thus no realistic time profile and persistence, when using the latter simulation method. However, visual inspection of the synthetic time series, such as in figure 8.20, showed that for the entire set of synthetic time series the desired persistence was still present, but possibly in a slightly weakened form with respect to the univariate time series, as described in section 8.4.2.

A possible explanation for the effectiveness of this newly developed method is the fact that the strongest dependence, the cases of univariate time dependence, was simulated first in a D-vine. These results could then be plugged into the second D-vine, describing multivariate dependence, as the input in which a considerably lower dependence was observed, as can be seen when comparing table 8.3 and 8.9. This resulted in only minor alterations of the already developed persistence within univariate time series, while the multivariate dependence was included.

No additional research was performed on why this significant difference occurred in the properties of the synthetic time series between the two methods, so no solid evidence can be given to support these statements.

Still, applying the '*univariate time dependence → multivariate dependence*' has proven to be an effective method for simulating time series which have both multivariate dependence and univariate time dependence. This application of copulas and vines has up to now not been seen in literature and may well be a new approach for simulating these dependences, based on data. It is advisable to perform more research on the

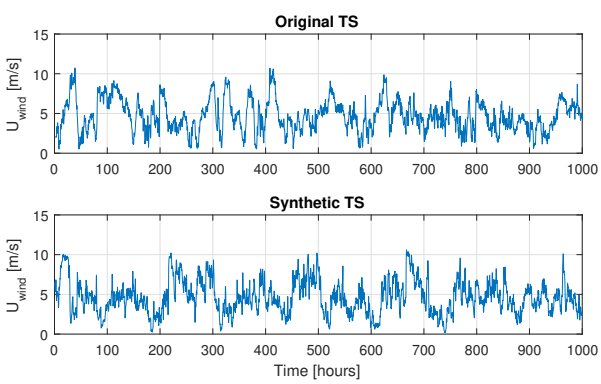

(a) U_{wind} time series

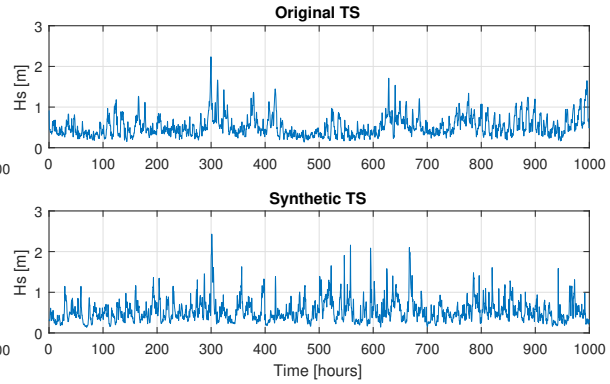

(b) H_s time series

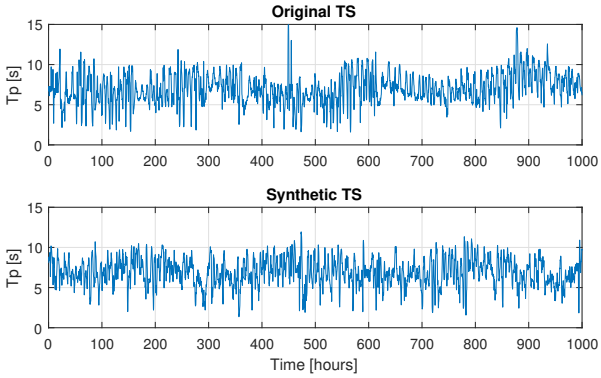

(c) T_p time series

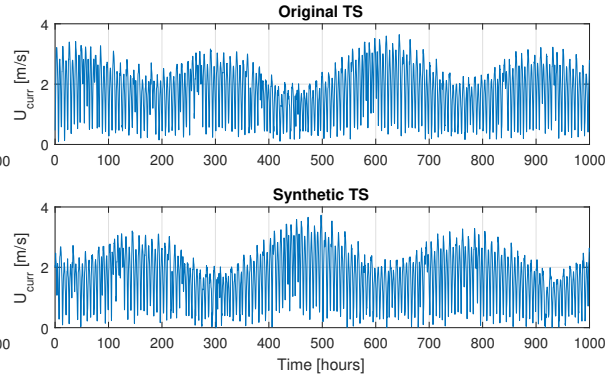

(d) U_{curr} time series

Figure 8.20: Comparison of original time series and one synthetic time series realization

definite effects of applying this simulation method on other types of data with the same dependences, but different magnitudes.

8.4.5. Synthetic time series validation

A validation study has been performed to justify the application of the simulated synthetic time series to represent the actual measurements. The validation is based on a comparison of the cumulative distributions of the weather window persistence in the original and synthetic time series. This approach has already been used in a similar study [58], which also includes multivariate dependence modeling.

For the valudation in this research the weather window persistence is observed for one maintenance task, namely the 'TEC replacement' task. The task is exensively described in subsection 6.1.1. It has operational limits for the H_s, U_{wind} and U_{curr} and therefore can be effectively used to validate the multivariate time series. The task has the following operational limits:

- H_s limit: 1.5 m
- U_{wind} limit: 6.0 m/s
- U_{curr} limit: 2.0 m/s

Figure 8.21a shows the cumulative distribution functions of the persistence for 1000 simulated time series, using the newly developed algorithm, and compares it with the weather window persistence in the original time series. It can be observed that the results from the synthetic time series are well clustered around the original time series. This is a strong indication that the synthetic time series have nearly identical statistical properties, whilst including randomness to represent the uncertainty. Figure 8.21b further substantiates this claim, as the mean persistence of the synthetic time series closely follows that of the original time series.

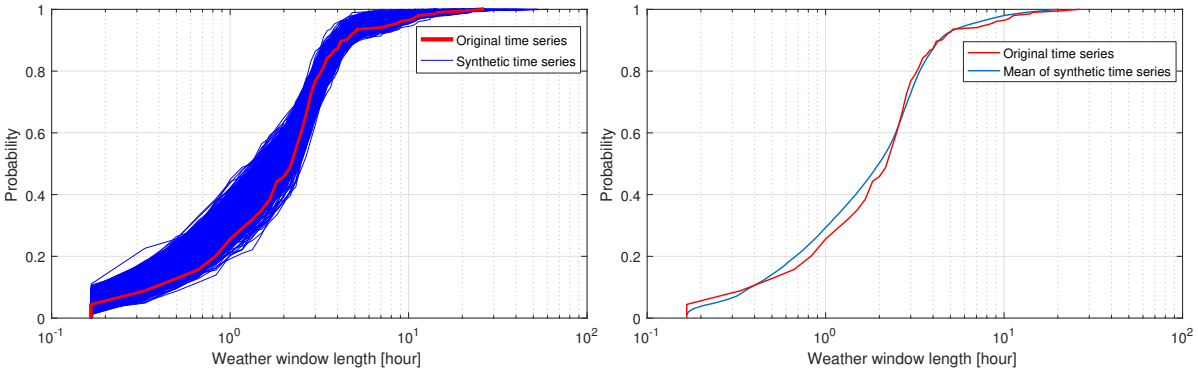

(a) CDF of the persistence in the original and synthetic time series (N_{sim} = 1000)

(b) CDF of the persistence in the original and mean persistence of the synthetic time series

Figure 8.21: Comparison of the cumulative distribution functions of the persistence in the original and synthetic time series

It is therefore concluded that the developed algorithm for simulating synthetic time series with both multivariate dependence and time dependence can be effectively implemented in the overall maintenance model, as these show a strong resemblance to the weather window persistence of the original time series.

8.5. Added value of using copulas for time series simulation

In this chapter it has been shown that it is possible to use pair-copula constructions to simulate new realizations of time series with multivariate dependence. Besides that it is just as important to show the added value of implementing this method when considering functionality of the overall maintenance model, as is described chapter 7. An analysis is therefore conducted to identify the results of running the maintenance model with exclusively the original measurement data from EMEC, and running the model with the synthetic time series which have been generated by using copulas.

In this comparison study the developed maintenance model uses identical input parameters, so only the blue model block of the model framework overview (figure 7.1) is varied. No insight is given in this section in the maintenance model modules itself, as this will be extensively explained in chapter 9. Instead, the main focus will be on a comparison of the probabilistic maintenance activity duration for replacing an arbitrary number of TECs. This is directly influenced by the weather window uncertainty, which is induced by the interaction between the vessel's operational limits and the used environmental time series.

The following comparison studies will be conducted to determine the added value of using copulas for time series (TS) simulation:

1. Original TS ⟷ Synthetic TS
   (a) Fixed starting point (t=0)
   (b) Variable starting points
2. Synthetic TS with/without multivariate dependence

8.5.1. Original TS ⟷ Synthetic TS

Two scenarios are used when comparing the effect of the original time series to the synthetic time series. The first scenario compares the original and synthetic time series for a fixed starting point in order to determine what the influence is of generating more realizations to introduce uncertainty.

The second scenario enables multiple varying starting points in both the original and synthetic time series. This enables multiple simulations to be extracted from the same original time series in order to compare the probabilistic results of an approach without (original TS) and with copulas (synthetic TS).

For each analysis only the maintenance activity durations of replacing 1,5 and 10 TECs are depicted in this section. The full overview of activity durations from 1 up to and including 10 TEC replacements are available in appendix D.11.

Scenario 1: Fixed starting point (t=0)

Firstly, the original time series is directly fed into the maintenance model by assuming that the TEC failure takes place at $t = 0$. The corresponding maintenance activity durations of replacing 1,5 and 10 TECs will be compared to 100 synthetic time series, which use the same starting point to describe the TEC failure. This is achieved by excluding the random U_{curr} starting point, as is described in paragraph 8.3, and using identical U_{curr} samples for running all the D-vine simulations.

Figure 8.22 shows the activity durations for using the original and synthetic time series. The weather window limits have been selected to fully correspond to the base case, mentioned in subsection 6.1.2. Only one simulation can be run with the original time series data, so this results in a deterministic value, displayed by the red vertical line.

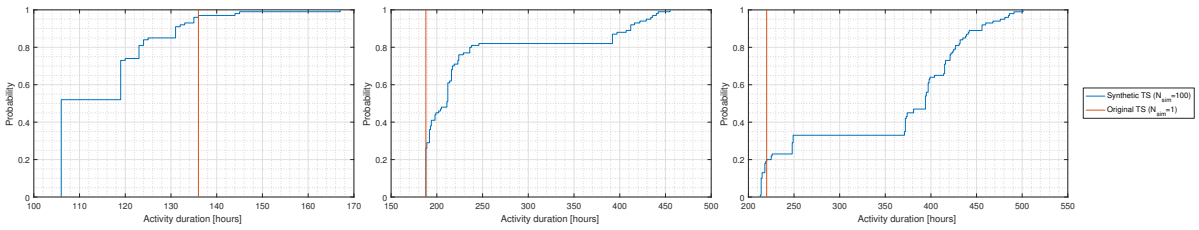

(a) Replace 1 TEC (b) Replace 5 TECs (c) Replace 10 TECs

Figure 8.22: Comparison of activity duration with original and synthetic time series (fixed starting point)

First of all it can be noted that, whilst keeping the current velocity time series fixed in all the simulations, still a large weather window uncertainty is introduced by applying the pair-copula construction to simulate synthetic time series. It is exactly this environmental randomness which can be included by simulating additional time series. Each of these synthetic time series is statistically identical to the original time series, but more realizations can be generated, resulting in a probabilistic representation of the maintenance activity durations.

Secondly, in this scenario it is interesting to observe that no fixed factor can be found which can convert the deterministic duration of the original time series to an arbitrary exceedence probability of the synthetic time series. Figure 8.22a may show the deterministic duration being close to the P90 exceedence probability, but figures and 8.22b and 8.22c reject this hypothesis.

Scenario 2: Varying starting points

The second scenario compares the set of 100 synthetic time series to an equally large set of quasi-original time series, which have been extract from the original measurements by shifting the starting point. These quasi-original time series have equally spaced starting points and describe a range of 14 days, to represent both the peak and neap tides which occur in one lunar cycle.

It can be seen in figure 8.23a and 8.23b that the quasi-original time series follows the synthetic time series reasonably well for the replacement of 1 and 5 TECs, respectively. However, as the number of tasks increase, and thus the number of required weather windows, the two approaches start showing a significant discrepancy. This effect can be observed in figure 8.23c and in appendix D.11, where each increment in TEC replacements in depicted.

By using the quasi-original time series is possible to describe weather window uncertainty due to the environmental randomness. An advantage of this approach is that it requires no measurement data analysis and copulas to simulate new synthetic time series, whilst still describing realistic multivariate dependence.

One major limitation of this approach is its restriction in generating more environmental realizations than is already captured in the original measurement data. Especially since the available dataset is very short, this results in major limitations when attempting to describe a full spectrum of possible environmental occurrences. Figure 8.23c is a good example of the considerable underestimation of the activity duration, which occurs due to only using copies of the original time series.

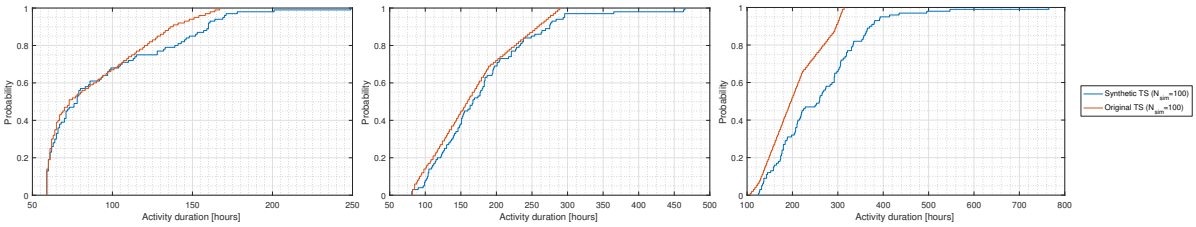

(a) Replace 1 TEC (b) Replace 5 TECs (c) Replace 10 TECs

Figure 8.23: Comparison of activity duration with original and synthetic time series (variable starting point)

Instead, by performing a copula analysis on the original time series and describing the identified in a PCC, it is possible to simulate as many synthetic time series as desired. This is a significant advantage of the vine simulation method used in this thesis, as more environmental realizations result in a more complete description of the weather induced uncertainty.

8.5.2. Synthetic TS with/without multivariate dependence

The second comparison study evaluates the added value of the PCC for its ability to include multivariate dependence. Other methods are available for simulating univariate time series, such as using an ARIMA model [38] to create forecasts of univariate time series, or by only using the method in subsection 8.4.2 to model univariate time dependence with a D-vine.

The effect of implementing multivariate dependence to the time series is assessed by comparing the resulting maintenance activity duration distribution for 100 simulations. The synthetic time series with multivariate dependence are simulated by using the developed algorithm, described in subsection 8.4.4. The time series without multivariate dependence are simulated by leaving out the second D-vine simulation step and directly couple the set of 4 univariate time series. Both methods use the same approach for selecting the U_{curr} time series, as is described in paragraph 8.3.

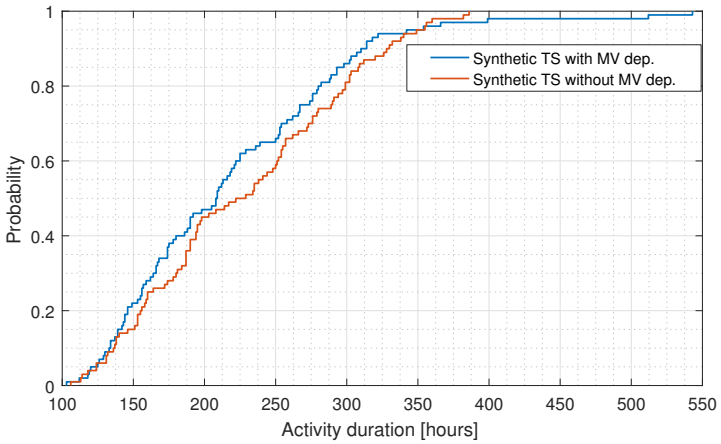

Figure 8.24: Comparison of activity duration of synthetic time series with and without multivariate dependence (replace 9 TECs)

In figure 8.24 it can be observed that excluding the multivariate dependence results in an increase of the maintenance duration, albeit not a significant one as the mean increase is less than 10%, Still, it must be said that by including multivariate dependence the simulated time series represent the actual situation more realistically and thus only bring advantages to the validity of the results. Whilst the added value for the current model configuration proves to be relatively small, the result can be perfectly explained and cases can be described in which the multivariate dependence may result in significant larger gains in validity.

Interpretation of results

First of all, the identified bivariate dependence between the four environmental variables, listed in table 8.3, showed relatively low rank dependence between most pairs, except for U_{curr}-T_p ($\tau = 0.35$). This implies that the peak wave period is reasonably well related to the current velocity, which is used as the simulation input. However, for the Damen base case it was decided that no limitations are applied with respect to the peak wave period. Any simulation advantage that would have been gained by implementing multivariate dependence would therefore be dismissed due to the absence of wave period related operational limits.

The remainder of the multivariate dependence pairs varied between independence ($\tau \approx 0$) and that of U_{wind}-H_s ($\tau = 0.12$). The discrepancy of the maintenance durations with and without multivariate in figure 8.24 is thus exclusively the result of the addition of this weak multivariate dependence. This may also be interpreted in such way that, in case T_p was included in the operational limits, the effect of including the multivariate dependence would be significantly larger.

Increased effect of multivariate dependence when modeling DP limits

In this thesis the operation limits are independently evaluated for each time step. The lack of applying multidimensional limits, which effectively captures the operable conditions for combinations of the four environmental variables, is assumed to be sufficient for this research. However, the developed maintenance model has been developed in modules in order to be upgraded independently. The connection with Damen's in-house DP model has already been established and it is thus possible to determine the vessel's station-keeping capabilities by means of advanced calculations. The DP limitations are therefore represented more realistically in the respective model, but is outside of this thesis' scope.

The implementation of DP limits will give a significant beneficial effect of using synthetic time series with a higher level of validity. DP operations are largely affected by the wave drift forces. Wave drift forces are very much dependent upon the wave period as short steep waves give higher forces than long waves with the same wave height. Therefore the wave spectrum and the selected wave period in relation to the wave height is very important in calculating the total wave drift force [103].

When the current velocity is low during its diurnal cycle, the possibility for a weather window may occur. However, as T_p is strongly dependent on U_{curr}, this will logically result in a reduction of the peak wave period during that same period. As is described above, this can lead to an increase in the total wave drift forces which negatively influence the weather window opportunities. The inclusion of multivariate dependence can thus be of great addition to represent the weather window opportunities as realistically as possible.

9

Maintenance policy optimization using Semi-Markov Decision Processes

RQ 2 How can the uncertainty in the maintenance activities of the TEC array be included in the model?

The focus of the chapter is to rearrange, modify and performing calculations on the parametric inputs that describe the entire system (tidal array with failing TECs which is to be maintained and are exposed to the environment) into a format which corresponds with a SMDP and thus can be optimized. As has been explained in chapter 3, this requires the system from part II to be represented as:

States describing the unique combination of TEC failures in the array

Decisions describing whether or not maintenance is performed in each state, and how many TECs are to be replaced

Transition probabilities describing what the probability is of going from one state to another, based on the selected decision of performing maintenance (maintenance based transition) or doing nothing (failure based transition)

Transition rates describing at what rate the transition form one state to another occurs. This is either induced by a TEC failure or the time is takes to perform maintenance.

Rewards describing the benefits and costs of being in a particular state. This is directly related to downtime of one or more TECs and the cost of performing maintenance.

This chapter is structured to describe the above mentioned SMDP elements in different sections. Section 9.1 and 9.2 describe the state state generation and decisions, respectively. As has been described in chapter 7, two main modules can be identified in the policy optimization model. Section 9.4 gives insight in the algorithms which calculate the SMDP properties of the failure related system processes and section 9.5 does this for the maintenance process. Section 9.6 explains how all data is combined, after which the optimal maintenance policy is determined. Lastly, section 9.7 describes the verification study for the model using multiple example cases.

9.1. State generation

The tidal system can be described by a set of states. The number of states can be selected arbitrarily, but it should be noted that this has a significant influence of the results. It is thus of great importance to choose both the quantity and the properties of the states well to find generate a good resemblance of the tidal system.

Within this research the number of states has been linked to the number of unique failure combinations within the tidal array. Two types of states have been defined in the model to resemble system well:

- Deterioration states (D-states, S_D)
- Maintenance states (M-states, S_M)

Each deterioration state thus describes a unique combination of failed TECs within the array. This effectively enables the model to include all transitions and costs which occur if the system changes from one state to another, by either performing maintenance of wait for another TEC to fail.

The maintenance states have a one-to-one relation with the deterioration states and describe the situation that occurs when the decision is made to perform maintenance, given the system was in a deterioration state before. This thus requires each deterioration state to have an copy, but with different properties, to which it is coupled. An except is the initial deterioration state, S_{D1}, which describes full availability of all TECs. In this state it is not possible to perform maintenance as the entire array is operational.

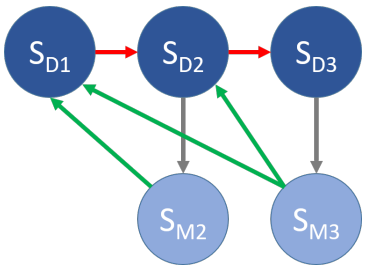

Figure 9.1: Example of deterioration and maintenance states

A simple serial example of the states and their interaction is depicted in figure 9.1, in which the arrows indicate direction of state changes, red being a TEC failure, gray the decision of performing maintenance and green the renewal process. The corresponding SMDP properties regarding the rewards, rates and decisions will be explained in more detail in the remainder of this chapter.

9.1.1. Unique states

The following model input parameters are used to generate the full set of states states:

$N_{platform}$ The number of tidal platforms which are present within the array.
N_{TEC} The number of TECs per tidal platform.
$N_{fail,max}$ The maximum number of of TECs which are allowed to have failed simultaneously in the array. This value cannot be exceeded in the model and will force the decision process to perform maintenance, effectively reducing the number of failed TECs.

Each failure combination within array is an unique state. It is self-evident that the total number of TECs is

$$N_{TEC,tot} = N_{platform} \cdot N_{TEC}, \tag{9.1}$$

and if each individual TEC and tidal platform was identified as an unique entity, the total number of failure combinations would be

$$N_{failcomb,max} = N_{S_D} = 2^{N_{tec} \cdot N_{platform}} \tag{9.2}$$
$$N_{S_M} = N_{S_D} - 1 \tag{9.3}$$
$$N_{S_{tot}} = N_{S_D} + N_{S_M} = 2 \cdot \left(2^{N_{tec} \cdot N_{platform}}\right) - 1 \tag{9.4}$$

For the base case the array consists out of 5 platforms with 16 TECs each. This would lead to $2.4179 * 10^{24}$ states in total. Even when only including either the platforms or TECs as unique entities, the number of required states is excessively high and showed to be too demanding to be run by the model.

A simplification has been performed, which reduces the number of states of the model, whilst not influencing the model results. This is due to the fact that all platforms and the TECs are modeled identically, so numerous quasi-identical failure combinations are present within the tidal array. All platforms and TECs are regarded

Table 9.1: Example of deterioration state duplicates (2 platforms with 2 TECs, 1 failure)

Platform 1		Platform 2	
TEC 1.1	TEC 1.2	TEC 2.1	TEC 2.2
×	✓	✓	✓
✓	×	✓	✓
✓	✓	×	✓
✓	✓	✓	×

generic and only the unique sets of failed TEC quantities are considered. Table 9.1 shows the duplicates for an array with 2 platforms and 2 TECs, of which all have unique entities and one has failed.

These duplicate states are merged into one state by an algorithm, based on the simplification that the system makes no distinction in costs and failure properties between the TECs at different platforms. This assumption is in line with the data availability and assumption of only including random failures, so no time varying failure rates are included. This has been covered in section 5.4.

An example of how the deterioration states are generated is depicted below in table 9.2, with $N_{platform} = 3$ and $N_{tec} = 2$. It shows that only 10 deterioration states ($N_{S_{tot}} = 19$) are identified instead of 64 ($N_{S_{tot}} = 127$), which would be the case if both TECs and platforms are considered as unique entities. This exponential reduction of states becomes especially useful for running simulations with large inputs.

Table 9.2: Example of deterioration state generation

State	Platform 1 ($N_{TEC,fail,1}$)	Platform 2 ($N_{TEC,fail,2}$)	Platform 3 ($N_{TEC,fail,3}$)
S_{D1}	0	0	0
S_{D2}	0	0	1
S_{D3}	0	0	2
S_{D4}	0	1	1
S_{D5}	0	1	2
S_{D6}	0	2	2
S_{D7}	1	1	1
S_{D8}	1	1	2
S_{D9}	1	2	2
S_{D10}	2	2	2

9.1.2. Maximum allowable array failures

The parameter $N_{fail,max}$ is implemented to limit the generation of excessive states which are irrelevant in the policy optimization. This is due to the fact that after a certain number of failures (e.g. after 20% total array failure) the system contains too many failed TECs which is undesirable and does not represent a realistic situation. Also, initial results may indicate a range of states where the the pivot point of going from the 'Do Nothing' decision to 'Perform Maintenance' is located. The successive states will, describing a larger number of failed TECs will thus never be reached and can be excluded without affecting the model results. This can significantly speed up the simulation.

9.2. Decisions

In the SMDP two sets of decisions have been defined, which correspond directly with the main questions which are to be answered by this model, as can be read in subsection 7.4.

It is important to note that, whilst the decisions have their own transition rates between states, the decision making moment is instantaneously upon entering entering the deterioration states from a previous state. More detailed information regarding the selected transition rates for each decision type is given in section 9.4 and 9.5.

9.2.1. Primary decision set: 'Should maintenance be performed?'

The first set of decisions can be chosen in any of the deterioration states and are as follows:

Decision 1 'Do Nothing' $(S_D \rightarrow S_D)$
Decision 2 'Perform Maintenance' $(S_D \rightarrow S_M)$

If decision 1 (D_1) is selected the system is left to deteriorate to a next state due to failure of an additional TEC. Selecting decision 2 (D_2) initiates maintenance and the respective maintenance state is entered. There are two exceptions which have already been briefly explained. In the fully operational state (S_D1) only decision one can selected, since there are no TECs to be repaired. In the deterioration states in which the number of failed TECs is equal to $N_{fail,max}$, decision 2 is forced.

9.2.2. Secondary decision set: 'If so, how many TECs should be replaced at once?'

The second set of decisions can be chosen in any of the maintenance states and are as follows:

Decision 2.1 'Replace 1 TEC $(S_M \rightarrow S_D$, with: $N_{TEC,fail,new} = N_{TEC,fail,old} - 1)$
Decision 2.x 'Replace x TECs, with: $1 \leq x \leq N_{TEC,fail}$ $(S_M \rightarrow S_D$, with: $N_{TEC,fail,new} = N_{TEC,fail,old} - x)$

Due to the state architecture, this decision set is only activated after the decision has been made to perform maintenance (D_2) in a deterioration state. In the maintenance state the decision can then be made a number of failed TECs, ranging between 1 and the number of failed TECs in the entire array, $N_{TEC,fail}$.

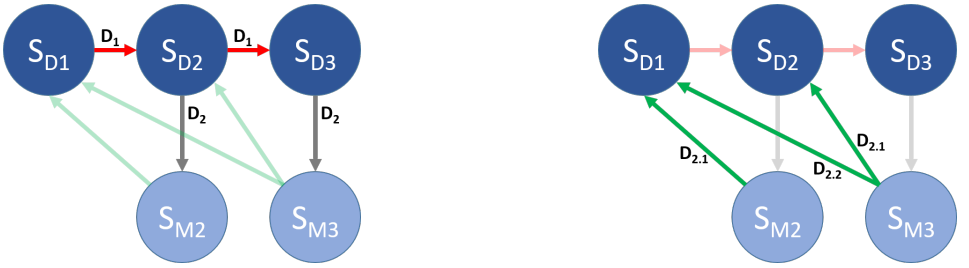

(a) Decision set 1: Deterioration states

(b) Decision set 2: Maintenance states

Figure 9.2: Decision sets for system states in SMDP representation

9.3. Illustrative example

For the remainder of the chapter a basic example is used to give more insight in the developed algorithm by means of a number of figures and numeric values. The example is identical to the system described in table 9.2 and contains 3 platforms with 2 TECs each. This expands the sequential state transitions to a slightly more complex network of states, which may contain multiple state transition probabilities due to having multiple platforms in the array, as is visualized in figure 9.3.

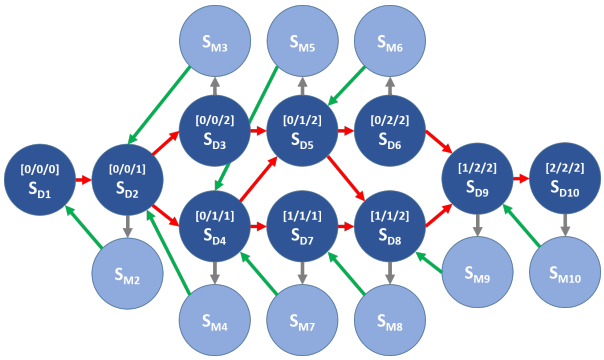

Figure 9.3: Tidal array example: deterioration & maintenance states

The numbers between brackets tell how many TECs have failed at the three platforms and the arrows represent the transitions based on the selected decision, identical to the method described in section 9.1.

The reason for selecting this specific tidal array selection is that larger systems become virtually impossible to represent visually. Still, the developed algorithms can be applied identically for larger tidal systems, so no difference is made.

9.3.1. Clarification on observed maintenance transitions

A number of processes can be observed in figure 9.3, of which two maintenance related ones are required to elucidate. Firstly, not all possible decisions are displayed, since this would result in a complex visualization. All of primary decisions $D1$ and $D2$ ('Do Nothing' & 'Perform Maintenance') are included, but only secondary decision $D2.1$ ('Replace one TEC') is visualized. Despite not being visualized, the other maintenance decisions will still be fully explained in section 9.5.

Secondly, the maintenance decisions do not allow a transition back to any deterioration state, due to the algorithm rules which describe the maintenance process. This can be seen at state S_{M5} and S_{M9} and is further explained in subsection 9.5.2.

9.4. Deterioration module

In this section the methods will be explained to determine the transition rates, probabilities and rewards for the deterioration related process. This process is directly related to decision 1 (D_1: 'Do Nothing'), so that the failures of TECs result in the transition from one deterioration state to another ($S_D \rightarrow S_D$), with increasing number of failed TECs ($N_{TEC,fail}$). Figure 9.4 depicts all deterioration states and transitions of the example from section 9.3.

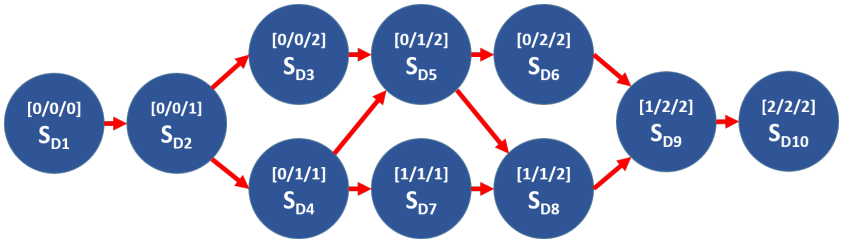

Figure 9.4: Tidal array example: deterioration transitions (decision: D_1)

9.4.1. Failure transition probabilities

Transitions between the deterioration states do not necessarily have one predefined path, as the introduction of multiple platforms within the system allows multiple destination states in some cases. Figure 9.3 clearly shows this, as state S_{D2} and S_{D5} each have two destination states to which it may transfer upon the event of a TEC failure.

For each deterioration state the transition probabilities of ending up in another deterioration state are calculated in a two-step process.

Step 1 Identify the deterioration states which have one more failed TEC than the departing state ($N_{TEC,fail,to} = N_{TEC,fail,from} + 1$)

Step 2 Calculate the transition probabilities of going from the departing state to the arrival state ($P_{S_{D,from} \rightarrow S_{D,to}}$)

The first step is accomplished by using Algorithm 2 for every deterioration state. Once the possible transitions are formally identified, the transition probabilities can be calculated. Since the system is represented by a number of identical TEC subsystems with a constant failure rate (λ_{TEC}), the transition probabilities can be easily calculated based on the ratio between the number of possible TEC failures which force the transition to the departure state and the total number of possible TEC failures of the departure state.

$$P_{S_{D,from} \rightarrow S_{D,to}} = \frac{N_{TEC,fail,pos,from \rightarrow to}}{N_{TEC,oper}} \tag{9.5}$$

$$N_{TEC,oper} = N_{TEC,tot} - N_{TEC,fail} \tag{9.6}$$

$$N_{TEC,fail} = \sum_{i=1}^{N_{platform}} N_{TEC,fail,i} \tag{9.7}$$

It should be noted that the summation of all departing transition probabilities per decision have to add up to one.

$$\sum_{i=1}^{N_{D,to}} P_{S_{D,from} \rightarrow S_{D,to,i}} = 1 \tag{9.8}$$

As a numerical example, table 9.3 gives the transition probabilities for state S_{D2}, S_{D4} and S_{D5} from figure 9.3. The transition probabilities of the other deterioration states are not given, as it is evident that they each only have one possible transition and the corresponding probabilities are thus equal to one.

Table 9.3: Examples values of transition probabilities

From	To	$N_{TEC,oper}$ [−]	$N_{TEC,fail,pos,from \rightarrow to}$ [−]	$P_{S_{D,from} \rightarrow S_{D,to}}$ [−]
S_{D2}	S_{D3}	5	1	0.20
S_{D2}	S_{D4}	5	4	0.80
S_{D4}	S_{D5}	4	2	0.50
S_{D4}	S_{D7}	4	2	0.50
S_{D5}	S_{D6}	3	1	0.33
S_{D5}	S_{D8}	3	2	0.67

9.4.2. Failure transition rates

In a SMDP all state transitions are represented as exponential distributions, as is described in chapter 3. This fully corresponds with the exponential distributions that describe the failure rate of a TEC. Therefore, the transition rate from one deterioration state to another is determined by the failure rate of the combined failure options which lead to the arrival state. To formalize this expression, the following equation describes the transition rate for any arbitrarily deterioration state transition.

$$\lambda_{S_{D,from} \rightarrow S_{D,to}} = N_{TEC,fail,pos,from \rightarrow to} \cdot \lambda_{TEC} \tag{9.9}$$

The number of TEC failure possibilities ($N_{TEC,fail,pos,from \rightarrow to}$) depends on which two deterioration states are considered and cannot be solved analytically. Algorithm 2 can be used to determine the quantity and the results for the example tidal array are listed in table 9.4. The TEC failure rate is chosen to be identical as in the case described in paragraph 5.4.4, thus $\lambda_{TEC} = 0.2920$.

In the table the corresponding MTBF between the states are also listed, which describes the transition time in years. It shows that for the given example, the state transitions occur between 0.57 years and 3.42 years, depending on the observed state.

9.4.3. Production downtime costs ('*Reward*')

For decision 1, 'Do Nothing', the associated costs entire consist out of the downtime costs, also defined as the indirect cost of maintenance. This is because a TEC failure results in a lack of electricity production. The

Table 9.4: Example values of deterioration transition rates

From	To	$N_{TEC,fail,pos,from\rightarrow to}$ [−]	$\lambda_{S_{D,from}\rightarrow S_{D,to}}$ $[1/year]$	MTBF $[year]$
S_{D1}	S_{D2}	6	1.7520	0.57
S_{D2}	S_{D3}	1	0.2920	3.42
S_{D2}	S_{D4}	4	1.1680	0.86
S_{D3}	S_{D5}	4	1.1680	0.86
S_{D4}	S_{D5}	2	0.5840	1.71
S_{D4}	S_{D7}	2	0.5840	1.71
S_{D5}	S_{D6}	1	0.2920	3.42
S_{D5}	S_{D8}	2	0.5840	1.71
S_{D6}	S_{D9}	2	0.5840	1.71
S_{D7}	S_{D8}	3	0.8760	1.14
S_{D8}	S_{D9}	2	0.5840	1.71
S_{D9}	S_{D10}	1	0.2920	3.42

downtime costs of a single TEC is the net price of the electricity which would have been produced in the period of downtime, had the TEC not failed or undergoing maintenance.

This cost is obtained by multiplying the net amount of missed electricity with the feed-in tariff which applies to the tidal location. The total amount of electricity losses in a state is multiplied with the number of failed TECs to obtain the costs of transition between deterioration states. The equation which is applied to calculate these deterioration costs is as follows:

$$C_{S_{D,from}\rightarrow S_{D,to}} = E_{S_{D,from}\rightarrow S_{D,to}} \cdot FiT \tag{9.10}$$

$$E_{S_{D,from}\rightarrow S_{D,to}} = N_{TEC,fail} \cdot P_{TEC,mean} \cdot \left(MTBF_{S_{D,from}} \cdot 365 * 24\right) \tag{9.11}$$

$$N_{TEC,fail} = \sum_{i=1}^{N_{platform}} N_{TEC,fail,i} \tag{9.12}$$

$$MTBF_{S_{D,from}} = \frac{1}{\lambda_{S_{D,from}}} \tag{9.13}$$

In this equation the costs upon transition ($C_{S_{D,from}\rightarrow S_{D,to}}$) are expressed in euros and it is important to note that the transition time ($MTBF_{S_{D,from}}$) should be converted from years to hours, because the mean TEC electricity production ($P_{TEC,mean}$) is defined in kW and the FiT in e/kWh. The FiT for the tidal array at the EMEC location has been described in paragraph 5.1.1 and is $0.12e/kWh$.

Mean electricity production ($P_{TEC,mean}$)

The mean electricity production of a TEC can be calculated once the TEC's power curve, described in subsection 5.3.1 is known and a time series of U_{curr} is available.

The most straight forward method would be to simulate synthetic time series with corresponding duration as the transition time, which is equal to the MTBF. However, since the failure rate of a TEC is dependent on the model input parameters (namely the assembly failure rates), this is not preferable as new time series would need to be generated each time the assembly parameters are changed. Also, the time series do not have a duration (T_{sim} = 1000hours = 41.67days) which fully corresponds with one full lunar cycle (27.5days), so it is not possible to calculate the mean electricity production by merely using one time series.

Instead, this model takes advantage of the fact that the current velocity has a recurring sinusoidal profile and a large set (N_{sim} = 1000) of synthetic time series has been generated. The set of synthetic time series, of which the properties have been discussed in chapter 8, each include a shifted copy of the original U_{curr} time series, with a randomly selected starting point, using an uniform distribution. The mean electricity production of a

TEC which is used in the model has been calculated by taking the mean of all individual mean TEC production values relating to the synthetic time series.

The procedure is calculating the model value for $P_{TEC,mean}$ is done as follows:

Step 1 Calculate the individual mean power production for each of the N_{sim} synthetic time series
- **1.1** Discretize power curve in N_{bin} bins (figure 9.5a)
- **1.2** Determine the histogram of the full length U_{curr} time series with identical bins (figure 9.5b)
- **1.3** Multiply the discretized bins with each other and to calculate the generated power per bin (figure 9.5c)
- **1.4** Divide by the number of samples ($T_{sim}/\triangle t = 6000$) to obtain the mean power production for one simulation (figure 9.5d)

Step 2 Calculate the overall $P_{TEC,mean}$ by taking the mean of all N_{sim} values (figure 9.5d, red line)

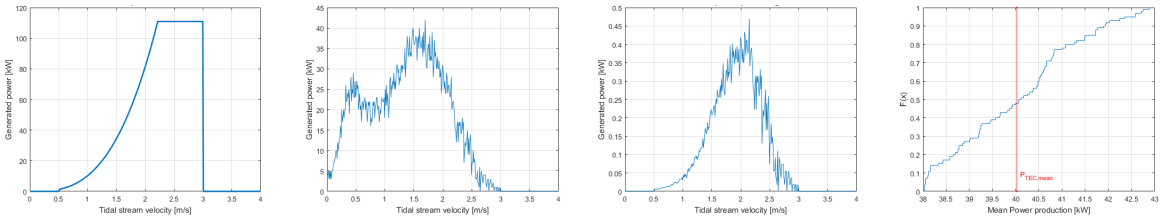

(a) TEC power curve

(b) Histogram of U_{curr} time series (1 simulation)

(c) Power production per histogram bin (1 simulation)

(d) CDF of all simulated TEC mean power production

Figure 9.5: Process for calculating the TEC's long term mean power production

In this example, using the base case TEC parameters and 1000 synthetic time series from the simulation method in chapter 8, the long term mean power production $P_{TEC,mean} = 40.0264kW$. This value will be applied to all downtime cost calculations which occur upon transition from one deterioration state to another, as a result of selecting decision 1, 'Do Nothing'.

9.5. Maintenance module

Using a similar structure as the previous section, this section will present the methods to determine the transition rates, probabilities and rewards for the maintenance related process. This process is initiated when decision 2 (D_2: 'Perform Maintenance') is selected in a state, after which the set of sub-decisions ($D_{2.x}$) determine how many TECs should be replaced at once.

Unlike the deterioration transitions, deciding to perform maintenance will result in two state transitions, as is depicted in figure 9.2. The primary decision of performing maintenance (D_2) results in the transition from one deterioration state to its coupled maintenance state ($S_D \rightarrow S_M$), whereas the secondary decision on the number of TECs to be replaced results in a transition back from the maintenance state to a deterioration state ($S_M \rightarrow S_D$) with a reduced number of failed TECs, corresponding to the number of replacements.

The primary decision D_2 does not represent any physical process and imposes no costs (($C_{D2} = 0$). Upon selection of this primary decision, the state changes instantaneously (($T_{D2} = 0$) from the deterioration state to its corresponding maintenance state with full probability (($P_{D2} = 1$)

Having said that, the transition rates, probabilities and rewards for the maintenance related process are thus exclusively related to the secondary decision set $D_{2.x}$ and will be explained in the remainder of this section.

9.5.1. Transition probabilities

Two decision rules have been implemented which determine the transition probabilities when performing a maintenance activity:

1. The maintenance priority

2. The chance of a TEC failure during maintenance

Maintenance priority

Important to mention is that the algorithm is designed to always maintain the platform with the most TEC failures first. This ensures that, if it is decided to replace multiple TECs, the number of platforms which are required to enter 'maintenance mode' is kept to a minimum. This ensures that less time is spent waiting in the array by the vessel until a new weather window occurs for the consecutive platform to be maintained, after the first one is fully renewed and the vessel still has functioning TECs loaded. The implementation of this design rule ensures that each maintenance decision can only lead to one arrival state, if no TEC failure occurs during the maintenance activity.

It can be seen in figure 9.6 that three possible maintenance possibilities are possible in maintenance state S_{M5}, after decision D_2 was selected upon entering the corresponding deterioration state S_{D5}. Each of these maintenance decisions is going to renew the system to a certain extend, reducing the number of $N_{TEC,fail}$ in the arrival state.

Decision $D_{2.1}$, replacing one TEC, shows a transition to state S_{D4}, but not S_{D3}. This is due to the previously explained model limitation that the algorithm only allows one possible transition per maintenance decision, and thus the algorithm prioritizes maintenance on the platform with most failures. This is all under the assumption that no TEC failure occurs during the activity.

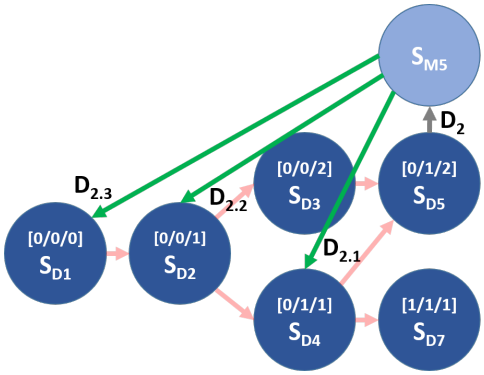

Figure 9.6: Tidal array example: Maintenance transitions from S_{M5}

TEC failure during maintenance

The previous paragraph described in what decision rules are applied to determine what the arrival state is of a maintenance activty. However, this is also affected by the possibility of a TEC failure. As has been mentioned in the model assumptions, this model allows one TEC to failure during the execution of a maintenance activity.

The algorithm has been extended in such way that, whilst still fulfilling the previously mentioned rules, it calculates what the chance of a TEC failure is during the respective maintenance operation and uses this to reallocate the transition probabilities of the maintenance activities. In other words, even if the decision was taken to replace 1 TEC, the final state may contain just as many failures (but not more, due to the limit of 1 TEC failure per activity) as the departure maintenance state.

The chance of a TEC failure during the maintenance activity is

$$P_{TEC,fail} = min\left(\frac{T_{act}}{(MTBF_{array} * 365 * 24)}, 1\right) \tag{9.14}$$

$$MTBF_{array} = \frac{1}{\lambda_{array}} \lambda_{array} \qquad = N_{TEC,oper} \cdot \lambda_{TEC} \tag{9.15}$$

with $MTBF_{array}$ being the failure time until one TEC fails in the array, given the current state.

Three characteristic situations may occur in the system:

- $T_{act} << MTBF_{array} \rightarrow P_{TEC,fail} \approx 0$
  This applies to most cases, since maintenance tasks usually last considerably shorter than the array failure time.
- $T_{act} \approx MTBF_{array} \rightarrow P_{TEC,fail} \approx 1$
  Especially in large arrays the $MTBF_{array}$ due to the large number of TECs. The failure probability increases as maintenance takes longer, or the time between TEC failure decreases.
- $T_{act} > MTBF_{array} \rightarrow P_{TEC,fail} = 1$
  If the maintenance activity duration exceeds that of the $MTBF_{array}$, it is assumed that a TEC will always fail during operation.

If $P_{TEC,fail}$ is calculated, the transition probabilities are calculated as follows:

$$P_{S_{M,from} \rightarrow S_{D,nofail}} = 1 - P_{TEC,fail} \tag{9.16}$$

$$P_{S_{M,from} \rightarrow S_{D,fail,i}} = P_{TEC,fail} \cdot P_{S_{D,nofail} \rightarrow S_{D,fail,i}} \tag{9.17}$$

The transition rate to the designated D-state without failure is $P_{S_{M,from} \rightarrow S_{D,nofail}}$, and the transition rate to any of the possible D-states when failure during the maintenance operation is described by $P_{S_{M,from} \rightarrow S_{D,fail,i}}$. The latter parameter uses the deterioration probabilities of the state that would have been arrived in, had failure not occurred. Similar to the deterioration transition probabilities should the sum of all outgoing transition probabilities be equal to 1 for each maintenance state.

Table 9.5 shows a numerical example, based on figure 9.6, in which decision $D_{2.2}$ is selected from maintenance state S_{M5}. The value for $P_{TEC,fail} = 0.2$ is assumed in this example.

Table 9.5: Examples values of maintenance transition probabilities

From	To	$P_{S_{D,from} \rightarrow S_{D,to}}$	Description
S_{D2}	S_{D3}	0.20	Deterioration due to TEC failure
S_{D2}	S_{D4}	0.80	Deterioration due to TEC failure
S_{M5}	S_{D2}	0.80	Maintenance, no TEC failure during activity
S_{M5}	S_{D3}	0.0.04	Maintenance, TEC failure during activity
S_{M5}	S_{D4}	0.0.16	Maintenance, TEC failure during activity

TEC failure transitions not visualized

Important to mention is that all state transition related figures in this thesis exclusively show the maintenance transition in which no TEC failure occurs. Still, the transition probability will be integrated in the model and used to plot the results.

9.5.2. Maintenance task generation algorithm

An algorithm has been developed which determines the required order of maintenance tasks, described in section 6.1, for the set of maintenance decisions ($D_{2.x}$). As has been mentioned in subsection 9.2.2, the number of possible replacements in an arbitrary maintenance state is between one and $N_{TEC,fail}$.

The developed algorithm works identically as the process flow described in subsection 6.1.1. It loops through the set of deterioration states and generate all possible replacement activities per state, based on the following model variables:

$N_{TEC,vessel}$ The maximum number of 'as new' TECs that can be replaced at once by the vessel
$N_{TEC,fail}$ The total number of failed TECs in the array
$N_{TEC,fail,i}$ The number of failed TECs at platform 'i'

The task generation for the example in figure 9.6 can be seen in appendix C.2.1, which also shows how the algorithm responds when more TECs need to be repaired than can be loaded at once.

9.5.3. Maintenance activity duration algorithm ('*Transition rates*')

Once all task sets are generated in the previous algorithm, it is possible to calculate the corresponding durations. This occurs in a four step process, which is repeated N_{sim} times for each generated activity in the system.

Step 1 Non-operable time steps per task are identified within the synthetic time series
Step 2 All possible weather windows per task are calculated
Step 3 The generated task sets per activity are fitted onto the synthetic time series
Step 4 The maintenance activity duration is the sum of all individual task durations ($T_{act} = \sum_{i=1}^{N_{task}} T_{task}$)

Each of the process steps will be explained more in detail the next paragraphs and visual examples will be provided accordingly. Unless stated otherwise, the combination of only one synthetic time series and one activity ($D_{2.1}$, replacement of one TEC) will be used.

Identifying non-operable time steps

The operable time steps per task are identified by applying the operational limits onto the synthetic time series. First, this is done individually per environmental variable, after which the overall non-operability can be determined by adding all the non-operable time steps. Within this model it is assumed that there is no dependence between the environmental limits and thus the time step is defined as non-operable as soon as one of the four (H_s, T_p, U_{wind}, U_{curr}) environmental limits is exceeded. Per simulation, this will generate ten data sets, one for each identified task, that describe whether the environmental limits are exceeded or not for each time step.

Figure 9.7 shows the result when the operable time steps of task 'TEC replacement' are identified for a 48 hour segment of the original time series. As mentioned in subsection 6.1.2, operation limit type 3 applies, so non-operable time steps are expected to be found in the time series. As said before, in this research no limits are set for T_p so this figure is not included.

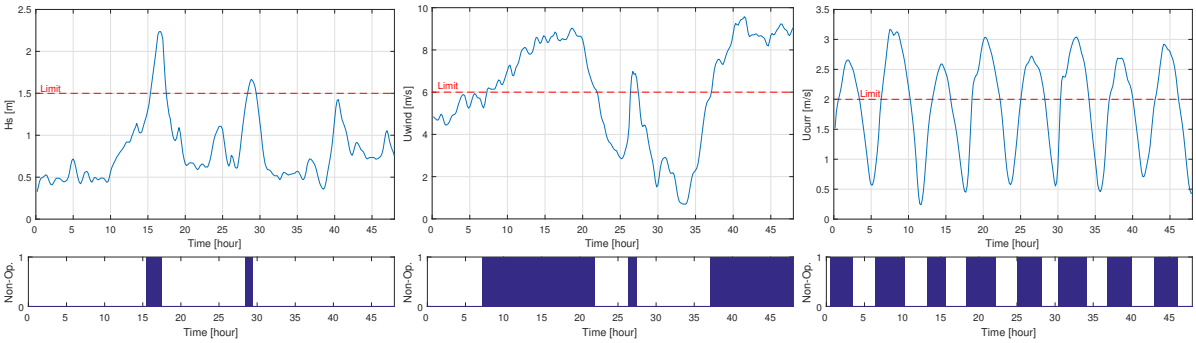

(a) Hs non-operability (b) Uwind non-operability (c) Ucurr non-operability

Figure 9.7: Fitting limits on time series and identifying non-operability

The overall non-operability for this specific task is found by adding all independent results of the environmental variables. The result for this example is shown in figure 9.8.

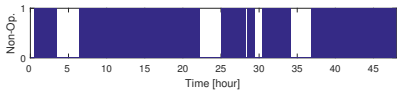

Figure 9.8: Overall non-operability for task 'TEC replacement' for the observed time series

Calculate weather windows

After having identified the non-operable time steps per task for all of the synthetic time series, the next step is to calculate which periods of availability are long enough, and thus provide a weather window, to perform the task of interest.

An algorithm calculates this for each task by pasting the task durations at each of the identified time steps which describe operability. If the entire duration concurs with operable time steps, this time step (at which the task commenced) is flagged as a suitable weather window. On the other hand, if the duration cannot be fully executed, it will mark this time step as unsuitable.

Figure 9.9 shows the example of fitting the 'TEC replacement' ($T_{act,5}$ = 1 hour $\rightarrow 6 \times \triangle t$) on a small segment (T = [6:13 hour]) of the found results in figure 9.8. The time steps ($\triangle t = 10min$) are shown in instances of 10 min, as this is the applied time series interval in this model.

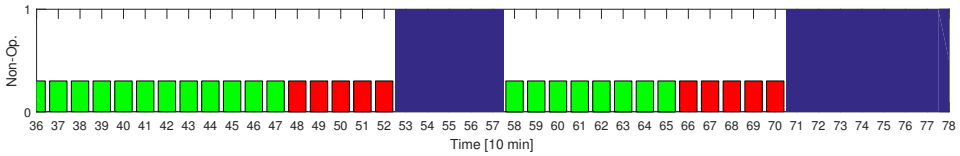

Figure 9.9: Weather window starting points for task 'TEC replacement' (green = pass, red = no pass)

Realistic weather window fitting

The algorithm for calculating the activity duration including the weather window has a number of features which attempt to represent the decision maker's behavior more realistically. It ensures that the tidal system remains longer in the 'maintenance mode' than is strictly necessary. This is done by including intelligence to the algorithm, which uses the following rules:

1. The vessel will not unnecessarily leave the port (residing in task **'waiting for weather window'**) until the following tasks can be performed at once:
   - 'port-array transport'
   - 'platform emerging'
   - 'TEC replacement' (all of intended replacements)
   - 'platform submerging'
2. The vessel will not unnecessarily initiate the 'maintenance mode' of a new tidal platform after finishing replacements on another (residing in task **'intra-array transport'**) until the following tasks can be performed at once:
   - 'platform emerging'
   - 'TEC replacement' (all of intended replacements)
   - 'platform submerging'

The general process for fitting the task list of an activity in the calculated weather windows of a synthetic time series is as follows:

Step 1 A TEC failure is assumed to occur at $t = 0$ of the synthetic time series
Step 2 The first task from the generated task list is fitted on the first 'pass' flagged time step, indicating a suitable weather window
Step 3 Starting at the time step after the just finished task, the next task from the generated task list is attempted to be fitted in the time series
Step 4 This process continues until all tasks from the activity's task list have been fitted

The addition of these realistic rules result in an adjustment to the general process which now no longer fits each task sequentially after the previous one has been completed, but for the 'waiting for weather window' and 'intra-array transport' tasks it will attempt to fit a multi-task weather window (of the above listed tasks) which should fit all at once, without non-operable time steps.

Probabilistic maintenance durations

The maintenance activity duration algorithm loops the entire set of generated activities through the set of N_{sim} synthetic time series to introduce the probabilistic property of the MC simulation.

In figure 9.10 a significant spreading of the activity duration can be observed due to the implemented necessity to 'wait for weather window' and in a lesser extend due to waiting in the 'array-port transport' task.

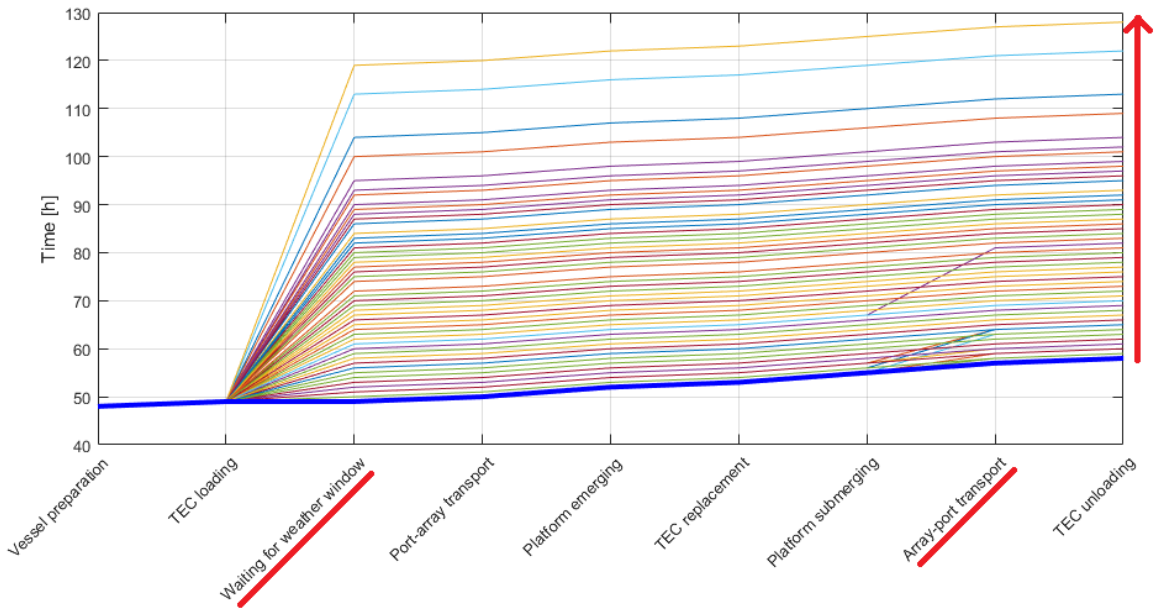

Figure 9.10: Cumulative task durations for the replacement of 1 TEC: $D_{2.1}$ (1000 simulations)

This proves that, whilst the synthetic time series are statistically identical to each other, the randomness still results in a huge uncertainty of the maintenance activity duration.

Even for the decision of only replacing one TEC, which requires the shortest weather window to perform the 'maintenance mode' related tasks, it can be observed that a number of simulations require an activity time of more than two times ($T_{act,max} = 128$) the absolute minimum time required ($T_{act,min} = 58$). The absolute minimum is represented by the bold blue line and describes the situation in which no weather window limitations occur during operation.

Activity time for multiple TEC replacements

As was mentioned, the conservative case ($D_{2.1}$) already imposes a significant spreading in the activity durations. In order to give more insight in the effect of performing multiple TEC replacements, the model has been run for different scenarios. Figure 9.11 shows the result of replacing between one and six TECs, running each scenario with 1000 independent synthetic time series.

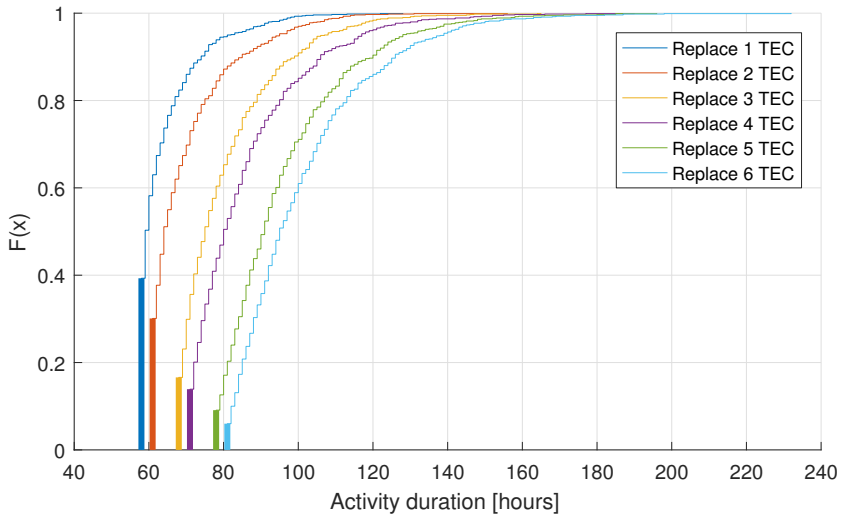

Figure 9.11: Cumulative task durations for the replacement of 1 to 6 TECs: $D_{2.1} \rightarrow D_{2.6}$ (1000 simulations)

The characteristics of figure 9.11 will be explained in much more detail in the sensitivity study. For now it is interesting to mention that the fraction of simulated activity durations that are equal to the minimum activity duration, and thus have no weather window limitations, reduces as the number of TECs which are to be replaced at once increases. The fraction which is equal to the minimum activity duration is highlighted in the figure by the bold vertical line. This decrease in number of activities without delay was expected, due to the implementation of the intelligent task fitting algorithm.

Conversion to transition rates

It is required to convert the calculated activity durations (state transition times) to rates, which represent the mean transition rate (λ) in the exponential distribution function which is the building block for the SMDP. Identically to the equation used in the Deterioration Module, the relation between the mean time to repair (MTTR) and λ can be determined.

$$\lambda_{MTTR} = \frac{1}{MTTR} \tag{9.18}$$

$$MTTR = T_{act} \tag{9.19}$$

Under the assumption that the calculated deterministic duration of the maintenance activities is in fact the MTTR of the corresponding exponential maintenance activity duration distribution, the maintenance transition rates can be easily determined.

9.5.4. Maintenance costs ('*Rewards*')

The cost of executing a maintenance activity, and thus the costs when changing states due to the maintenance decision $D_2.x$, consists out of three independent cost contributions, namely:

- Vessel activity costs
- Characteristic TEC product costs
- Downtime costs

For an arbitrary maintenance operation the following holds:

$$C_{maint} = C_{act} + C_{TEC,tot} + C_{DT,tot} \tag{9.20}$$

Vessel maintenance costs

For each maintenance activity the individual task durations have been calculated per synthetic time series. This was done in paragraph 9.5.3. To obtain the vessel maintenance costs, also referred to as the direct costs of maintenance, the task durations are to be multiplied with their respective cost rate. These cost rates have been described in paragraph 6.2.3 and included the vessel day rate, fuel costs and wages of the specialized personnel.

$$C_{act} = \sum_{i=1}^{N_{task}} T_{task} \cdot C_{rate,task} \tag{9.21}$$

Assumptions

Within this research it has been assumed that no additional vessel costs apply, except for those described.

Also, the task durations are used in their original precision, so not rounding off to days or other time intervals is performed.

Characteristic TEC product costs

The characteristic TEC product costs describe the mean repair costs of a TEC due to the 'as new' replacement of the failed assembly. This cost, based on the ratio of assembly failure rates and assembly product costs, has been calculated in paragraph 5.4.4 and is found to be $C_{TEC} = €10405$ per TEC reparation.

The total TEC related costs per maintenance activities can be easily calculated by multiplying the number of TECs to be replaced by the characteristic TEC product cost. Naturally, the number of TECs to be replaced is decided by the secondary decision set $D_{2.x}$.

$$C_{TEC,tot} = C_{TEC} \cdot N_{TEC,repl} \tag{9.22}$$

Assumptions

Determining the characteristic TEC product costs by the method described in this research is only valid when looking at the system from a long-term perspective, as the individual assembly failures may give different results (with a large standard deviation) when observing the problem for a short amount of time in reality.

Also, this method assumes that the reparation costs can be assigned to the operation which places the respective TEC back into operation. In reality the costs will have been made already after this TEC failed at an earlier point in time. Still, when looking at the system from a long-term perspective, the assumption holds due to the fact that the number of stock TECs onshore need not to exceed the number of TEC in the array, so reparation of the failed assembly is always preferred to constructing a completely new TEC and thus the TEC repair costs will stabilize in time.

Downtime costs

The downtime costs during the maintenance activity are calculated in a similar way as is done for the deterioration related downtime costs. However, the main difference is the observed duration. Whereas the deterioration downtime costs describe a long-term process, and thus the mean production of a TEC was used, the downtime during maintenance is significantly shorter.

Two types of TEC downtime during a maintenance activity are identified:

- Direct downtime of the failed TECs
- Indirect downtime of all TECs when a tidal platform is in 'maintenance mode'

An algorithm uses the initial number of TEC failures as a starting point and then calculates for each task within the activity's task list how many TECs are non-operating. Figure 9.12 shows the number of non-operating TECs for the replacement of two failed TECs, each positioned on a different platform. ($S_{M4} \rightarrow S_{D1}$)

The procedure of calculating the downtime costs is as follows:

Step 1 Discretize the TEC power curve in N_{bin} bins
Step 2 For each maintenance task in the activity:
- **2.1** Determine the histogram of the $U_{curr}(t_{task,start} : t_{task,end})$ time series with identical bins
  - $t_{task,start}$ is moment the task is started
  - $t_{task,end}$ is the moment the task is completed
- **2.2** Multiply the discretized U_{curr} and power curve bins with each other and divide by '[1 hour $/\triangle t$]' to calculate the generated power per bin in kWh
- **2.3** Sum the power of all bins to the generated electricity of one TEC during that task
- **2.4** Multiply with the number of failed TECs to obtain the net generated electricity during that task

Step 3 Sum all generated power in each of the tasks
Step 4 Multiply the total generated electricity with the FiT to obtain the total downtime costs

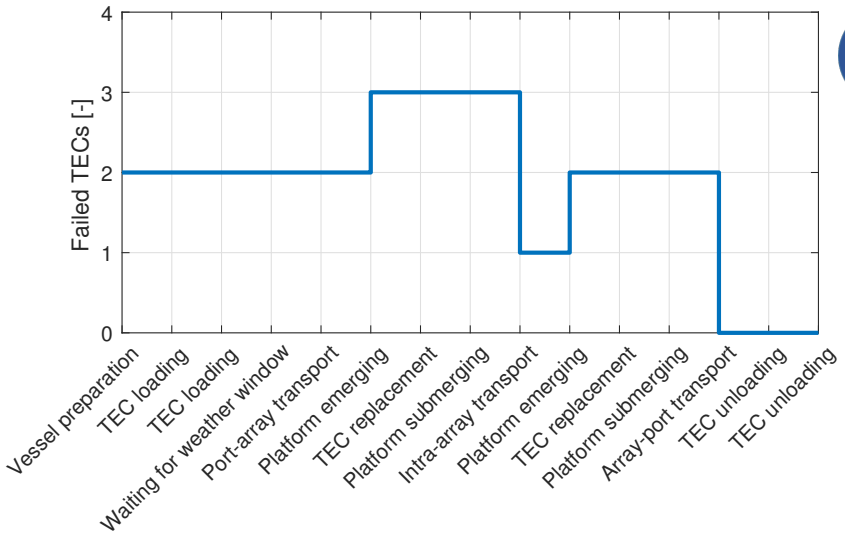

(a) Failed TECs per maintenance task

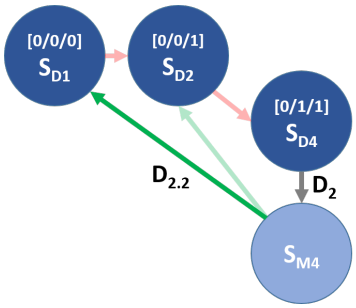

(b) Maintenance activity $D_{2.2}$ ($S_{M4} \rightarrow S_{D1}$)

Figure 9.12: Tidal array example: $N_{TEC,fail}$ during the maintenance activity

9.6. Policy optimization module

Once the tidal system has been effectively described in states, decisions, transition rates, probabilities and rewards, it is possible to use the unichain policy iteration algorithm, described in subsection 3.4.1, to optimize the policy. Within the model no alternations have been done on the existing algorithm, the interpretation of results has shown to play an important role within this research.

9.6.1. Primary output interpretation

For a single simulation the policy optimization module produces two primary outputs:

- The optimal policy of the system
- The maintenance cost rate (gain of the system)

Optimal policy

The optimal policy of the system describes what the most economical decision is to make in each state. Important to remember is that the SMDP is based on exponential distributions, so the Markov property describes that the system is memoryless. This implies that, regardless of how the system has made it to the state, the proposed decision remains optimal. An example output of the model for the example array (3 platforms, 2 TECs each) is shown below in table 9.6.

Table 9.6: Example array: Optimal policy (1 simulation)

State	$N_{TEC,fail,i}$	Opt. decision	$N_{TEC,repl}$
S_{D1}	[0/0/0]	'Wait'	0
S_{D2}	[0/0/1]	'Maintenance'	1
S_{D3}	[0/0/2]	'Wait'	0
S_{D4}	[0/1/1]	'Maintenance'	2
S_{D5}	[0/1/2]	'Maintenance'	3
S_{D6}	[0/2/2]	'Maintenance'	4
S_{D7}	[1/1/1]	'Maintenance'	3
S_{D8}	[1/1/2]	'Maintenance'	4
S_{D9}	[1/2/2]	'Maintenance'	5
S_{D10}	[2/2/2]	'Maintenance'	6

The first two columns of the model output display for which deterioration state, and its TEC failure combination, the decision is determined. The third column 'Optimal decision' answers the question of whether or not to perform maintenance in case the system arrives in that state. The last column '$N_{TEC,repl}$' mentions, if decided to perform maintenance, how many TECs should be replaced in one activity.

It can be observed that in all maintenance is initiated in all states, except for S_{D3}. Also, if maintenance is to performed, the maximum number of TECs will be replaced for every condition. These example results can be extensively analyzed, but this will be done in chapter 10.3 in which the base case is plugged into the model.

Maintenance cost rate

The optimization model also determines the system's gain rate, which is interpreted as the reward rate, given that the optimal policy is executed. In this model the rewards are represented by the costs, so the model will attempt to minimize the maintenance cost rate for the tidal array. The generated maintenance cost rate includes all costs which are included in the model, namely:

- Downtime costs
  - Failed TEC
  - Non-operating TECs during 'maintenance mode'
- TEC repair costs (characteristic TEC product costs)
- Maintenance activity costs
  - Vessel day rate
  - Fuel consumption
  - Personnel wages

In this example the obtained maintenance cost rate is equal to 10.98 €/hour. Since the SMDP optimization assumes an infinite horizon, the cost rate can be multiplied with the duration of interest to calculate how much in total is spent on the listed maintenance related costs. Naturally this is bounded by the described assumptions in the research and additional costs may apply.

9.6.2. Probabilistic output due to environmental randomness

The strength of this model is not producing an optimal policy, and corresponding cost rate, based on one simulation. Instead, the interface with the newly developed vine model for simulating large numbers of synthetic time series enables to analyze the effect of the weather uncertainty on the model outputs. This implementation of uncertainty within the model gives a realistic representation of the randomness of the weather. Therefore, the focus of the output is to combine the results of all N_{sim} simulations and bundle it to support the decision making.

Once finished, the model presents the gain rate for all simulations. Figure 9.13a shows the maintenance cost rates of the example case for 1000 simulations.

9.6.3. Decision making

By using the output of N_{sim} simulations to generate uncertainty, it is possible to support the decision making. The model provides a graphical overview of the ratio of the optimal policy's occurrence with respect to the total number of simulations. This ratio can be interpreted as the probability that the policy of interest does indeed lead to the desired results. For each policy, the corresponding gain distribution can be generated to connect the probability of selecting the optimal policy with its results.

Having provided this insight, it is then up to the decision maker to decide which policy is to be executed. This decision can thus be made on basis of the combination of risk and its costs. For the example in this chapter the optimal policies are shown in figure 9.13b and the gain distributions are provided for the three most occurring policies. Notice that many optimal policies only occur once or twice, this can be explained due to a simulation specific discrepancy in the optimal decision for a single state with respect to the major policies.

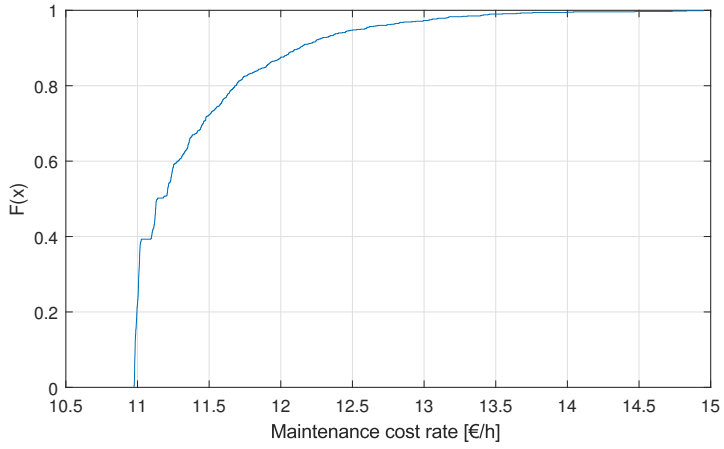

(a) Cumulative distribution of the gain rate

(b) Pie chart of optimal policy occurrences

Figure 9.13: Example tidal array: Maintenance cost rates and optimal policies for $N_{sim} = 1000$

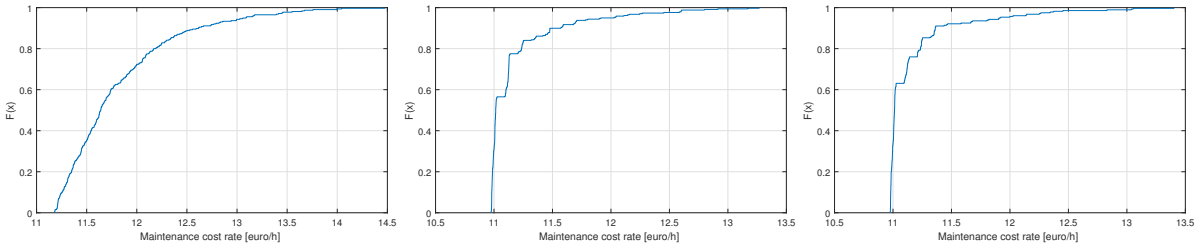

(a) Policy A

(b) Policy B

(c) Policy C

Figure 9.14: Example tidal array: Maintenance cost rates for $N_{sim} = 1000$

Given the near identical ratios of occurrence, the most economically favorable decision would be to implement policy C, closely followed by policy B. Policy A, whilst being optimal in 32% of the simulations, provides a more unfavorable cost rate distribution and thus is not economically optimal overall. Still, if the decision maker desires to make decisions with a large certainty, it still may be advised to select the slightly more expensive policy A. This type of analysis will be extensively described for the base case in the next chapter.

9.7. Model verification

A verification study has been performed to ensure the optimization model works as expected. Each of the individual calculations has been tested during development, but now the entire model and its output will analyzed by means of a degeneracy testing approach. Degeneracy testing [112] consists of checking that the model works for the extreme values of system and workload (input) parameters. Although extreme cases may not represent typical cases, degeneracy testing can help to find bugs that would not otherwise have been discovered.

Numerous degenerate cases with extreme input values have been developed, but for this research only the most relevant cases are provided.

9.7.1. Case 1a: High set-up vessel, low variable costs costs

This case is executed with an extreme cost rate for the 'vessel preparation' task, as this only occurs once during each activity. The variable costs (price for a TEC replacement) is kept to a minimum. The system consists out of 1 tidal platform with 3 TECs. The remainder of the parameters are identical to the base case, with $N_{sim} = 100$.

Hypothesis: all optimal policies decide to wait until $N_{TEC,fail} = 3$, then replace all 3 TECs at once

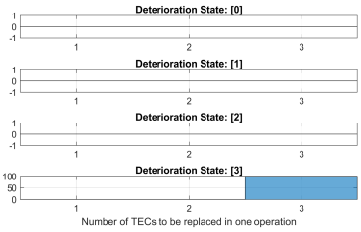

Figure 9.15: Optimal policy results of case 1a

The results of this case show indeed that the hypothesis is fulfilled. An empty bar means no TEC replacement in the respective state. 100% of the simulations decide to replace 3 TECs at once when $N_{TEC,fail} = 3$.

9.7.2. Case 1b: Low set-up vessel, High variable costs costs

This case is executed with a low cost rate for the tasks that only occur once, and an extreme cost rate for the variable 'TEC replacement' task. The system consists out of 1 tidal platform with 3 TECs. The remainder of the parameters are identical to the base case, with $N_{sim} = 100$.

Hypothesis: all optimal policies decide to wait until $N_{TEC,fail} = 3$, then replace only 1 TEC

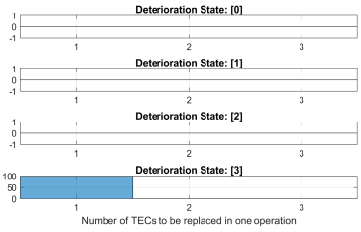

Figure 9.16: Optimal policy results of case 1b

The results of this case show indeed that the hypothesis is fulfilled. An empty bar means no TEC replacement in the respective state. 100% of the simulations decide to replace 1 TEC when $N_{TEC,fail} = 3$.

9.7.3. Case 2: No weather window requirements

This case is executed without the requirement of weather windows, implying that the vessel is not limited by the weather conditions and can operate under any conditions. The system consists out of 1 tidal platform with 3 TECs. The remainder of the parameters are identical to the base case, with $N_{sim} = 100$.

Hypothesis: all maintenance activity durations are identical and maintenance costs are nearly identical

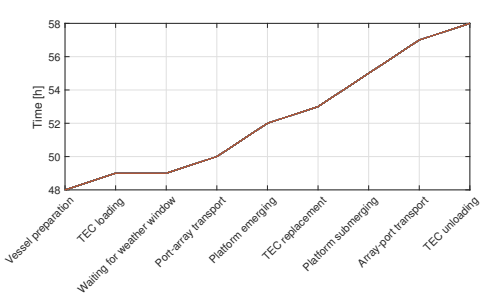

(a) Maintenance task duration for 3 TEC replacement ($N_{sim} = 100$)

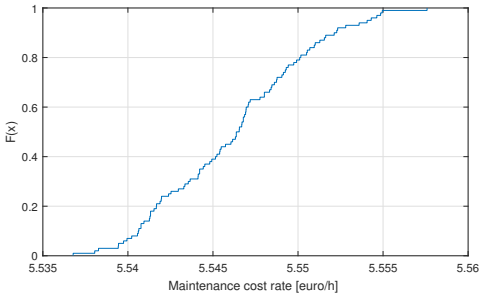

(b) Cost rate distribution for case 2

Figure 9.17: Results of case 2

The results of this case show indeed that the hypothesis is fulfilled. Figure 9.17a shows that all simulations are

identical to the minimum activity duration, plotted on top of each other. Also, the variation in maintenance costs in figure 9.17b show only minute variations, which can be explained due to the down time costs, which vary due to the use of randomly synthetic time series. This also proves that these downtime costs only account for small variations in the cost rate.

9.7.4. Case 3a: High TEC failure rate

This case is executed with an extremely high TEC failure rate (λ_{TEC}), which will result in short transition times between the deterioration states. The system consists out of 1 tidal platform with 3 TECs. The remainder of the parameters are identical to the base case, with $N_{sim} = 100$.

Hypothesis: all optimal policies decide to wait until $N_{TEC,fail} = 3$, then replace 1 TEC

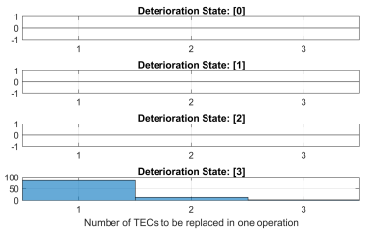

Figure 9.18: Optimal policy results of case 3a

The results of this case show that the hypothesis is partially fulfilled. An empty bar means no TEC replacement in the respective state. 85% of the simulations decide to replace 1 TEC when $N_{TEC,fail} = 3$.

Explanation of unexpected result

However, for this case it should be noted that the degree of increasing the TEC failure rate has influence on which optimal policy is presented. For this case the TEC failure rate was increased by 10^3 (to $\lambda_{TEC} = 292$ [failures/year]). Incrementally increasing the failure rate showed that the optimal policies changed from $D_{2.3} \rightarrow D_{2.2} \rightarrow D_{2.1}$. This indicates that either failure rate caused the system to be near a break even point of the boundary of the model applicability has been reached.

Further increasing the failure rate caused more unexpected behavior and it was found that this is due to the assumption that during the maintenance activity, only one TEC can fail. When $\lambda_{array} >> \lambda_{MTTR}$ this assumption no longer holds and the model does not realistically represent the system, providing incorrect policies and maintenance rates.

9.7.5. Case 3b: Low TEC failure rate

This case is executed with an extremely low TEC failure rate (λ_{TEC}), which will result in long transition times between the deterioration states. The system consists out of 1 tidal platform with 3 TECs. The remainder of the parameters are identical to the base case, with $N_{sim} = 100$.

Hypothesis: all optimal policies decide to replace $N_{TEC,fail}$ in each state

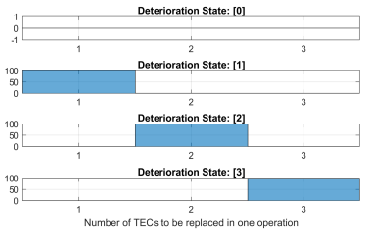

Figure 9.19: Optimal policy results of case 3b

The results of this case show indeed that the hypothesis is fulfilled. An empty bar means no TEC replacement in the respective state. 100% of the simulations decide to replace $N_{TEC,fail}$ in each of the states.

10

Model results

This chapter answers the third research question, namely

RQ 3 How can the resulting optimal maintenance strategy influence the decision making?
- (a) How does this model relate to other generic analytic group based maintenance models?
- (b) What are the main sensitivities that affect the total maintenance cost?

In this chapter the base case, developed by Damen, is analyzed to determine which group maintenance policy is recommended. Also, a sensitivity study will be performed for multiple cases, which each describe a possible alteration in the system. These results will provide more insights in the effect of the assumptions within this research and the uncertainties in the selection of the model input parameters.

10.1. Damen base case

As already discussed in part II, the Damen base case describes a tidal array located at EMEC. Five platforms, each with 16 TECs, are located in the array, and each each fulfill the conditions set by the assumptions of this model. The complete overview of model input parameters can be found in appendix E.1.

10.1.1. Complete description of uncertainty

The model has been run with 1000 (=N_{sim}) independently generated synthetic time series, which were generated using the developed vine algorithm that includes both univariate time dependence and multivariate dependence of the environmental parameters. It has been assumed that the number of simulations is large enough to represent any possible random occurrence of sea states, given the equality of the statistical parameters. This implies that this probabilistic approach fully describes the uncertainty that is introduced by the randomness of the environmental conditions.

10.1.2. General findings

Power production

When inspecting the data used for determining the mean power production per TEC ($P_{TEC,mean}$), it was found that the current design of the TEC may have some improvements regarding its cut-out velocity. From figure 10.1 it can be seen that the current cut-out velocity of 3.0 m/s is not fully in line with the occurring current velocities at the EMEC tidal site.

Whilst it is outside the scope of this research to propose an improved TEC design, including the working ranges of its assemblies, the effect of a higher cut-out velocity may very well impact the results of this maintenance optimization. By only increasing the cut-out velocity to 3.1 m/s, an improvement of 3.53% in $P_{TEC,mean}$ can already be observed.

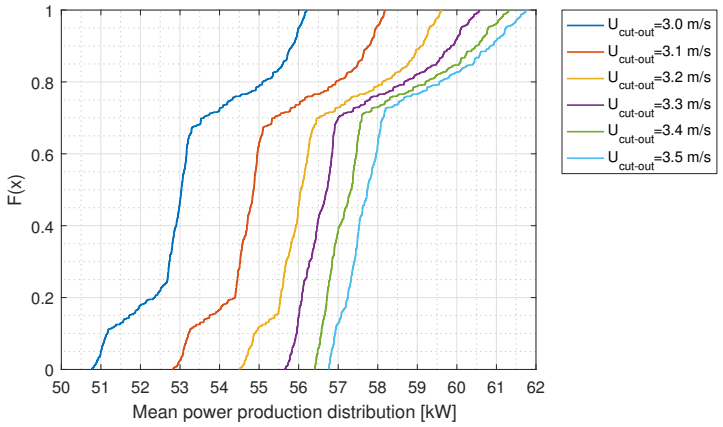

Figure 10.1: Mean power production distribution for different cut-out velocities

The power production and load factor for multiple cut-out velocity values are listed below. It can be seen that the beneficial effect of increasing the cut-out velocity stagnates for the EMEC location as it becomes closer to 3.5 m/s.

Table 10.1: Power production properties for different cut-out velocities

U_{cutout}	[m/s]	3.0	3.1	3.2	3.3	3.4	3.5
$P_{TEC,mean}$	[kW]	53.35	55.23	56.54	57.21	57.81	58.25
Load Factor	[%]	48.50	50.21	51.40	52.01	52.55	52.96

Failure times

It has been calculated how long it takes to reach a certain number of failed TECs if no maintenance is performed, regardless of the failure combination. Figure 10.2a depicts the failures of all 80 TECs in the array, distributed over 5 platforms with 16 TECs each. The time until the 30'th TEC failure looks more or less like a linear relation. This fully corresponds with the theory on parallel component failure with a constant failure rate, described in subsection 4.3.2. As more TECs are included, the time leading to a full array failure only slightly increases, since it is proportional to the partial sum of the harmonic series.

The failure time of the first ten TECs has been shown in figure 10.2b. As a result of the large number of TECs in the array, the first TEC already fails after 15.6 days. This time between failures can effortlessly applied for the consecutive failures in the figure, as the increase in failure time is negligible.

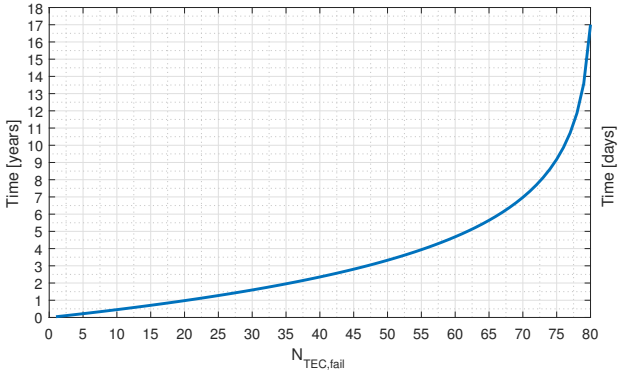

(a) Time to failure for 80 TECs

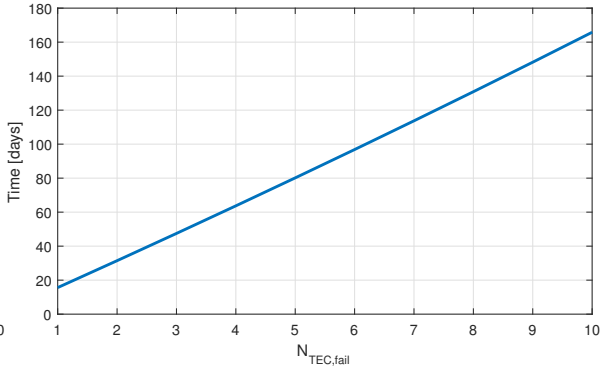

(b) Time to failure for 10 TECs

It is important to check whether the condition is met that the shortest failure time does not become smaller than the corresponding maintenance replacement duration. This condition is required to be met, since the

Table 10.2: Comparison of failure times and maintenance activity durations

N_{TEC}	T_{fail} [days]	T_{maint} [days]
1	15.6	6.4
2	31.2	7.5
3	46.8	8.8

maintenance model only allows maximum one TEC failure during a maintenance activity. Table 10.2 shows the comparison of the failure times and the respective activity durations for one, two and three TECs. Since there are multiple failure combinations for 2 and 3 TEC failures, only the combination is observed during which all failures are on the same platform. The P90 value is used as an indication for the activity duration with a high certainty.

It can be observed that the increase in the MTBF up to the n'th TECs increases faster than the corresponding maintenance time required to replace all the failed TECs. It can therefore be concluded that the required condition will always hold for this base case and that the possibility of a TEC failure during maintenance is modeled realistically.

10.1.3. Identifying optimal policies

Lower limit of maintenance cost rates

Having run the model, an optimal policy was found for each of the independent simulations. This set of optimal policies can best be interpreted as the theoretical lower limit for performing maintenance, given that the weather forecast is fully known for the decision maker at any moment in time. This should, theoretically, give him the required information to always select the best decisions for that specific state, given the full insight in the weather conditions for the time span of the all possible activities.

Each of these identified optimal policies is the best policy to implement in that single simulation and has its own corresponding maintenance cost rate. The cumulative distribution of the maintenance cost rates is depicted in figure 10.3a and represents the absolute minimum cost rate distribution of the base case, under the assumption mentioned in subsection 10.1.1.

Set of optimal policies

Contrary to the ideal situation in which no (environmental) uncertainties are present, in reality it most common to operate by means of fixed decision rules, namely the maintenance policy. These dictate what decision should be taken in each state, without having full insights in the upcoming weather conditions. This requires us to narrow down the set of identified optimal policies to one recommended policy, which approaches the global optimum and thus has a cost rate distribution which is nearly identical to that in figure 10.3a.

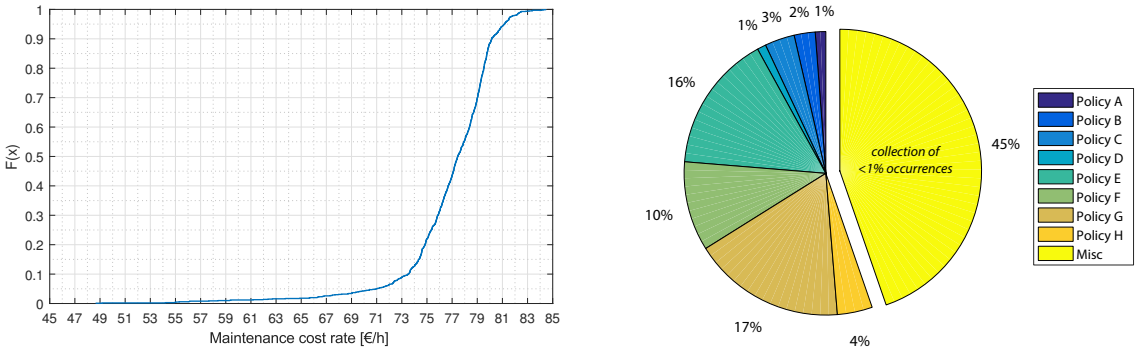

(a) CDF of the optimal maintenance cost rate

(b) Ratio of optimal maintenance policies

Figure 10.3: Maintenance cost rates and optimal policies of the base case

It may be possible to identify a single policy which is optimal in all of the simulations, and thus concluding that the policy selection is insensitive to the environmental uncertainty. However, as can be seen in figure 10.6c a large set of different optimal policies can be found in simulations. In total 363 unique policies have been found to represent the absolute optimum. All policies which occurred less than one percent of the total simulations have been collected in the 'miscellaneous' slice.

TEC replacements of the optimal policies

Before comparing the identified optimal policies to determine which is recommended, the TEC replacement properties of the theoretical lower limit are analyzed. It has been found that in most of the states the optimal policy dictates that either none or the the maximum number of failed TECs ($N_{TEC,fail}$) should be replaced. This can be seen in figure 10.4, in which the percentage of non-maximum replacements is shown per state.

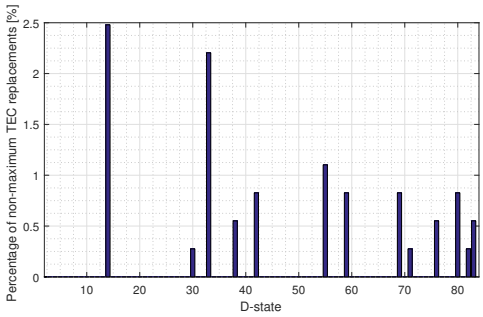

Figure 10.4: Percentage of non-maximum TEC replacements if maintenance is initiated

The two states with the highest number of non-maximum TEC replacements are state 14 and 33, which have been observed more in detail. The distribution of the number of TEC replacements for both states for the identified optimal policies have been depicted in figure 10.5. All occurrences in which a non-maximum replacement is performed describe a maintenance activity in which one TEC less is replaced.

The selected Utility Vessel can carry three TECs at once, as described in chapter 6. In the situation 5 TECs were to be replaced instead of 4, the vessel would require to have a tidal platform enter maintenance three times, instead of only twice. For this small number of simulations the weather window must have been unfavorable, so the additional waiting time (and corresponding costs) was less optimal than replacing one more TEC.

This phenomenon is also observed in the other occurrences of non-maximum replacements and is the proof that subdividing the TECs over the tidal platforms, requiring independent tasks to perform the maintenance on each platform, has a noticeable effect on the policy outcomes, and also influences the maintenance cost rate.

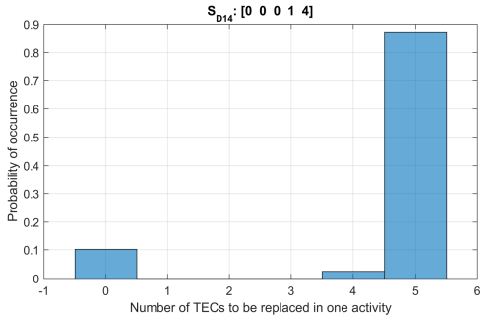

(a) TEC replacements of optimal policies in S_{D14}

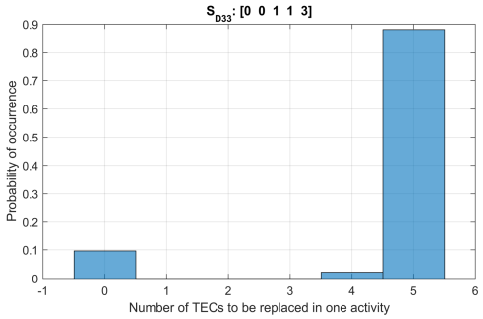

(b) TEC replacements of optimal policies in S_{D33}

Figure 10.5: TEC replacements in states with high non-maximum replacements

Still, it can be said that in a vast majority of the simulations the optimal decision in a state is to either perform no maintenance or replace the maximum number of TECs. This corresponds with the conclusions of existing analytical group replacement models [6]. Still, this preliminary model conclusion will be looked into once more in the recommended policy, which is be described in subsection 10.1.5.

10.1.4. Comparison of optimal policies

For determining the recommended policy in the base case, it has been decided to compare the maintenance cost rates of the three most occurring optimal policies. The policies which are included are listed below, including their occurrence within the set of identified optimal policies.

- Policy E (16%)
- Policy F (10%)
- Policy G (17%)

As mentioned before, the approach in this research is to use this initial set of identified optimal policies to narrow down the observed policies, which will then be applied once more to all 1000 simulations. Again, it is important to state that, whilst being the optimal policy in at least one simulation, it does not necessarily have to result in being a global optimal policy. Still, being optimal in some cases and possibly sub-optimal in others increases the chance of at least approaching the global optimal policy.

Decision regimes

When comparing the three policies and their respective decisions per state, an interesting decision pattern was observed. It was found that three Decision Regimes (DRs) can be set up, which are related to the number of TEC failures ($N_{TEC,fail}$) of the respective states. The distribution of TEC failures among the tidal platforms did not affect these regimes.

The three DR which were identified in the analyzed optimal policies are:

DR 1 Maintenance should never be performed
DR 2 Maintenance should be performed, based on the failure combination
DR 3 Maintenance should always be performed

In DR 1 the renewal of the failed TECs never outweighs the cost due to the TEC downtime. The system is therefore left to deteriorate to subsequent D-states until the economical break-even point is achieved.

DR 2 can be seen as the transition between the D_1 ('Do Nothing') and D_2 ('Perform Maintenance') set of decisions. All three policies have very similar DR boundaries, but an unique set of decisions in DR 2. This shows that each of the three observed policies have near identical decisions and only differ slightly. It should be noted that for all three policies the maximum number of TECs are replaced if decided to perform maintenance.

All decisions in DR 3 are to perform maintenance and replace $N_{TEC,fail}$, regardless of the failure combination. This can be explained by the physical representation that the added cost of long maintenance activities (including sailing back and forth to the port to load more TECs) never becomes more expensive than the downtime costs of the non-replaced TEC(s). Also, the fixed mobilization costs of the vessel only have to be paid once when replacing all TECs in one maintenance activity.

The regime boundaries which apply to the three policies are shown in table 10.3 and are defined by the number of failed TECs. These may be subjected to change when observing other policies. In this analysis the DR boundaries of policy G describe the largest envelop when interested in DR 2. Policy E and F have slightly shifted boundaries between DR 1 and 2, but in this analysis the decisions will be shown for that of policy G to depict all.

Having developed this new method for describing maintenance policies with a large set of decisions, it is now possible to perform a clear comparison of the three maintenance policies. DR 1 and 3 describe the situation of performing no TEC replacement and $N_{TEC,fail}$ TEC replacements, respectively. These states and decisions will not be plotted as these are evident, based on the DR properties. The decisions per state of the three policies of DR 2 are shown below in figure 10.6.

Table 10.3: Boundaries of the decision regimes for analyzed policies

DR	Lower boundary $[N_{TEC,fail}]$	Upper boundary $[N_{TEC,fail}]$
1	0	2 (3*)
2	3 (4*)	5
3	6	9

* the respective boundaries of policy E and F

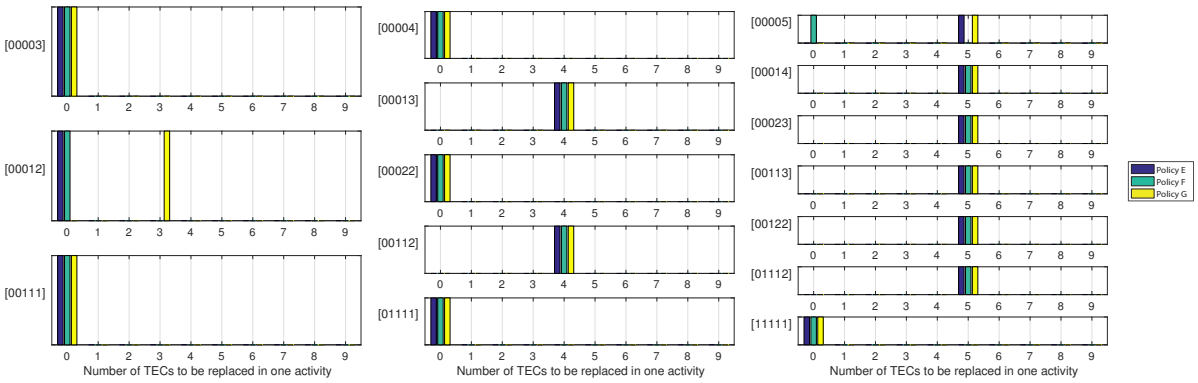

(a) States with $N_{TEC,fail} = 3$ (b) States with $N_{TEC,fail} = 4$ (c) States with $N_{TEC,fail} = 5$

Figure 10.6: Decisions per state for the three analyzed policies within DR 2 of policy G

It can be observed that policy G is the only policy which initiates maintenance when $N_{TEC,fail} = 3$ in the case that two TECs have failed on one platform and the third TEC on a different platform.

For the states with $N_{TEC,fail} = 4$ all policies have identical decisions. It may seem that the states with failure combination $N_{TEC,fail,i}$ = [00004] and [00013] have identical properties, since the situation after replacing three out of four TECs (due to $N_{TEC,vessel}$) is one failed TEC. It must not be forgotten that the policy optimization also takes the possible next outcomes (the arrival states in case of D_1 - 'Do Nothing') into account, which are in fact much different.

For the states with $N_{TEC,fail} = 5$ policy E and G initiate maintenance in one more state with respect to policy F. Overall policy G can be seen as the most maintenance eager policy, followed by policy E and lastly policy F. Still, this observation does not say anything about the corresponding maintenance cost rate and merely provides insight in how these policies differ compared to each other.

Maintenance cost rates

Having defined what makes each of the analyzed policies unique, it can be said there is a noticeable difference in the lower threshold until maintenance is initiated, at least in the cases shown in figure 10.6. Still, this difference is relatively small considering the set of possible decisions is many times greater due to the presence of 83 D-states.

To quantify the difference in terms of maintenance cost rates, each of the three policies has been plugged into the model once more to execute its set of decisions for each of the synthetic time series. Having assumed that the 1000 simulations fully describe all environmental uncertainty, this will thus lead to the effective maintenance cost rate distribution per policy. The cumulative distribution of the three policies are depicted in figure E.20a.

Confidence levels

Also, figure E.20b shows which policy provides the lowest maintenance cost rate, given a certain confidence level. Policy E and G fully describe the range of confidence levels, with policy G showing lower cost rates between 0% and 11%, and in the range of 52.5% up to the 100% confidence level. Industry values for the

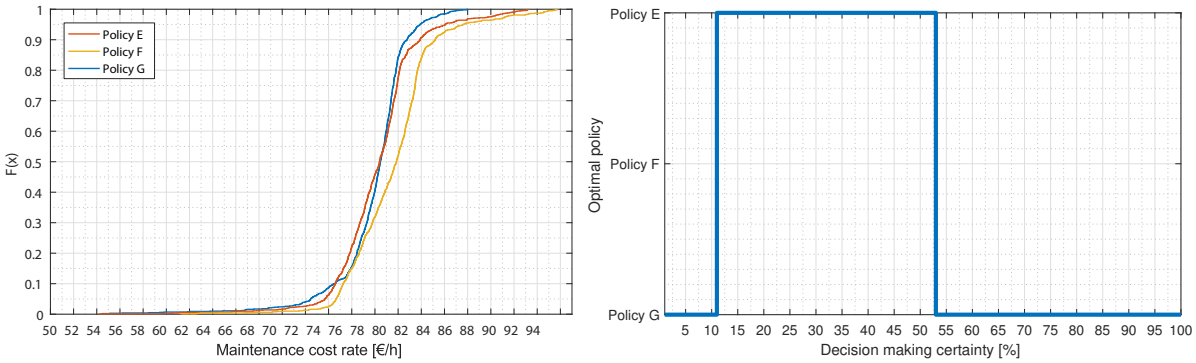

(a) Maintenance cost rates of selected policies (b) Recommended policy based on decision making certainty

Figure 10.7: Comparison of the maintenance cost rate per analyzed policy

applied confidence levels are usually ranging between P50 and P99, depending on how much risk is taken by the decision maker. Especially for these kind of costly operations with a high uncertainty, it is highly advised to implement a conservative confidence level, implying the P-value should be close to 100.

The maintenance cost rates for the described confidence levels are listed in table 10.8, in which also the theoretical lower limit is given, which corresponds to the previously described situation in which the decision taker has full insight in all (future) uncertainties at the moment of deciding. It can be seen that especially for P90 the theoretical lower limit is close to that of policy G, implying that this policy is very cost effective to implement.

Table 10.4: Maintenance cost rates of the identified optimal policies for different confidence levels

Confidence level	Policy E [€/h]	Policy F [€/h]	Policy G [€/h]	Lower limit [€/h]
P50	**78.34**	79.86	78.47	77.45
P90	81.89	83.21	**80.77**	80.15
P99	89.86	92.57	**84.41**	82.42

Recommended maintenance policy

It should be mentioned clearly that the selection of the confidence level is entirely up to the decision maker and the output of this decision support tool can merely give advice on the risks and gains which are related to different levels. Still, since the scope of this research describes the early stage development of a novel tidal platform system, the recommended policy in this thesis will be policy G, using a relatively conservative confidence level of P90.

10.1.5. Analysis of recommended maintenance policy

This subsection describes the analysis which has been performed to provide more insight in the recommended policy, policy G. The decisions per state have already been described by means of the different DR levels of the policy, listed in table 10.3, and the decisions in DR 2, shown in figure 10.6.

Maintenance loops

When applying policy G, the tidal system will be left to deteriorate from its fully renewed state ($N_{TEC,fail} = 0$) until it arrives in one of the states listed in table 10.1.5. In any of those D-states, decision D_2 is selected and the SMDP transits immediately to the corresponding M-state. Since the policy replaces the maximum number of TECs when a maintenance activity is performed, the loop is closed and the process of deterioration starts again in its initial state.

These loops, each with their own unique arrival state, are called maintenance loops and describe a closed set of states and transitions in which the system acts, given that the maintenance policy is followed at all times. Table 10.1.5 gives the unique maintenance loops of policy G, including the fraction that the system will end in that arrival state due to deterioration. A visualization of all states and transitions within the closed set is shown in appendix E.13.

Table 10.5: Unique maintenance loops of policy G

Loop	$N_{TEC,fail}$	Arrival state	Arrival probability
1	3	[0 0 0 1 2]	60.26%
2	4	[0 0 0 1 3]	7.46%
3		[0 0 1 1 2]	17.98%
4	5	[0 0 0 0 5]	0.24%
5		[0 0 0 1 4]	1.28%
6		[0 1 1 1 2]	10.10%
7	6	[1 1 1 1 2]	2.69%

10.2. Reference case: Optimal policy without unique failure combinations

This section describes the results of a simplified alternative approach for finding an optimal maintenance policy, without making distinction between the unique failure combinations and assuming that always $N_{TEC,fail}$ TECs will be replaced if maintenance is performed. The results from this calculation can then be used to determine the added value of the newly developed maintenance optimization model.

10.2.1. Approach

This approach uses the same data as the developed model, which has already been presented in subsection 10.1.2. The approach is as follows:

Step 1 For each $N_{TEC,fail}$, determine:
- **1.1** Time up to failure
- **1.2** Total downtime costs up to failure
- **1.3** P90 value of the total maintenance cost for the least expensive failure combination

Step 2 Add the downtime costs and maintenance costs to obtain the total costs (if maintenance were to be performed at that moment)

Step 3 Divide the total costs by the time up to the failure to obtain the maintenance cost rate

Step 4 The bottom of the curve shows the optimal value of $N_{TEC,fail}$ when maintenance should occur

In this approach the least expensive maintenance operation is selected to provide the absolute lower boundary of costs. Also, the possibility of a TEC failure during maintenance is excluded, which should lower the overall maintenance cost rate of this approach even further.

10.2.2. Comparison of results

Figure E.20a shows the corresponding maintenance cost rate for each of the possible maintenance policies. It can be observed that the cost rate decreases when decided to postpone maintenance until more TECs have failed. Since $Nfail,max = 9$, the cost rates for the remainder of $N_{TEC,fail}$ cannot be inspected, but it clearly shows that the cost rate flattens out at $N_{TEC,fail} = 9$ and will not decrease much more. Therefore, this value will be assumed to give the minimum maintenance cost rate for this approach.

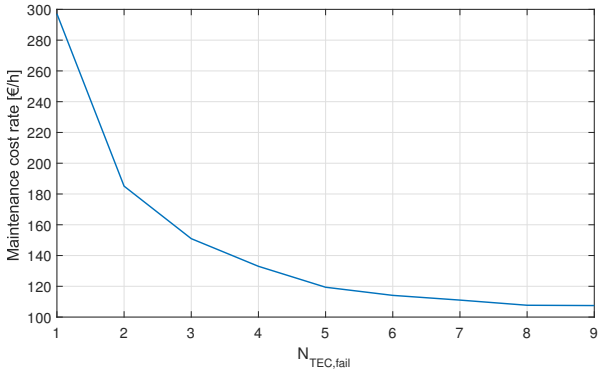

Figure 10.8: reference case: Optimal maintenance cost rate

When comparing the minimum cost rate of this approach to that of the policy G, from the developed model, a significant difference can be observed. The P90 values of the optimal policy for both approaches are listed below in table 10.6. By implementing the more complex policy optimization model, the overall maintenance costs can be reduced by almost 25% with respect to an already partially optimized result.

Table 10.6: Comparison of P90 values for minimum cost rates

Approach	P90 cost rate [€/h]	Relative difference [%]
Reference case	107.50	100 %
Developed model	80.77	75.13 %

This result is very significant and proofs that the development of this model brings great advantages in terms of minimizing the maintenance cost rate for complex systems, such as a tidal array. Having included a more detailed description of the tidal array, by means of describing unique failure combinations, the optimal maintenance policy can also differentiate between these unique states, as they each have their own duration and cost distribution for the corresponding maintenance activity.

In this comparison the optimal policies from both approaches also differed, showing that the uncertainty and its effects are described more extensively in the model, after which it was included in the optimization of the maintenance policy. It must be mentioned that all additions to this model greatly increase the number of possible states and unique decision sets within the system. The choice of representing the tidal array in a SMDP has been an absolute necessity in terms of finding an optimal policy within a considerable amount of time.

10.3. Sensitivity analysis

10.3.1. Selecting representative simulations

To reduce the overall simulation time for the sensitivity analysis, only 20 simulations have been selected ($N_{sim} = 20$). For every 5 percentile of the identified optimal cost rate distribution, the corresponding simulation has been identified. This reduction leads to a lower accuracy, but will have a similar distribution as the full simulation with $N_{sim} = 1000$.

10.3.2. Scenario 1: TEC failure rate

A large uncertainty at this point in the design is the failure rate of the individual assemblies, which are used to calculate the model parameter λ_{TEC}. As stated in subsection 5.4.2, reference values of 300kW wind turbines are used in this model. In table 5.2 it was observed that a reduction of power production, from 1MW to 300kW, leads to significant reductions in the failure rate. By assuming this trend also applies to the assemblies of a tidal platform, it results in lower failure rates of the TEC, since its rated power (P_{rated}) is only 110kW.

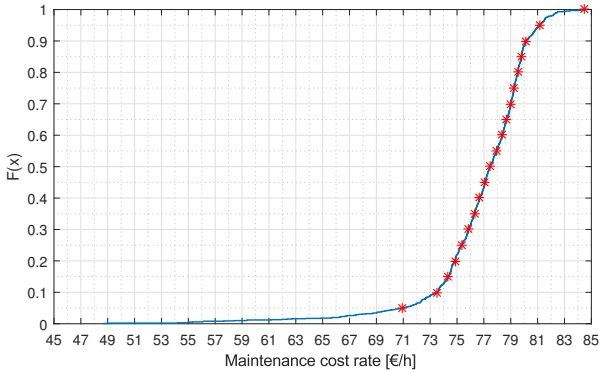

Figure 10.9: Selection of simulation points from identified optimal policies

On the other hand, the harsh marine environment may induce additional loads on the system, accelerating the wear of the system. This can theoretically result in an increase in failure rate (of at least the assemblies which are in contact with the water, such as the blades), but it requires additional research to quantify these conversion factors. As mentioned, in subsection 5.4.3, there are researches which indeed increase the failure rates with adjustment factors to take the naval underwater environment into account.

It is thus of great interest to investigate the effect on the optimal policy and maintenance rate distribution when both increasing and decreasing the failure rate. This will give insight in how this large uncertainty influences the results.

Model limitations when increasing λ_{TEC}

In the model description (subsection 9.5.1 and 9.7.4) it was already described that the applicability of the model is bounded by the ratio between λ_{array} and λ_{MTTR}, since only the possibility of one TEC failure is implemented during maintenance. For the majority of the cases this assumption holds, but in cases where either the number of TECs in the array ($N_{TEC,tot}$) is very large or the TEC failure rate λ_{TEC} is larger than currently assumed, this assumption no longer holds due to $\lambda_{array} >> \lambda_{MTTR}$ and unrealistic results are found.

This limitation will be overcome by running the sensitivity analysis of λ_{TEC} twice:

Run 1 describes the example array, described in section 9.3 ($N_{platform} = 3, N_{TEC} = 2$), with both reduced and increased TEC failure rates to give insight in the qualitative influence of changing λ_{TEC}.

Run 2 describes the Damen base case ($N_{platform} = 5, N_{TEC} = 16$) with reduced TEC failure rates with respect to the base case, to provide quantitative results when λ_{TEC} is lower than assumed.

Qualitative results: Run 1

The maintenance cost rates distributions plotted in figure 10.10a show an increase as the failure rate increases, which is as expected. More interesting is to note that the cost rate does not scale linearly with the change of failure rate. The relative difference of the P90 values have been listed in table 10.7, which shows that doubling the original failure rate only results in an increase of 48.8% of the total maintenance cost rate. This can be explained by the existence of fixed set-up costs for maintenance and variable costs. This implies that regardless of the TEC failure rate, the cost rate always consists of a fraction which can be seen as the fixed (minimum) costs for maintaining the system.

A second observation is that of the changing maintenance decisions as the failure rate increases. This is represented in figure 10.10b, which shows the identified optimal decisions in $S_{D2} = [001]$. As the failure rate increases, the time between consecutive failure decreases. A trend can be identified of maintenance that maintenance is postponed until a later moment as the failure rate increases. The dark blue bar shows that all optimal decisions choose to perform replace the single failed TEC, if the failure rate would be half the original failure rate. From 2.5 times the original failure rate all optimal decisions choose to postpone the maintenance until a later state.

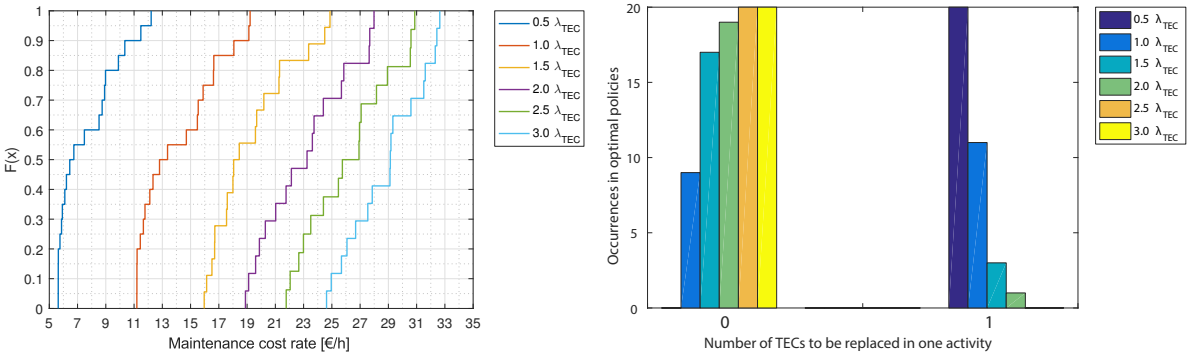

(a) Cumulative distribution of maintenance cost rates

(b) Identified optimal decisions in S_{D2} = [001]

Figure 10.10: Maintenance cost rates and optimal decisions for different λ_{TEC}

Table 10.7: Relative difference in maintenance cost rate at P90 due to changing λ_{TEC}

$X \cdot \lambda TEC$	Rel. diff. at P90
0.5	59.7%
1.0	100.0%
1.5	129.9%
2.0	148.8%
2.5	164.5%
3.0	174.3%

The listed results are only for obtaining qualitative insights in the sensitivities, so the actual maintenance cost rates are not related to the base case. However, since the failure rate data of tidal assemblies is mostly unavailable and solely relies on offshore wind reference data, it is important to conclude that this maintenance model is not highly sensible to discrepancies in the failure rates.

Quantitative results: Run 2

Performing the same sensitivity analysis for the Damen base case, it can be observed that the same effect occurs when decreasing the TEC failure rates. A decrease in the failure rate results in a larger (positive) change in the corresponding maintenance cost rates, whilst an increase in the failure rate has a less significant (negative) impact on the maintenance cost rate.

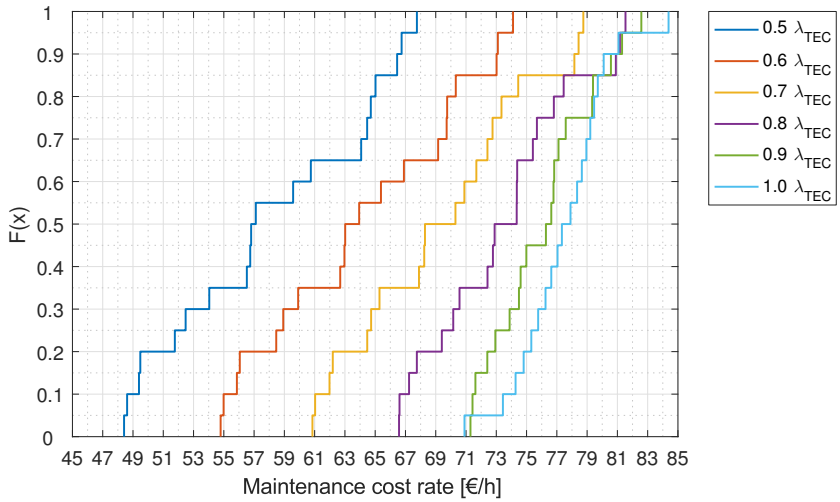

Figure 10.11: Cumulative distribution of maintenance cost rates for different λ_{TEC}

This effect is very favorable, especially in the current phase of development. The resulting maintenance cost rate for the Damen base case can therefore be a good first estimate, as uncertainty in the failure rates of tidal assemblies can be easily accounted for by adding a correction factor, which should be in line with the relative cost differences of this sensitivity scenario.

Table 10.8: Maintenance cost rates of simulations with varying λ_{TEC} values for different confidence levels

Confidence level	$0.5 \cdot \lambda_{TEC}$ [€/h]	$0.6 \cdot \lambda_{TEC}$ [€/h]	$0.7 \cdot \lambda_{TEC}$ [€/h]	$0.8 \cdot \lambda_{TEC}$ [€/h]	$0.9 \cdot \lambda_{TEC}$ [€/h]	$1.0 \cdot \lambda_{TEC}$ [€/h]
P50	56.96	63.48	69.30	73.62	76.46	77.62
P90	66.60	73.06	78.30	81.03	80.94	80.59
P99	67.76	74.11	78.75	81.54	82.58	84.38

10.3.3. Scenario 2: Array size

The second scenario which has been studied is the increasing number of tidal platforms in the array. The results of this scenario may either be of interest to give insight in the consecutive placement of platforms, or by finding the optimal number of platforms which can be maintained by one vessel.

Figure 10.12 depicts the maintenance cost rates for increasing the number of platforms from one to five. It is expected to see an increase in the total maintenance costs, but this gives a distorted view on the actual effectiveness, as the corresponding increase in electricity production capabilities are not plotted.

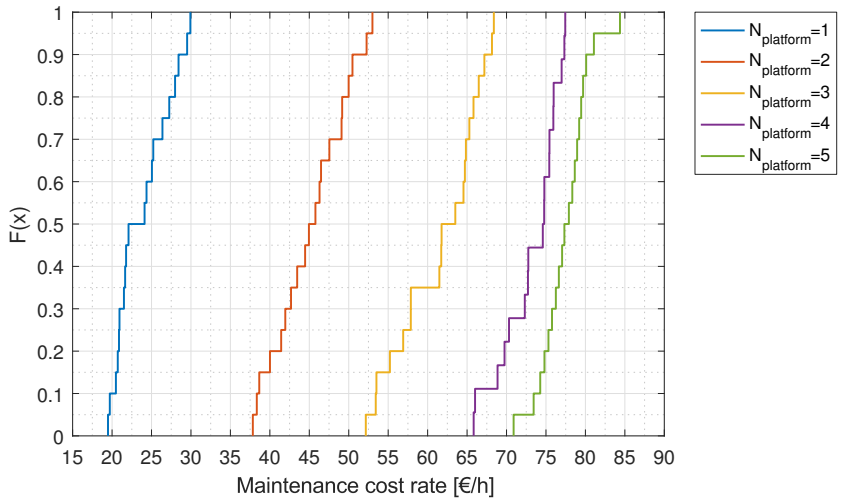

Figure 10.12: Cumulative distribution of maintenance cost rates for different $N_{platform}$

Therefore the P90 value of the maintenance cost rates have been normalized to represent the cost of maintaining one tidal platform. The results are listed in table 10.9 and show a decrease in the normalized maintenance cost rate as the number of tidal platforms in the array increases. It is therefore recommended, under the assumption that the application of a constant failure rate is valid, to directly construct and commission the five tidal platforms at once and initiate the operational phase. However, in reality this may result in a undesirable event in which a significant part of the TECs fail within a short amount of time due to wear-out failures.

Table 10.9: Normalized maintenance cost rates for different $N_{platform}$

$N_{platform}$	1	2	3	4	5
P90 total [€/h]	28.97	51.37	67.67	77.16	80.59
P90 normalized [€/h]	28.97	25.68	22.55	19.28	16.11

10.3.4. Scenario 3: Maintenance vessel

The last scenario which is analyzed in this sensitivity study is that of fluctuating vessel day rates. The base case value is depicted as the red line in figure 10.13, whilst the blue and yellow line describe the lower and upper boundary of the vessel day rates, respectively. These day rates have been identified in subsection 6.2.3.

Similar to the first two scenarios, an increase of the day rates by 100% (base case to upper bound: €13.5k to 27.0k) results in an significantly smaller increase of the total maintenance cost rate, namely 35%. However, by decreasing the day rate by almost 60% (base case to lower bound: €13.5k to 5.6k), the new cost rate is only reduced by 20% with respect to the original value.

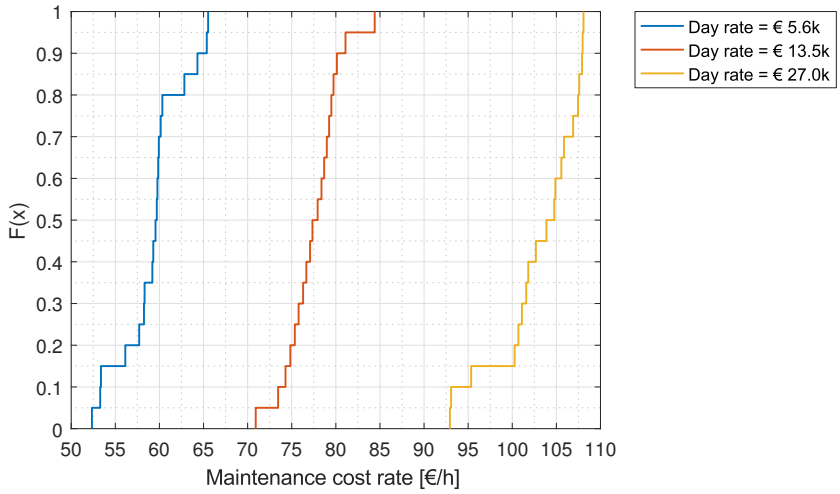

Figure 10.13: Cumulative distribution of maintenance cost rates for different vessel day rates

A reasonable explanation for this is the presence of the other maintenance cost related factors, which do no scale with the changing day rates in this analysis. The TEC repair costs remain constant in all three cases and also the fuel and crew costs fixed, regardless of the day rate changes. Of course the market is highly unpredictable and a fluctuation of one factor, such as vessel day rates, may also be related to price fluctuations of other related maintenance costs. It is therefore recommendable to rerun this model if any of the cost factors changes noticeably.

11

Conclusions & recommendations

11.1. Conclusions

RQ 1 *How can the environmental effects at tidal hotspots be realistically modeled?*
- (a) *Can dependence between the variables be identified and explained?*
- (b) *What model is best used to generate time series which includes multivariate dependence?*

The EMEC tidal field measurement data provided unexpected results when analyzing the bivariate dependence between the wind velocity, significant wave height, peak wave period and the current velocity. A negligible dependence was found between the wind and wave compared to results from open water locations [65]. This may be explained by the sheltered location and shallow waters of the tidal location, but no additional research was performed on this behavior as no long-term data was available from EMEC.

Secondly, the bidirectional current seemed to have a significant influence on the wave propagation direction. The occurrence of tidal lumps [55], which could be identified in numerical models of the EMEC field, could not be identified in the measurement data. Contrary to that, it was observed that the general wave propagation direction would follow the current direction in more than 90% of the samples, and samples with opposing flow directions only describing relatively small wave heights. This gave enough arguments to assume that the directionality of the waves, current and wind could be neglected when creating synthetic time series, as this would not contribute in terms of environmental harshness of changes in persistence.

Another analysis of the EMEC measurement data concluded that no improved dependence could be found between the waves and current when observing the high-frequency components of the respective phenomena. A frequency analysis showed the best correspondence between the waves and current in the lower frequencies, which corresponds to the semi-diurnal character of the tide. It was thus concluded not to implement high frequency observations for describing dependence between the wave and current variables.

The four environmental parameters (H_s,T_p,U_{wind} and U_{curr}) would therefore be used in their normal state, excluding directionality, to develop the vine. A D-vine structure showed to be the best fit for describing the multivariate dependence. The only significant bivariate dependence in the data was between the current velocity and the peak wave period, followed by weak dependence between the wind velocity and significant wave height, and significant wave height and peak wave period.

Due to the relatively short set of measurement data, it proved to be impossible to obtain time independent samples. This condition normally is required for an effective representation by copulas, as each set of simulated samples is generated by random seeds and thus does not include variable properties from previous time steps. Therefore, a new vine simulation method has been developed for including both time dependence and multivariate dependence in the synthetic time series. This has been achieved by using a sequential sampling method which first samples the set of univariate time series and then plugs the generated output into the existing multivariate dependence simulation algorithm, instead of using random uniform input. This method proves to work very well for the EMEC data and contains both types of dependence in the dataset. The validity of applying the synthetic time series has been presented as the weather window lengths closely resembled

that of the original data set.

The added value of using the new simulation method consists of two main factors. Firstly, by using a pair-copula construction to simulate synthetic time series, more realizations can be generated than by using the original measurement set. This significantly contributes to providing a more complete description of the weather window uncertainty. Secondly, the inclusion of multivariate dependence in the synthetic time series gives a more realistic representation, which is expressed as a slight reduction of the maintenance activity durations compared to using time series without multivariate dependence. The beneficial effect of including multivariate dependence can be strengthened if the operational limits of weather windows are based on (combinations of) all four environmental variables.

RQ 2 *How can the uncertainty in the maintenance activities of the TEC array be included in the model?*

Chapter nine describes the development of the model which includes the maintenance and failure related activities. A semi-Markov decision process has been chosen to represent the decision making in the model. The tidal array is to be represented in unique states, after which the transition rates and corresponding costs need to be determined. The unichain policy optimization algorithm can then be applied to converge to an optimal maintenance policy, which describes the best decision for each state.

Maintenance activities are included by a number of simplifications which describe the process of replacing TECs by means of a numerical approach, which uses a single synthetic environmental time series. Interaction between the environmental phenomena and the vessel activity is modeled by means of describing weather windows for the identified maintenance tasks. The vessel is required to wait until a weather window occurs for the consecutive tasks, similar to what would happen in reality.

Maintenance uncertainty due to the environment is introduced to the model by applying a Monte Carlo simulation on the decision making model. Each synthetic environmental time series is randomly generated, whilst having near identical long-term properties. By using a large number of synthetic time series, it can be safely assumed that the maintenance uncertainty is fully described by the distributed model results.

RQ 3 *How can the resulting optimal maintenance policy influence the decision making?*
- (a) *How does this model relate to other generic analytic group based maintenance models?*
- (b) *What are the main sensitivities that affect the total maintenance cost?*

Chapter ten describes the results of the base case run of the decision support model. The maintenance uncertainty has a direct effect on the corresponding optimal policies. For every individual simulation an optimal policy is found, but it has been found that the optimal policy is subjected to change due to varying maintenance duration and costs. The set of optimal policies each correspond to different maintenance cost rates, which thus can be described by a distribution based on its occurrence.

Given the limited data availability of the tidal system properties, a relatively detailed representation of the tidal system has been developed. The model developed in this thesis has proven to generate a maintenance policy which is almost 25% more cost effective compared to more generic optimization studies. This has been achieved by expanding the set of unique states in which the tidal array can reside in, compared to the definitions of a more general group maintenance model. This corresponds closely with the literature on semi-Markov decision processes, which state that the quality of the model results is mostly dependent on the state representation of the observed system.

By analyzing the results of the optimal base case maintenance policy it was found that a significant difference in maintenance costs was found, merely based on varying one state decision. It was thus observed that the more detailed description of the tidal array in unique failure combinations per tidal platform proved to be a significant improvement, but would not have been able if an existing analytical model was used.

The sensitivity study included three scenarios, namely the variation in TEC failure rates, the number of tidal platforms in the array and the fluctuation in vessel day rates. For each scenario it was observed that an arbitrary increase of the parameter of interest would result in a smaller increase of the corresponding maintenance cost rate. The most important conclusions from the sensitivity study are that the model's sensitivity to a change in either the failure rate or vessel day rate is well described and the deployment of multiple tidal platforms in the array is very favorable for the normalized maintenance cost rate.

11.2. Recommendations

The developed decision support tool has shown to be of significant value for giving a good estimate of the maintenance cost rate for an arbitrary tidal energy array. The tool can be used by design engineers in its current state, but nevertheless a number of recommendations can be made to further improve its validity and range of application.

Besides that, the environmental analysis conducted on the tidal location characteristics may provide a starting point for further research. The recommendations regarding the environmental analysis and time series simulation will therefore be discussed separately from the maintenance model recommendations. However, it may be clear that these recommendations also enhance the quality of the maintenance decision support tool and are certainly of interest for the overall model improvements.

11.2.1. Environmental analysis and modeling

Analyze long term data

In this research the measurement data described two months during the calm summer period. The findings are therefore not directly applicable to describe year-round weather conditions, as the winter conditions are usually harsher. The analysis of long term data could therefore contribute significantly to identify seasonality in the data, which can then be applied to give a better representation of the environmental conditions at a tidal location. Currently a long term measurement campaign is ongoing at another tidal hotspot in the Bay of Fundy, Canada, by Fundy Ocean Research Center for Energy (FORCE). Performing a similar research on the multivariate dependence could also help identify generic dependences of tidal hotspots.

Advanced copula families

The multivariate dependence is described in this research by a D-vine construction which only allowed five basic copula families to be included. The included copulas can be used to describe the basic upper and/or lower tail dependence, but more advanced copulas are available. These copulas enable the description of skewness in bivariate data of the observed time series and thus may give a more accurate representation of the actual dependence.

Additional environmental variables

The inclusion of additional variables for representing the environment may contribute to the quality of the generated time series. Literature states that waves height and period are significantly influenced by the changing water depth at the shallow tidal hotspots. Including this variable may possibly result in new dependence, which has not yet been included in this research.

Validate developed simulation algorithm

A sequential D-vine simulation algorithm has been developed which first models univariate time dependence after which the multivariate dependence is generated. This method has shown to be effective for creating synthetic time series with comparable persistence compared to the original time series. The described time dependence proved to be significantly larger than the multivariate dependence, but this ratio may be well different for other cases. In order to apply this algorithm for general use, it is therefore highly recommended to first perform a validation study on the effects on both the multivariate dependence and persistence if this ratio differs.

11.2.2. Decision support tool

Validate operational data

In this preliminary stage of design, a large uncertainty is in the assumptions regarding the operational data, such as assembly failure rates, vessel operation limits and task durations. For the validity of the model it is therefore of great importance to perform validation studies on the failure rate representation. This can

either be done by interpreting the results of existing reliability studies which describe closely corresponding components or by means of deploying a tidal prototype for obtaining real data.

Advanced failure rate distributions

Once more operational reliability data of the TEC components become available, the failure rate distribution should be reconsidered to represent the actual failures more accurately. In this model an exponential failure distribution is applied, which considers a constant hazard rate and is only suited to describe the operational lifetime. Evidently, the failure rate will increase once the component's design lifetime approaches. By merely describing the failures in the TEC array with a constant failure rate, either the hazard rate is overestimated during the operational lifetime or the wear-out failures are underestimated.

The corresponding wear-out failures can effectively be described by means of a Weibull or log-Normal distribution. However, implementation of these advanced failure rate distributions requires failure data to be present in order to estimate the distribution parameters. If these data become available in the future, several models [77, 106] are available for calculating and optimizing maintenance policies.

Advanced vessel operations

In this thesis the operation limits are independently evaluated for each time step. A desired addition to the model would be to include multidimensional limits, which effectively captures the operable conditions for combinations of the environmental variables. This also enables the coupling of existing models to describe the limits during station-keeping and dynamic crane operations.

Secondly, the decision making behavior of the vessel can also be improved. During a replacement operation it may be desirable to deviate from the predefined set of tasks if the alternative, such as returning to port if the forecast describes no weather window, proves to be more cost effective.

Lastly, the inclusion of multiple vessels to perform maintenance in the same array would resemble the actual situation better. Each vessel may have different characteristics and be responsible for its own tasks, be it a maintenance activity or system monitoring.

Different maintenance strategy

In this research a corrective group maintenance strategy was applied, for which the optimal policy has been approached. A different maintenance strategy could possibly lead to further cost reductions, despite having found an optimal policy for the current strategy. Whilst this strategy was employed to describe the upper limit of maintenance cost, for further development of the tidal system it is highly recommended to also include a preventative maintenance strategy. Especially during the operational phase, this strategy can bring significant improvements due to being executed in the least harsh environmental conditions.

A

Copulas and Vines

A.1. Common methods for describing dependence

A.1.1. Pearson product-moment correlation coefficient

The Pearson product-moment correlation coefficient is a measure of the linear correlation between two variables X and Y, giving a value between +1 and -1 inclusive, where 1 is total positive correlation, 0 is no correlation, and -1 is total negative correlation.

$$Pearson's \quad \rho_{X,Y} = \frac{Cov(X,Y)}{\sqrt{\sigma_X^2 \sigma_Y^2}} \tag{A.1}$$

As can be seen in figure A.1, the Pearson correlation coefficient is inadequate for fully describing the dependence between the distribution and does not take skewness, symmetry and other non-linear phenomenon into account.

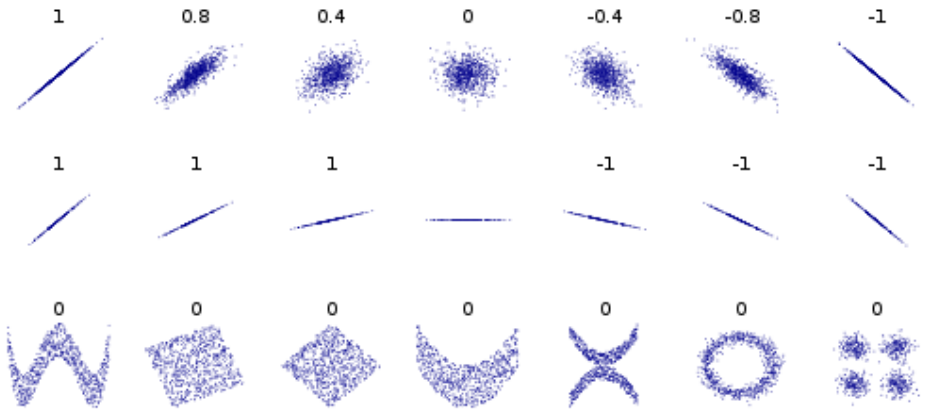

Figure A.1: Pearson Linear Correlation cases

A.1.2. Spearman's rank correlation coefficient

The Spearman correlation [91] between two variables is equal to the Pearson correlation between the rank values of those two variables; while Pearson's correlation assesses linear relationships, Spearman's correlation assesses monotonic relationships (whether linear or not). If there are no repeated data values, a perfect Spearman correlation of +1 or -1 occurs when each of the variables is a perfect monotone function of the other.

$$Spearman's \quad \rho_{X,Y} = \frac{12}{n(n^2-1)} \sum_{i=1}^{n} \left(rank(X_i) - \frac{n+1}{2} \right) \left(rank(Y_i) - \frac{N=1}{2} \right) \tag{A.2}$$

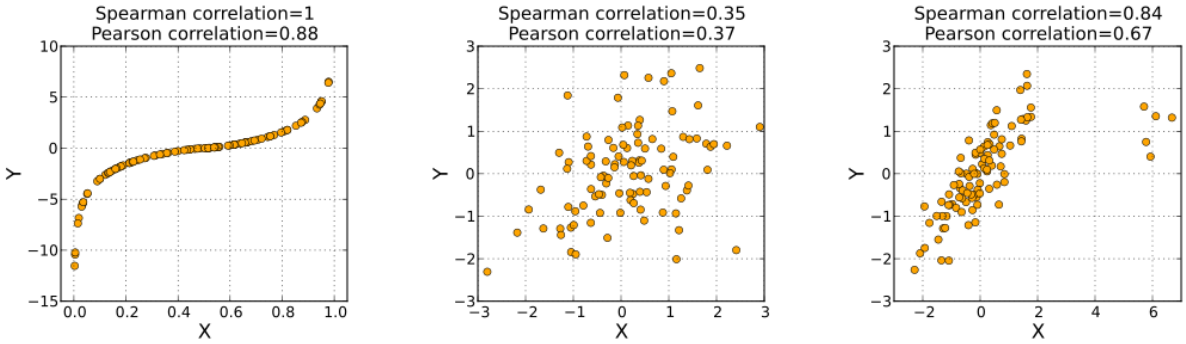

Figure A.2: Differences between Pearson and Spearman correlation

A.1.3. Kendall rank correlation coefficient

The Kendall rank correlation coefficient [49] is a statistic used to measure the ordinal association between two measured quantities. Contrary to the Spearman correlation, the Kendall correlation is not affected by how far from each other ranks are but only by whether the ranks between observations are equal or not. The Kendall Tau correlation

$$Kendall's \quad \tau_{X,Y} = \frac{2}{n(n-1)} \sum_{i<j} sign[(X_i - X_j)(Y_i - Y_j)] \tag{A.3}$$

A.2. Properties of the copula construction methods

Joe [47] has performed extensive research on the analytical elucidation of each of the listed copula construction methods and discussed some desirable properties of copula models, and summarized which of them can be satisfied for the various constructions.

Table A.1: Satisfaction or not of properties for various constructions

Class	A1	A2	A3	A4	B	C1	C2	D
Gaussian	yes	yes	no	no	yes	no	yes	yes
multivariate t_ν	no	yes	yes	no	yes	no	yes	yes
Archimedean	yes	no	no	bivariate	yes	yes	yes	yes
mixture of max-id	yes	yes	bivariate	bivariate	yes	yes	yes	partly
vine PCC	yes	yes	yes	yes	no	no	yes	yes
factor	yes	yes	yes	yes	yes	no	partly	yes

A1 inclusion of independence and comonotonicity copulas
A2 flexible and wide range of dependence
A3 flexible tail dependence
A4 flexible tail asymmetries
B1 closure property under marginalization
C1 closed-form cdf
C2 closed-form density
D ease of simulation

'*Bivariate*' in a cell means that the property holds for bivariate but not general multivariate

A.3. A pair-copula decomposition of a general multivariate distribution

Consider a vector $X = (X_1, \ldots, X_n)$ of random variables with a joint density function $f(x_1, \ldots, x_n)$. This density can be decomposed in the following non-unique way

$$f(x_1, \ldots, x_n) = f_n(x_n) \cdot f(x_{n-1}|x_n) \cdot f(x_{n-2}|x_{n-1}, x_n) \cdot \ldots \cdot f(x_1|x_2, \ldots, x_n) \tag{A.4}$$

Using the copula properties, as described in ..... and assuming F to be absolutely continuous with strictly, increasing marginal densities $F_1, \cdots, F_n$, we get

$$\begin{aligned} f(x_1, \ldots, x_n) &= \frac{\partial F(x_1, \ldots, x_n)}{\partial x_1, \ldots, \partial x_n} \\ &= \frac{\partial C(x_1, \ldots, x_n)}{\partial x_1, \ldots, \partial x_n} \\ &= c_{12\ldots n} \cdot f_1 \cdot \ldots \cdot f_n \end{aligned} \tag{A.5}$$

The second step is done by using Sklar's theorem and the last step by applying the chain rule. The result in (4.2.2) can be used to represent (4.2.1) with pair-copulas and univariate distribution functions alone. We make use of the following type of factorizations

$$f_{1|2} = \frac{f_{12}}{f_2} = \frac{c_{12} \cdot f_1 \cdot f_2}{f_2} = c_{12} \cdot f_1 \tag{A.6}$$

$$f_{1|23} = \frac{f_{123}}{f_{23}} = \frac{f_{12|3} \cdot f_3}{f_{2|3} \cdot f_3} = \frac{c_{12|3} \cdot f_{1|3} \cdot f_{2|3}}{f_{2|3}} = c_{12|3} \cdot c_{13} \cdot f_1 \tag{A.7}$$

$$f_{1|234} = \frac{f_{1234}}{f_{234}} = \frac{f_{12|34} \cdot f_{34}}{f_{2|34} \cdot f_{34}} = \frac{c_{12|34} \cdot f_{1|34} \cdot f_{2|34}}{f_{2|34}} = c_{12|34} \cdot c_{13|4} \cdot c_{14} \cdot f_1 \tag{A.8}$$

Note that (4.2.3) and (4.2.4) are not unique in that a change in the conditioning set in step two would give different results, i.e. different pair-copulas in the final results. We see that each term in (4.2.1) can be decomposed by the following iterative procedure [2]

$$f_{x|v} = c_{xv_j|v_{-j}} \left(F_{x|v_{-j}}, F_{v_j|v_{-j}} \right) f_{x|v_{-j}} \tag{A.9}$$

for a n-dimensional vector v. Here vj is a component of v, and v-j is the v-vector without component j. Decomposing a distribution function with four variables could then be done as follows:

$$\begin{aligned} f_{1234} &= f_1 \cdot f_{2|1} \cdot f_{3|12} \cdot f_{4|123} \\ &= f_1 \cdot c_{12} f_2 \cdot c_{23|1} c13 f_3 \cdot c_{34|12} c_{24|1} c_{14} f_4 \\ &= c_{34|12} c_{23|1} c_{24|1} c_{12} c_{13} c_{14} \prod_{i=1}^{4} f_i \end{aligned} \tag{A.10}$$

There are 24 different combinations for the four-dimensional case [2]. With this is mind, it is desirable to have a decomposition that describes and preserves the (in advance) known information about the dependence structure among the variables as good as possible. This is where the concept of vines is a good aid. Vines will be treated in subsection 2.4.2.

A.4. Vine density distributions

Bedford and Cooke [10] give the density of an n-dimensional distribution for the C- and D-vine, which may be written as follows:

A.4.1. D-vine

$$f_{1,2,\ldots,n} = \prod_{k=1}^{n} f_k f_k \prod_{j=1}^{n-1} \prod_{i=1}^{n-j} C_{i,i+j|i+1,\ldots,i+j-1} \tag{A.11}$$

A.4.2. C-vine

$$f_{1,2,\ldots,n} = \prod_{k=1}^{n} f_k f_k \prod_{j=1}^{n-1} \prod_{i=1}^{n-j} C_{j,i+j|1,\ldots,j-i} \tag{A.12}$$

A.5. D-vine copula simulation algorithm

A.5.1. D-vine

Algorithm 1 D-vine simulation algorithm [2]

Sample $w_1, \ldots, w_n$ independent uniform on [0,1]
$x_1 = v_{1,1} = w_1$
$x_2 = v_{2,1} = h^{-1}(w_2, v_{1,1}, \theta_{1,1})$
$v_{2,2} = h(v_{1,1}, v_{2,1}, \theta_{1,1}$
for $i = 3:1:n$ **do**
  $v_{i,1} = w_i$
  for $k = i-1:-1:2$ **do**
    $v_{i,1} = h^{-1}(v_{i,1}, v_{i-1,2k-1}, \theta_{k,i-k})$
  end for
  $v_{i,1} = h^{-1}(v_{i,1}, v_{i-1,1}, \theta 1, i-1)$
  $x_i = v_{i,1}$
  if $i == n$ **then**
    STOP
  end if
  $v_{i,2} = h(v_{i-1,1}, v_{i,1}, \theta i, i-1$
  $v_{i,3} = h(v_{i,1}, v_{i-1,1}, \theta i, i-1$
  if $i > 3$ **then**
    for $j = 2:1:i-2$ **do**
      $v_{i,2j} = h(v_{i-1,2j-2}, v_{i,2j-1}, \theta_{j,i-j})$
      $v_{i,2j+1} = h(v_{i,2j-1}, v_{i-1,2j-2}, \theta_{j,i-j})$
    end for
  end if
  $v_{i,2i-2} = h(v_{i-1,2i-4}, v_{i,2i-3}, \theta_{i-1,1})$
end for

A.5.2. Node labels

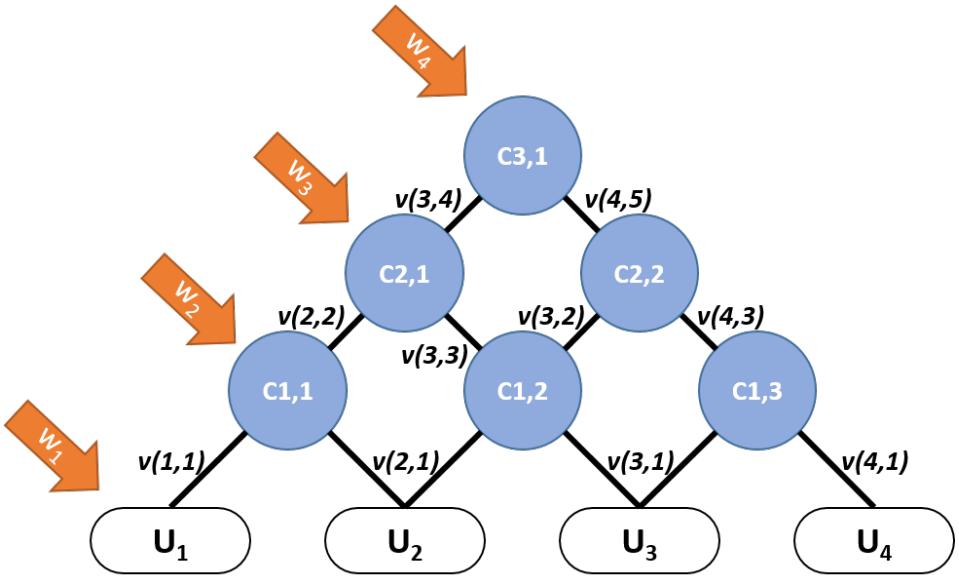

Figure A.3: D-vine node labels

B

Darrieus turbine power generation

B.1. Types of Darrieus turbines

A vertical-axis wind turbine is of Darrieus-type when it is driven by aerodynamic lift [12, 86]. The Darrieus turbine consists of two or more aerofoil-shaped blades attached to a rotating vertical shaft. The wind blowing over the aerofoil contours of the blade creates aerodynamic lift and actually pulls the blades along. In this section, general mathematical expressions that describe the aerodynamic models of Darrieus-type VAWTs are presented.

The Darrieus turbine was initially developed for application in the wind industry, but much research has already been performed on its applicability for tidal currents. Over the course of the years three main Darrieus variants have been developed, as can be seen in figure B.1. Whilst the rotor geometry differs, all types still rely on the lift generating properties due to the foil blade profile.

Figure B.1: Darrieus types

B.2. Power curve

Damen Research has developed a darrieus model to determine the power curve parameters. The model uses a quasi-static approach for calculating the TSR-C_p ratio, based on the Darrieus design. Literature on blade

aerodynamics [43, 86] was used to develop the model and the Darrieus configuration, including its dimensions, were found iteratively by combining recommended designs from existing research [12, 74] with in-house cost and efficiency analyses.

B.2.1. Power coefficient

The power coefficient, (C_p) is a quantity that expresses what fraction of the power in the wind is being extracted by the wind turbine. It is generally assumed to be a function of both tip-speed ratio and pitch angle.

B.2.2. Darrieus swept area

For Darrieus turbines the swept area is constant, as the Vertical Axis Turbine (VAT) is omni-directional and can operate with currents from all directions. The swept area for a Darrieus is calculated as follows,

$$A = 2R \cdot H \tag{B.1}$$

which implies that the vertical surface area, formed by twice the radius (R) and the height(H) of the Darrieus determines the swept area (A) of the PM.

B.2.3. Power coefficient

The power coefficient, (C_p) is a quantity that expresses what fraction of the power in the wind is being extracted by the wind turbine. It is generally assumed to be a function of both TSR and pitch angle.

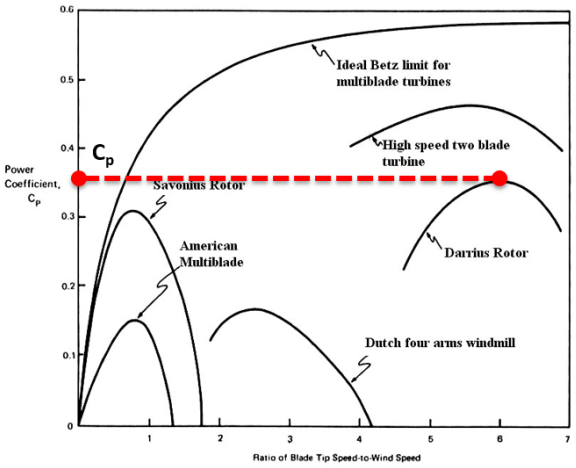

Figure B.2: TSR-C_p relation for different PMs

Tip-speed ratio

The tip-speed ratio (TSR) is the ratio between the tangential speed of the tip of a blade (ωR) and the actual speed of the flow (U_{curr}). This ratio is especially important since it is related to efficiency, as a relation exists between the TSR and the C_p of the system.

$$TSR = \frac{\omega R}{U_{curr}} \tag{B.2}$$

Optimal control strategy

Using a control strategy enables the PM to operate at its optimal TSR, either by changing its pitch angle or by adjusting the rotational speed of the blades. Optimizing TSR for each current flow velocity maximizes C_p and thus results in an increase of the power production.

The slowly changing character of the current velocity enables the use of a quasi-static approach for determining the optimal control strategy. It is therefore assumed that the fluctuations in U_{curr} are slow enough for the control system to always use the best TSR for the optimal power coefficient.

C

Model properties

C.1. Deterioration Module

C.1.1. Calculate $N_{TEC,fail,pos}$

The number of TEC failure possibilities between two D-states can be calculated, given the requirement that the number of failed TECs in a state are written in a row vector, which must be sorted in ascending order. The TEC failure representation in figure 9.3 and table 9.2 show an example of the correct row vector format.

Algorithm 2 Calculates the number of TEC failure possibilities between two D-states

```
for ii = 1:Nstate

    Dind = State(ii,:);
% Individual combination per deterioration phase

    PMavail = Npm*ones(1,Ntec) - Dind;

    Sred = repmat(Dind,[Ntec 1]) + eye(Ntec);
% Matrix with all possible failures to next deterioration phase from the 'From' state

    [Rind,~] = find(Sred>Nfailmax);
% Find entries which exceed Ntec,fail,max
    Sred(Rind,:) = [];
% Remove entries

    [Rind,~] = find(Sred>Npm);
% Find entries which exceed Ntec
    Sred(Rind,:) = [];
% Remove entries

    Ssort = sort(Sred,2);
% Sort remaining entries

    for jj = 1:size(Ssort,1)

        col = ismember(State,Ssort(jj,:),'rows');
% Find the column index of the deteriorated state
        Trans(ii,col) = Trans(ii,col) + ( PMavail(jj)/sum(PMavail) );
        Fpos(ii,col) = Fpos(ii,col) + PMavail(jj);
% Number of TECs which can fail for that failure comb
    end

end
```

C.2. Maintenance Module

C.2.1. Numerical example of maintenance task generation

It can be seen in figure C.1 that three possible maintenance possibilities are possible in maintenance state S_{M5}, after decision D_2 was selected upon entering the corresponding deterioration state S_{D5}. Each of these maintenance decisions is going to renew the system to a certain extend, reducing the number of $N_{TEC,fail}$ in the arrival state.

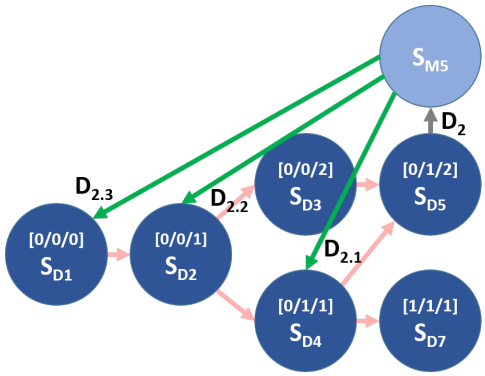

Figure C.1: Tidal array example: Maintenance transitions from S_{M5}

Decision $D_{2.1}$, replacing one TEC, shows a transition to state S_{D4}, but not S_{D3}. This is due to the previously explained model limitation that the algorithm only allows one possible transition per maintenance decision, and thus the algorithm prioritizes maintenance on the platform with most failures.

In table C.1 the output of the task generation algorithm is shown for state S_{M5}. The maximum number of functioning TECs on the vessel ($N_{TEC,vessel}$) is two in this example to show the influence on the task generation.

Table C.1: Tidal array example: Maintenance task generation

Decision $D_{2.1}$	Decision $D_{2.2}$	Decision $D_{2.3}$
Vessel preparation	Vessel preparation	Vessel preparation
TEC loading	TEC loading	TEC loading
Waiting for weather window	TEC loading	TEC loading
Port-array transport	Waiting for weather window	Waiting for weather window
Platform emerging	Port-array transport	Port-array transport
TEC replacement	Platform emerging	Platform emerging
Platform submerging	TEC replacement	TEC replacement
Array-port transport	TEC replacement	TEC replacement
TEC unloading	Platform submerging	Platform submerging
	Array-port transport	Array-port transport
	TEC unloading	TEC unloading
	TEC unloading	TEC unloading
		TEC loading
		Waiting for weather window
		Port-array transport
		Platform emerging
		TEC replacement
		Platform submerging
		Array-port transport
		TEC unloading

D

Environmental analysis

D.1. Acoustic Wave and Current ADCP

Acoustic Doppler Current Profilers (ADCPs) are most often used to measure the velocity profile, but wave data may be obtained when using an AWAC subtype [95], of which an picture is shown in appendix D.1. The wave height is estimated with a vertical beam that measures the distance to the surface using the echo from short pulses and simple peak estimation algorithms. The wave direction is found by cross correlating the along-beam velocity estimates and the wave height measurement from the vertical beam.

Figure D.1: Acoustic wave and current ADCP

D.2. Filtering & smoothing

The environmental dataset contains raw measurement data and has not been quality checked by EMEC. It contains both negative and extreme values for H_s and T_p, including a small period of no measurements. In order to determine the multivariate dependence using copulas, the measurement data of all four variates needs to be usable for each sample. By filtering the dataset for each of the four variables, the time samples for negative (if applicable) and extreme values are identified, so these can be removed from the analysis. Furthermore, the data is smoothed to reduce local fluctuations and measurement errors.

The process of filtering and smoothing is shown below and its effect is depicted in figure D.3,D.4,D.5 and D.6:

1. Remove all NaNs and negative values
2. Remove all extreme values

3. Apply a Hampel filter to remove outliers

D.2.1. Extreme value removal

Unrealistically high peaks in the datasets are removed increase the dataset accuracy and ensure that the more advanced Hampel filters more effectively. The cut-off values, listed in table D.1, for the four variates are selected in consultation via personal contact with EMEC's data technician [97] to apply expert knowledge for validation purposes.

Table D.1: Extreme value limits for EMEC dataset

Variate	threshold value	unit
H_s	5	[m]
T_p	15	[s]
U_{wind}	20	[m/s]
U_{curr}	5	[m/s]

D.2.2. Outlier filtering

A Hampel filter [37] is applied to the input vector, x, to detect and remove outliers. For each sample of x, the function computes the median of a window composed of the sample and its k_{ham} surrounding samples, three per side. It also estimates the standard deviation of each sample about its window median using the median absolute deviation (MAD). In statistics, the MAD is a robust measure of the variability of a univariate sample of quantitative data [59]. If a sample differs from the median by more than $N_{sig,ham}$ standard deviations, it is removed from all four variate time series.

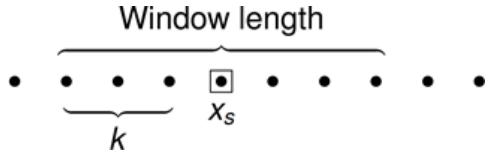

Figure D.2: Window used for the median absolute deviation

$$MAD_i = median(|X_i - median(X)|) \tag{D.1}$$

For the data sets the following Hampel parameters are used, also based on personal contact with EMEC's data technician [97], to perform the outlier filtering.

- k_{ham} = 40
- $N_{sig,ham}$ = 3

D.3. EMEC measurement data

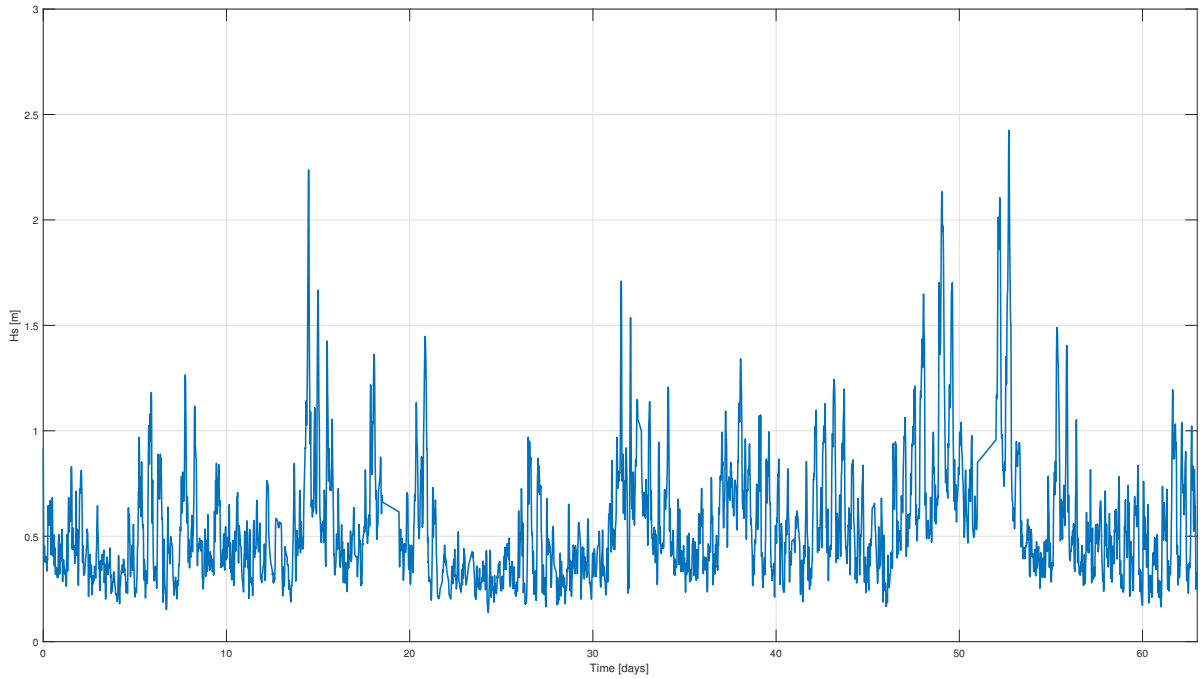

Figure D.3: Timeseries of H_s

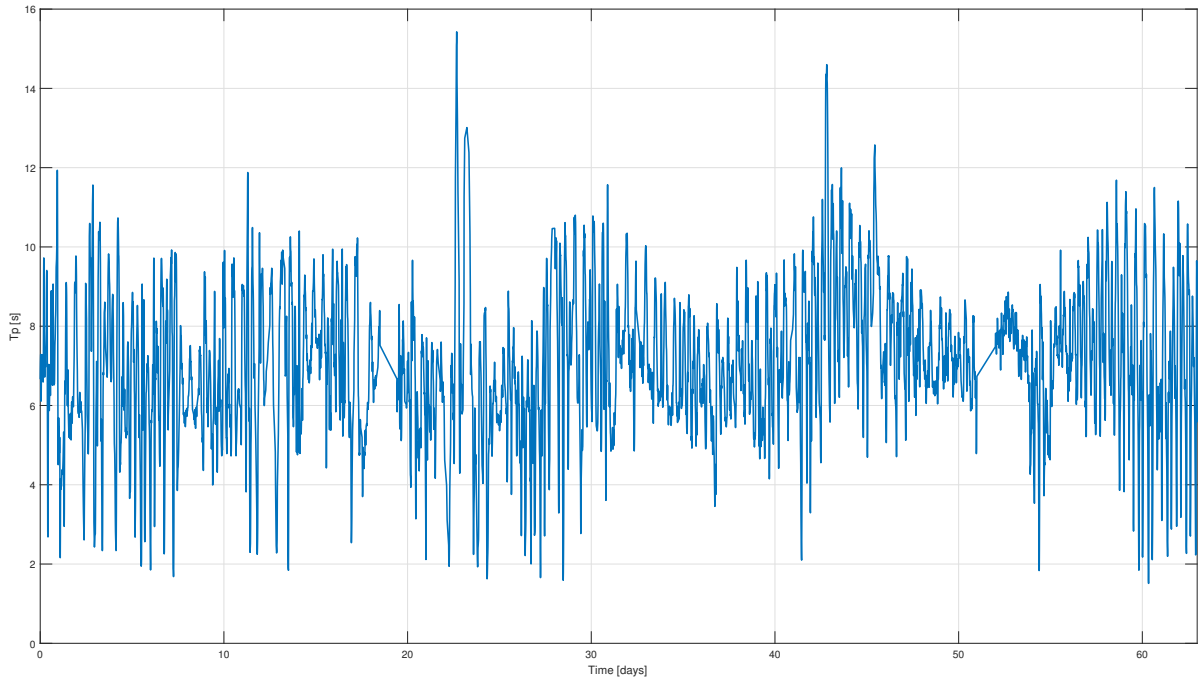

Figure D.4: Timeseries of T_p

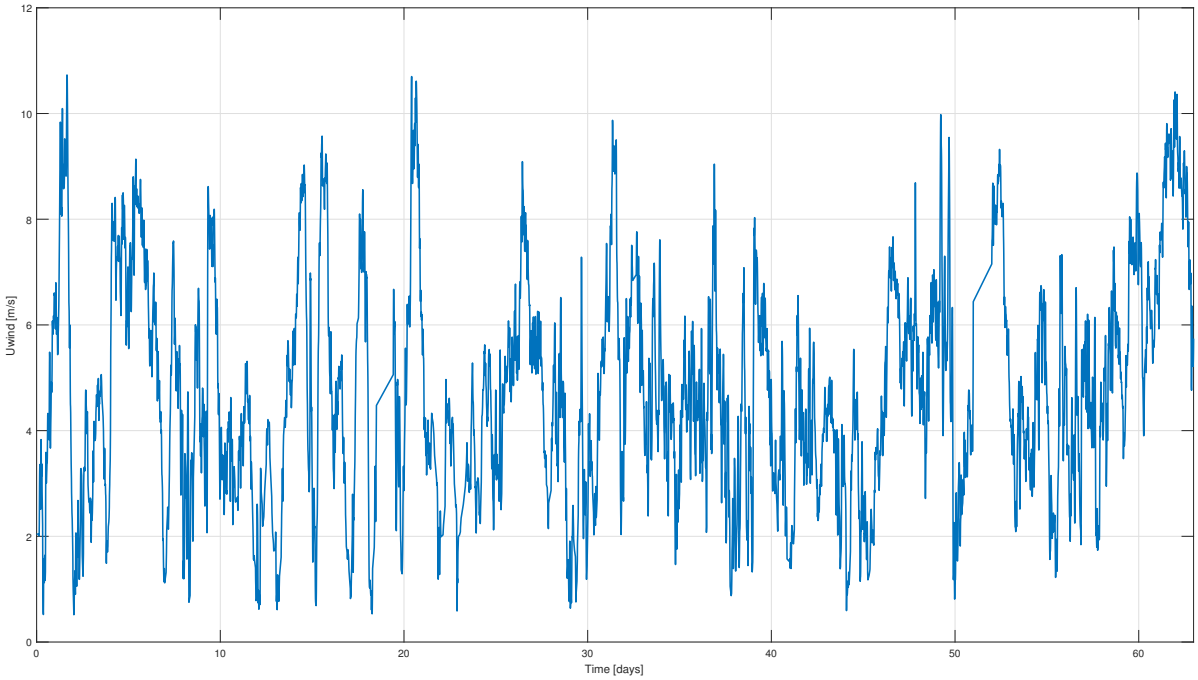

Figure D.5: Timeseries of U_{wind}

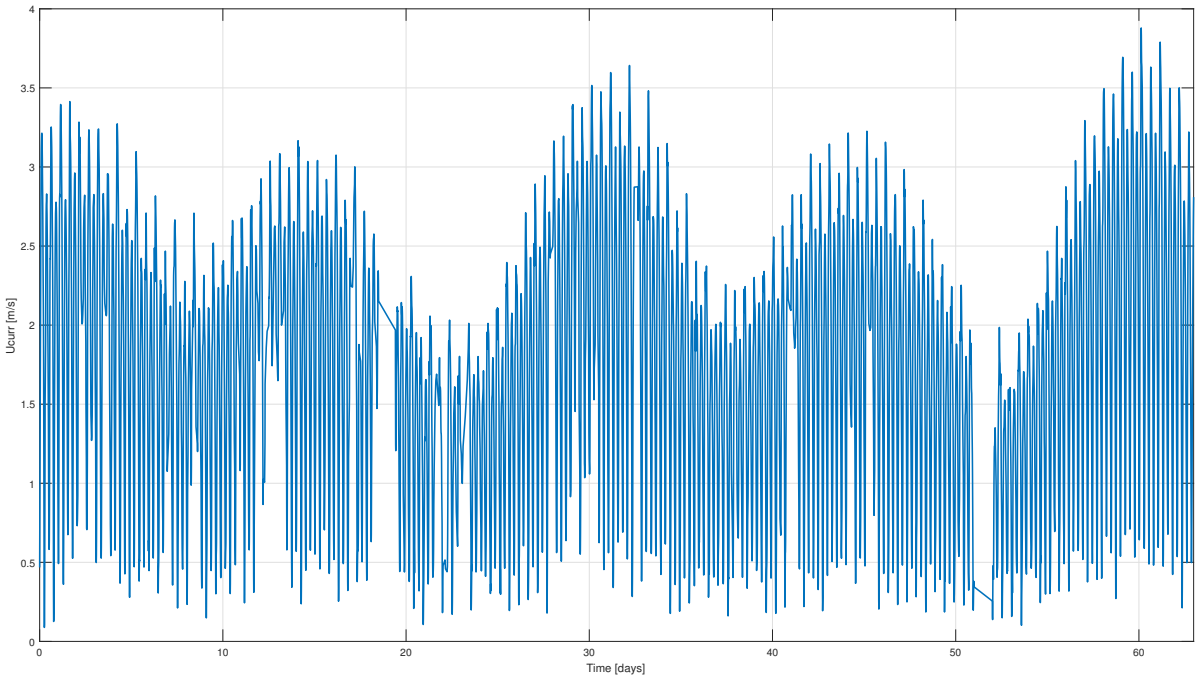

Figure D.6: Timeseries of U_{curr}

D.4. Influence of directionality on wave-current interaction

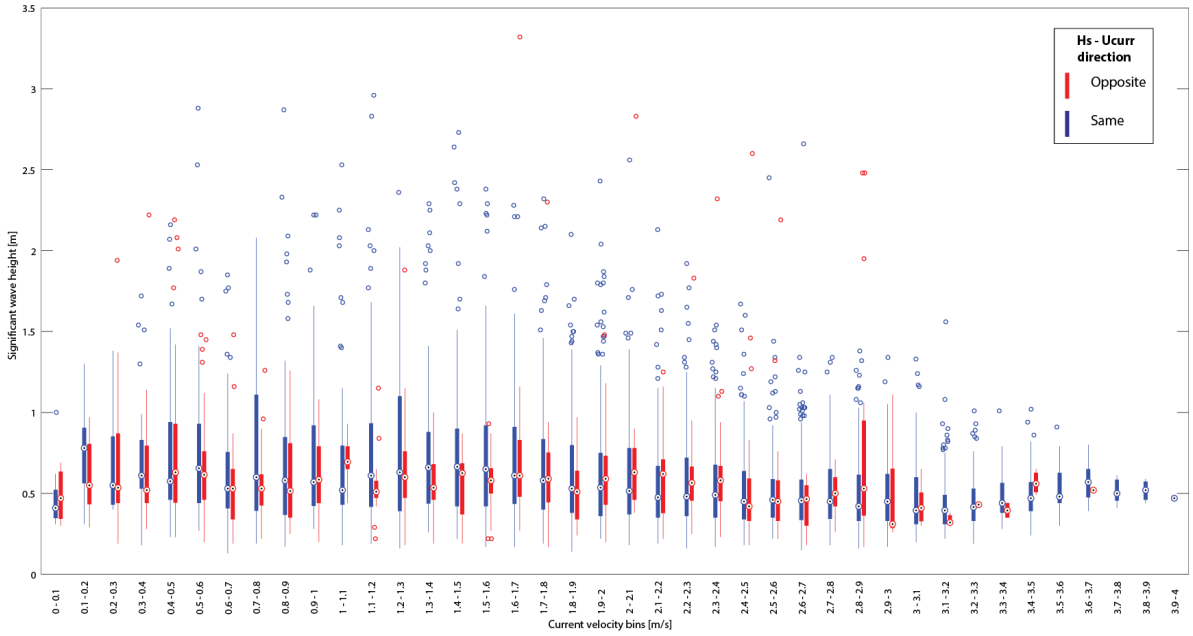

Figure D.7: Boxplot of significant wave height per current velocity bin: same and opposite direction

D.5. Reference study on dependence of sea state variables

Montes-Iturrizaga and Heredia-Zavoni [65] have conducted research on the dependence of sea states using hindmost time series of tropical storms (hurricanes) and extra-tropical events (northers) in the period from 1958 to 1999 for a site at 650 meter water depth located in the Gulf of Mexico.

The time series include data for significant wave height H_s, peak spectral period T_p, and 10-m hourly wind speed U_{wind}. The significant wave height for extreme sea states are taken as those for which $H_s \geqslant H_s^{th}$ provided H_s at time t_{peak} is a peak value within time windows $t_{peak} + \triangle T_{cluster}$ and $t_{peak} - \triangle T_{cluster}$ using a de-clustering time window of $\triangle T_{cluster}$ = 30 hours and a treshold value H_s^{th} =4.5m The threshold value here comes from an analysis of extreme value data based on the POT approach [31] and the time-window was taken from previous analysis of the data for statistical independence of peak values [66]. The values of all other associated environmental parameters are taken as those occurring at the same time t_{peak} as the peak values of significant wave height.

Table D.2: Kendall's Tau rank correlations of reference study on sea states

	Hs	Tp	Uwind
Hs	1	0.563	0.555
Tp	0.563	1	0.164
Uwind	0.555	0.164	1

D.6. All possible factorisations and their combined Tau values

Table D.3: All possible factorisations and their combined Tau values

position 1	position 2	position 3	position 4	$\sum_{k=1}^{3} \mid \tau_k \mid$
Uwind	Hs	Tp	Ucurr	0,591834
Uwind	Hs	Ucurr	Tp	0,583649
Uwind	Tp	Hs	Ucurr	0,234735
Uwind	Tp	Ucurr	Hs	0,551169
Uwind	Ucurr	Hs	Tp	0,149161
Uwind	Ucurr	Tp	Hs	0,473781
Hs	Uwind	Tp	Ucurr	0,602592
Hs	Uwind	Ucurr	Tp	0,517018
Hs	Tp	Uwind	Ucurr	0,168104
Hs	Tp	Ucurr	Uwind	0,473781
Hs	Ucurr	Uwind	Tp	0,159919
Hs	Ucurr	Tp	Uwind	0,551169
Tp	Uwind	Hs	Ucurr	0,277972
Tp	Uwind	Ucurr	Hs	0,159919
Tp	Hs	Uwind	Ucurr	0,200583
Tp	Hs	Ucurr	Uwind	0,149161
Tp	Ucurr	Uwind	Hs	0,517018
Tp	Ucurr	Hs	Uwind	0,583649
Ucurr	Uwind	Hs	Tp	0,200583
Ucurr	Uwind	Tp	Hs	0,168104
Ucurr	Hs	Uwind	Tp	0,277972
Ucurr	Hs	Tp	Uwind	0,234735
Ucurr	Tp	Uwind	Hs	0,602592
Ucurr	Tp	Hs	Uwind	0,591834

D.7. D-vine contours

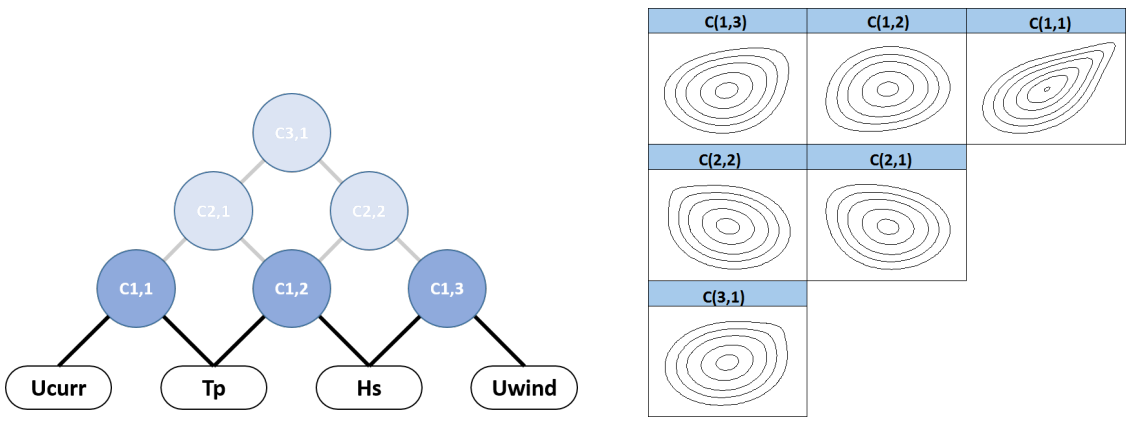

(a) D-vine with copula indices

(b) Copula contours per tree of the D-vine

Figure D.8: Properties of the used D-vine

D.8. Time independence analysis

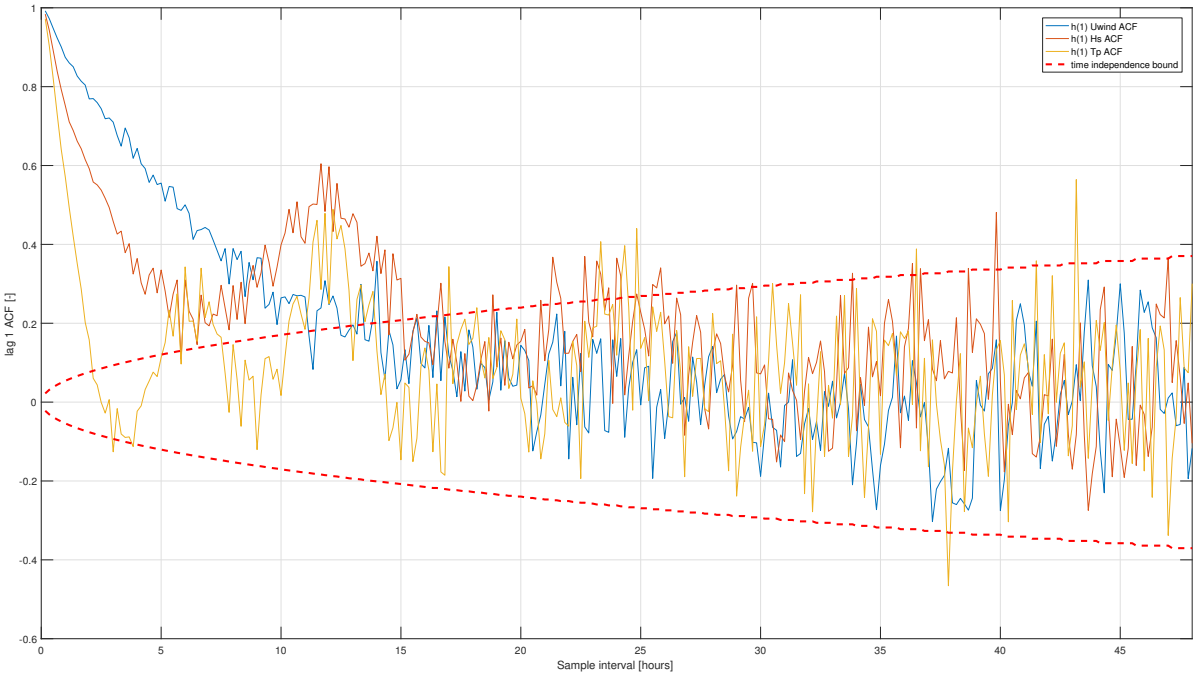

Figure D.9: Time independence analysis

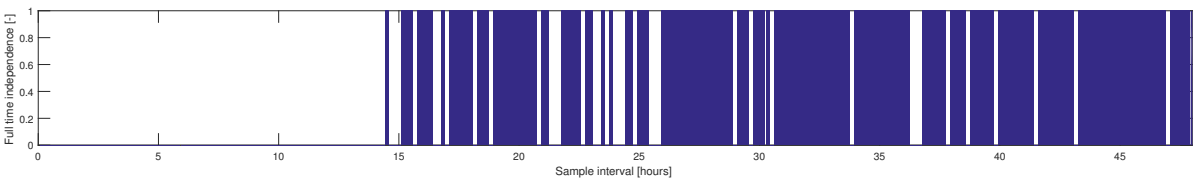

Figure D.10: Required time interval for full time dependence of all 4 variables

D.9. Auto- and Cross-correlations of EMEC data

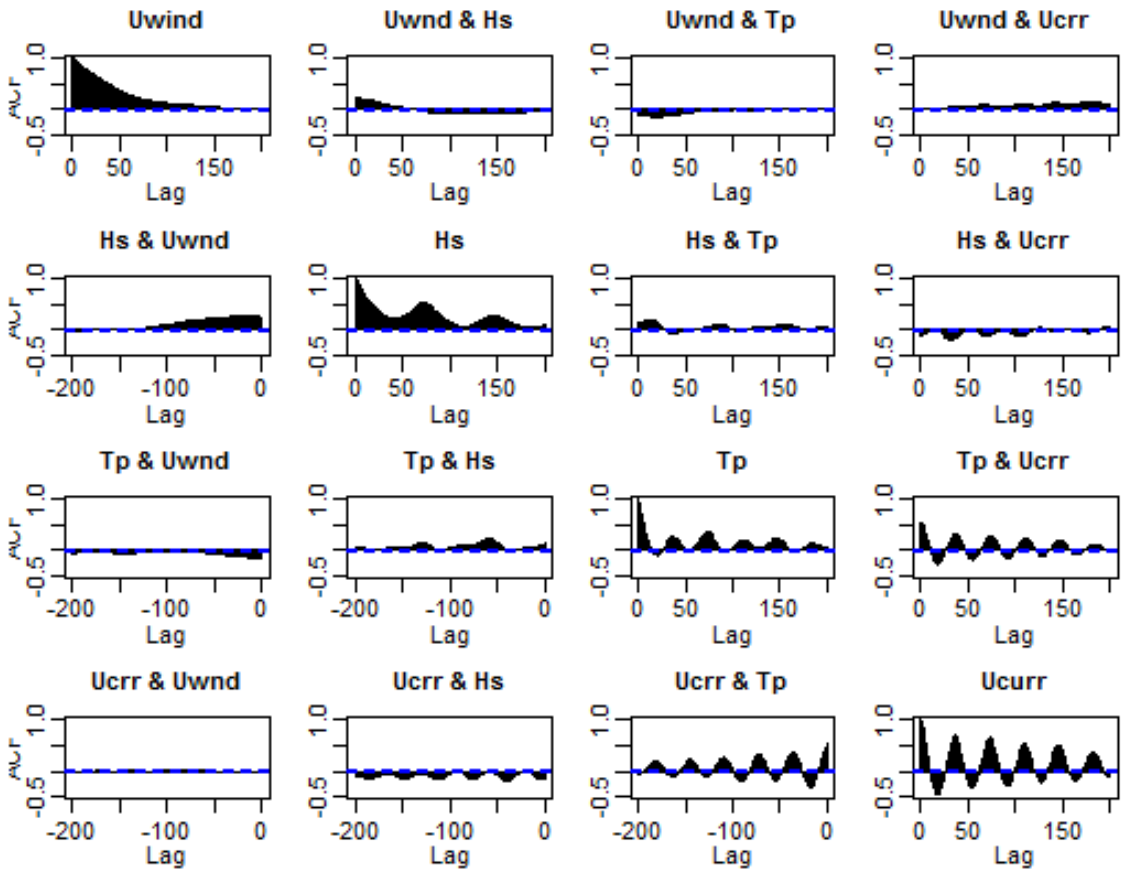

Figure D.11: Auto- and Cross-correlations of EMEC data

D.10. Simulated time series of U_{wind} for different lags and time steps

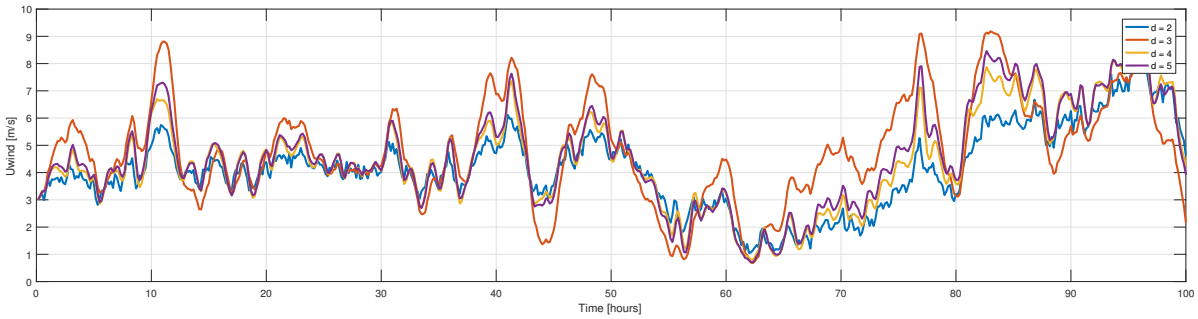

Figure D.12: Simulated time series of U_{wind} for different lags (Δt = 10 min)

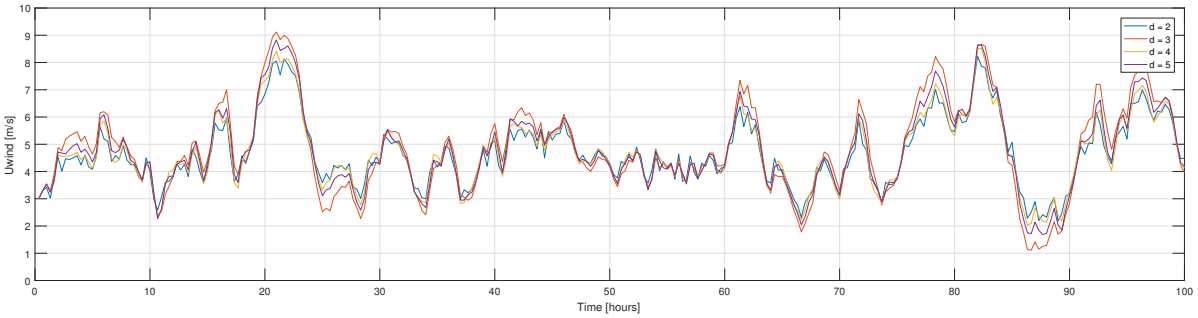

Figure D.13: Simulated time series of U_{wind} for different lags ($\triangle t$ = 20 min)

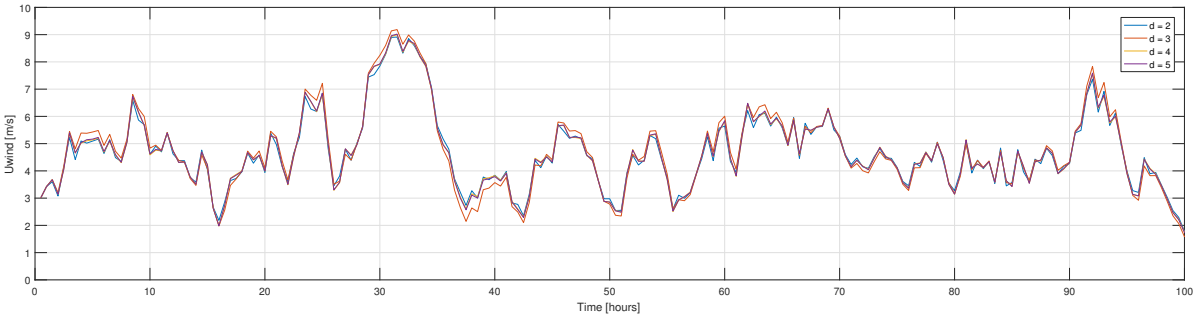

Figure D.14: Simulated time series of U_{wind} for different lags ($\triangle t$ = 30 min)

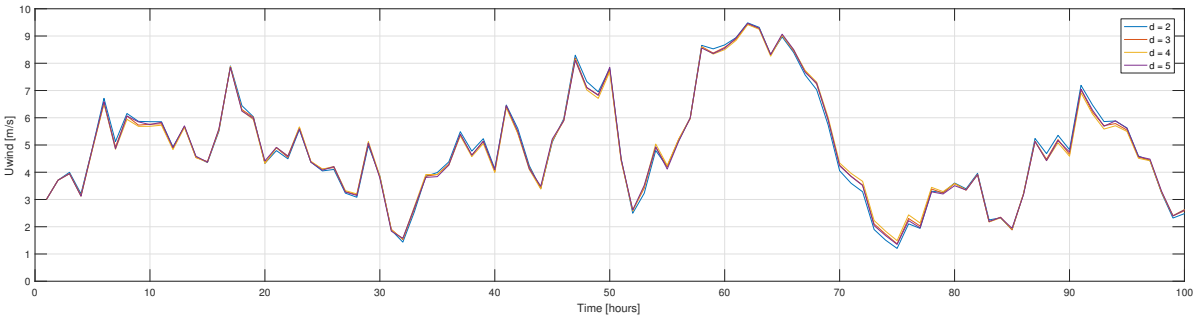

Figure D.15: Simulated time series of U_{wind} for different lags ($\triangle t$ = 1 hour)

D.11. Copula comparison study

In this section all activity duration plots for the analyses are depicted. The comparison study considers one up to ten TEC failures.

D.11.1. Original TS ⟷ Synthetic TS

Scenario 1: Fixed starting point (t=0)

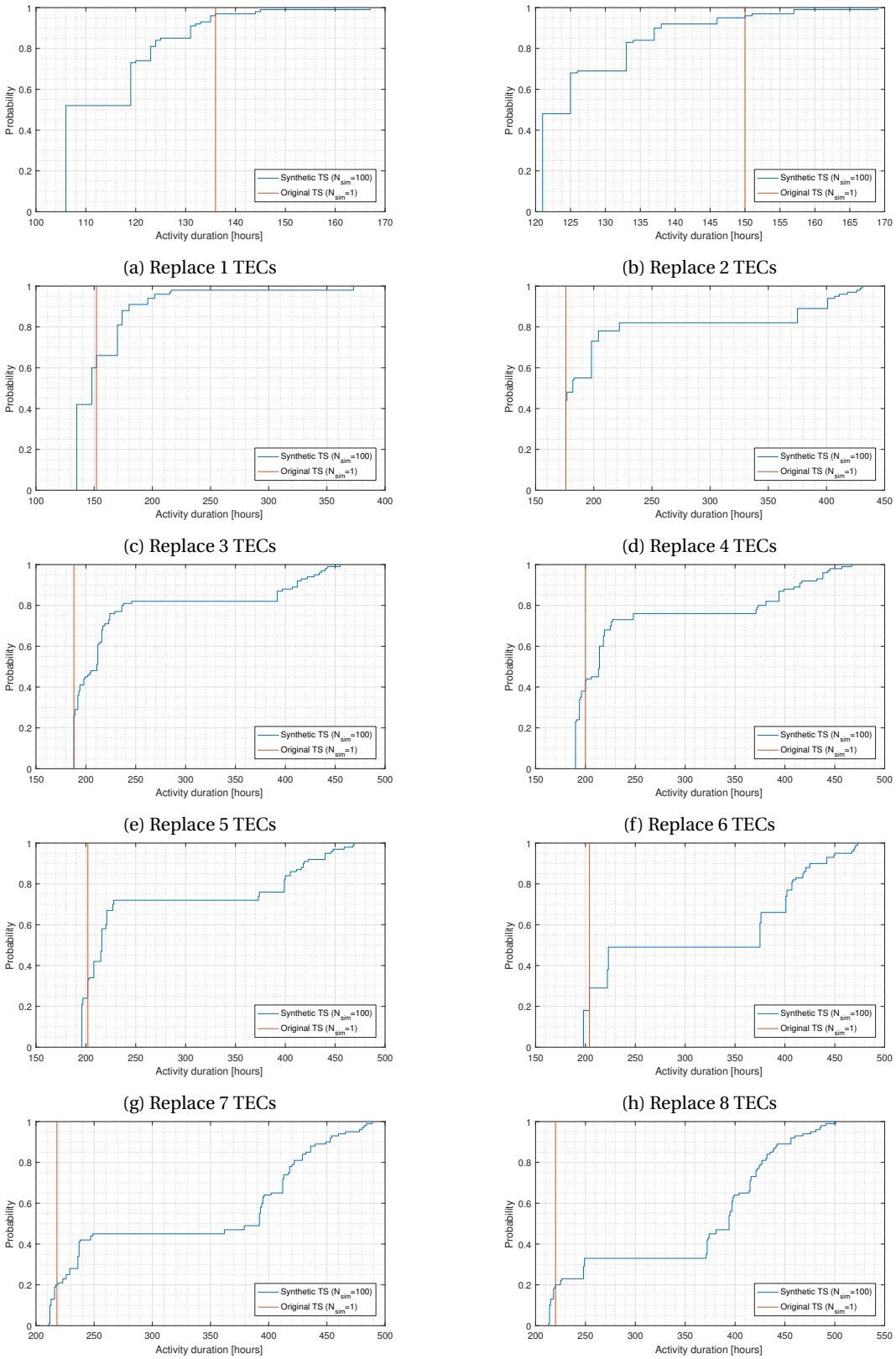

(a) Replace 1 TECs

(b) Replace 2 TECs

(c) Replace 3 TECs

(d) Replace 4 TECs

(e) Replace 5 TECs

(f) Replace 6 TECs

(g) Replace 7 TECs

(h) Replace 8 TECs

(i) Replace 9 TECs

(j) Replace 10 TECs

Figure D.16: Comparison of activity duration with original and synthetic time series (fixed starting point)

Scenario 2: Varying starting points

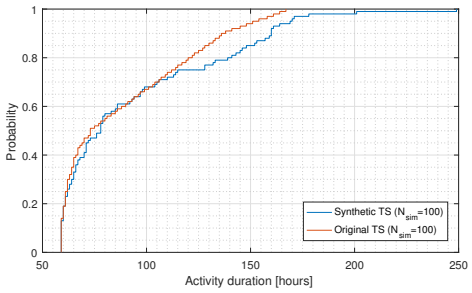

(a) Replace 1 TECs

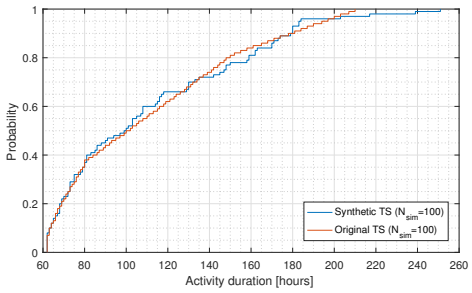

(b) Replace 2 TECs

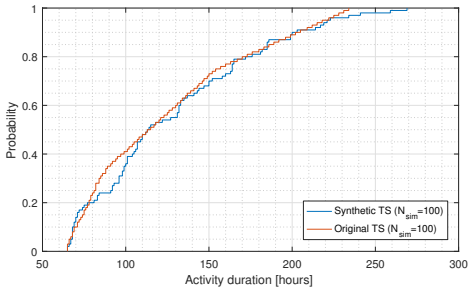

(c) Replace 3 TECs

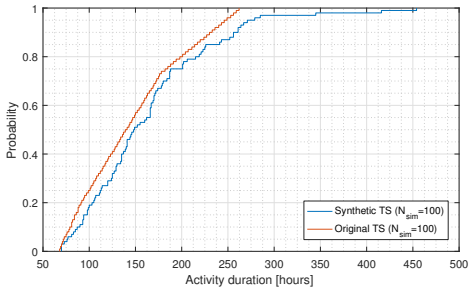

(d) Replace 4 TECs

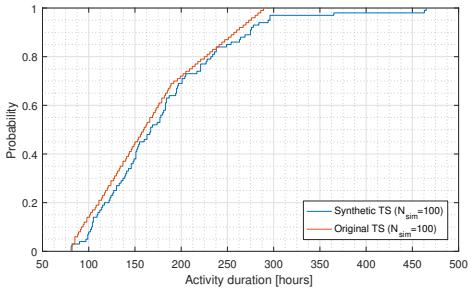

(e) Replace 5 TECs

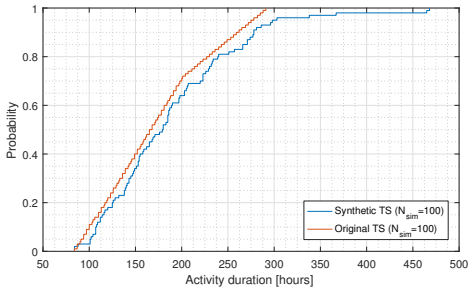

(f) Replace 6 TECs

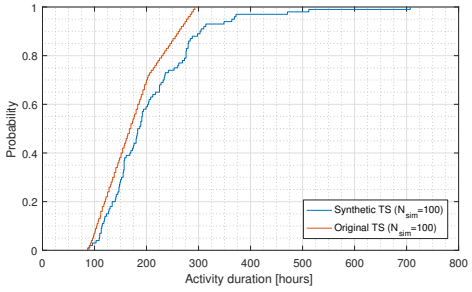

(g) Replace 7 TECs

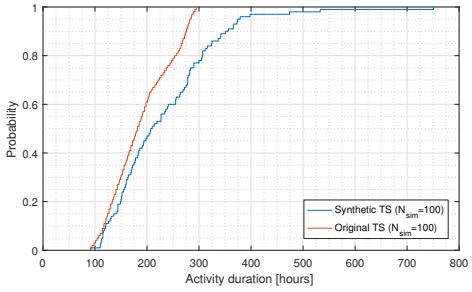

(h) Replace 8 TECs

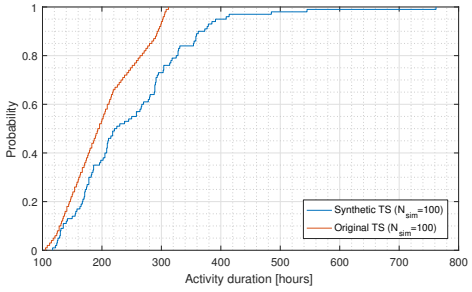

(i) Replace 9 TECs

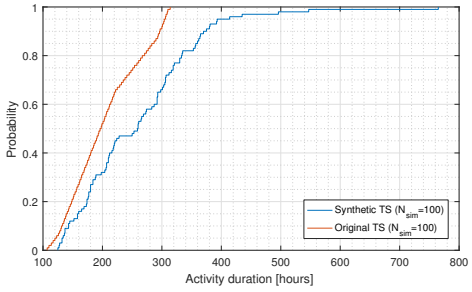

(j) Replace 10 TECs

Figure D.17: Comparison of activity duration with original and synthetic time series (variable starting point)

E

Model results

E.1. Base case input parameters

Environmental Analysis

Data Input

parameter			unit
Name of the tidal location	FieldName	EMEC	[-]
Directory with sensor data	Dir_data	D:\Dropbox\THESIS\MATLAB Code\DATA\Environment\EMEC	[-]
Filename of MET data	File_MET	Eday Wind speeds jul-oct 2015.xlsx	[-]
Filename of ADCP data	File_ADCP	ADCP-data-Jul-Sept-15.csv	[-]

Monte Carlo simulation loops

parameter			unit
Binsize of current velocity histogram	bin_size	0,01	[m/s]

Outlier data Filtering (Hampel filter parameters)

parameter			unit
Hs			
Number of neighbors on either side of each sample of x in the measurement window	Filter_k_Hs	40	[-]
number of standard deviations by which a sample of x must differ from the local median for it to be replaced with the median	Filter_nsigma_Hs	3	[-]
Tp			
Number of neighbors on either side of each sample of x in the measurement window	Filter_k_Tp	30	[-]
number of standard deviations by which a sample of x must differ from the local median for it to be replaced with the median	Filter_nsigma_Tp	3	[-]
Uwind			
Number of neighbors on either side of each sample of x in the measurement window	Filter_k_Uwind	30	[-]
number of standard deviations by which a sample of x must differ from the local median for it to be replaced with the median	Filter_nsigma_Uwind	3	[-]
Ucurr			
Number of neighbors on either side of each sample of x in the measurement window	Filter_k_Ucurr	30	[-]
number of standard deviations by which a sample of x must differ from the local median for it to be replaced with the median	Filter_nsigma_Ucurr	3	[-]
	FeedInTariff	0,11	€/kWh
	Tsim	6000	[10 * 'sample_int' min]
	Nsim	1000	[-]
	rho_w	1025	[kg/m3]
	smoothing	9	
	sample_int	1	

Figure E.1: Input - Simulation data

Activity Name	Duration [hours]	Fixed COST [€]	Variable COST [€\h]	Hs limit [m]	Tp limit [s]	Uwind limit [m/s]	Ucurr limit [m/s]
Vessel preparation	48	€ 36.480,00					
TEC loading	1	€ -	€ 580,00				
Port-array transport	2	€ -	€ 980,00	2,5		9	
Platform emerging	2	€ -	€ 875,00	2		7	2,5
TEC replacement	1	€ -	€ 875,00	1,5		6	2
Platform submerging	2	€ -	€ 875,00	2		7	2,5
Array-port transport	2	€ -	€ 980,00	2,5		9	
TEC unloading	1	€ -	€ 580,00				
Intra-array transport	0,5	€ -	€ 980,00	2,5		9	
Waiting for weather window	0	€ -	€ 580,00				

Figure E.2: Input - Operational data

System Parameters

Array

parameter	Symbol	value	unit
Number of TECs	Ntec	5	[-]
Mean distance between TECs	Xtec	500	[m]
Distance to port	Xport	10	[km]

TEC

parameter	Symbol	value	unit
Number of primer movers	Npm	16	[-]

TEC Efficiency

Prime Mover & Power Curve

parameter	Symbol	value	unit
Rated power of a PM	Prated	110	[kW]
Cut-in velocity	V_i	0,5	[m/s]
Cut-out velocity	V_o	3	[m/s]
Cut-in efficiency	Cp_i	0,38	[-]
Rated efficiency	Cp_r	0,38	[-]
Darrieus length	L	11,2	[m]
Darrieus radius	R	2,6	[m]

Misc. Components

parameter	Symbol	value	unit
Drive train efficiency	eff_DT	90	[%]

(a) Input - System data

System Parameters

parameter	Symbol	value	unit
Maximum failures of PMs	Nfailmax	9	[-]

Electricity Generation

Assembly	Failure rate [1/yr]	Component Cost [€]
Blades	0,078	€ 1.260,00
Generator	0,059	€ 10.200,00
Brake	0,029	€ 10.200,00
Gearbox	0,079	€ 13.950,00
Shaft/bearings	0,002	€ 11.100,00
Converter	0,045	€ 20.400,00

(b) Input - Failure data

Vessel Parameters

parameter	Symbol	value	unit
PM capacity per vessel	Npm_vessel	3	[-]
Vessel sailing speed	V_sail	12	[kt]

(c) Input - Vessel data

E.1.1. Determining $N_{fail,max}$

The value for $N_{fail,max} = 9$ was set after several iterations. This value can be arbitrarily set to anything between 1 and $N_{TEC,tot}$, but it was found that for all combinations of $N_{fail} = 8$ and 9, the decision was to replace the maximum number of TECs. This meant that the upper boundary for found and following deterioration state would never be reached.

E.2. General results

E.2.1. Maintenance activity

Decision D2.1 - Replace 1 TEC

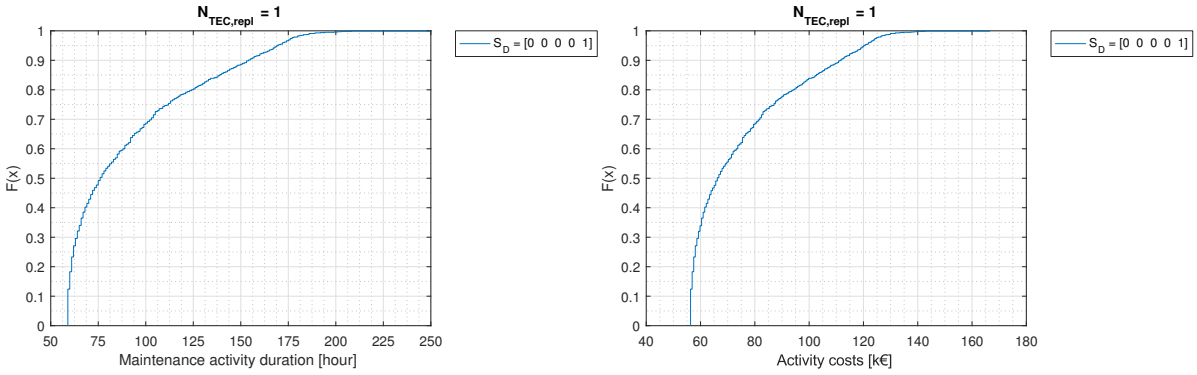

(a) Maintenance activity duration distribution

(b) Maintenance activity cost distribution

Figure E.4: Maintenance activity duration and costs of maintenance for Decision D2.1: 'Replace 1 TEC'

Decision D2.2 - Replace 2 TECs

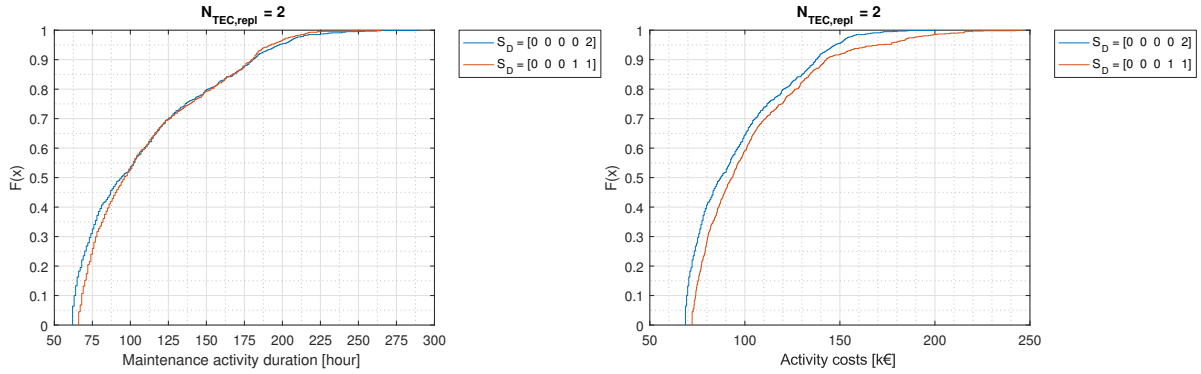

(a) Maintenance activity duration distribution (b) Maintenance activity cost distribution

Figure E.5: Maintenance activity duration and costs of maintenance for Decision D2.2: 'Replace 2 TECs'

Decision D2.3 - Replace 3 TECs

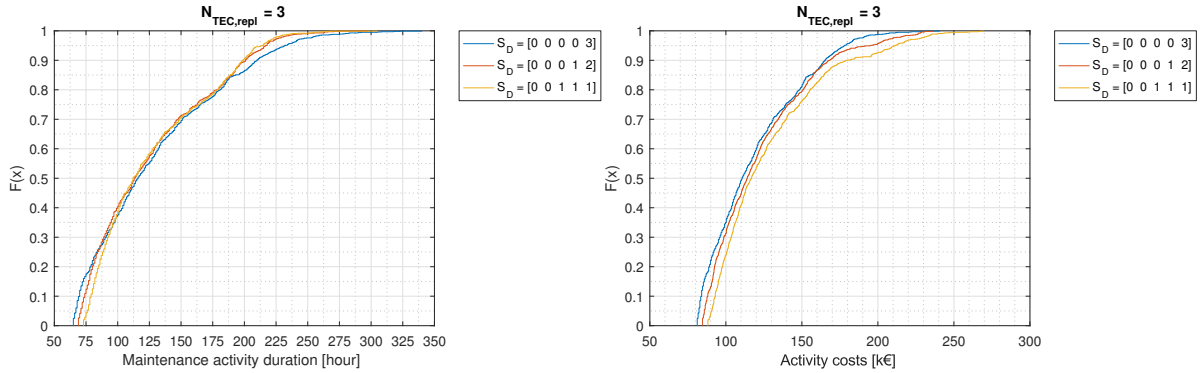

(a) Maintenance activity duration distribution (b) Maintenance activity cost distribution

Figure E.6: Maintenance activity duration and costs of maintenance for Decision D2.3: 'Replace 3 TECs'

Decision D2.4 - Replace 4 TECs

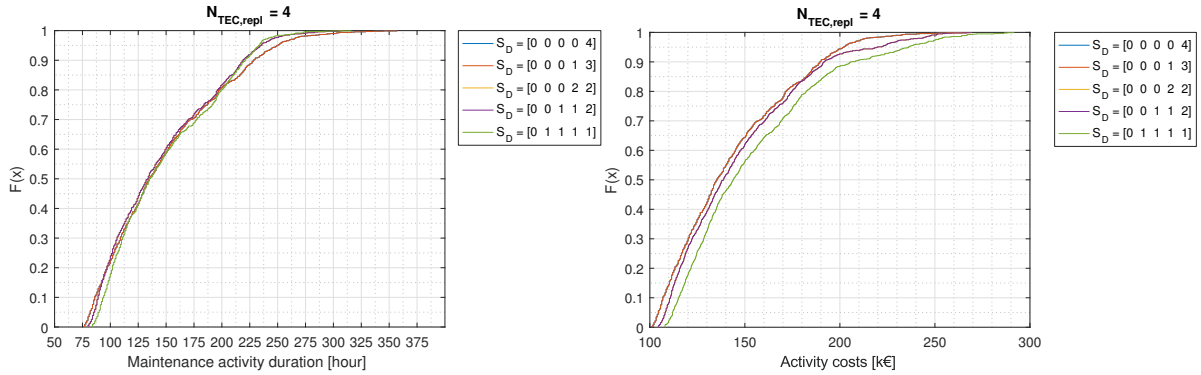

(a) Maintenance activity duration distribution (b) Maintenance activity cost distribution

Figure E.7: Maintenance activity duration and costs of maintenance for Decision D2.4: 'Replace 4 TECs'

Decision D2.5 - Replace 5 TECs

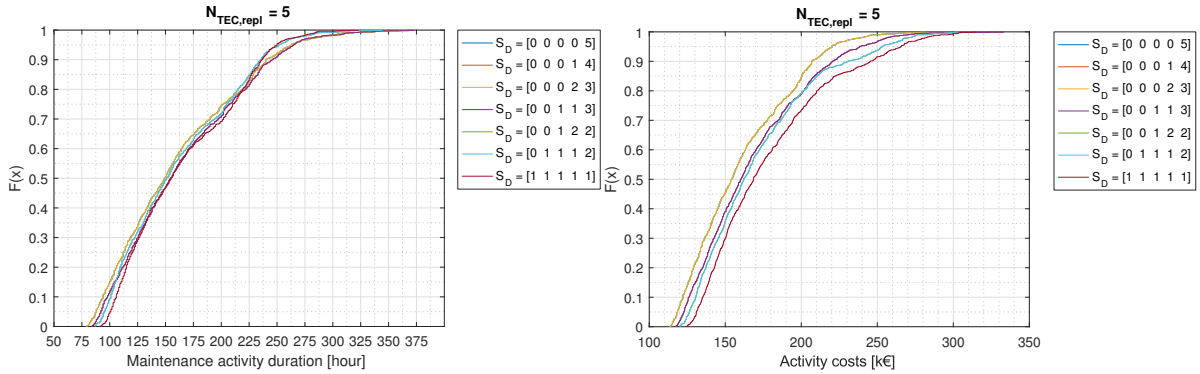

(a) Maintenance activity duration distribution (b) Maintenance activity cost distribution

Figure E.8: Maintenance activity duration and costs of maintenance for Decision D2.5: 'Replace 5 TECs'

Decision D2.6 - Replace 6 TECs

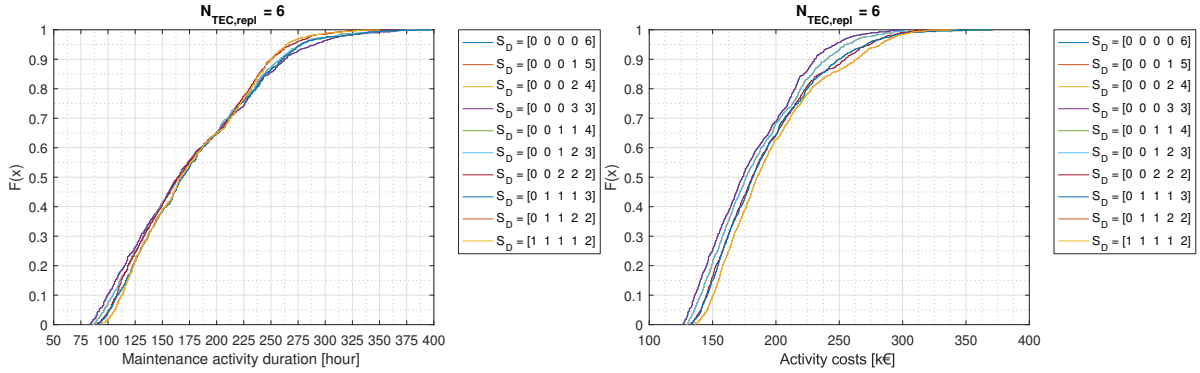

(a) Maintenance activity duration distribution (b) Maintenance activity cost distribution

Figure E.9: Maintenance activity duration and costs of maintenance for Decision D2.6: 'Replace 6 TECs'

Decision D2.7 - Replace 7 TECs

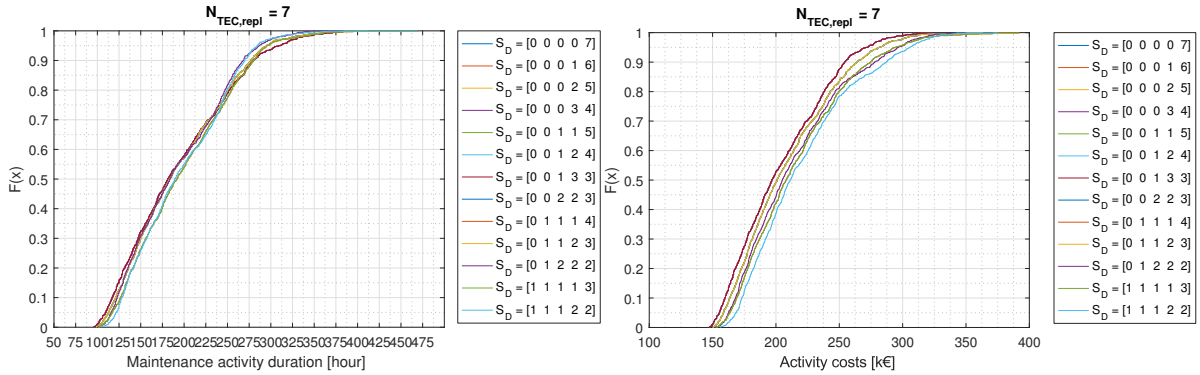

(a) Maintenance activity duration distribution (b) Maintenance activity cost distribution

Figure E.10: Maintenance activity duration and costs of maintenance for Decision D2.7: 'Replace 7 TECs'

Decision D2.8 - Replace 8 TECs

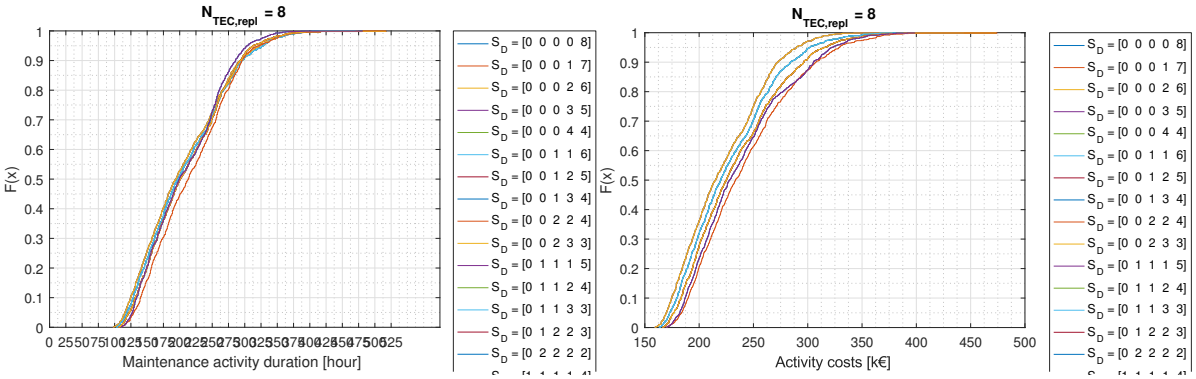

(a) Maintenance activity duration distribution (b) Maintenance activity cost distribution

Figure E.11: Maintenance activity duration and costs of maintenance for Decision D2.8: 'Replace 8 TECs'

Decision D2.9 - Replace 9 TECs

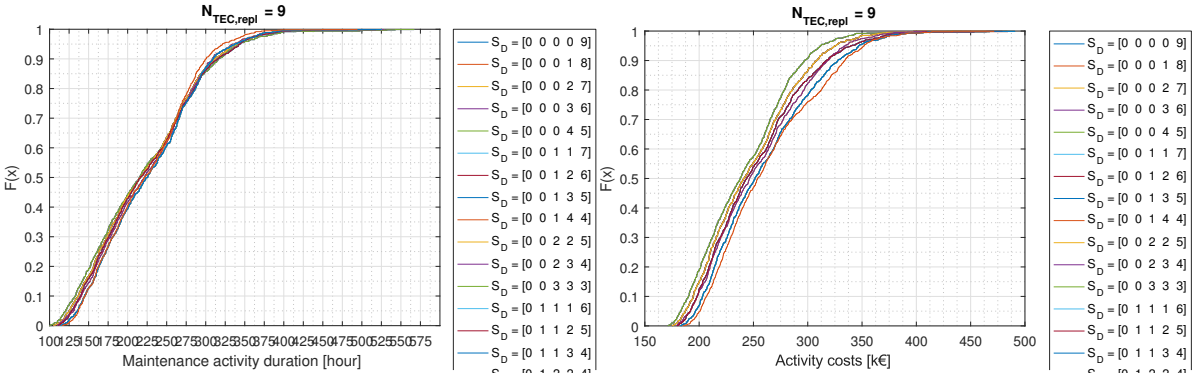

(a) Maintenance activity duration distribution (b) Maintenance activity cost distribution

Figure E.12: Maintenance activity duration and costs of maintenance for Decision D2.9: 'Replace 9 TECs'

E.3. Properties of policy G

E.3.1. Flowchart of D-states and transitions

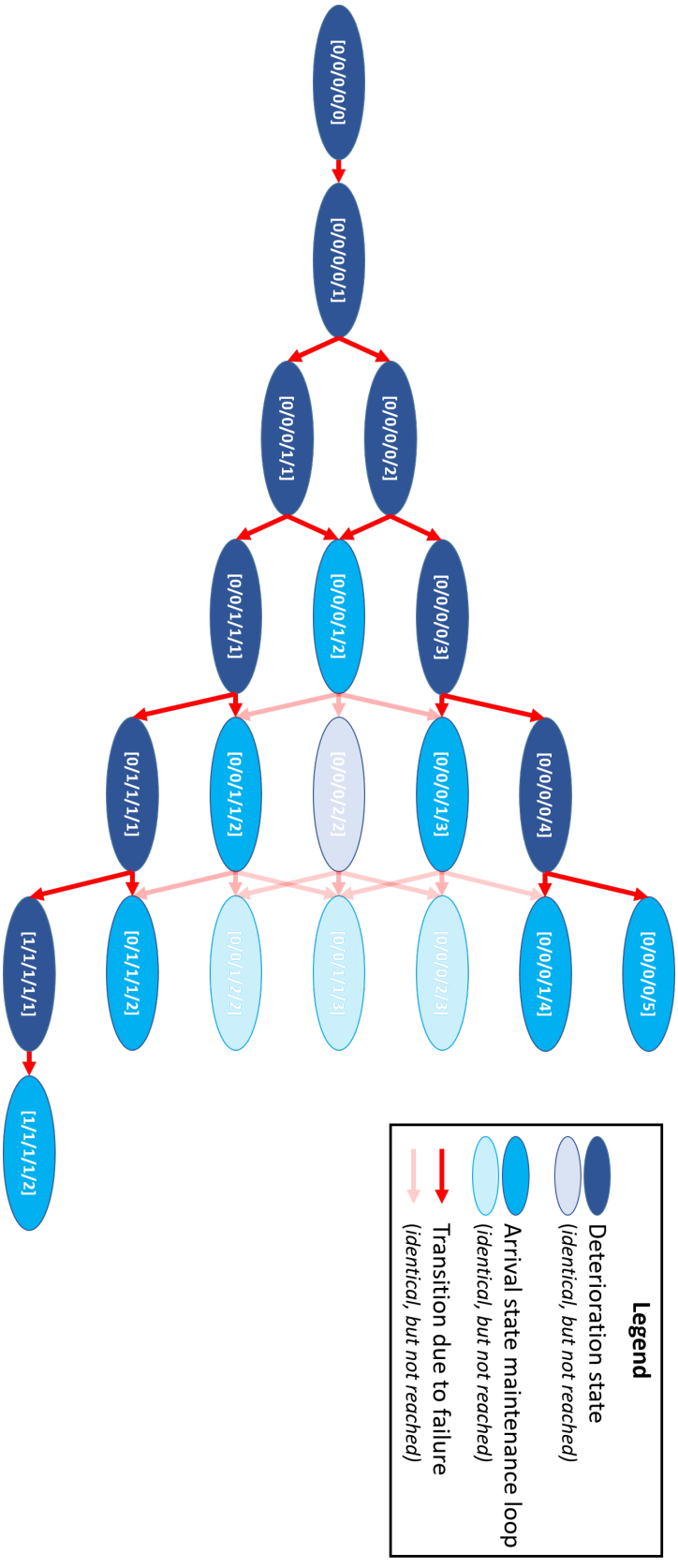

Figure E.13: Flowchart of D-states and transitions of policy G

E.3.2. Maintenance loop activity properties

Loop 1: Arrival state [0 0 0 1 2]

State properties:

- $N_{TEC,fail,i} = [00012]$
- $N_{TEC,repl} = 3$

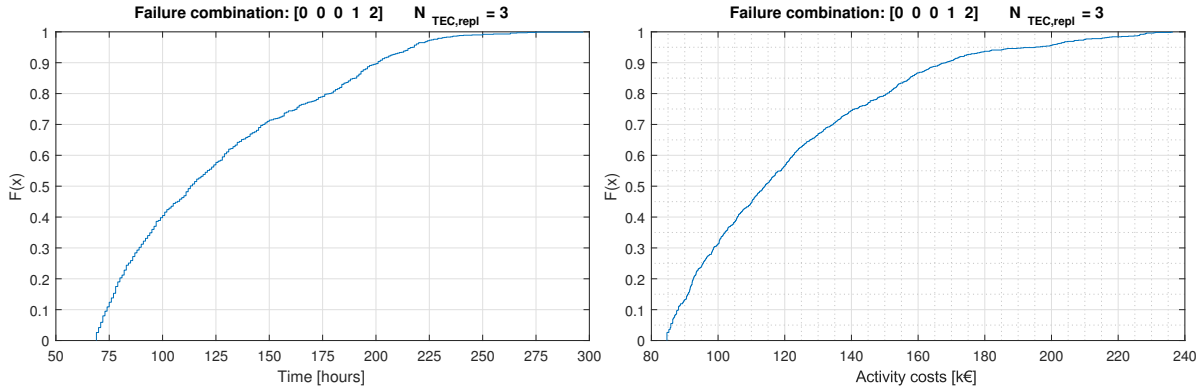

(a) Maintenance activity duration distribution (b) Maintenance activity cost distribution

Figure E.14: Maintenance activity duration and costs of maintenance loop 1

Loop 2: Arrival state [0 0 0 1 3]

State properties:

- $N_{TEC,fail,i} = [00013]$
- $N_{TEC,repl} = 4$

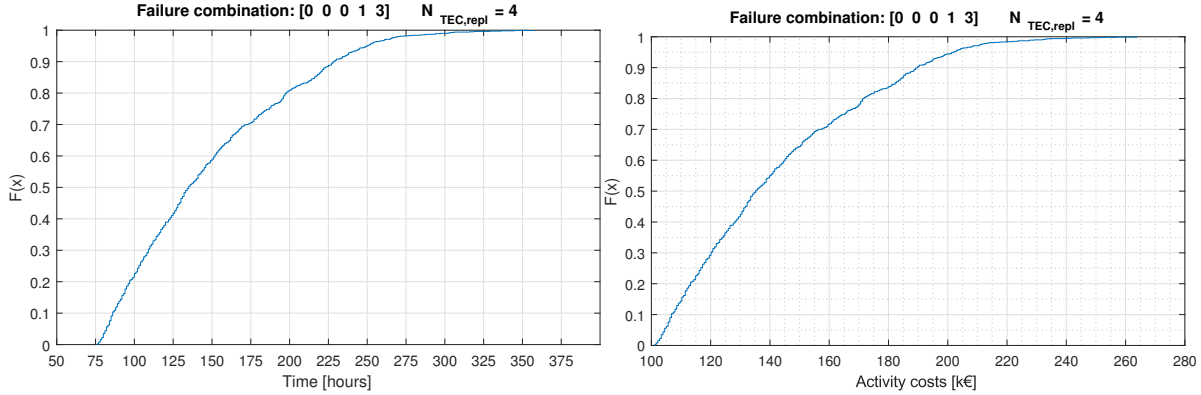

(a) Maintenance activity duration distribution (b) Maintenance activity cost distribution

Figure E.15: Maintenance activity duration and costs of maintenance loop 2

Loop 3: Arrival state [0 0 1 1 2]

State properties:

- $N_{TEC,fail,i} = [00112]$
- $N_{TEC,repl} = 4$

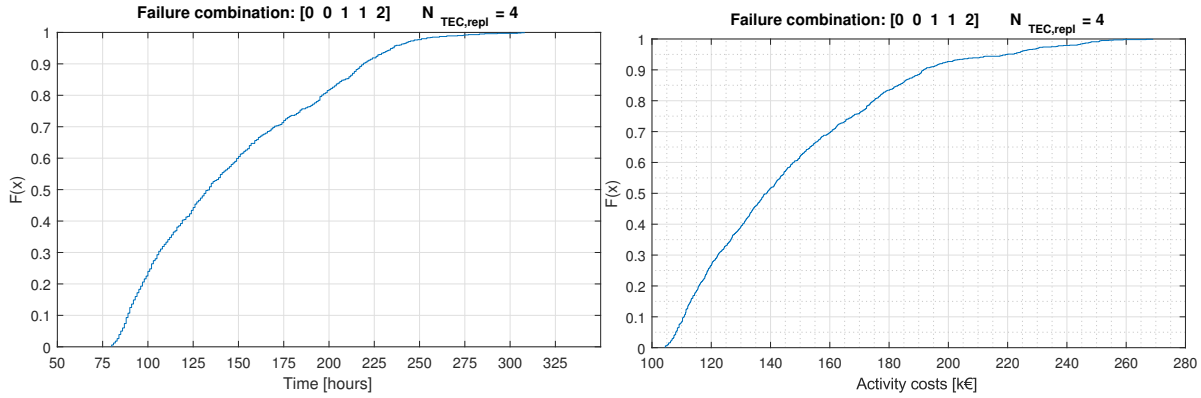

(a) Maintenance activity duration distribution (b) Maintenance activity cost distribution

Figure E.16: Maintenance activity duration and costs of maintenance loop 3

Loop 4: Arrival state [0 0 0 0 5]

State properties:

- $N_{TEC,fail,i} = [00005]$
- $N_{TEC,repl} = 5$

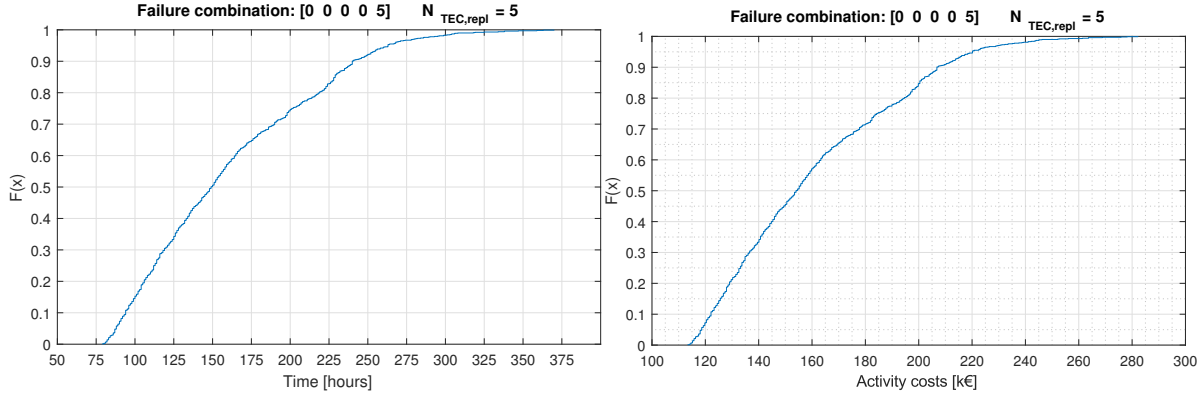

(a) Maintenance activity duration distribution (b) Maintenance activity cost distribution

Figure E.17: Maintenance activity duration and costs of maintenance loop 4

Loop 5: Arrival state [0 0 0 1 4]

State properties:

- $N_{TEC,fail,i} = [00014]$
- $N_{TEC,repl} = 3$

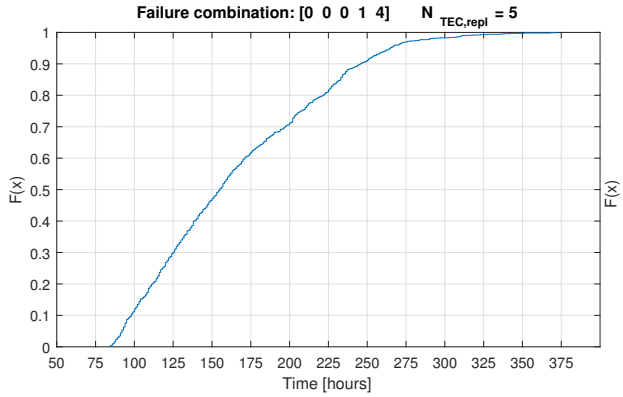

(a) Maintenance activity duration distribution

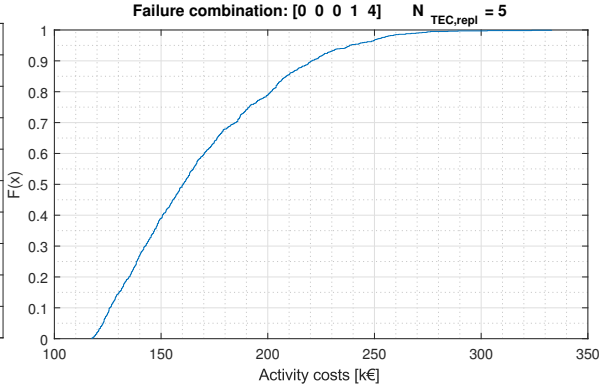

(b) Maintenance activity cost distribution

Figure E.18: Maintenance activity duration and costs of maintenance loop 5

Loop 6: Arrival state [0 1 1 1 2]

State properties:

- $N_{TEC,fail,i} = [01112]$
- $N_{TEC,repl} = 5$

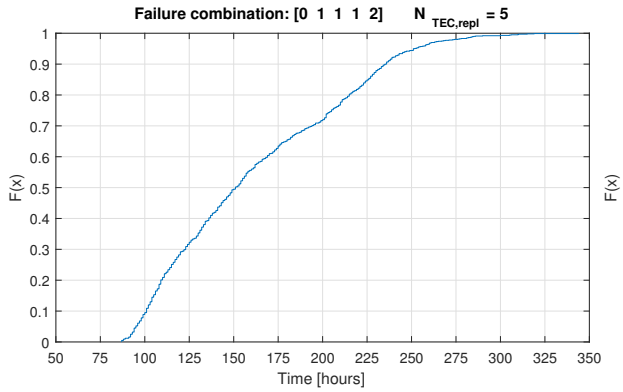

(a) Maintenance activity duration distribution

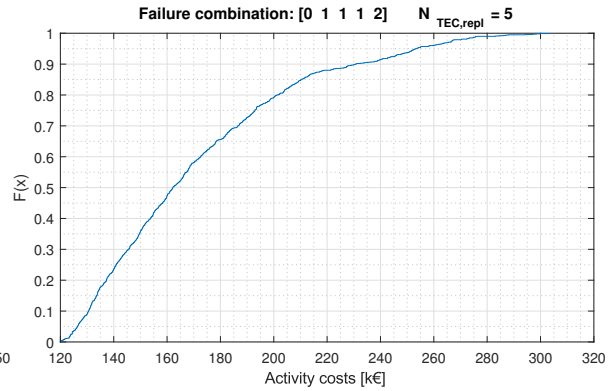

(b) Maintenance activity cost distribution

Figure E.19: Maintenance activity duration and costs of maintenance loop 6

Loop 7: Arrival state [1 1 1 1 2]

State properties:

- $N_{TEC,fail,i} = [11112]$
- $N_{TEC,repl} = 6$

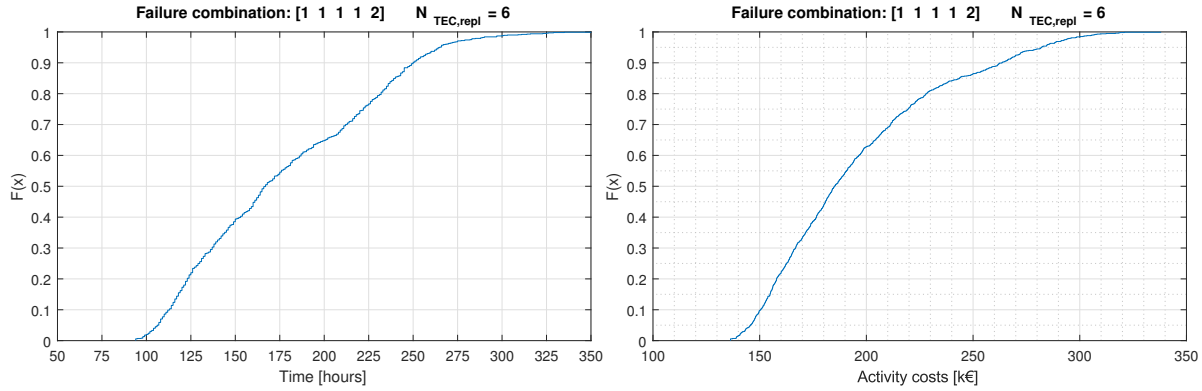

(a) Maintenance activity duration distribution

(b) Maintenance activity cost distribution

Figure E.20: Maintenance activity duration and costs of maintenance loop 7

Bibliography

[1] Kjersti Aas and Daniel Berg. Models for construction of multivariate dependence – a comparison study. *The European Journal of Finance*, 15(2006):639–659, 2009. ISSN 1351-847X. doi: 10.1080/13518470802588767.

[2] Kjersti Aas, Claudia Czado, Arnoldo Frigessi, and Henrik Bakken. Pair-copula constructions of multiple dependence. *Insurance: Mathematics and Economics*, 44(2):182–198, 2009. ISSN 01676687. doi: 10.1016/j.insmatheco.2007.02.001.

[3] H Akaike. Information theory and an extension of the maximum likelihood principle. In *International Symposium on Information Theory*, pages 267–281, 1973. ISBN 9780387983554. doi: 10.1016/j.econlet.2011.12.027.

[4] H. Arabian-Hoseynabadi, H. Oraee, and P. J. Tavner. Failure Modes and Effects Analysis (FMEA) for wind turbines. *International Journal of Electrical Power and Energy Systems*, 32(7):817–824, 2010. ISSN 01420615. doi: 10.1016/j.ijepes.2010.01.019.

[5] Fabrice Ardhuin. The Interaction of Ocean Waves and Wind. *Eos, Transactions American Geophysical Union*, 86(17):174, 2005. ISSN 0096-3941. doi: 10.1029/2005EO170005.

[6] David Assaf. Optimal Group Maintenance Policies with Continuous and Periodic Inspections. 33(11):1440–1452, 2016.

[7] Atlantis Resources Limited. A Route to the Cost-Effective Deployment of Large Arrays. *Bristol Tidal Energy Forum 5*, page 9, 2013.

[8] Atlantis Resources Limited. Global Resource, 2014. URL `http://atlantisresourcesltd.com/marine-power/global-resources.html`.

[9] M. Baykal-Gürsoy. Semi-Markov Decision Processes. *PhD Proposal*, 1:1–12, 2015. ISSN 1098-6596. doi: 10.1017/CBO9781107415324.004.

[10] Tim Bedford and Roger M. Cooke. Probability density decomposition for conditionally dependent random variables modeled by vines. *Annals of Mathematics and Artificial Intelligence*, 32(1-4):245–268, 2001. ISSN 10122443. doi: 10.1023/A:1016725902970.

[11] Tim Bedford and Roger M. Cooke. Vines - A new graphical model for dependent random variables. *Annals of Statistics*, 30(4):1031–1068, 2002. ISSN 00905364. doi: 10.1214/aos/1031689016.

[12] MM Aslam Bhutta, Nasir Hayat, and AU Farooq. Vertical axis wind turbine–A review of various configurations and design techniques. ... *Energy Reviews*, 16(4):1926–1939, 2012. ISSN 13640321. doi: 10.1016/j.rser.2011.12.004. URL `http://linkinghub.elsevier.com/retrieve/pii/S136403211100596X$\delimiter"026E3B2$nhttp://www.sciencedirect.com/science/article/pii/S136403211100596X`.

[13] Rodolfo Bolaños, Jennifer M. Brown, and Alejandro J. Souza. Wave-current interactions in a tide dominated estuary. *Continental Shelf Research*, 87:109–123, 2014. ISSN 02784343. doi: 10.1016/j.csr.2014.05.009.

[14] Tim Bollerslev. Generalized autoregressive conditional heteroskedasticity. *Journal of Econometrics*, 31(3):307–327, 1986. ISSN 03044076. doi: 10.1016/0304-4076(86)90063-1.

[15] Z. I. Botev. The normal law under linear restrictions: simulation and estimation via minimax tilting. *Journal of the Royal Statistical Society: Series B (Statistical Methodology)*, pages n/a–n/a, feb 2016. ISSN 13697412. doi: 10.1111/rssb.12162. URL `http://doi.wiley.com/10.1111/rssb.12162`.

[16] Zdravko Botev. CRAN - Package TruncatedNormal, 2015. URL https://cran.r-project.org/web/packages/TruncatedNormal/index.html.

[17] G E P Box, G M Jenkins, and G C Reinsel. Time Series Analysis: Forecasting & Control. *Holden-Day*, Rev ed., 1994. doi: 10.1016/j.ijforecast.2004.02.001.

[18] Bunker Index. Price Index, News and Directory Information for the Marine Fuel Industry, 2016. URL http://www.bunkerindex.com/prices/neurope.php.

[19] CEN (European Committee for Standardization). EN 13306:2001 Maintenance Terminology, 2001.

[20] Clarksons Platou. Global Support Vessel Monthly. (December), 2015.

[21] David R. Cox. *The Statistical Analysis of Series of Events*. Springer Verlag, 1 edition, 1966. ISBN 9789401178037.

[22] Adolfo Crespo Márquez. *The Maintenance Management Framework: Models and Methods for Complex Systems Maintenance*. 2007. ISBN 9788578110796. doi: 10.1017/CBO9781107415324.004.

[23] Damen Shipyards. Damen Utility workboat 6516 with large deck area, 2016. URL http://products.damen.com/en/ranges/utility-vessel/utility-vessel-6516.

[24] EIA. International Energy Statistics - Electricity Generation 2012, 2012. URL http://www.eia.gov/cfapps/ipdbproject/iedindex3.cfm?tid=2{&}pid=alltypes{&}aid=12{&}cid=regions{&}syid=2008{&}eyid=2012{&}unit=BKWH.

[25] Paul Embrechts, Filip Lindskog, and Alexander Mcneil. Ch.8 Modelling dependence with copulas and applications to risk management. *Handbook of Heavy Tailed Distributions in Finance*, pages 329–384, 2003. doi: 10.1016/B978-044450896-6.50010-8. URL http://www.sciencedirect.com/science/article/pii/B9780444508966500108.

[26] Energy Numbers. Capacity factors at Danish offshore wind farms, 2016. URL http://energynumbers.info/capacity-factors-at-danish-offshore-wind-farms.

[27] Energy Numbers. UK offshore wind capacity factors, 2016. URL http://energynumbers.info/uk-offshore-wind-capacity-factors.

[28] Ernst & Young. Cost of and financial support for wave , tidal stream and tidal range generation in the UK. (October):1–56, 2010. URL http://webarchive.nationalarchives.gov.uk/20121205174605/http:/decc.gov.uk/assets/decc/whatwedo/ukenergysupply/energymix/renewableenergy/explained/wave{_}tidal/798-cost-of-and-finacial-support-for-wave-tidal-strea.pdf.

[29] ETI. Insights into Tidal Stream energy.

[30] European Ocean Energy Association. Oceans of energy: European Oceans Energy Roadmap 2010-2050. *OEA-Technical-Library*, 2010. URL http://www.ocean-energy-systems.org/library/countries-roadmaps/document/european-ocean-energy-roadmap-2010-2050/.

[31] J. A. Ferreira and C. Guedes Soares. An Application of the Peaks Over Threshold Method to Predict Extremes of Significant Wave Height. *Journal of Offshore Mechanics and Arctic Engineering*, 120(3):165, 1998. ISSN 08927219. doi: 10.1115/1.2829537. URL http://offshoremechanics.asmedigitalcollection.asme.org/article.aspx?articleid=1453559.

[32] Gabriel Frahm, Markus Junker, and Alexander Szimayer. Elliptical copulas: Applicability and limitations. *Statistics and Probability Letters*, 63(3):275–286, 2003. ISSN 01677152. doi: 10.1016/S0167-7152(03)00092-0.

[33] Christian Genest and Anne-Catherine Favre. Everything You Always Wanted to Know about Copula Modeling but Were Afraid to Ask. *Journal of Hydrologic Engineering*, 12(4):347–368, 2007. ISSN 1084-0699. doi: 10.1061/(ASCE)1084-0699(2007)12:4(347).

[34] Geoscience Australia. Australian Energy Resource Assessment. *Australian Energy Resource Assessment*, (2):285 – 308, 2014.

[35] Google Maps. Map data ©2016 Google 500 ft, 2016.

[36] Franciszek Grabski. Ch. 15: Semi-Markov decision processes. *Semi-Markov Processes: Applications in System Reliability and Maintenance*, pages 229–244, 2015. doi: 10.1016/B978-0-12-800518-7.00015-6. URL http://linkinghub.elsevier.com/retrieve/pii/B9780128005187000156.

[37] Frank R. Hampel. The Influence Curve and its Role in Robust Estimation. *Journal of the American Statistical Association*, 69(346):383–393, 1974. ISSN 0162-1459. doi: 10.1080/01621459.1974.10482962. URL http://www.tandfonline.com/doi/abs/10.1080/01621459.1974.10482962.

[38] S.L. Ho, M. Xie, S. L. Ho, and M. Xie. The use of ARIMA models for reliability forecasting and analysis. *Computers & Industrial Engineering*, 35(1-2):213–216, oct 1998. ISSN 03608352. doi: 10.1016/S0360-8352(98)00066-7. URL http://linkinghub.elsevier.com/retrieve/pii/S0360835298000667.

[39] Don Hoogendoorn. Personal contact with D. Hoogendoorn: Damen tidal project manager. 2016.

[40] Ronald. A Howard. Semi-Markov and Decision Processes. *Dynamic Probabilistic Systems*, 2, 1971.

[41] Intel Corp. Systems Quality/Reliability Handbook, 1987.

[42] International Renewable Energy Agency. IRENA Ocean Energy Technology Brief 3. (June), 2014.

[43] Mazharul Islam, David S K Ting, and Amir Fartaj. Aerodynamic models for Darrieus-type straight-bladed vertical axis wind turbines, 2008. ISSN 13640321.

[44] Nancy L Jacob and Keith V Smith. Optimal m-failure policies with random repair time. *Finance*, 27(2): 2411, 2012. doi: 10.13140/2.1.4874.0482.

[45] Harry Joe. Families of m-Variate Distributions with Given Margins and m(m-1)/2 Bivariate Dependence Parameters. *Lecture Notes-Monograph Series*, 28:120–141, 1996. ISSN 07492170. doi: 10.1214/lnms/1215452614. URL http://www.jstor.org/stable/4355888.

[46] Harry Joe. *Multivariate models and dependence concepts*. Number 1960. 1997. ISBN 0412073315. doi: ExportDate21May2013.

[47] Harry Joe. Dependence Modeling with Copulas. *CRC Press*, page 479, 2015.

[48] I.G. Jonsson. Wave-current interaction. *Ocean Engineering*, 9A:65–120, 1990.

[49] Maurice G Kendall. A New Measure of Rank Correlation. *Biometrika*, 30(1):81–93, 2012.

[50] Monika Kereszturi, Jonathan Tawn, and Philip Jonathan. Assessing extremal dependence of North Sea storm severity. *Ocean Engineering*, 118:242–259, 2016. ISSN 00298018. doi: 10.1016/j.oceaneng.2016.04.013.

[51] Yuka Kikuchi, Takeshi Ishihara, W C Skamarock, J B Klemp, J Dudhia, D O Gill, D M Barker, W Wang, and J G Powers. Assessment of weather window for the construction of offshore power plants by using wind and wave simulations Validation of simulation for wave and wind. *MMAB Technical Note*, 276194, 2009.

[52] Georgia-Ann Klutke, Peter C Kiessler, and M A Wortman. A Critical Look at the Bathtub Curve. *IEEE TRANSACTIONS ON RELIABILITY*, 52(1), 2003. doi: 10.1109/TR.2002.804492.

[53] Bernd J. Kröger, Verena Graf-Borttscheller, and Anja Lowit. Modeling of vessel and equipment cost for the maintenance activities of an offshore tidal energy array. *Proceedings of the Annual Conference of the International Speech Communication Association, INTERSPEECH*, pages 2639–2642, 2008. ISSN 19909772. doi: 10.1016/j.buildenv.2006.10.027.

[54] W. Kuo, W.T.K. Chien, and T. Kim. Reliability and Stress Burn-In. 1998.

[55] J. Lawrence, H. Kofoed-Hansen, and C. Chevalier. High-resolution metocean modelling at EMEC's (UK) marine energy test sites. In *8th European Wave and Tidal Energy Conference*, 2009. ISBN 0908-8857. doi: 10.1111/j.2007.0908-8857.03909.x.

[56] Claire Legrand, Black and Veatch, and Emec. *Assessment of Tidal Energy Resource*. 2009. ISBN 9780580656422.

[57] Georgios Leontaris. Design of a probabilistic decision support tool for the cable installation of an Offshore Wind Farm. 2015.

[58] Georgios Leontaris, Oswaldo Morales-Nápoles, and A. R M (Rogier) Wolfert. Probabilistic scheduling of offshore operations using copula based environmental time series – An application for cable installation management for offshore wind farms. *Ocean Engineering*, 125:328–341, 2016. ISSN 00298018. doi: 10.1016/j.oceaneng.2016.08.029. URL http://dx.doi.org/10.1016/j.oceaneng.2016.08.029.

[59] Christophe Leys, Olivier Klein, Philippe Bernard, and Laurent Licata. Detecting outliers: Do not use standard deviation around the mean, use absolute deviation around the median. *Journal of Experimental Social Psychology*, 49(4):764–766, 2013. ISSN 00221031. doi: 10.1016/j.jesp.2013.03.013.

[60] Marine Current Turbines Limited. Marine Current Turbines to deploy tidal farm off Orkney after securing Site Lease from the Crown Estate, 2010. URL http://www.marineturbines.com/3/news/article/31/marine{_}current{_}turbines{_}to{_}deploy{_}tidal{_}farm{_}off{_}orkney{_}after{_}securing{_

[61] A.A. Markov. The theory of Algorithms. *Trudy Mat. Inst. Steklov.*, 42:3–375, 1954.

[62] Rebecca Martin, Iraklis Lazakis, Sami Barbouchi, and Lars Johanning. Identification and Quantification of Important Offshore Wind Operations and Maintenance Factors.

[63] MathPages. Infinite Parallel Redundancy. URL http://www.mathpages.com/home/kmath326/kmath326.HTM.

[64] Alexander J. McNeil, Rüdiger Frey, and Paul Embrechts. *Quantitative risk management: Concepts, techniques, and tools*. 2005. ISBN 0691122555.

[65] R. Montes-Iturrizaga and E. Heredia-Zavoni. Multivariate environmental contours using C-vine copulas. *Ocean Engineering*, 118:68–82, 2016. ISSN 00298018. doi: 10.1016/j.oceaneng.2016.03.011. URL http://www.sciencedirect.com/science/article/pii/S0029801816001189.

[66] R. Montes-Iturrizaga, E. Heredia-Zavoni, F. Silva-González, and D. Straub. Nested reliability analysis of mooring lines for floating systems. *Applied Ocean Research*, 34:107–115, 2012. ISSN 01411187. doi: 10.1016/j.apor.2011.09.005.

[67] Markus Nævestad. Multivariate Distributions Through Pair-Copula Construction : Theory and Applications. (June), 2009.

[68] Vincent S Neary, Michael Lawson, Mirko Previsic, Kathleen C Hallett, Andrea Copping, Jeff Rieks, Alison Labonte, and Dianne K Murray. Methodology for Design and Economic Analysis of Marine Energy Conversion (Mec) Technologies. *2nd Marine Energy Technology Symposium*, pages 1–6, 2014.

[69] Roger B. Nelsen. *An Introduction to Copulas*, volume 2. 2006. ISBN 9788578110796. doi: 10.1017/CBO9781107415324.004.

[70] T. Obdam and T. van der Zee. ECN O&M Tool Case Study for a Far Offshore Wind Farm. 2011.

[71] Ocean Energy Systems. International Levelised Cost Of Energy for Ocean Energy Technologies. (May): 1–48, 2015.

[72] Office of Gas and Electricity Markets. Feed-in Tariff Generation & Export Payment Rate Table for Non-Photovoltaic Installations. 2015.

[73] K. Okumoto and E. A. Elsayed. An optimum group maintenance policy. *Naval Research Logistics Quarterly*, 30(4):667–674, 1983. doi: 10.1002/nav.3800300412. URL http://doi.wiley.com/10.1002/nav.3800300412.

[74] I Paraschivoiu. Wind Turbine Design: With Emphasis on Darrieus Concept. *Montreal : Polytechnic International Press*, page 438, 2002.

[75] BP p.l.c. BP Energy Outlook 2035: February 2015. (February):96, 2015. ISSN 08496757. doi: 10.5555/jan.010a.2013. URL http://www.bp.com/content/dam/bp/pdf/Energy-economics/Energy-Outlook/BP{_}World{_}Energy{_}Outlook{_}booklet{_}2035.pdf.

[76] BP p.l.c. BP Statistical Review of World Energy: June 2016. (June):1–2, 2016.

[77] Elmira Popova and JG Wilson. Group replacement policies for parallel systems whose components have phase distributed failure times. *Annals of operations research*, 91:163–189, 1999. ISSN 02545330. URL http://link.springer.com/article/10.1023/A:1018941521644.

[78] VGB PowerTech. Levelised Cost of Electricity. 2015. URL www.vgb.org.

[79] D. Pudjianto, D. Pudjianto, C. Ramsay, C. Ramsay, G. Strbac, and G. Strbac. Virtual power plant and system integration of distributed energy resources. *Renewable Power Generation, IET*, 1(1):10–16, 2007. ISSN 17521416. doi: 10.1049/iet-rpg. URL http://ieeexplore.ieee.org/xpls/abs{_}all.jsp?arnumber=4159950.

[80] Martin L Puterman. Markov Decision Processes: Discrete Stochastic Dynamic Programming, 1994. ISSN 0040-1706. URL http://portal.acm.org/citation.cfm?id=528623.

[81] Peter E. Robins, Simon P. Neill, Matt J. Lewis, and Sophie L. Ward. Characterising the spatial and temporal variability of the tidal-stream energy resource over the northwest European shelf seas. *Applied Energy*, 147(January):510–522, 2015. ISSN 03062619. doi: 10.1016/j.apenergy.2015.03.045. URL http://www.sciencedirect.com/science/article/pii/S0306261915003293.

[82] J. L. Romeu. Understanding Series and Parallel Systems Reliability. *Reliability Analysis Center*, 11(5):8, 2012.

[83] S. Ross. Stochastic Processes. 1996.

[84] Peter Scheijgrond and Alex Raventos. Dutch Wave & Tidal energy sector. *TKI Wind op Zee*, (June), 2015.

[85] Ulf Schepsmeier, Jakob Stoeber, Benedikt Graeler, Thomas Nagler, and Tobias Erhardt. R and 'VineCopula' package, 2016.

[86] Frank Scheurich, Timothy M. Fletcher, and Richard E. Brown. Simulating the aerodynamic performance and wake dynamics of a vertical-axis wind turbine. *Wind Energy*, 14(2):159–177, 2011. ISSN 10954244. doi: 10.1002/we.409.

[87] Gideon Schwarz. Estimating the dimension of a model. *The Annals of Statistics*, 6(2):461–464, 1978. ISSN 0090-5364. doi: 10.1214/aos/1176344136. URL http://projecteuclid.org/euclid.aos/1176344136.

[88] Mahmood Shafiee, Feargal Brennan, and Inés Armada Espinosa. Whole Life-Cycle Costing of Large-Scale Offshore Wind Farms.

[89] By Masaaki Sibuya. Bivariate extreme statistics. *the Institute of Statistical Mathematics*, 10(1):195–210, 1960.

[90] Abe Sklar. Fonction de répartition à n dimensions et leurs marges. *Publications de l'Institut de Statistique de l'Université de Paris*, 8:229–231, 1959.

[91] Charles Spearman. Spearman's rank correlation coefficient. *Amer. J. Psychol.*, 15:1–8, 1904. ISSN 1756-1833. doi: 10.1136/bmj.g7327.

[92] Magnus Stålhane, Hanne Vefsnmo, Elin E Halvorsen-Weare, Lars Magnus Hvattum, and Lars Magne Nonås. Vessel fleet optimization for maintenance operations at offshore wind farms under uncertainty. *Energy Procedia*, 94:357–366, 2016. doi: 10.1016/j.egypro.2016.09.195.

[93] Strategic Initiative for Ocean Energy. Ocean Energy: Cost of Energy and Cost Reduction Opportunities. (May):29, 2013. URL `http://si-ocean.eu/en/upload/docs/WP3/CoEreport3{_}2final.pdf`.

[94] N. M. (Noel M.) Swerdlow and O. (Otto) Neugebauer. *Mathematical astronomy in Copernicus's De revolutionibus*. Springer-Verlag, 1984. ISBN 0387909397.

[95] Eugene A Terray, Blair H Brumley, and Brandon Strong. Measuring Waves and Currents with an Upward-Looking ADCP.

[96] Inc. The MathWorks. MATLAB and Statistics Toolbox Release 2016a, 2016.

[97] Joe Thompson. Personal contact with J. Thompson: EMEC data technician, 2016.

[98] Tidal Sails. Tidal Sails: about us, 2013. URL `http://tidalsails.com/about-us/`.

[99] H C Tijms. Semi-Markov Decision Processes. 7, 2003.

[100] Henk C. Tijms. Stochastic Modeling and Analysis: A Computational Approach. 1986.

[101] Curtis L. Tomasevicz and Sohrab Asgarpoor. Optimum maintenance policy using semi-Markov decision processes. *Electric Power Systems Research*, 79(9):1286–1291, 2009. ISSN 03787796. doi: 10.1016/j.epsr.2009.03.008.

[102] Curtis L Tomasevicz, Member Ieee, and Sohrab Asgarpoor. Optimum Maintenance Policy Using Semi-Markov Decision Processes. *Electrical Engineering*, pages 23–28, 2006.

[103] B.v. Ubisch. Station Keeping Criteria for Dynamically Positioned Vessels. In *DYNAMIC POSITIONING CONFERENCE: Design and Control*, 2004.

[104] U.S. Energy Information Administration. Electric Power Monthly: Table 6.7.B. Capacity Factors for Utility Scale Generators Not Primarily Using Fossil Fuels, January 2013-May 2016, 2016. URL `http://www.eia.gov/electricity/monthly/epm{_}table{_}grapher.cfm?t=epmt{_}6{_}07{_}b`.

[105] F. Vagliasindi. Gestire la manutenzione. Perche e come. *Perche e come*, 1989.

[106] Jasper van Casteren. Power System Reliability Assessment using the Weibull-Markov Model Department of Electric Power Engineering. *Engineering*, 2001.

[107] Vroon B.V. Vessel Datasheet: VOS PRINCIPLE, 2016. URL `https://www.vroon.nl/Files/VesselParticulars/VOSPRINCIPLE20160727095856.pdf`.

[108] Ronald E Walpole, Raymond H Myers, Sharon L Myers, and Keying Ye. *Probability and Statistics for Engineers and Scientists*, volume 3rd. 2012. ISBN 0132047675.

[109] J. Wolf and D. Prandle. Some observations of wave-current interaction. *Coastal Engineering*, 37(3-4): 471–485, 1999. ISSN 03783839. doi: 10.1016/S0378-3839(99)00039-3.

[110] D Meseguer Yebra, S Nyborg Rasmussen, C Weinell, and L Thorslund Pedersen. Marine Fouling and Corrosion Protection for Off-Shore Ocean Energy Setups. *3rd International Conference on Ocean Energy, 6 October, Bilbao*, pages 1–6, 2010.

[111] X Yu, M R Starke, L M Tolbert, and B Ozpineci. Fuel cell power conditioning for electric power applications : a summary. *IET Electric Power Applications*, 1(5):643–656, 2007. ISSN 17518660. doi: 10.1049/iet-epa.

[112] David Zimmerman. Model validation and verification of large and complex space structures. *Inverse Problems in Science and Engineering*, 8(2):93–118, 2000. ISSN 1068-2767. doi: 10.1080/174159700088027722.